UNIVERSITY OF SOUTHAMPTON

Resistive Properties and Detection of Fish

by

Graham Adrian Fewings

A Thesis Submitted to the University of Southampton for the Degree of Doctor of Philosophy

School of Ocean and Earth Science,
Southampton Oceanography Centre,
European Way,
Southampton,
SO14 3ZH.

January, 2001

UNIVERSITY OF SOUTHAMPTON

ABSTRACT

FACULTY OF SCIENCE

OCEAN AND EARTH SCIENCES

Doctor of Philosophy

RESISTIVE PROPERTIES AND DETECTION OF FISH

By Graham Adrian Fewings

A review of the methods available for non-invasive migratory salmonid stock monitoring suggests that there is a need for a new method of assessment of stock size and composition. Both of these measures are important for the success of salmonid population research, management and protection. This thesis details the development of a new method of fish detection and measurement that is designed for operation across a river channel without the need for a permanent man-made structure.

The method is based on an array of small sensor units that may be extended to monitor an entire river width. An electronic resistance sensor, personal computer interface control and automatic calibration were developed and tested for the detection and measurement of resistive targets. The sensor could detect 306 mm resistive targets at a range of 700 mm with a basic accuracy of 25 ppm.

Stainless steel rod and freshly killed fish targets produced very similar changes in the electrical resistance measured between wide-spaced point electrodes. Subsequent measurements indicated relationships between resistance change signal (RCS) and resistive target length, position, water depth, water conductivity and electrode separation. Mathematical models were developed to describe the relationship between RCS and electrode separation, target length and target range from the plane of the electrodes.

The mathematical models were incorporated into computer simulations of two methods of target range compensation. Both of these methods were shown to reduce the target length estimation error, compared with no target range compensation, by $\geq 62\%$. A system that used six point electrodes to compensate for target range was shown to length targets with high accuracy compared with existing systems ($\pm$ 40 mm length error ($1.96 \cdot \sigma$) at a range of 650 mm).

The prototype sensor array was also tested in semi-field conditions using a moving stainless rod and live Atlantic salmon (*Salmo salar* L.) as resistive targets. The ability to record RCS measurements in real time and translate the measurements into predictive models was demonstrated. Measurements of RCS during the passage of salmon over the sensor array were also recorded. These records indicated that salmon-sized fish could be detected by the prototype system and that the RCS were substantially larger than expected from measurements of freshly killed fish.

The results of this study indicate that the technique investigated could provide an additional method of migratory salmonid stock enumeration and measurement at reduced cost and increased accuracy than existing systems.

LIST OF CONTENTS

LIST OF FIGURES

LIST OF TABLES

LIST OF PLATES

ACKNOWLEDGEMENTS

I would like to thank Dr. S. Hutchinson, Dr. L. E. Hawkins, Mr. N. W. Jenkinson and Professor A. P. M. Lockwood for their guidance and critique throughout this investigation. I would also like to express my gratitude to Mr. J. Chandler and Mr. L. Talks for their support and for making this study possible whilst in the employment of the National Rivers Authority and subsequently the Environment Agency. I am also especially grateful to my wife, Sue, for all the time she has spent proof reading and generally being supportive over an extended period.

DEFINITIONS

Model Parameters

λ = 10·log resistance change signal (RCS)

λ_0 = 10·log RCS at T_r =0

T_r = target range (*mm or m dependent on application*)

C_r = corner range (*mm*) ◊

a = difference in RCS (*10·log Ω*) ◊

b = slope coefficient (*10·log Ω mm^{-1}*) ◊

γ = target length (*mm*)

ρ = RCS ratio (*dimensionless*)

α = acoustic coefficient of absorption (*dimensionless*)

σ_{bs} = back scattering cross section (*dimensionless*)

V = voltage difference across conductor (*volt*)

I = current flowing in the conductor (*ampere*)

R = resistance of the conductor (*ohm or Ω*)

Spatial Definitions

Longitudinal axis	axis of river channel or z axis, +ve upstream
Lateral axis	axis across river channel or x axis, +ve to right looking upstream
Vertical axis	axis from river bed to the water surface, +ve upwards

◊ Descriptions as provided by Fox and Shotton (1995)

CHAPTER ONE

GENERAL INTRODUCTION

CHAPTER ONE

1 GENERAL INTRODUCTION

1.1 The Need for Accurate Stock Assessment Methods

The Atlantic salmon is considered to be an important fish species of the North Atlantic. This is because of its value in economic and symbolic terms at both a local and international level. The presence of substantial Atlantic salmon populations is often considered to be indicative of high water quality and effective river management. Their presence can also support substantial rural communities through commercial netting and recreational fishing. In England and Wales the present economic value of each live wild salmon has been estimated at over £14,000 *(at 1997 prices)* (Radford *et al.,* 1991), considerably more than the £10 to £20 value of the same fish's value for food. For these, and other reasons, governments and private fisheries interests are prepared to allocate substantial resources to support existing salmon populations that are in decline and to invest in the reinstatement of salmon populations where they have been absent for decades. Two examples of such reinstatement projects currently underway are the rehabilitation of the River Thames in England and the River Seine in France (Gough, 1989,1990,1991;Euzenat and Larinier, *pers comm*[α]).

On rivers with populations of Atlantic salmon, management of both river and salmon resources are essential to prevent over-exploitation. Effective management of these assets requires high quality information describing the status of the resource and of resource impacting factors. Whilst the technologies for routine, accurate monitoring of river water quality and quantity are well established, these goals have been difficult to achieve for monitoring salmon populations.

[α] (1993). Referring to the rehabilitation programme on the R. Seine in Northern France by Conseil Superieur de la Pêche.

1.2 The Salmon Life Cycle and Salmon Stock Assessment

The life cycle of the Atlantic salmon is complex, largely because the species is anadromous in nature. Eggs are laid in gravelled reaches of fast flowing, high water quality rivers. Once hatched, the juveniles remain in freshwater for one to four years before migration to sea at an approximate length of 150 mm. Salmon emigrants from northern Europe then rapidly gain weight as they undertake a feeding migration around the North Atlantic (see Figure 1). Fish destined to return to their natal rivers after one year at sea make a truncated migration including the Faroe Islands and Iceland, before turning southward to Irish and UK waters. Fish that remain in the sea for a second year appear to feed off the coast of Greenland before returning (Mills, 1989).

Once back in home waters, fish may enter freshwater immediately and make a sustained upstream migration, or more commonly arrive in the tidal reaches of rivers and then wait for suitable conditions for upstream migration. Typically, substantial upstream migrations are made during periods of elevated river discharge (Banks, 1969). Once suitable spawning areas are located at the correct time of year, normally around December, spawning takes place. It is during the period of upstream migration that the opportunity exists to gain valuable information regarding the number and size of surviving adult salmon using automatic salmon counters.

One of the earliest uses of automatic fish counters was to determine the environmental impact of physical barriers to migratory fish movement such as hydro-electric dams (Lethlean, 1953) and they are still used for this purpose (Harte, 1993). A more recent use, requiring new approaches to fish counting, is the determination of environmental impact because of the building of tidal barrages (Euzenat and Larinier, *pers comm.*[α]). In this case, optical counters are required because of the large range in water

---

[α] (1993). Referring to the rehabilitation programme on the R. Seine in Northern France by Conseil Superieur de la Pêche.

conductivity at barrage sites, high acoustic noise and the need for a high degree of species discrimination.

In some cases barriers to fish movement are a behavioural response to environmental stimuli such as water velocity, temperature or light. Such environmental effects can be caused by water abstraction schemes and therefore counters have been used in these circumstances to determine operational limits for water abstraction (Fewings, 1993; Gregory, 1987).

Other investigations have been concerned with furthering the understanding of in-river migration process so that migratory fish populations may be safeguarded. An additional benefit of this type of investigation is the enumeration of total returning stock size in addition to the calculation of exploitation rate and spawning escapement (Solomon and Potter, 1992).

Figure 1 Map of North Atlantic showing approximate migration routes

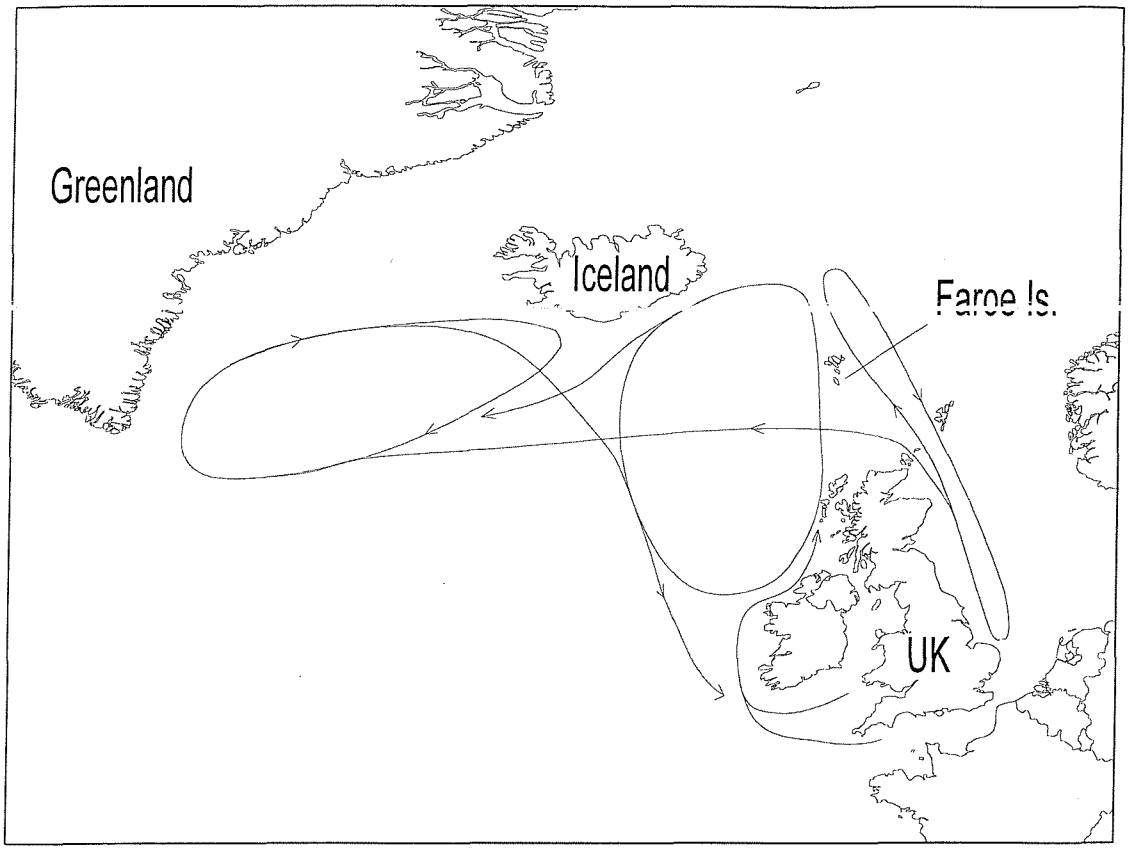

(modified from Mills, 1989)

The management of salmon populations can take many forms. In Canada, some provinces have opted for a system where exploitation in the river cannot proceed until the target number of adult fish has passed through the zone fished. This system can only operate if some means exists to estimate the number of fish that have passed through the fishing zone. Similarly, in England and Wales, salmon spawning targets have been set on many of the main salmon rivers in order to optimise the size of the exploitable stock. Although this is a relatively new method to the UK it has already been used to support the implementation of controls on fishing exploitation on all of the salmon rivers in England and Wales. In order to determine the salmon stock status of rivers in relation to their spawning targets, methods are required to estimate, with known precision, the stock size and approximate age composition each year.

Ideally, salmon population monitoring should yield high quality data that is non-destructive to the fish, non-invasive to migration and inexpensive to collect. The present work describes the initial research and development of a method to count and size salmon with greater accuracy and at reduced cost than existing systems.

1.3 Fish Detection Methods

1.3.1 Introduction

The techniques in use and under development for automatic fish detection are essentially sensor systems that can detect some difference between the fish and the water in which they are immersed. Freshwater has only a limited number of transmission "windows" through which it is possible to penetrate. These "windows" are confined to the electromagnetic waves of long radio waves (wavelengths > 0.1 m), visible light, X-rays and gamma rays. X-ray and gamma ray bands are too expensive or dangerous to place in river counting situations, leaving only the visible and radio bands suitable for use. Water is also transmissive to electric current and sound thus the major groups of methods that can transfer information through water are the transmission categories of light, radio, sound and electric current.

Each method has strengths and weaknesses, which should be carefully considered prior to selection at each potential monitoring location. Fewings (1994) and Hellawell (1973) have carried out reviews of such methods but a brief description serves to establish the context of the goals set out for this investigation.

1.3.2 Existing Fish Detection Methods

1.3.2.1 Optical Fish Detection

Light has been widely utilised by man and other predators to detect fish. One of the major reasons for the evolution of the visual sense is its supreme flexibility and resolution. These natural systems possess the ability not only to recognise objects but estimate size, range, texture and colour. The method applied to fish counting has the advantage of potentially high resolution and accuracy for both detection and counting. The disadvantage of the method is its susceptibility to the transmission losses that occur when rivers are in spate. It is precisely in these high turbidity periods that many salmon migrate upstream therefore leading to potentially substantial inaccuracies in

counting systems. Potentially successful systems have specifically addressed this problem of high transmission loss.

Many rivers that support populations of migratory salmonids have normally low water turbidities and would therefore be suitable for optical counting methods. Some attempts have been made to use machine vision systems for the identification and sizing of fish (Johnson *et al*, 1988) but these have been limited in their success by the speed of computers to process the visual images. The system developed by Johnson *et al* could process video tapes of fish passing through a fish counting area but only when the tape was replayed at reduced speed.

Visual images contain vast amounts of information that the human visual system can process extremely quickly. Serial processing computers process one instruction after another and therefore have to be very fast to process the great deal of information present in a single image. In practice, only a very small proportion of the information from an image is required for counting and sizing and therefore many of the procedures involved with machine vision processing are merely for searching simple but large data sets.

For these reasons, the methods that show greatest promise have incorporated powerful methods for the reduction of the amount of data to be searched for a fish pattern. Two methods have been used to acquire visual data from a counting area. The most obvious uses a video camera to convert light to an electronic signal that can be processed by computer. Data reduction has been achieved with the design of specialist illumination systems to provide very clear, high contrast images in the form of silhouettes. The alternate method uses linear arrays of light emitters and detectors to determine the presence or absence of an opaque object between them. Data reduction is achieved by the sampling of relatively few detectors that are favourably arranged and only provide the information that an object is in the light path or not.

It was recognised that the detection of fish shapes by machine could be enhanced by the simplification of the video images. One way of simplifying images is to represent

them as a series of points on a grid that are either black or white with no shades of grey between. This data reduction technique may be carried out by the computer once an image is in memory or prior to capture by a video camera. The former approach uses valuable computer time and can lead to errors in interpretation on conversion from a grey scale image to a binary one. By simplifying an image prior to capture, variation in the quality of images can be reduced and simplifying an image prior to capture may increase the range of turbidities under which a machine vision system can operate. These two advantages can be achieved with an increase in the contrast of subjects to their background. This is the aim of silhouette imaging systems.

Pippy (cited by Fewings, 1994) achieved very significant contrast enhancements by employing a highly structured arrangement of lighting, camera and reflective backing. This system is based around the properties of the retro-reflective material frequently used on road signs. This material has the useful characteristic that it reflects incedent light almost directly back toward the source, very little light is reflected off this axis.

Pippy arranged an illumination system that supplied light from the axis of the camera using 50% reflective mirrors. Contrast was enhanced since the backing material returned a high proportion of the incident light to the camera. A salmon has a reflective underside but does not reflect light as efficiently as the background. Therefore the fish appeared very dark against a very bright white background. The technique was further refined by the construction of a counting tube with background surfaces at precise angles to the camera/light source axis and a mirror so that the video image showed fish targets both in plan and side elevation.

The simplified video image was processed using a motion detector unit which triggered a time-lapse video recorder on detection of an object moving in the field of view. Such units are readily available for security applications and merely search the video image for areas of darkness, over a preset size, that change position on subsequent images. The system produces a series of time-lapse images with the periods of low activity removed. This processing massively simplifies the task of viewing time-lapse video records since only suspect events are included.

These video records were used to supply the input of a machine vision system called SCIAC model 101 which was constructed around a standard video digitiser card for a personal computer. Video images were digitised in real-time and small areas of the images checked for movement of objects into the counting area. The downstream area is searched first, at right angles to the movement of the water.

If an object was detected then similar searches were carried out at a lateral displacement to the first search but on subsequent images to determine the direction of movement of the object. Once an object was determined to be fully in the counting area then a search was carried out to determine the length of the object. Certain logical criteria were required in order that a count was given and a length was attributable to that count. For example, an object was required to traverse the counting area in a pre-set time and exit from the opposite end of the counting area to the entry point.

In 1992 the system was used for counting the ascending salmon in a southern river of Newfoundland by collecting the motion detector directed video and by subsequent processing by the machine vision system and human interpreter. More recently the machine vision system has been made fast enough to operate on-site without intermediate recordings. An accuracy of over 95% was reported when less than three fish were present in the view. In addition, the system was shown to discriminate between salmonids and eels (*Anguilla anguilla* L.) but not between salmon and migratory trout of similar size.

The limitations of such systems are due to the low volume of water that can be sampled with the counting tube described. Clear, high contrast images are required for the successful identification and sizing of fish. This condition cannot be met if the turbidity of the water is too high since the intensity of the light reflected from the background will decrease markedly as the turbidity of the water increases. As the field of view was increased in order to sample greater volumes of water the relative size of the subject fish became smaller. This increased the search task and reduced the spatial resolution of the output results.

The custom software for the fish counting system on the personal computer was under development during 1992 but significant improvements in performance were still being made. These improvements were largely concerned with optimising the search algorithms for speed and reliability with variable fish behaviour. Such technological limitations will recede as the host computers become faster and the software development programs become more efficient.

Travade (1990) used a video motion detector unit to switch a time lapse video recorder from slow record (0.3 fields s^{-1}) to normal record (50 fields s^{-1}) when an object was detected moving in a preset direction. Evaluation of these machine edited video recordings when compared with continuous time-lapse video recordings showed that counting accuracies of 90-100% were possible under favourable conditions. In addition the analysis system had the ability to discriminate species using shape factors. Images were collected using a side aspect-viewing window with illumination by halogen lamps. Highly reflective background made fish appear in silhouette to enhance contrast. High-count accuracies were achieved with channel widths of 0.3 to 1 m, dependent on the turbidity of the water.

An image analysis system is now under development by Larinier and Travade (1992) to incorporate a fast digital image processor on a unit to be used within a personal computer host. Target identification, tracking and sizing were achieved within the unit and the processed information is transferred to the host computer for additional processing and storage. Fish targets were tracked and constituent features of the fish target were combined to construct a composite target image for further analysis. The target tracking allowed account to be made of the direction of target travel for counting statistics. Shape parameters were extracted from this composite and used in a discriminant analysis process to determine species. Recognition of fish targets was observed at rates of 90 – 100% for fish greater than 0.25 m in length. Significant problems were found in the discrimination of multiple targets that appear to overlap on the silhouette image.

Reson System A/S of Denmark have developed a fish counting and sizing system based on similar principles to that of the Pippy and Larinier systems called the Sealook 9000 submersible weighing system (cited by Fewings, 1994). Silhouette images are generated with structured lighting in an enclosed sensing zone of approximately 0.3 m^3 through which fish swam. The images were digitised and processed using fast micropocessors and software optimised for speed and resolution. The system was designed to be accurate and flexible as it is portable and field programmable. The precision of the unit was claimed by the manufacturers to be within 5% for weight of single fish, 2% for total biomass calculation and counting error is said to be less than 1%. The analysis method is designed for salmon and trout in the size range 0.3 to 8 kg. Since the view of the fish silhouette is restricted to the width of the counting zone (0.3 m) the system must calculate the mass of passing fish from a combination of width and length measurements. To establish the length of an individual fish the speed of passage must be determined from the movement of shape markers past the camera. Mass is calculated using trout and salmon shape relationships.

Reson System claim that two fish may be identified by a length axis separation of just 0.05 m. Furthermore, two fish may be simultaneously counted and sized even if they were alongside each other but one slightly higher than the other to expose one of the fish edges. The weight estimate in this instance was a combined mass although two fish were counted.

Although the system has been used successfully in fish farm situations its overall accuracy will depend upon the turbidity of the water sampled. No figures were supplied regarding the counting of non-fish objects or turbidity ranges applicable to the device. This system has advanced capabilities compared to other silhouette imaging systems but until such devices can be tested alongside each other then they will be difficult to compare.

The alternate method of optical fish detection involves the use of linear arrays of light sources and detectors.Two groups, Vaki Aquaculture Systems of Iceland and Mr Karl

Kilvik of Norway (cited by Fewings, 1994) developed almost identical solutions to machine vision fish counting. A series of light emitting diodes (LED) were arranged in a vertical line at 5 mm centres on one side of a rectangular cross-section channel. Opposite each LED was placed a sensitive light detector also arranged at 5mm centres. This arrangement was then repeated a few centimetres upstream of the first array. Each emitter/detector pair was activated in succession to determine if there was an object between. Since these pairs were sampled at a high rate a whole line of 200 pairs were sampled in a fraction of a second.

Consider a fish moving upstream through the counting area. As the fish body passes through the sensor array the sensor pairs that were obscured map out the vertical height of the fish body. To transform this spatial information into the outline of the fish, the rate of fish movement past the array was determined from the time delay between coincident points on the shape as they pass the second array displaced upstream from the first. With both sets of data available, a complete outline of the fish was calculated. The resolution of fish lengthing was dependent upon the reliability of the algorithm searching for coincident points on the fish. The direction of fish passage was determined from the order in which the vertical arrays are traversed.

Both of the systems developed used infrared emitter/detector pairs that transmit coded pulses of light. The transmission of coded signals allowed screening of signals to reject extraneous light thus improving the signal to noise ratio. Such a scheme not only reduced the likelihood of false positive signals but enabled transmission of signals through turbid water or over greater range than simple light transmissions. Although the two groups developed the technique independently, the problem and the technology available contributed to this convergent development.

The Norwegian system, the FL60, is smaller than the Vaki system and therefore cannot sample as large a volume of water per unit time. Data from the FL60 array was transmitted as digital information in serial form to a logic unit that may be tens of metres from the array. The logic unit performs the function of fish recognition, determination of direction, length and swimming height. All of these parameters were

recorded along with the time in digital form and either output to a small display or printer.

Under test conditions the counter has shown a minimum accuracy of 93% but this was achieved in less than ideal conditions. Where debris and air bubble entrainment were kept to a minimum the counting accuracy was increased to 100%. The developer assures that current developments in the fish recognition software will increase the counter's reliability under such unfavourable but realistic conditions.

The Vaki system had the additional capability to reconstruct fish outlines using a number of coincident points on the fish shape, thus it can cope with variation in fish traversal speed therefore giving a more robust estimate of fish length. It is possible for the Vaki system to output the actual shapes of passing objects for validation purposes where quality assurance data is required. At present the information is not available to determine if the size difference of the two systems is due to the design ranges of turbidity under which the devices are expected to operate.

1.3.2.2 Hydro-Acoustic Fish Detection

One other transmission band available in water is that of compression waves of frequencies between a few hertz and 500 kHz otherwise known as the sound or acoustic channel. Fish use this band for communication, passive location of prey and short range active location for shoaling and object avoidance. Juvenile salmonids are known to communicate in narrow frequency bands and avoid particular sound sources (Knudsen *et al.*, 1992). Fish also use low frequency compression waves to locate prey using the lateral line, an organ present in almost all fish, highly specialised for the reception of low frequency sound (Bleckmann, 1986). A less well known use of the lateral line is its use for shoaling and object avoidance. Tail movement produces low frequency pressure waves and these pressure waves are reflected off nearby fish or inanimate objects. The lateral line detects the reflected pressure waves and therefore can avoid large rocks etc. in darkness.

Since salmonids are very streamlined and move through water very efficiently, little of the propulsive energy of a swimming fish is converted into acoustic energy that could be detected passively. Therefore all the effort to detect migrating salmonids using the acoustic band have employed active methods. The term active refers to the release of acoustic energy into water and measurement of the acoustic energy reflected off objects in the water. The first devices for fish detection were developed in the 1930's. Sund (1935) reports the use of a very early echo sounder for the detection of cod *Gadus morhua* L. Obviously the technologies available for the development of hydro-acoustic systems are far more advanced than in these early days and can now be applied to the difficult technical task of individual fish detection, sizing and positioning.

In order to discuss the relative merits of the presently available systems and the difficulties involved in fish detection, some theory of hydro-acoustics must be described. Oscillations of a submerged surface displace the adjacent water molecules, which then displace their neighbouring water molecules. In this way sound is transmitted through water as series of compression waves that radiate from the source. This spreading of the sound over the area of the wave front leads to a reduction in the intensity of the sound. This reduction in intensity is therefore proportional to the area over which the sound is spread. Since the area of the wave front is related to the square of the range from the source then the intensity decreases in inverse proportion to the square of the range.

Intensity of sound at range is further reduced by absorption losses. Such losses are dependent on factors such as temperature, pressure and frequency. Acoustic absorption increases linearly with range but the effects in freshwater are generally considered small except for frequency related absorption.

Sound reflects off objects of differing density from the propagation medium, in this case water, and it is this reflected sound that is required for fish detection. Not all targets reflect sound in the same manner. The technical term for the ability of an object to reflect sound is called the backscattering cross section and equates to the acoustic

size of an object. With teleost or bony fish most of the sound reflection is due to the presence of the swim bladder as this organ has a low density.

Intensity of sound can normally vary over several orders of magnitude and therefore is cumbersome to relate in linear units. For this reason sound intensity is measured on a logarithmic scale called the decibel (dB). A further advantage of using decibel units is the ease of manipulation. To multiply values add their decibel equivalents and to divide values , subtract their decibel values.

In order for sound to be reflected off a target it must first be generated. Since the direction of a target from the sound source is desirable information, it is important that the sound source is directional. Ideally sound would be projected from the source or transducer along a single axis. In practice it has proven difficult to achieve this and so transducers are available with a single primary axis but with smaller secondary axes. These secondary axes are usually referred to as side lobes. Transducers are classified in their directionality, the angle off axis at which the acoustic energy is reduced by half (-3dB point) is usually the beam angle quoted. This is important since the angle off axis of the target will affect the apparent size of the acoustic target.

The sound transducer not only converts electrical pulses into acoustic pulses but also generates electrical impulses when excited by incident reflected sound. Beam angles typically range from 2° to 45° and are usually circular in cross-section. When used in shallow water elliptical beams are sometimes used to "view" horizontally.

Acoustic pulses consist of short bursts of sound at the operating frequency of the transducer. Since these pulses have a finite duration and travel at about 1480 ms^{-1} the resolution of separate targets at similar ranges will be limited by this pulse duration. The greater the pulse duration the lower the range resolution. A typical pulse width for scientific sonar would be 0.2 ms, therefore the pulse length would be 1480 x 0.0002 or 0.296 m. Targets could be theoretically resolved at a range separation of half this distance or 0.148 m.

Acoustic energy spreads spherically and is absorbed on transmission through water, this transmission loss is predictable and quantifiable. On both the projection and reflection path the acoustic intensity decreases by approximately 20 x Log Range due to spreading. Therefore the total loss is

$$\mathbf{40Log\ T_r}$$

where T_r is the range to the target

The losses due to absorption are also known and quantified by

$$\mathbf{2\alpha\ T_r}$$

where α is the coefficient of absorption

The range to target can be determined by timing the interval between release of the sound energy and the detection of its reflected image as the speed of sound in water is known. With this information it is possible to compensate for the effects of range to the target and calculate a size estimate for a given target. Scientific sonar has this compensation scheme built in as a feature called time varied gain (TVG).

The observed target strength (T_S) can be related to the acoustic size or back-scattering cross section by the following equation.

$$\mathbf{TS = 10\ Log\ \sigma_{bs}}$$

where σ_{bs} is the back scattering cross section

Unfortunately, the target strength estimate is dependent on the shape, size and orientation of the acoustic target relative to the acoustic beam. For a given orientation

of fish the target strength is negative and proportional to the length of the fish, i.e. -20dB for large fish targets and -65dB for small fish targets. Most of the back scattered acoustic energy is reflected from the swim bladder. Since the swim bladders of most fish have a large side aspect and small end aspect the largest target strengths are derived from side aspect views of fish targets. For this reason it is important that fish behaviour is taken into consideration for site selection, i.e, that fish should swim past the site presenting a side aspect normal to the beam axis.

Further determination must be made to successfully detect and size fish targets, this is the axial position of the target in the acoustic beam. The further off-axis the target is the smaller the target will appear. Two methods are presently in use to determine this axial position of a target.

The dual beam method uses two acoustic transducers on the same axis but with different beam angles. As target strengths from each transducer are processed separately but in a short time span the off axis angle can be determined and therefore used to compensate target strengths. The alternate method uses a single transducer that is divided into four discrete reception units. The four units are combined for the transmission of the acoustic pulse but on reception of reflected energy the data from each unit is processed separately. Acoustic energy reflected from an on-axis target is received simultaneously in each of the four quadrants. As the target moves off-axis the sound energy is received at slightly different times in each quadrant leading to phase shifts between adjacent quadrants. These phase shifts can resolve the off-axis angle and therefore enable axial position compensation. Single beam systems cannot determine the off-axis angle and are therefore limited in their usefulness for salmon counting applications since accurate target strengths cannot be calculated.

One other factor is important for the success of acoustic salmon counting operations, that the site must have a low background noise level so that small fish targets are not obscured. Such noise is generally derived from three sources, ambient acoustic energy, electronic noise in the equipment and from reverberation or unwanted targets. The accepted methods for minimising these undesirable effects are good site selection and

planning, extensive electronic and digital filtering and the use of thresholding. Thresholding sets acoustic limits below which signals are rejected and is used extensively in sonar applications. If ambient noise is very high it may be possible to shift to another frequency band to avoid the noise.

Since the target strength measurements should be accurate and repeatable between years and between sites calibrations must be made at regular intervals to maintain data quality. This is normally accomplished with standard acoustic targets such as a competition ping pong ball or tethered live fish of similar size and species to that required for monitoring. For ultimate analogy to the natural passage, fish can be trapped upstream of the counting site and released downstream of the site at low activity times. Individual targets can then be tracked and used for calibration as they swim upstream through the counting site. This technique was used at the counting site on the Moisie River, Quebec Province, Canada, by Groupe Environment Schooner Inc.(Fewings, 1994). Tethered fish were used by Hydroacoustics Technology Inc. on the Yukon River, Alaska (Johnston *et al.,* 1993).

Positioning of the standard acoustic target at alternate ranges and angles off axis enables calibration of the TVG, off axis determination and mapping of the effective counting zone. This latter calibration allows the estimation of the river cross section not covered by the counting zone and therefore the scaling required to give overall passage numbers.

For salmon counting applications it is also important to determine the direction of travel of the acoustic targets. Such determinations can help discriminate fish and non-fish targets since debris rarely move contrary to river currents. Target tracking is an important feature of modern sonar counting systems although the methodologies vary dependant on the type of sonar being used. It is possible to track targets with a single beam system by arranging the acoustic axis to view slightly downstream. Fish swimming upstream through the counting zone are detected at progressively reduced range with an initially small target strength, increasing to a peak and then reducing again as compensation cannot be made for off-axis error. This technique can also be

used with a dual beam system with improved accuracy because of axial compensation. The problem with this approach is that most upstream moving targets will present a sub-maximal target strength due to their non-normal orientation relative to the acoustic axis.

The favoured method of operation with dual beam systems uses two dual beam transducers mounted alongside each other and normal to the flow of the river, sometimes referred to as a quad or paired system. Targets are detected and tracked with both acoustic beams although targets will exhibit a time delay between detection in one beam relative to another. The order in which the targets are detected indicates the direction of travel. Since none of the transducers can be active simultaneously they must be activated sequentially in order that they do not interfere with each other, this is termed multiplex operation. Two quad systems can be used at the same site, one pair on each bank viewing across to the other, this ensures maximum coverage of the river cross section. In these configurations different beam angles are often chosen for each bank dependent on channel slope.

An example of a hydro-acoustic fish counting study site is that on the river Moisie, Quebec, Canada (1990) and serves to illustrate some of the practical difficulties involved in the operation of a hydro-acoustic fish counting site.

The site was selected in 1990 due to a combination of desirable features. These included a gently shelving bottom profile, laminar flow and sufficient distance from the estuary to ensure consistent upstream movement of salmon. The river was 140 m wide at the study site, flows from north-east to south-west and has a three-degree slope on the south-eastern shore and an eight-degree slope on the north-western shore.

Four dual beam sonar units were used in multiplex fashion, with a three-degree narrow beam angle on the gently sloping shore and a six-degree narrow beam angle on the steeply sloping shore. This arrangement was to maximise the coverage of the river profile. All transducers operated at a frequency of 420 kHz with the adjacent

transducers aligned to overlap their respective beams. By overlapping the acoustic beams targets could be tracked through the counting zone as described earlier.

Acoustic calibrations of the equipment were carried out in the laboratory prior to field operation and then standard acoustic targets were used to calibrate the equipment during the study period. In addition to this calibration, live salmon were trapped upstream of the counting site and transported downstream of the acoustic arrays; the fish's progress was then monitored, where possible, through the counting zone. Video cameras were mounted at the end of each deflecting fence and recordings were made of fish passage during daylight hours.

Since limitations of the equipment required the use of only one dual beam pair at one time, a larger proportion of each hour was spent recording activity on the gently shelving shore. This decision was made based on experience gained in previous years at the site, which indicated more fish passage on this shore. It was also known that the spatial coverage was not complete from standard target tests and released fish target experiments. Expansion of the number of fish detected due to spatial and temporal limit coverage was carried out by incorporation of the data from released fish passages and the known proportion of time each area was sampled. This revealed a detection rate of 71% of the released fish passing through the detection area. A statistically significant correlation was also observed between the hydro-acoustic upstream counts and the daily trap catch upstream ($r_{critical} = 0.497$; d.f. = 14; $\alpha = 0.05$; $r = 0.67$; Harte, 1993). The major conclusion drawn from this study was an estimate of between 4556 and 4862 salmon passed the study site in 1992 and that these estimates were considered accurate.

Acoustic methods have therefore been shown to be effective for salmon population estimation in the major rivers of North America and are presently being used in major rivers of Scotland, Wales and the north-west of England. The method can sample entire river widths of over 150 m but requires considerable care in specific installation and monitoring. Species discrimination is based on estimated target size, which is dependent on the orientation of the fish and is therefore of moderate resolution.

Problems have also been noted with the discrimination of fish from water-borne debris (Harte, 1993).

1.3.2.3 Electrical Resistance Change Fish Detection

Electrical resistance change methods provide the basis on which many automatic salmon counters have been built. The first (Lethlean 1953), was built around the Wheatstone resistance bridge principle which offered high sensitivity to resistance change but had the unfortunate inability to distinguish fish moving upstream from volumes of high resistance such as air entrained debris moving downstream.

Currently used systems all operate on a similar principle. Three electrodes are mounted across the flow of a channel each separated by approximately 450 mm. An oscillating signal, either a square or sine wave, is applied to the centre electrode. This signal can be arranged to provide a constant current to the electrode or a constant voltage. Ohm's law can then be used to determine the resistance between the centre electrode and the other two electrodes. This law states that the electrical current that flows through a conductor is determined by the voltage difference across the conductor and the resistance of the conductor.

Ohm's Law:

$\mathbf{V = I \cdot R}$ where

V = voltage difference across conductor

I = current flowing in the conductor

R = resistance of the conductor

Therefore if a constant voltage is applied to the centre electrode then by measuring the current in the other arms of the array the resistance between the electrodes can be determined. Similarly if a constant current is applied to the outer two electrodes then the voltage required to drive this current will enable the determination of resistance between the electrodes. By division of the sensing area into two regions it was possible to determine the order in which the regions were traversed and therefore the direction of fish travel.

Fish have a lower electrical resistivity than the water they displace unlike plastic bags, wood and rafts of weed and therefore they can be distinguished from other objects that pass over weirs.

As a fish swims over such a counting weir it forms a low resistivity path in parallel with the background water resistance. Since there is always a serial resistance in addition to this parallel resistance the overall change in resistance is necessarily small (excepting fish that literally touch both adjacent electrodes). This change in resistance is transient and may vary size by several orders of magnitude especially with fish targets that are longer than the separation of the electrodes. The observed change in resistance for a given size fish is dependent on a number of variables some related to the sensing zone conditions and some related to the behaviour of the fish.

The background water resistance determines the resistivity change that occurs with a fish present by providing an alternate conduction path for the sensing electrical signal. Normally the background resistance is smaller than the fish resistance therefore the absolute change in resistance when a fish is present is not very large.

Parallel resistances combine in the following manner

$$R_{total} = 1/ ((1/R_{Fish}) + (1/R_{Background}))$$

If the difference between the background resistance and the fish resistance is small i.e. short electrodes, low conductivity water with shallow depth then the presence of the fish resistance provides a relatively large change in the combined resistance. If the background resistance is very small in comparison to the fish resistance i.e. long electrodes, high conductivity water of significant depth then the addition of the fish resistance provides a small change in the combined resistance.

Therefore in a typical case of background resistance of 100 Ω and an apparent fish resistance of 2,500 Ω the peak signal would be

$$= R_{Background} - (1/ ((1/R_{Fish}) + (1/R_{Background})))$$

$$= 100 - (1/ ((1/100) + (1/2{,}500)))$$

$$= 3.85\ \Omega$$ change in resistance or maximum fish signal

If $R_{Background}$ were 20 Ω the change in resistance for a similar fish resistance is calculated as only 0.16 Ω. This demonstrates that this type of counting system must include environmental compensation if reliable long-term results are required.

Many factors can modify the background resistance such as the electrode surface area, water depth, water conductivity and electrode separation. Modern resistivity fish counters attempt to compensate for these variations to maintain a near constant response to a standard fish passage at a given range from the counting electrodes. Although this has not been achieved to date as indicated by the analyses of Nicholson *et al.* (1995).

Whilst modern counters can attempt to compensate for environmental variation in the counting zone it is much more difficult to compensate for variations in fish swimming behaviour. The magnitude of resistance change also depends on the range of the fish to the electrodes for a given size fish. The greater the range the smaller the resistance change with a fish present. This reduction in apparent size is not linear

but of the reciprocal form, each increase in range of 50 mm can reduce the signal produced by the presence of the target by a factor of two (Fewings, 1994).

Normally, for reliable counting of fish larger than 50 cm at short range, signal amplification or gain is set which excludes such fish at ranges greater than half the separation of the electrodes or 225 mm. It is possible to set count thresholds and gain to count fish at greater range but this can cause inaccuracies by inclusion of small fish such as young migratory trout (*Salmo trutta* L.) that pass close to the electrodes. Inclusion of such small fish can dramatically increase the error count since these fish are often present in much higher numbers than the larger target species. Where adult salmon are the only fish likely to pass the counting station, gain for counting may be set high with little risk of counting undesired species but yields increased detection of salmon at larger range. No methods exist, at present, to compensate for range to the fish target and therefore methods have been developed to encourage fish to swim close to the electrodes.

These methods exploit the energy saving behaviour patterns of anadromous fish. When challenged with a region of fast flowing water with a distinct velocity profile, fish often swim in the lowest velocity paths (Dunkely and Shearer,1989; Hellawell *et al.*, 1974). These conditions must be met whilst maintaining a relatively constant water volume over the counting zone. If this water volume is allowed to fluctuate with a similar period to that of a fish passing then it is difficult to remove this resistivity noise from the fish signals. Fish signals have a period of 0.5 to 4 seconds and therefore large ripples and waves fall into this noise-generating category.

It is possible to create favourable counting conditions using a number of tried and tested techniques. The first method employed was used by Lethlean in 1953 and involves forcing fish to swim through a submerged tube. Three ring electrodes were set in the tube at approximately 450mm separation. Since the tube was submerged there was no opportunity for the volume of water to change in the tube and therefore a high signal to noise ratio was maintained.

Although the fish travelling through the tube were surrounded by electrodes, significant range effects remain. This effect is described by Lethlean and due to the variation in field density as the distance from the electrodes increases i.e. as a fish traverses closer to the central axis of the tube. Lethlean showed that a given size fish

longer than the separation of the electrodes that passes through the centre of the tube could give an arbitrary output signal of 100 units. The same length fish that passed very close to the electrodes would then give an output signal of 300 units; clearly range was still important even in tube counting systems. Where laminar flow is presented to the ascending salmon it is thought that most will seek the lower velocity paths. In a tube counter situation the lowest velocities can be found closest to the tube walls which also corresponds to the positions of largest signal response.

The major problem with tube type counting systems remains the potential for blockage and that fish must be guided to the counter or prevented from using alternate routes by fish screens. This usually involves costly maintenance checks and therefore detracts from the advantages of high signal to noise ratio.

An alternative to tube counting uses open crested weirs with the electrodes set into the downstream face of the weir. The advantages with this method include its immunity to blockage and the visibility of the objects that swim or float past. The disadvantages include the increased problems of environmental compensation due to variable water depth, low signal to noise ratios, low sensitivity on wide weirs and construction problems.

The Crump guaging weir (Crump, 1952) is the most commonly used type of weir for open channel fish counting. It is triangular in cross section with an upstream face of slope 2:1 and downstream slope of 5:1. It is particularly suitable for this purpose due to the laminar flow conditions and range of velocities that can be achieved.

Low signal to noise ratios are due to the open nature of weirs which make them susceptible to wind induced waves over the counting zone and entrainment of bubbles due to the proximity of channel partitions etc. Signal to noise ratio is also highly dependent on the depth of water over the electrode set. Successful designs of this type of weir ensure that a minimal depth of half the separation of the electrodes is maintained (225 mm). It is also desirable that the depth does not exceed the separation of the electrodes for more than a modest proportion of the year as unnecessary water depth provides more opportunity for fish to ascend the weir at significant ranges from the electrodes.

Approach slopes should not be truncated since ascending fish may not have sufficient distance to align near the bottom of the water column before entering the electrode array. This may lead to fish ascending the weir at markedly different heights in the water column for each of the two halves of the electrode array. This has the effect of reducing the symmetry of the processed fish passage waveform. If the amplitudes of the upstream and downstream portions of the waveform are too dissimilar the counting logic may not be satisfied and the count may not be made.

Fewings (1988) quotes 95% confidence limits for length estimation of ascending salmon at two open channel counting sites using two resistivity fish counters. These estimates vary from ±8 cm to ± 21cm and appear to depend on water depth. Nicholson *et al.* (1993) also suggests lengthing accuracies of ± 20 cm are normal over significant changes in background resistance. Greater water depth tends to provide poorer lengthing accuracy as there is the opportunity for more variability in fish swimming depth.

This limitation in the ability of the sensor system to estimate the length of fish has significant relevance to overall count accuracy when the river reach under study contains both migratory trout and salmon. Fewings (1997) demonstrates that although counting accuracy was high at a site on the River Test, Hampshire, the number of salmon counted was generally an over-estimate and that the number of migratory trout counted was generally an under-estimate. This was primarily due to the presence of some salmon size migratory trout and that some young migratory trout were too small to be counted. This remains a problem at many sites where visual verification is not available.

The Logie fish counter has been evaluated and refined for several years by collaboration between the manufacturers, Aquantic of Montrose, Scotland, and many government agencies.

This counter is significantly different from previous fish counters since it incorporates a number of features, which are designed to decrease the inaccuracies caused by changes in the conductivity and quantity of water over the electrodes. The most significant features of the counter are the environmental compensation techniques employed, the relatively sophisticated fish discrimination algorithm and the data archiving of "pseudo sizes" for the fish detected.

Environmental compensation is achieved by a combination of techniques. The background water resistance is determined by automatic insertion of a known test resistance with automatic gain adjustment to give a constant response. This test procedure is carried out every 30 minutes. Water conductivity is measured with an external probe and the length of the electrodes is input at the system keypad. With this combination of measured and manually input information the Logie constructs internal lookup tables for signal gain adjustment. Testing has shown that much of the variation in performance due to environmental fluctuations is compensated for with this system although by no means all (Nicholson *et al.*, 1995).

The fish discrimination algorithm is one of the most important features of the Logie fish counter and has proven to be robust in its application to distinguish fish and non-fish passage events. It was known from earlier experience of fish counters by the Department of Agriculture and Fisheries for Scotland, who co-developed the Logie counter, that wind induced ripples, ice and various items of river borne debris could seriously degrade counter performance by causing false counts. The Logie counter applies rather more discriminant rules to the event waveforms than previous resistivity fish counters. Most counters have preset thresholds for each of the upstream and downstream pairs of electrodes. A count would normally be given if both thresholds are met or exceeded within a given time period of approximately three seconds. In the Logie counter, additional rules are applied to the waveform requiring both waveform peaks to be similar in size and significantly larger than the noise in the sample.

This approach has worked well at most sites but care must be taken when this method is used at sites with a rectangular cross section since some fish have not been counted because of dissimilar peak estimates in the upstream and downstream sections. Dissimilar waveform peaks can be caused by fish ascending or descending during passage over the counting electrodes. Modifications have been made to the fish discrimination algorithm that relax this criterion. As a result this problem has been solved but it illustrates the importance of optimum site conditions. It is unlikely that such sites will be able to achieve as high count accuracies as purpose built sites that minimise behavioural variation of passing salmon.

Another feature of the Logie counter that distinguishes it from the other resistivity counters is the storage of event time and a "pseudo size" estimate for the event. Events that satisfy the count criteria are given a size estimate based on the amplitude

of the largest waveform peak observed. These sizes are values from 0 to 127, the larger the value the larger the size estimate for the fish. Comparison of observed fish length and fish counter size estimates by Nicholson *et al.* (1995) has yielded relationships between the pseudo-sizes and the real length of the migrant salmon.

The Mk X fish counter from Scottish Hydro was first available in 1987 and has since been refined by continuous development and extensive field testing. This fish counter was primarily developed for use in Scottish rivers to monitor the passage of salmon past barriers imposed by hydro-electric schemes. To this end it was optimised for use in smaller channels, with low conductivity water and low power consumption for remote use. Many of the counting sites were positioned at the upstream exit of Borland fish lifts where fish exit is highly sporadic and therefore the maximum counting rate was important.

The Mk X design had to achieve count accuracies of 90% or better to meet the specification set by the government's Scottish Office for its monitoring role in Scottish hydro-electric schemes. Johnson and Clarke (1987) report that this specification was met at various sites in Scotland. The counter is microprocessor based and designed to be flexible in use. Core plug-in modules can be augmented by ancillary modules for tasks such as data logging, external switching of cameras or data recorders and output of analogue resistivity change data. Internal batteries provide enough power for three days of stand alone operation but provision is made for extended operation from external batteries. Few controls are available on the unit as gain is set by digital push button settings. Recent versions have 32 gain settings, which can be tested *in-situ* by momentarily switching in preset resistances.

Resistance measurement is made in an unusual manner that has some advantages over other methods. In the standard three-electrode configuration the centre electrode is excited with a constant voltage waveform with the current in each of the other electrode circuits measured. This arrangement allows direct determination of the type of change in resistance of each section in the counting zone, ie. it is explicitly known if a resistance change is due to a high or low conductivity object. Measurement techniques based on the bridge principle of resistance measurement could not directly determine if a change in resistance was due to a high resistivity volume in one section or a low resistivity volume in the other section.

1.3.2.4 Summary of Existing Fish Detection Methods

In summary electrical resistivity methods are able to operate in high water turbidity and under a wide range of water conductivity (10-550 $\mu S.cm^{-1}$). The method is limited in its species discrimination and fish sizing but can sample moderate water flow up to approximately 20 m^3s^{-1} per unit and has been shown to provide fish counting accuracies of >90% for Atlantic salmon (Woods, 1995; Nicholson *et al.*, 1995). Species discrimination is based on estimates of fish length, which have been evaluated to accuracies of *circa* ± 80 mm [95% CI] (Fewings, 1988; Nicholson *et al.*, 1995).

All of these methods require significant capital expenditure either for equipment purchase or site installations. Maintenance and operating costs are also significant, so clear benefits must be available to justify this expenditure. In general terms, hydro-acoustic counters can provide count estimates of approximately 80% accuracy and are suitable for moderate to large rivers. The equipment and operating costs are significant since complex equipment, a high level of training and post processing are required to achieve this quoted accuracy. In contrast, optical counters are often placed within existing structures such as fish passes and traps and require relatively little operational costs. Resistivity counters generally have low running costs, but may be sited on existing structures or on high cost purpose built structures. This leads to a large range in the installation costs for resistivity counters. A comparison of such costs is presented in the table below.

Table 1 Comparison of installation and operation costs of fish counters

Cost (£1,000's)	Hydro-acoustic counter	Optical counter	Resistivity counter
Structure	0	2	2-200
Equipment	60	15	10
Manpower	15	3	3
Validation	8	3	3

Automatic fish counters are presently being used for a number of purposes such as behavioural research, environmental impact assessment and routine stock monitoring which demonstrates the need for salmon count data.

The identification of species type is especially important where significant populations of other migratory species exist. For example, many of the salmon rivers of England and Wales have substantial populations of migratory trout . These fish can cause a significant error in the estimation of total returning stock of salmon if the fish counter cannot discriminate between the two species.

Suitable siting of the counting system is also important in order to observe relevant behaviour patterns and to maximise the accuracy of the resultant data. If a counter is situated too far down a river system, significant vacillation effects may be observed as fish that are not committed to a given migration route retreat downstream to ascend another channel. Placement of the hydro-acoustic counting site on the Moisie River, Canada was not only a matter of selection of good river profile and flow patterns, but also the position upstream from the estuary (Harte, 1993).

The resolution and accuracy of a counting system decreases as the volume of water to be sampled increases. Virtually all of the automatic fish counting systems presently available use light, electric effects or sound to detect fish. The properties of the fish, freshwater and the detection method place limits on the resolution and accuracy of the counting system and usually constrain the siting and operation of such systems.

1.3.2.5 Natural Electrical Detection Methods

It is often the case that if a particular ability conveys a selective advantage to an individual then that ability can be found in nature. Fish are hunted in nature using light, sound and even using electric fields. Fish conduct electricity better than the

freshwater they displace and generate electric fields from muscle activity, which enable the passive and active methods of electrical detection.

Passive detection methods sense electrical activity generated by the fish and are analogous to insect predators listening for the sound of a flying insect. The stingray (*Dasyatis sabina* (Lesueur)) is known to employ this method of detection in order to locate prey buried under several centimetres of sand (Blonder and Alevizon, 1988). Sharks have also been shown to possess similar electroreceptive abilities that enable the detection of prey (Kaljmin, 1982).

Active electrical methods detect a change in the conductivity or capacitance within a field generated by the sensing system, an analogy being a bat generating sound and listening to the reflections of that sound from prey such as a flying insect. Fish, such as the weakly electric fish *Apteronotus albifrons* (L.) has also employed this active method (Lannoo and Lannoo, 1993). These fish emit low frequency direct current (d.c.) pulses (750 to 820 Hz). Distortions to this field are sensed by arrays of voltage sensitive 'pores' on the flanks of the fish. Fish that stray into the field generated by the fish change the shape of the field perceived by the pores since the prey has a different electrical conductivity to the water it displaces. Some fish that possess the sense of active electrolocation can not only detect objects more conductive than the surrounding medium, but also objects that differ in either conductivity or capacitance to this medium (Moller, 1995).

Estimates of fish conductivity vary from 357 $\mu S.cm^{-1}$ to 1270 $\mu S.cm^{-1}$ (Whitney and Pierce, 1957; Monan and Engstrom, 1963) whereas most rivers in the UK have water conductivity of between 10 and 300 $\mu S.cm^{-1}$. This demonstrates that most fish should be detectable since they have a higher conductivity than the water they displace. Fish species that have evolved electrical sensory apparatus often live in dark or very turbid conditions or hunt prey that are well camouflaged optically. In addition, most of the African and South American rivers that have populations of fish that use electrolocation also have a low water conductivity. Emde (1993) showed that the ability of *Gnathonemus petersii* (Günther) to detect capacitive objects was a function

of water conductivity. As water conductivity increased, the minimum detectable capacitance increased until the water conductivity reached 800 $\mu S.cm^{-1}$. At water conductivities greater than this threshold the subjects could not discriminate capacitive and resistive objects.

Lissmann (1963) observed that *Gymnarchus niloticus* (Cuvier), produced weak electric pulses at a constant 300 $pulses.s^{-1}$ and reacted violently to the presence of a small magnet or an electrified insulator near the fish's aquarium. He concluded that the fish was sensitive to very small electric fields of the order $<1\ \mu V$. Further experiments used conditioned fish to distinguish between containers with an insulator inside and containers with conductors inside. It was also noted that most of the body surface of *Gymnarchus* was covered with a skin that was an unusually good insulator.

In certain areas, especially near the head, the skin was perforated with pores filled with a jelly-like substance, which led into tubes, and eventually a capsule called a mormyromast. These mormyromasts have afferent nerve fibres that combine to form one of the major sensory nerves leading to the brain. Lissmann showed that although the frequency of discharges remained almost constant, the frequency of nerve impulses from the mormyromasts increased as the amplitude of the electric signal at the sensory cells increased.

Further experimentation revealed that sensory stimulus was a function of both frequency and amplitude at the mormyromasts. Since the frequency and amplitude of the excitation discharges were held constant by the fish the only variable at the mormyromast was the local voltage which was dictated by the electrical conductivity of the volume surrounding the fish. The mechanism used by the fish to filter background signals was determined to be one of time integration over a period of approximately 25 ms. Such a period corresponds to the collection of information from seven or eight discharges. This sensory mechanism has therefore been shown to be effective in the natural world and has features making it suitable for study as a fish detection method.

1.4 Initial Objectives

The objective of this investigation was to provide a basis for a new method of non-invasive migratory fish stock monitoring. Existing methods are expensive because of their high manpower requirement or large investment cost in purpose-built structures. Any new method should reduce or remove these features in its operation.

The electrical resistance change method was chosen for further investigation in this study since it offered a high immunity to false targets; the opportunity for operation in turbid water and hence potentially wide application in varied river conditions. Nature has also demonstrated that there is considerable scope for enhancements to the existing resistance change detection methods.

1.5 Improvements to Existing Methods

Although electrical resistance change fish counting has a high immunity to false signals and requires only simple in-river components it has a number of limitations that restrict the method's usefulness. These limitations are largely concerned with the range over which fish can be detected. For example, installations are largely confined to weirs or fish passes, as the detection range is relatively low compared to acoustic methods, typically 0.3 m or less. In addition, sites have generally been selected which encourage the fish to swim quickly through the counting zone without significant vacillation. This has the effect of simplifying the resistance change signals associated with fish and reduces the number of opportunities for misinterpreting these signals.

Some of the errors that can occur are because of the inability of existing systems to compensate for changes in the range of the fish from the sensor system. An example is that of a fish that swims upstream through the counting zone close to the sensor system but then drops back downstream at a greater range from the sensors so that it is not detected moving downstream. Other errors, which can occur with existing systems, involve the passage of multiple fish at the same time. If two fish pass through the counting zone in parallel then only one fish is normally counted, even if they are substantially separated laterally in the counting zone. This is caused by the sensor electrodes extending across an entire section of river channel. If two fish were to pass through the counting zone, slightly overlapping in the longitudinal direction then this would normally be counted as one fish.

To overcome these limitations and to increase the resolution and target detection range of the resistance change method, investigation was directed toward enhanced performance of small sensor "cells" and possible methods for range compensation. A cellular approach was adopted since it would enable deployment in a range of river channel widths as sensor cells could be sampled sequentially to detect fish targets across a wide channel. If electrodes were separated more widely than those in the present systems the relatively high inter-electrode resistance would aid sensitivity and provide increased range since the excitation field extends further from the plane of the electrodes (Webster,1990). This effect is also demonstrated with conventional strip electrodes as described by Lawson (1975). In this case fish resistance change signal was positively related to electrode separation for a given fish length, fish range and water conductivity.

Present resistance change counting methods[α] cannot discriminate between objects that have a resistivity higher or lower than the water it displaces. The reason for this

---

[α] Except for the discontinued North of Scotland Hydro Board MkX counter which used parallel current measurements to discriminate high and low conductivity objects.

limitation is that the actual parameter measured is the resistance difference between two pairs of electrodes. Thus the effect of a high resistance volume between the downstream pair of electrodes causes the same output as a low resistance between the upstream pair. This can lead to false detections of objects such as rafts of weed or lumps of ice. A replacement method should discriminate these two types of object.

CHAPTER TWO

SENSOR CONSTRUCTION

CHAPTER TWO

2 SENSOR CONSTRUCTION

2.1 Specification

This section considers issues with existing resistance change fish counting systems that might be addressed by the specification, design and testing of a new sensor system. Previous resistivity-based sensor systems have been designed to count fish over a given size. To achieve this, they have an optimised arrangement of the electrodes in the water to suit this purpose (Lethlean, 1953). The electrodes were placed on the bottom of a river channel or in a tube with a longitudinal separation approximately equal to the length of the smallest fish to be counted (usually 450-500 mm) as shown in Figure 2. These strip electrodes ensured that fish spanning two electrodes evoked a large resistance change between the electrodes and therefore gave a large signal to noise ratio (SNR). The following subsections describe how existing systems might be improved.

2.1.1 Simplified Fish Length Estimation

Fish that at least span the electrodes produce a large signal. As fish length increases, the volume of the fish between the electrodes and not purely its length increasingly affects the fish-induced resistance change. This leads to non-linearity in the fish length to resistance change relationship. This relationship could be simplified if the electrode separation was larger than the largest fish likely to be encountered.

2.1.2 Increased Detection Range

The proximity of the electrodes to each other ensures that the sensing zone is relatively close to the electrodes. Therefore effective counting takes place with targets less than half the electrode separation from the plane of the electrodes. In this case the effective range is only 200-250 mm. Sensitivity has been found to be reduced near the ends of the electrodes (Nicholson *et al.,* 1995).

Figure 2 Standard open channel resistivity change fish-counting weir

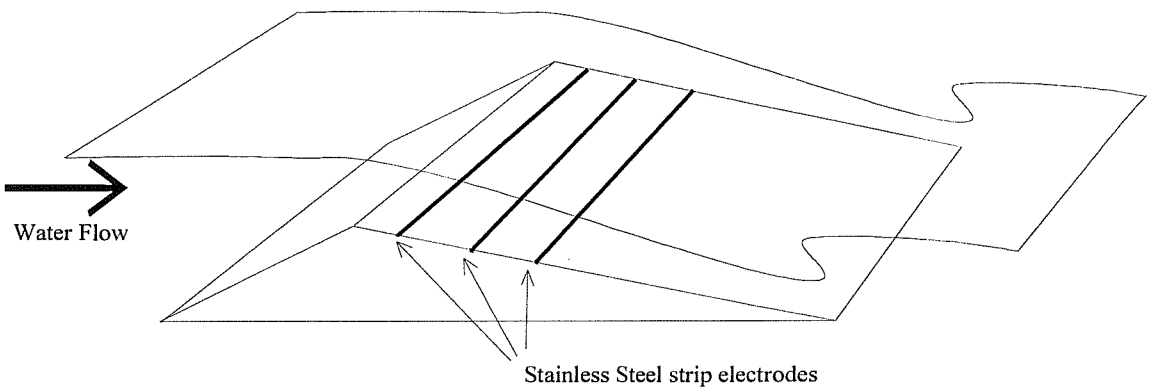

Figure 3 Diagram of proposed electrode array deployment

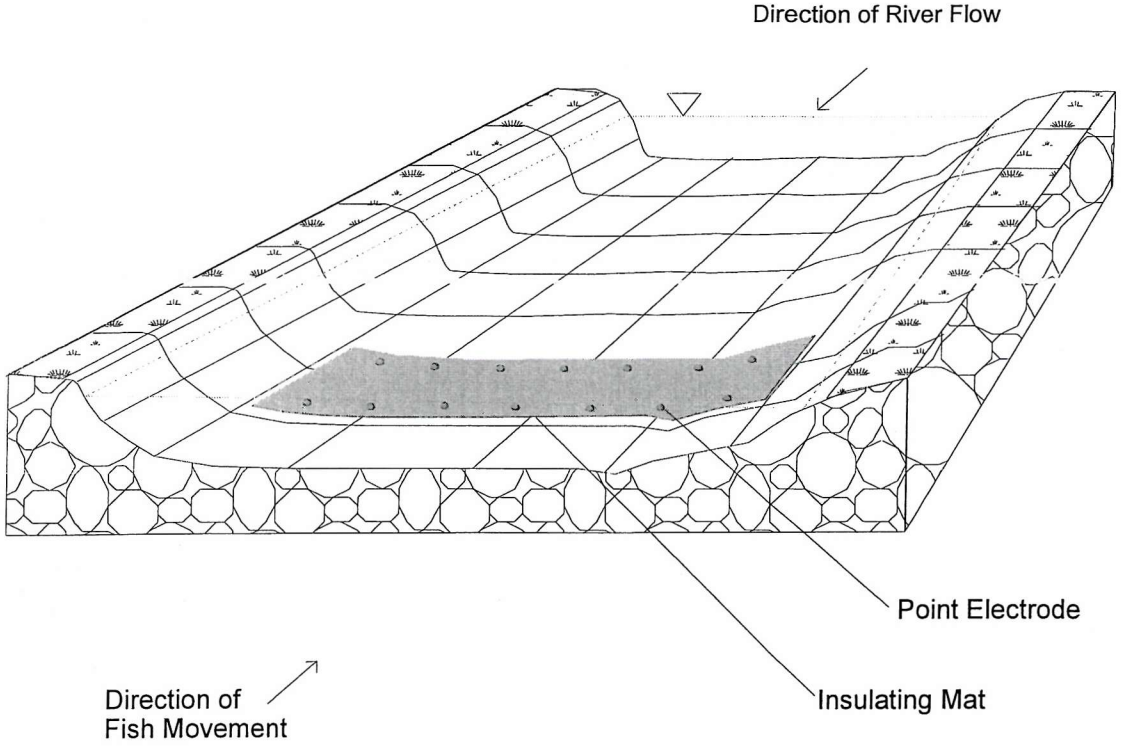

DEFINITIONS

Longitudinal axis	: axis of river channel or z axis, +ve upstream
Lateral axis	: axis across river channel or x axis, +ve to right looking upstream
Vertical axis	: axis from river bed to the water surface, +ve upwards

Thus fish that swim near the channel walls or more than 250 mm from the electrodes are less likely to be counted. Effective range could be increased using a larger separation of electrodes and edge effects could be removed by using point electrodes instead of strip electrodes. A suitable arrangement of the electrodes could be as shown in Figure 3.

2.1.3 Absolute Resistance Measurement

The resistance between electrodes is often measured by the application of an electrical signal to pairs of electrodes with either the signal peak voltage or the signal peak current held constant. If the former method is used then the current flowing in the circuit is measured to indicate the inter-electrode resistance. If the latter method is used then the voltage required to maintain a constant current is measured to indicate the inter-electrode resistance. Neither method has a particular advantage over the other but each requires the design and selection of specific circuit subsections. For this project the constant current method was chosen.

The requirement for absolute resistance measurement was because of the need to discriminate high and low resistivity objects that might pass through the counting zone. Existing resistance change sensors measure the difference in resistance between two pairs of electrodes. This is partly because of the need to remove the effects of background resistance and partly to resolve the direction of travel of the resistance targets.

Normally a fish, that has a lower electrical resistivity than the water it displaces, when swimming upstream would first decrease the resistance between the downstream pair of electrodes relative to the upstream pair. Subsequently, as the fish swims between the upstream pair of electrodes, the resistance between them is decreased. Since the measurement of change in electrical resistance is actually the difference in resistance between the two pairs of electrodes, errors in signal interpretation can occur. For example, a high resistivity object moving downstream would provide a resistance change signal similar to a low resistivity object moving upstream. However, if absolute

resistance measurements were taken then high and low resistivity objects could be resolved.

In addition to these benefits the background resistance provides information regarding the general electrical conditions between the electrodes such as depth of water and water conductivity. Each of these factors can affect the relative size of resistance change when a fish passes and therefore should be used in conjunction with water conductivity and water depth measurements to compensate for these environmental factors. The negative aspect of this absolute measurement approach is that it imposes higher specifications for resolution and accuracy of the sensor system as well as for the rejection of noise signals.

2.1.4 Longevity of Electrode Systems

For such measurements to be undertaken stable alternating current (a.c.) signal sources are required to maintain constant electrode excitation. To minimise the electrolytic and electroplating effects of passing currents through water using metal electrodes a.c. signals should be used.

2.1.5 Fish Signal Filtering

Fish swim through existing weir counting zones within a known range of velocities. Thus fish resistance signals have frequencies within a certain range. Normally this frequency range lies between 2 and 0.2 Hz. Therefore it is possible to exclude many non-fish signals that can be induced by slow changes in river depth, river conductivity or river temperature by using frequency band-pass filtering.

2.1.6 Fish Lengthing Accuracy

For a new detection system to be practically useful each electrode pair "cell" would require an operating range of >0.5 m with lengthing accuracy of better than ±50 mm. Existing resistance change counting systems approach this level of lengthing accuracy at some sites. An acceptable minimum fish size for detection would be approximately

250 mm, large enough for small migratory trout but small enough to exclude even large juvenile salmon from detection on their migration to the sea.

2.1.7 Operational Water Conductivity Range

Freshwater conductivity varies from approximately 10 to 600 $\mu S.cm^{-1}$ throughout the UK and therefore the design of a new system should be able to compensate for such environmental variation.

2.1.8 Extendable to Sample Entire River Widths

Since most rivers in the UK are less than 100 m wide and often comprise reaches of less than 1m in depth, the system should be capable of incorporating additional cells up to the width of the river. Each cell should individually compensate for the depth and conductivity of water flowing over it. To this end cells of approximately 1m longitudinal separation are suggested to maximise the signal available for fish detection and to maximise the ability of a system to compensate for local variations in water depth.

If large cells were used then the relative change in resistance between the measured electrodes when a fish passed between them would be decreased therefore making fish detection more difficult. In addition, compensation for the depth of water over each part an array would become more inaccurate.

If such a target specification could be met then the sensor system should significantly improve existing capabilities to monitor migratory fish stocks in many rivers of the UK.

2.2 Analogue Signal Source

Measurement of resistance using the methods discussed earlier requires the ability to generate a.c. signals of stable amplitude in order to provide a stable drive voltage or

current. Various a.c. signal types have been used in fish counter designs but the most common are of the sine and square wave type.

The frequency of these a.c. signals is usually between 500 and 3,000 Hz (Northrop, 1989; Gray, 1995). Generation of such signals is simple unless very stable amplitudes are required. In this instance an initial specification for amplitude stability was set at 12-bit accuracy or 1 in 4,096 (0.024%) as used in the field of electrical impedance tomography (EIT). EIT is a medical technique in which the distribution of electrical impedance in human tissues is measured to aid in disease diagnosis.

Figure 4 Wein bridge oscillator circuit (zener stabilised)

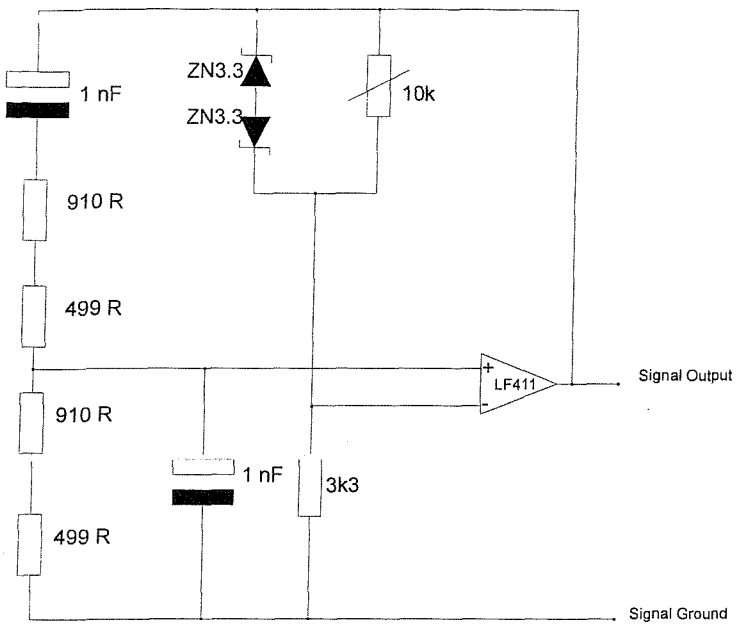

(after Horowitz and Hill, 1989)

Many of the sub-circuits used in EIT have been designed to solve similar measurement problems to that found in fish detection. Some subcircuits were therefore used as initial circuits in an attempt to achieve the above specification for sine wave generation at frequencies from 5 to 50 kHz and amplitudes up to 10 V peak to peak.

The recommended method for sine wave generation at such frequencies with stable amplitude is based on the "Wein Bridge" type circuit (Horowitz and Hill, 1989). The first circuit tested is described by Horowitz and Hill and shown in Figure 4. In this case the basic circuit had an additional section to provide stable amplitude control and low distortion. It was found that the circuit would not oscillate and the cause could not be determined therefore another simpler circuit was constructed using thermistor stabilisation to effect amplitude control.

This thermistor stabilised circuit is described by Marston (1990) (see Figure 5). In this case component values were chosen to provide 5 kHz and 50 kHz output frequencies with peak to peak amplitudes of 2 V. Under test this circuit did oscillate and was found to be reliable but the amplitude stability was not as high as required. The circuit is shown in Figure 4. Amplitude stability was tested using a complete resistance sensor with measurement of the output d.c. signal using a 12-bit analogue to digital converter as described in Section 2.6.1.

The final oscillator circuit, which was built and tested, was described by Van der Walt (1981) and was also based on the Wein bridge circuit. This variant was designed to oscillate at 50 kHz with an amplitude stability of better than 0.024%. This device was found to operate with less noise than previous oscillators and is shown in Figure 6. The improved amplitude stability of the circuit is largely due to the inclusion of a high performance automatic gain control section. This comprises a full wave active rectifier and integrator sections, which provide a d.c. signal used to set the output of a Wein bridge oscillator using a negative feedback loop.

Figure 5 Thermistor stabilised Wein bridge oscillator circuit

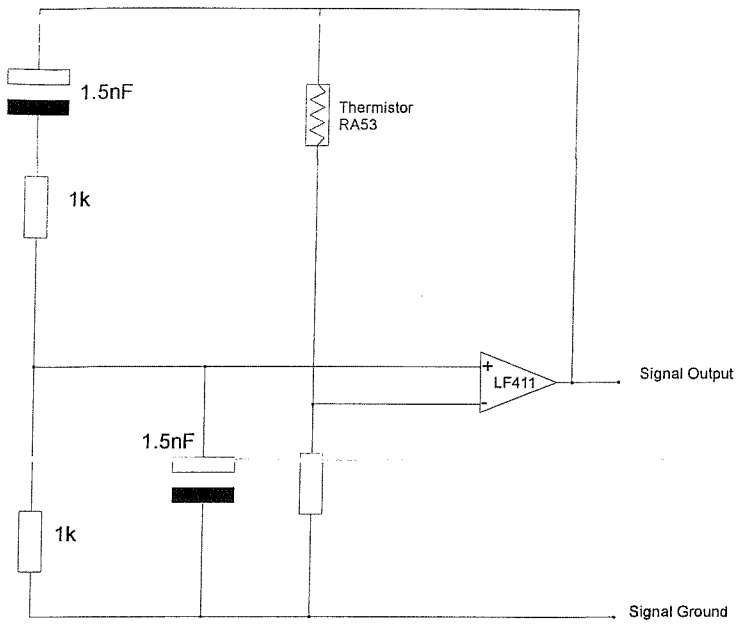

(*after Marston, 1990*)

Figure 6 Amplitude stabilised Wein bridge oscillator circuit

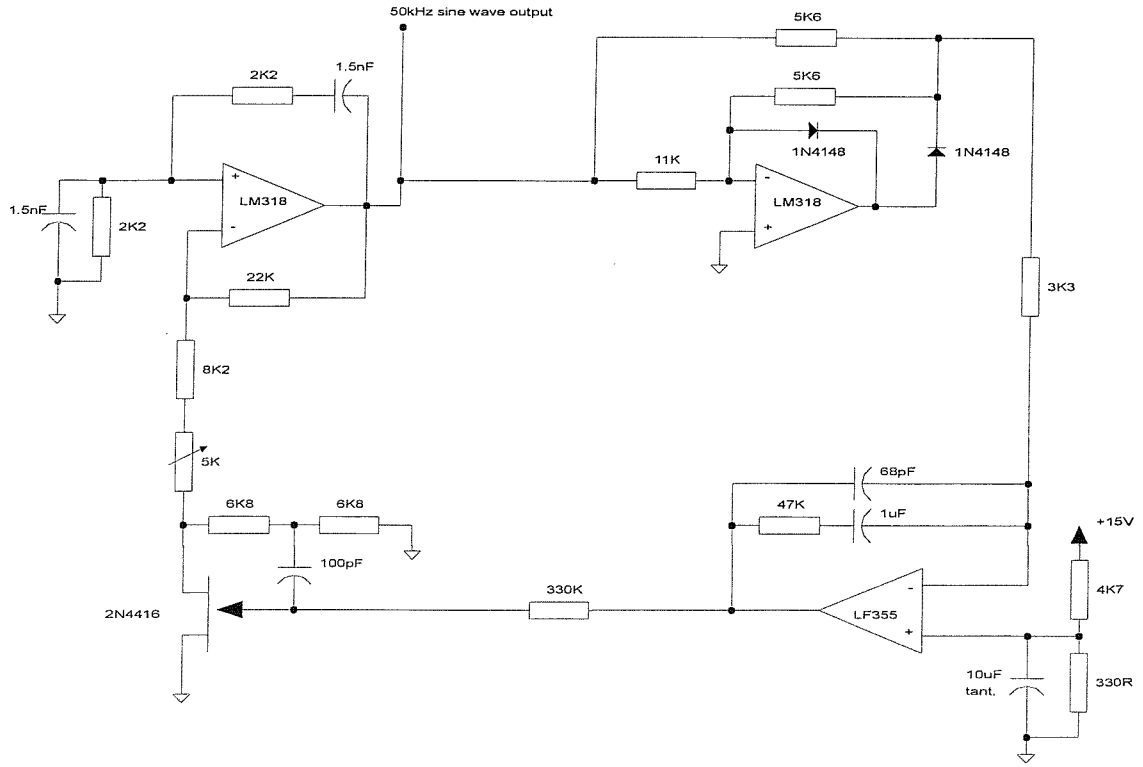

(after Van der Walt, 1981)

2.3 Current Source

Once a suitable excitation signal had been generated, an additional circuit was required to convert the constant amplitude voltage signal to a constant amplitude current signal. Under such conditions the resistance of the inter-electrode space determines the voltage drive required for a constant current in the sensor circuit. Thus the measured voltage at the drive electrode was proportional to the resistance of the circuit.

Three circuits were constructed and tested. The first circuit used a CA3080 transconductance amplifier to convert an input voltage to an output current. Unfortunately, the output signal was found to be distorted on measurement with an oscilloscope. The circuit also required a rather small input signal since the gain of the circuit was high. For these reasons alternative methods were investigated.

The second circuit was conceptually the simplest, consisting of an operational amplifier fed with the constant amplitude input signal to the non-inverting input and a test resistance connected between the output and the inverting input. Since the output of an operational amplifier changes in order to minimise the difference between the two inputs, the current in the feedback loop was proportional to the input voltage (see Figure 7). A disadvantage of this circuit was that the inverting input side of the test resistance cannot be grounded and must remain floating.

Horowitz and Hill (1989) describe the last circuit as a Howland Current source. This circuit uses four matched resistors and an operational amplifier to convert an input voltage to an output current with a gain proportional to the ratio of two pairs of these resistors. This circuit is referred to ground and therefore is simpler to interface to subsequent circuits (see Figure 8). Webster (1990) also describes a variant of this circuit for use in EIT. This Howland current source was found to be simple and reliable in operation using the industry standard LF411 and AD711 operational amplifiers with metal film resistors at 0.1% tolerance.

Figure 7 Simple current source

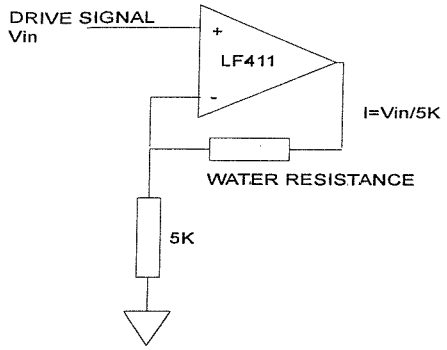

(after Horowitz and Hill, 1989)

Figure 8 Howland current source with input and output buffers

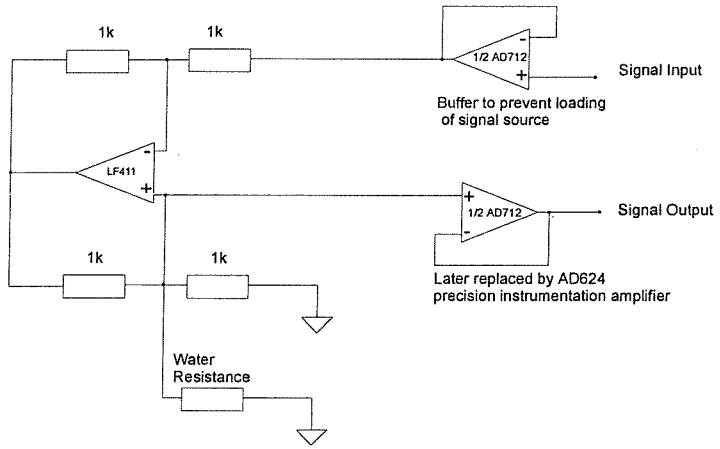

(after Horowitz and Hill, 1989)

The low temperature coefficient of these resistors (±15 ppm/°C) produced relatively little temperature dependence of the circuit. The circuit was therefore adopted as the basis of voltage to current conversion in all subsequent sensor circuits although calibration tests indicated improved performance was possible with additional buffer stages. These calibrations are described by Figure 9 to 12 and Table 2 to 5.

2.4 Signal Demodulation

The current drive method of resistance measurement is essentially an amplitude modulation technique where the load resistance, in this case the water between the electrodes, modulates the carrier signal amplitude. To measure the resistance information encoded in the amplitude (voltage) of the carrier signal, an amplitude demodulation method was required. The simplest methods convert the bipolar output signal (has both positive and negative voltage components) to a unipolar signal and then low-pass filter the output to remove the high-frequency carrier signal. This method is described in Figure 13.

To convert the output signal from a bipolar to a unipolar form the signal can be rectified. There are many methods available for this operation. The simplest uses a diode and a resistor. Diodes have the property of offering a low resistance to a positive potential difference above a threshold and a large resistance to a potential difference less than this threshold. The effect of this operation is to allow the transfer of positive signals through the circuit but not the negative components. One problem with the use of the simplest circuits of this type is that the signal passed has the threshold voltage subtracted from the signal giving a low signal output. This may be from 0.25-0.6V dependent on the type of diode used. Active circuits can be employed to remove this problem as described in Figure 14 to 15. These circuits also invert the negative components of the signal to full-wave rectify the input signal. Full wave rectified circuits provide a larger demodulated signal for a given input due to the retention of both negative and positive components of the input signal and also provide a smoother signal.

Figure 9 Performance of an unbuffered Howland current source at two drive currents

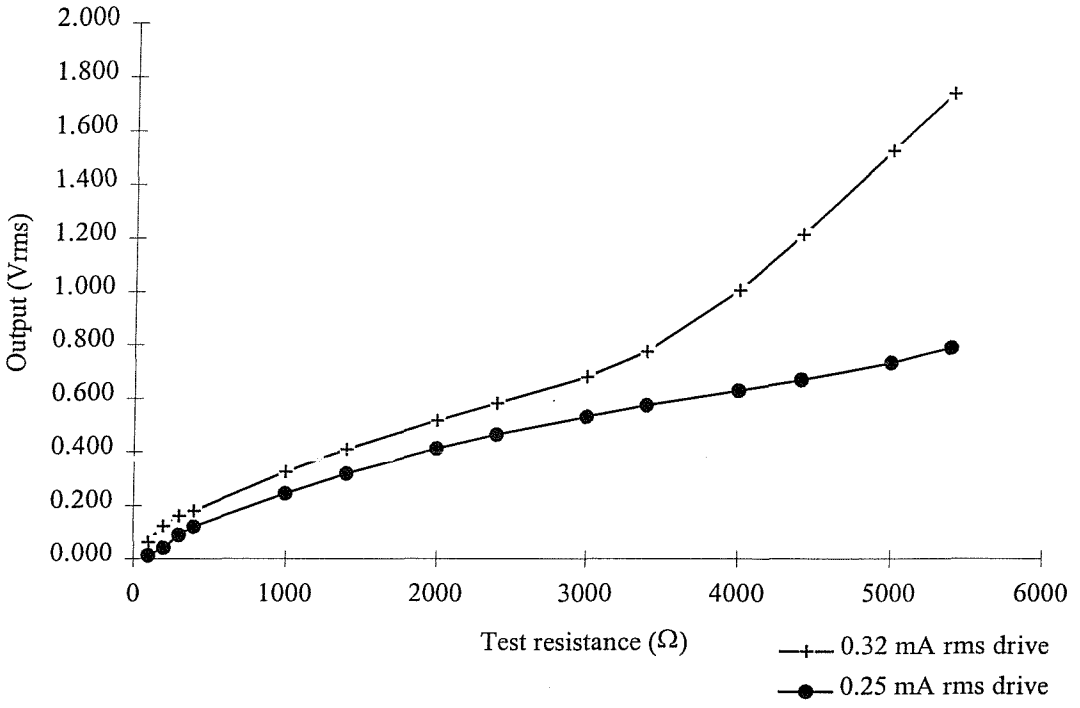

NB. The drive currents used were chosen arbitrarily

Table 2 Output from unbuffered Howland current source at two drive currents

Test resistance (Ω)	High current drive Output (Vrms)	Low current drive Output (Vrms)
100	0.063	0.012
200	0.122	0.041
300	0.161	0.090
400	0.180	0.121
1000	0.328	0.246
1400	0.410	0.322
2000	0.518	0.413
2400	0.585	0.466
3000	0.683	0.534
3400	0.777	0.576
4000	1.005	0.633
4400	1.216	0.672
5000	1.530	0.736
5400	1.742	0.791

1 mA/V Howland current source (unbuffered)
Power supply +/- 10V
100 kHz sine input

Figure 10 Comparison of input buffered and unbuffered current source performance

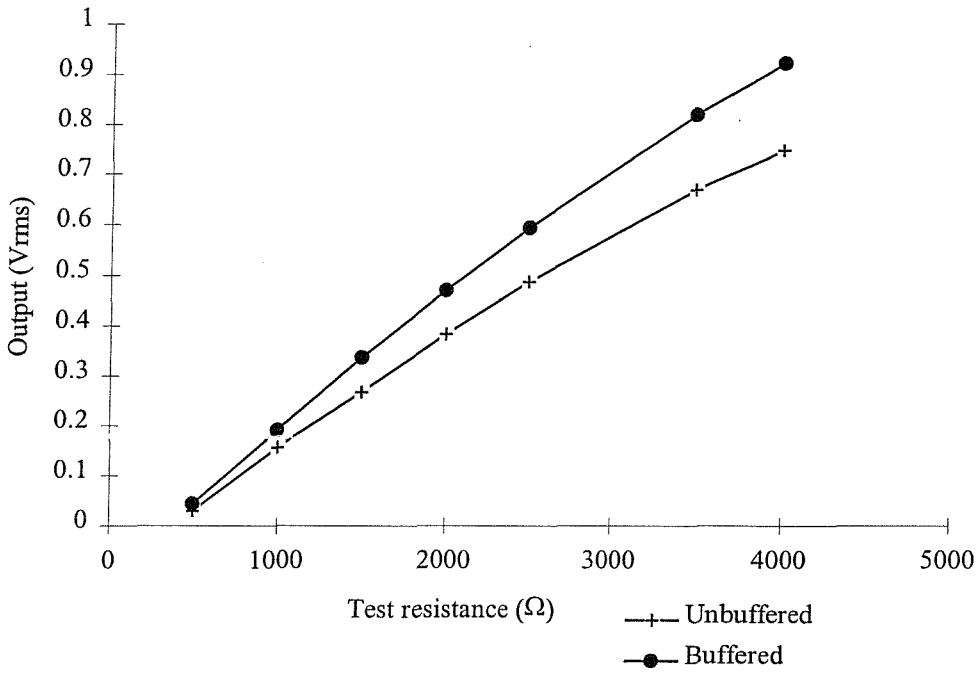

Circuit described by Figures 14 and 17

Table 3 Comparison of input buffered and unbuffered current source performance

Test resistance (Ω)	Unbuffered circuit output (V)	Input buffered circuit output (V)
500	0.0295	0.0441
1000	0.1569	0.1918
1500	0.2678	0.3366
2000	0.3835	0.4709
2500	0.4877	0.5942
3500	0.6687	0.8190
4000	0.7497	0.9238

Test conditions
100 kHz sine excitation from bench oscilator
Measurement of output by ADC
Demodulation by buffered rectifier and 2 stage RC low pass filter
Stage 1 = 159 Hz
Stage 2 = 1.59 Hz

Result

Max error unbuffered circuit	3.70% (0.5 to 4kΩ)
Max error buffered circuit	2.90% (0.5 to 4kΩ)

Figure 11 Comparison of dual buffered Howland current source with an ideal performance curve

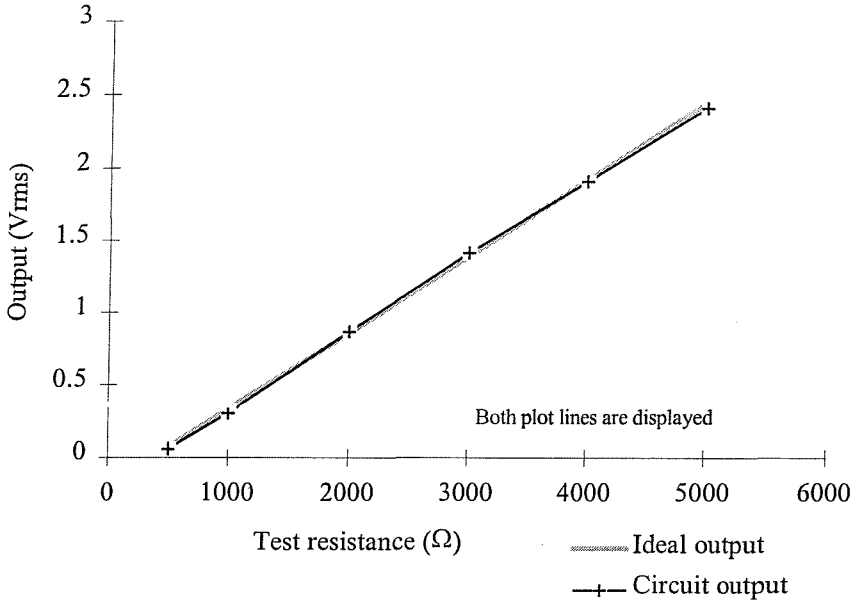

Table 4 Comparison of dual buffered Howland current source with an ideal performance curve

Test resistance (Ω)	Dual buffered circuit output (V)	Ideal output (V)	Point error (%)
500	0.058	0.065	0.290
1000	0.303	0.330	1.110
2000	0.870	0.861	-0.380
3000	1.415	1.391	-0.980
4000	1.914	1.921	0.290
5000	2.415	2.451	1.490

Test conditions
106 kHz sine excitation using thermistor
stabilised Wein bridge oscilatoor
Measurement of output by ADC
Demodulation by buffered rectifier and 2 stage
RC low pass filter
Stage 1 = 159 Hz
Stage 2 = 1.59 Hz

Result
Maximum point error 1.49% (0.5 to 4 kΩ)

Figure 12 Comparison of circuit output and ideal curves for amplitude stabilised signal source and dual buffered Howland current source

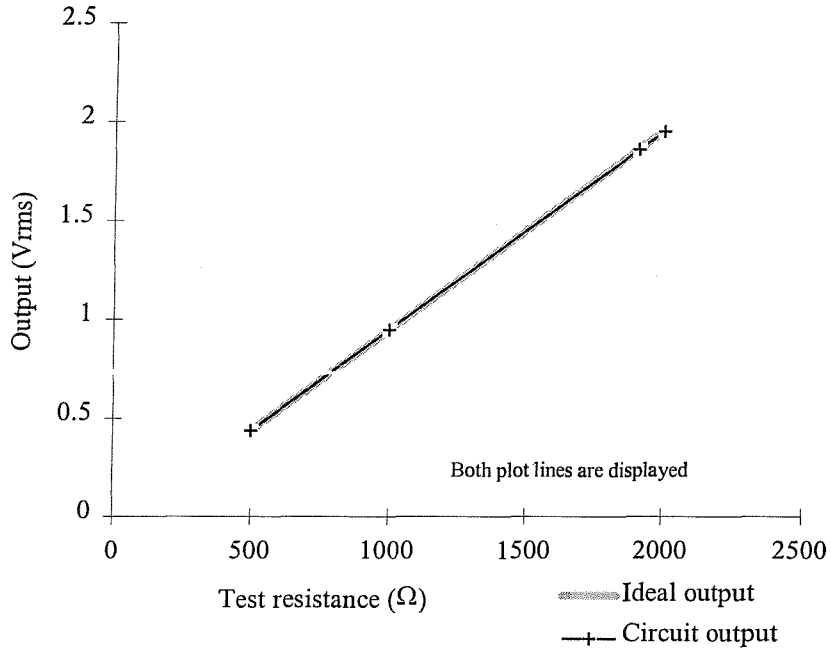

Table 5 Comparison of circuit output and ideal curves for amplitude stabilised signal source and dual buffered Howland current source

Test resistance (Ω)	Output (V)	Ideal output (V)	Error (V)	Error (%)
2000	1.954	1.958	0.004	0.204%
1909	1.864	1.865	0.001	0.054%
1000	0.947	0.944	-0.003	-0.318%
500	0.437	0.437	0.000	0.000%

Test conditions
50 kHz sine excitation using amplitude stabilised Wein bridge oscilator
1 mA/V dual buffered Howland current source electrode drive
buffered rectifier and 2 stage RC low pass filter
both stages 1.59Hz
Result
Maximum error 0.318%

Figure 13 The demodulation of an amplitude modulated signal

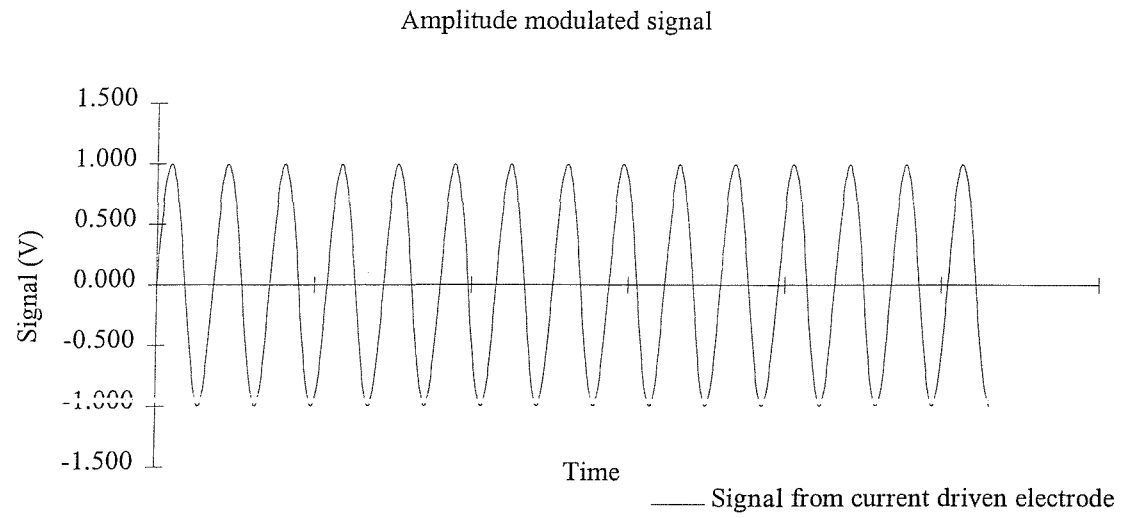

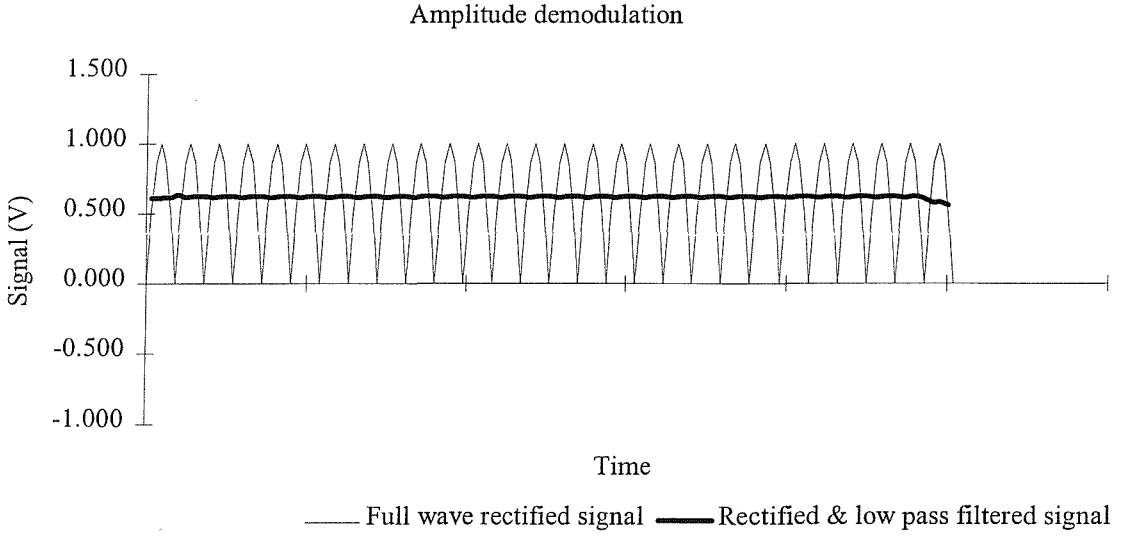

Figure 14 Full wave active rectifier circuit (i)

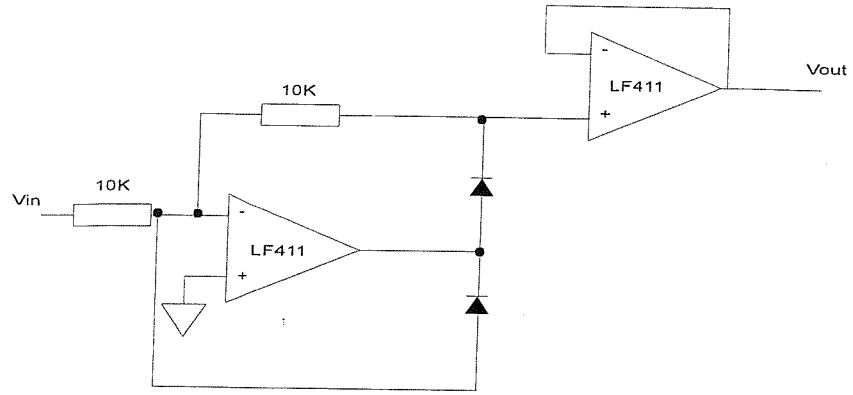

(after Horowitz and Hill, 1989)

Figure 15 Full wave active rectifier circuit (ii)

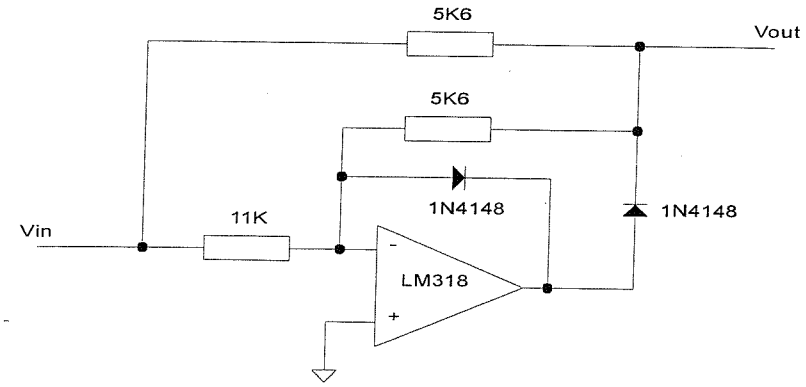

(after Van der Walt, 1981)

Figure 16 Full wave active rectifier circuit (iii)

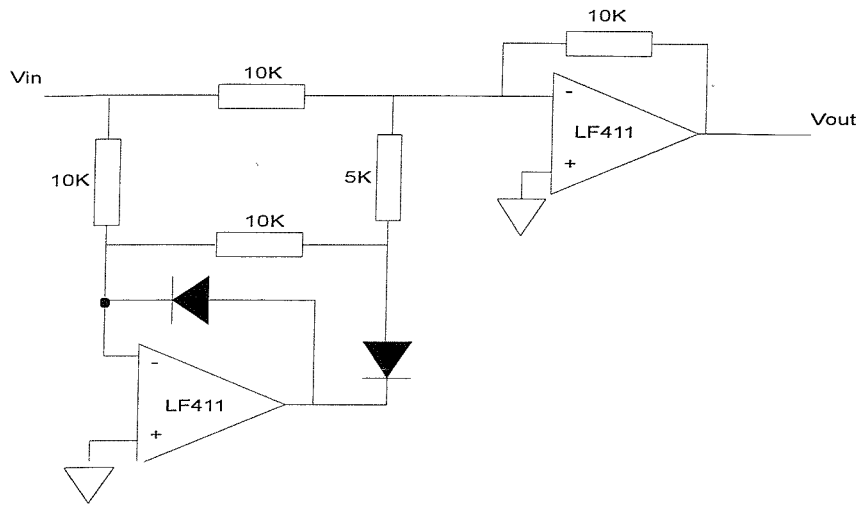

(after Horowitz and Hill, 1989)

Figure 17 Two stage 1.5 Hz dual buffered low pass filter

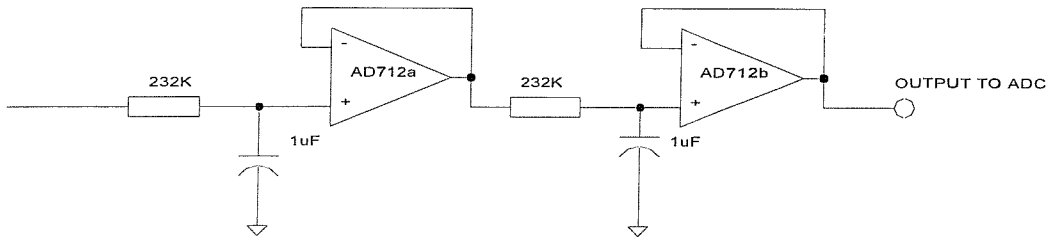

(adapted from Horowitz and Hill, 1989)

A number of these rectifier circuits were compared and the best selected for incorporation in the sensor interface. Selection was based on the degree of distortion introduced to the signal, the operational voltage range and the complexity of the circuit. Full wave rectifier circuit (ii) (Figure 15) was found to have the best performance according to the criteria above and was therefore used for most of the measurements described in chapter 3.

In addition to the rectification of the input signal the output must be low-pass filtered to remove the high-frequency components of the output signal. The cut-off frequency of the filter was set to exclude the maximum proportion of carrier and external noise which is typically centred on 50 Hz. Therefore low-pass filters were tested with cut-off frequencies (-3dB) of 1-10Hz. Both passive and active filters were constructed and tested with output buffering to prevent loading of the circuits by the computer analogue to digital converter (ADC) interface. This ADC had a specified input impedance of 100 kΩ. The circuit described by Figure 17 was found to give the lowest noise of all the low pass filter options tested. The amount of noise output was evaluated by calculation of the range of sample value in relation to the mean of the samples. Thus percentage noise values were determined.[α]

Two other demodulation techniques were tested but failed to provide sufficiently stable output for the purposes of this study. The first method utilised single chip root mean square (rms) to d.c. converters to demodulate the amplitude modulated resistance signal. "Analog Devices" converter chips AD536, AD636 and AD637 were tested using the manufacturers application note circuit described as standard rms connection. Each of these datasheets is included in Appendix A. Only the AD536 was made to operate satisfactorily but its performance was not as high as the active rectifier / low pass filter methods described above due to the presence of considerable low frequency noise in the output signal.

[α] Although these values were collected a subsequent computer failure destroyed the data.

Figure 18 Sensor system used for sine source tank measurements

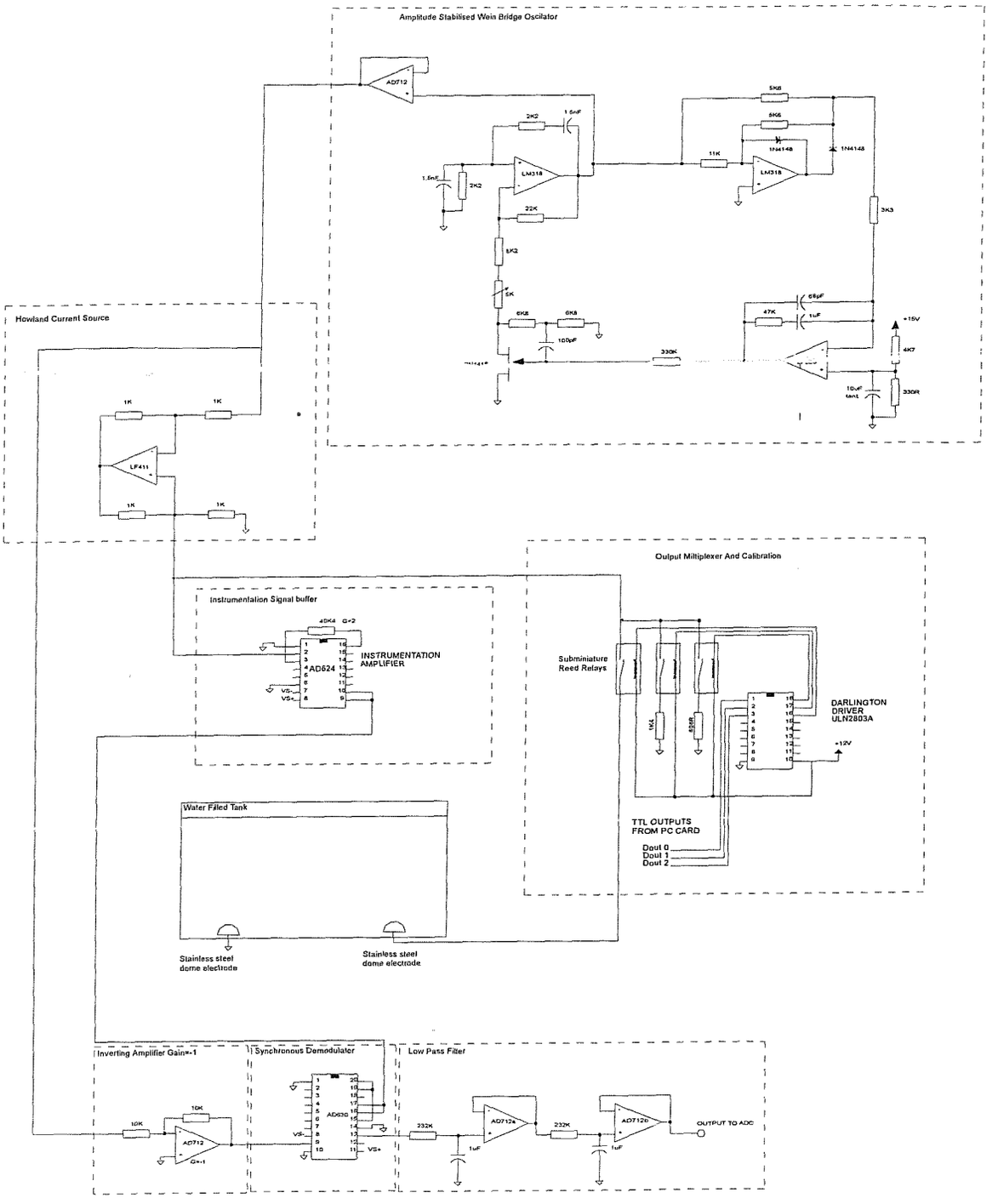

NB. Analogue ground cables and connections have been omitted for clarity

Plate 1 Analogue sensor circuit board

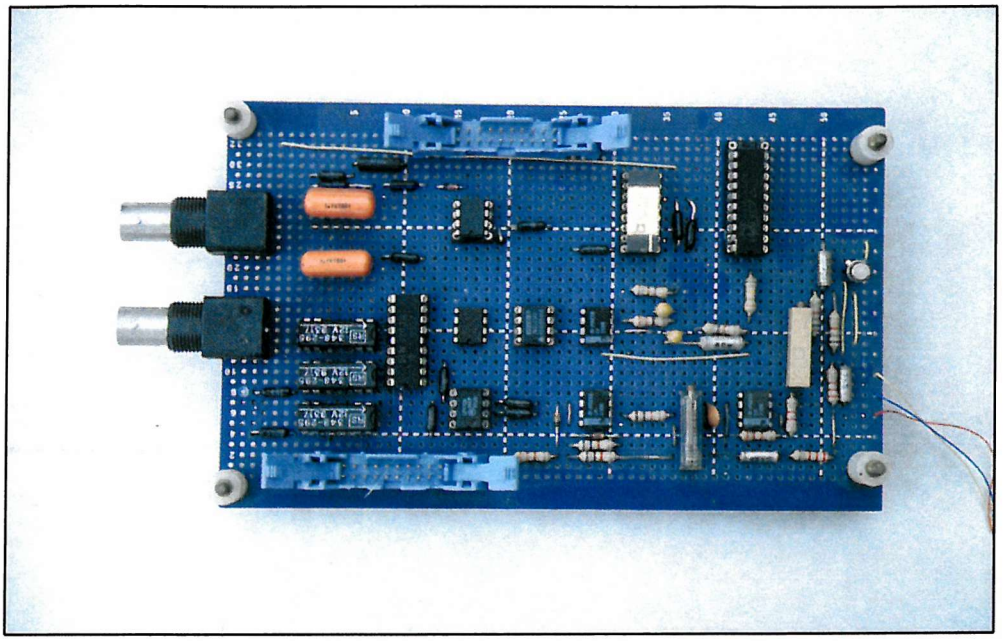

Plate 2 Digital sensor circuit board

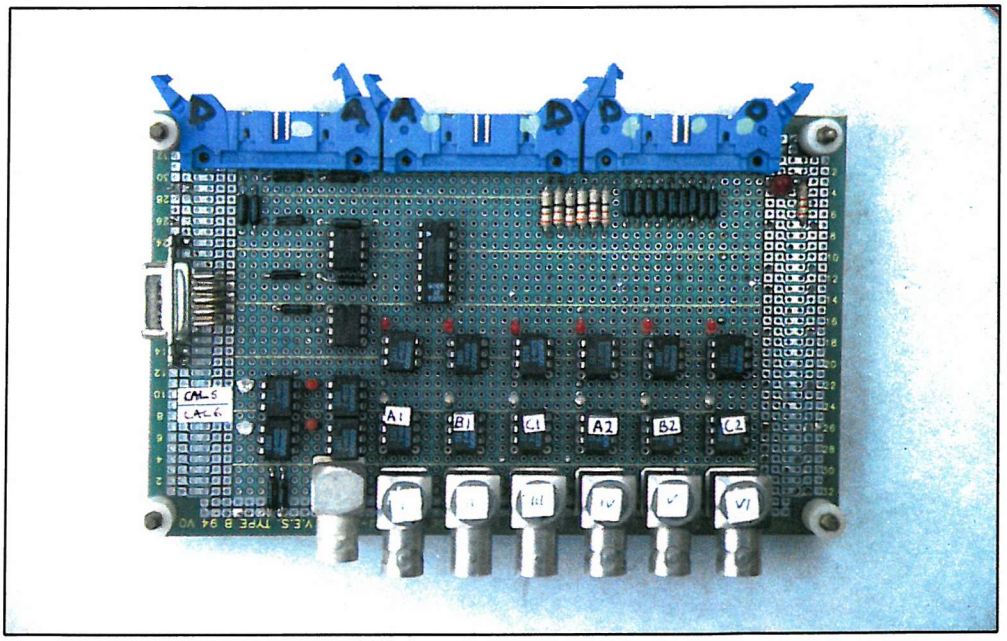

The alternative demodulation method used an analogue multiplier chip to divide the current drive signal by the voltage signal at the drive electrode. Since these devices have sufficient slew rate to track these signals at even 50 kHz the output was expected to be a voltage linearly proportional to the conductance of the load. Although two different analogue multipliers were tried in this configuration, the output contained sufficient low frequency noise to exclude their use for this purpose.

An analogue multiplier was also used as to divide demodulated current and voltage signals. Once again the output low frequency noise precluded their further use in this configuration. Finally an analogue multiplier was tested as a rectifier, this was achieved by squaring the voltage at the drive electrode. This produced a unipolar output of half the frequency of the input signal. Once low-pass filtered the output was found to contain considerable low frequency noise and therefore excluded from further experimentation.

One other method of signal rectification was tested, that of synchronous rectification. "Analog Devices" manufacture a synchronous demodulation integrated circuit, the AD630, which contains a synchronous rectification subsection. The device uses two inputs as described by the AD624 application notes (Appendix A), the amplitude modulated resistance signal found at the sensing electrode and an inverted drive voltage (see Figure 18 and Plate 1). The AD630 uses the inverted signal output of the Wein bridge oscillator to switch the gain of the modulated input signal from 1 to -1. The output from this device was thus a full wave-rectified resistance modulated voltage with the amplitude of the peaks proportional to the resistance applied between the electrodes. The AD630 is a high quality device specified for precision applications, it was therefore designed for low noise operation and high stability.

In summary, many demodulation techniques were tested with the most stable constructed using standard active rectifier and active low-pass filter subcircuits or high performance integrated circuit building blocks. Component operational amplifiers were chosen for high input impedance, high slew rate and low noise characteristics. To

this end the LF411 and AD711 operational amplifiers were found to provide satisfactory results.

2.5 Noise Rejection

It was found that measurements of resistance at resolutions necessary for fish detection at range were swamped by random noise in the interface and from input noise derived from the electrodes. Further investigation determined three suitable methods of noise reduction.

By substitution of the measurement electrodes and water with a precision "dummy" resistor, internal sources of noise were investigated. These sources of noise could be reduced by reduction of the output low pass-filter cut-off frequency, increased filter cut-off rate (i.e. more filter orders), improved output and input buffering and digital filtering of the digitised signal. The first three methods improve signal to noise ratio by improving the rejection of power supply a.c. interference through improved filter performance. The latter method improves resolution by selectively removing mains interference introduced in the computer interface itself.

Digital filtering was used in two ways, first a 50 Hz digital band reject filter was introduced sampling at 100 times 50 Hz (5 kHz) and averaging the signal over 200 samples i.e. two periods of a 50 Hz cycle. This was found to dramatically reduce the apparent noise in the sensor system. This type of noise was present for any source and therefore it was concluded that the source was the ADC card itself since it was located close to a 50 Hz power supply in the IBM computer. Digital filtering was therefore the only simple method of improving signal to noise ratio without modification of the ADC hardware. A number of alternative configurations (number of samples and sample rate) of filter were tested and this was found to be a good compromise between sample rate and noise rejection.

The second digital filter was a low pass filter, two types of these filters were tested, recursive and non-recursive. The former type has good filter performance but suffers from phase shift problems. This was thought to be undesirable for real time

measurement of fish proximity as the output from a target detection could be delayed by more than one second. Essentially this type of filter averages a new sample with the previous sample a preset number of times, the output of each averaging cycle is then fed back into the averaging process as input.

The non-recursive filter could also be described as a moving average filter. This filter also has a lag response but is generally smaller than that of the former filter and approximately equal to the sample rate multiplied by half the number of samples averaged. This method was found to be a good compromise between noise rejection and response time.

With the electrodes connected to the interface more noise was observed. Placing a hand on the side of the test-tank below the water line apparently decreased the resistance between the electrodes. Increasing hand area in contact with the tank surface increased the response. The response was not observed if a hand was placed above the water line. A hand placed near the unshielded drive electrode cable provided a similar negative resistance response. This was not observed if a hand was placed near the unshielded ground cable to the grounded electrode.

By shielding the electrode cables the response to hand proximity was markedly reduced but not eliminated. It was concluded that the effect was due to earthing of the tank water via the experimenter's body. Multiple earthing electrodes were therefore arranged at the surface of the water in the tank at the four corners (Figure 19). This addition further reduced the effects of human proximity to the tank.

Figure 19 General arrangement of test tank

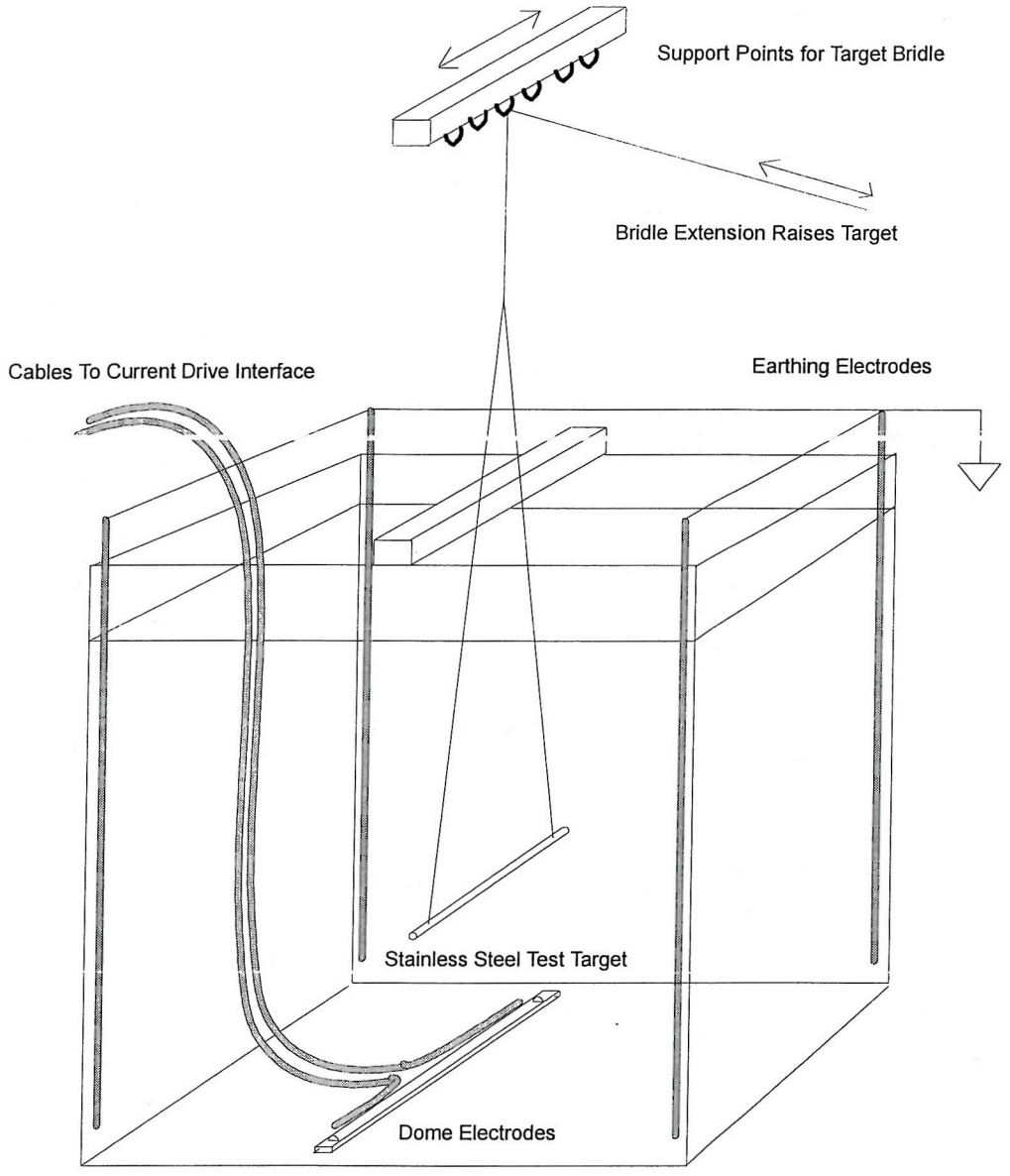

NB. Earthing electrodes were connected to the earth strap of the immediate building. Shielding and grounding considerations are discussed in Section 2.5 and chapter 3. In general the coaxial cable sheath was connected to analogue ground at the sensor interface and sealed to prevent connection with the water near to the electrode.

2.6 Sensor Evaluation

2.6.1 Calibrations

Each subcircuit was required to exhibit stable and expected behaviour before incorporation to the complete sensor. Once the sensor configuration was complete this was tested for stable and expected behaviour with a test resistance and the water load resistance.

Each complete sensor construct was tested for linearity over the resistance range of 100 to 1,000 Ω by placing precision metal film resistors in place of the test tank load resistance. Each resistor was previously measured using a digital resistance meter and connected to the interface using a prototyping breadboard. Combinations of serial and parallel resistances were used to provide a range of test resistances. The results of these calibrations with key sensor configurations are given in Figure 9 to 12 and Table 2 to 5.

Once the sensor configuration had been reasonably refined, an automatic calibration subsection was built into the sensor hardware and software. This circuit used computer control to switch in combinations of precision test resistances *in lieu* of the water load resistance. This calibration feature was incorporated to allow the routine collection of resistance data in SI units instead of units that required further translation to SI units via manual calibrations. Modifications to subcircuits, ageing of components, temperature drifts etc. were thereby taken into account each time the sensor was used. Figure 18 describes the automatic calibration sensor.

2.6.2 Sensing Electrodes

The electrodes used in the test tank were designed to provide point contact with the water and to be resilient to corrosion. To this end the electrodes were made of 316 stainless steel and were hemispherical in shape.

Figure 20 Electrode general arrangement

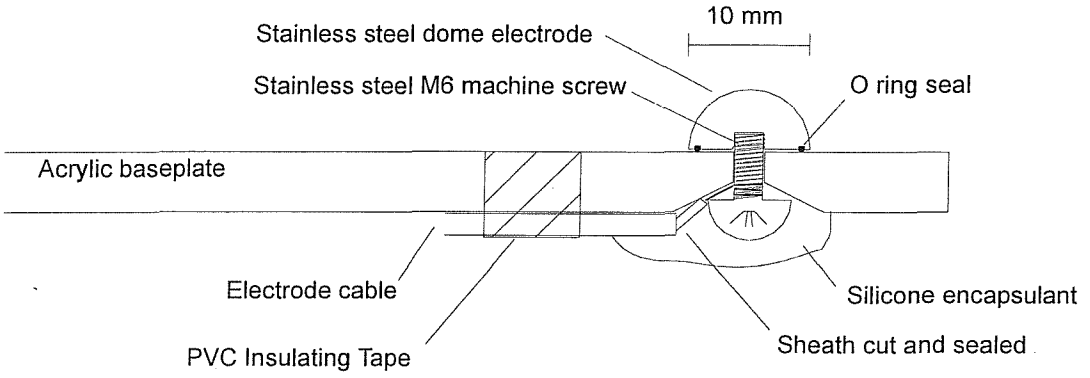

Stainless steel electrodes were used due to their electrical stability in freshwater

The flat surface of the electrode was recessed to allow an 'O' ring seal between the electrode and its mounting plate as shown in Figure 20. The purpose of this seal was to standardise the exposed surface of the electrode as much as possible. Fixture of the electrode to its substrate was achieved using an M6 machine screw made of the same quality stainless steel as the electrode body. The machine screw also served to hold the gold ring terminal soldered to the electrode cable. To promote a low resistance connection between the ring, machine screw and dome electrode the ring and threads were smeared with electrically conductive silver paint. Once this assembly was dry the underside of the acrylic sheet base plate was sealed with silicone encapsulant.

2.7 Digital Signal Source

After a series of tank test experiments it became clear that any operational fish counting system would require the ability to switch sensing electrodes in order to avoid interference between adjacent "cells". Unfortunately the existing sensor system was not suitable for such procedures since the low pass filter section required time to settle after changing electrodes as well as a means of removing the current signal prior to each change of electrodes. Since the filter cut off frequency was of the set at 1.5 Hz the time to settle was estimated at *circa* 1.33 seconds [twice the period of the cut off frequency]. As an operational unit would require to sample the electrode at least 20 times a second a more flexible sensing method was required.

Some fish counters were known to use square wave signal sources to drive the electrodes, therefore precision sources of square wave signals were investigated. In this case a ready source of square wave pulses was the PCL718 data acquisition card previously used for analogue to digital conversion, which also has a digital to analogue converter (DAC). In such an arrangement the data acquisition card has the ability to synchronise analogue input samples with the output pulse, there is therefore no need for demodulation circuits since the data acquisition card accomplishes it.

Figure 21 Single pulse resistance measurements multiplexer circuit

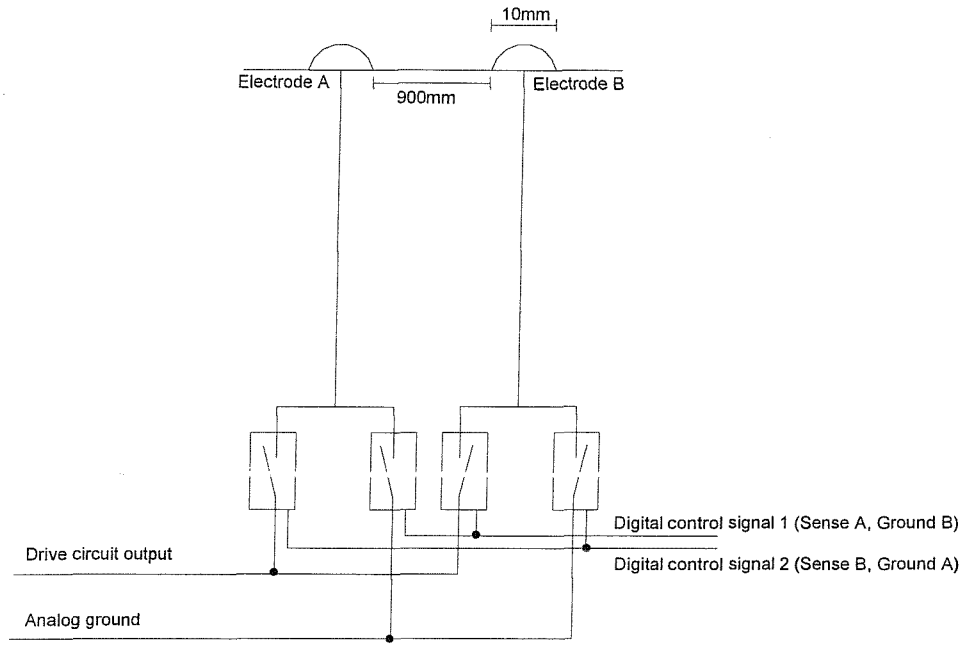

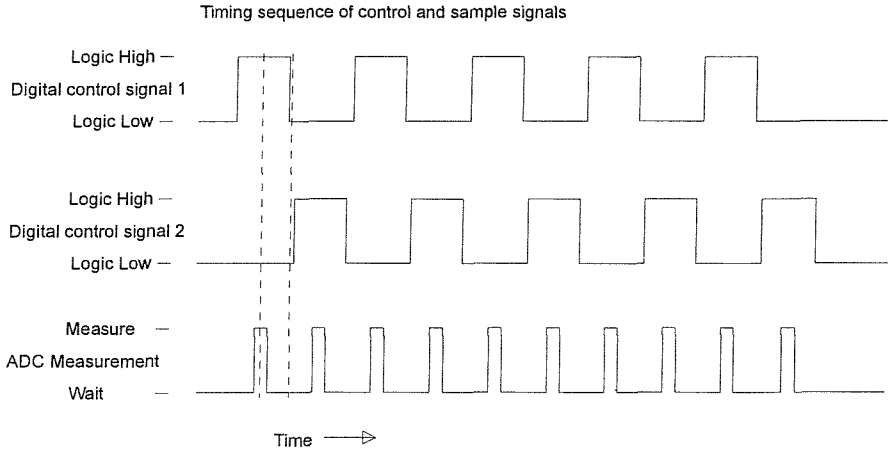

2.7.1 Single Pulse Measurements

A first attempt at resistance measurement using the DAC involved using a single pulse of direct current. The current pulse was initiated by a voltage pulse from the DAC, which was then converted to a current pulse by a buffered Howland current source as described by Figure 8. To avoid problems with electrolytic action an arrangement of digitally controlled switches was used to invert the current direction of the pulse. This is illustrated by Figure 21 in which initially electrode A was connected to the sensing circuit and B was connected to analogue ground due to the application of a logic high signal on digital control line 1 and a logic low signal applied to control line 2. After a measurement was taken, digital control line 1 was set low and control line 2 was set at logic high. In this state electrode B was connected to the sensing circuit and electrode A was connected to analogue ground.

Mechanical relays have a finite life of *circa* 1×10^7 operations and therefore solid-state relays were used since they are not constrained by this limitation. "PhotoMos" relays (see Appendix A) were utilised since they have a very low resistance to signals when in the "on" state and were easily interfaced to the TTL logic of the PCL718. Figure 22 describes their general connection arrangement. An indicator light-emitting diode was included in the design for diagnostic purposes.

The circuit was tested initially using additional "PhotoMos" relays in the calibration configuration used for the analogue signal driven sensor. Two relays were therefore used to switch two precision resistors into the circuit for calibration and stability testing. With one resistor of 806 Ω and one of 1,400 Ω three calibration resistances could be generated, the third by using both resistors in parallel giving a resistance of 511.51 Ω. The "on" resistance of the "PhotoMos" relays was measured using a digital resistance meter and found to be stable at *circa* 0.7 Ω. Using this arrangement of single pulse resistance measurement the estimates of resistance for the calibration resistors was found to be very consistent (variation in estimated resistance of $<\pm$ 0.01 Ω in 1,400 Ω).

Figure 22 Standard TTL control of "PhotoMOS" relay

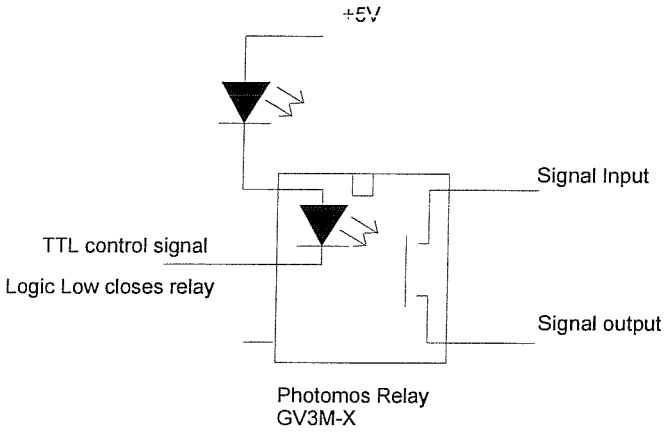

NB. A 249Ω resistor was used in series with the TTL control signal and the photomos diode.

This represents a resolution of 1 part in 140,000 or *circa* 17-bit resolution. This high resolution was largely due to averaging of a number of samples and obviously exceeds the resolution of the 12-bit ADC used.

When the sensor system was used with the two electrodes in the test tank the measurements were much more variable. The increased variability in measurements was thought to be due to a significant capacitance of the electrode arrangement, exacerbated by variations in the duration of the current pulses. It was also noticed that a bias in the measurements quickly formed between one electrode and the other. This meant that even with no targets present in the water, the resistance measured in one direction was not the same as if the electrodes were reversed.

2.7.2 Measurements Using Sequences of Pulses

To overcome the capacitance problem it was reasoned that if a precisely timed sequence of pulses which alternated between a positive and a negative current was used, then greater consistency and balance of charging each electrode could be achieved.

To investigate this solution a precise sequence of square wave pulses was generated by the DAC allowing measurements to be taken for a known time period. The output voltage of the DAC was converted to an output current by a dual buffered Howland current source (see Figure 24). These current pulses were configured to be of alternating polarity with respect to 0 volts and of constant amplitude (see Figure 23). It was possible to configure the data acquisition card to synchronise an output current pulse with the collection of a voltage sample. This voltage sample was derived from the sensing electrode voltage, ie. the voltage required to drive a preset current. This voltage was therefore proportional to the resistance between the electrodes.

Figure 23 Pulse sequence from digital to analog convertor

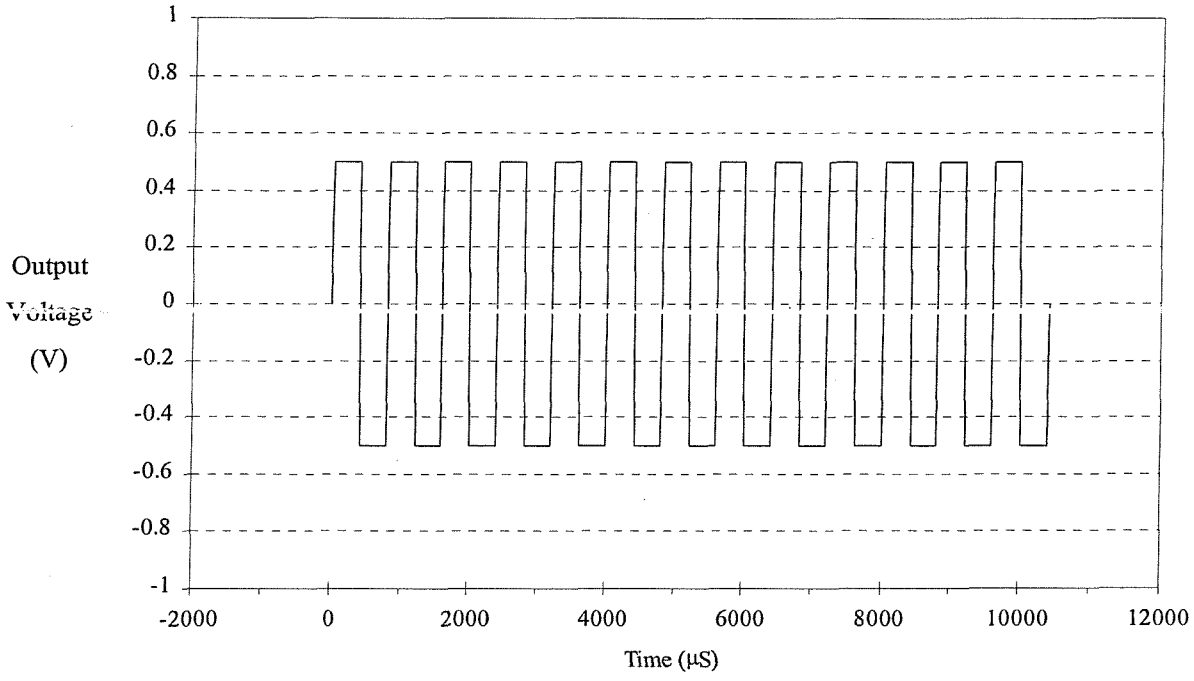

Figure 24 Digital to analog sensor circuit

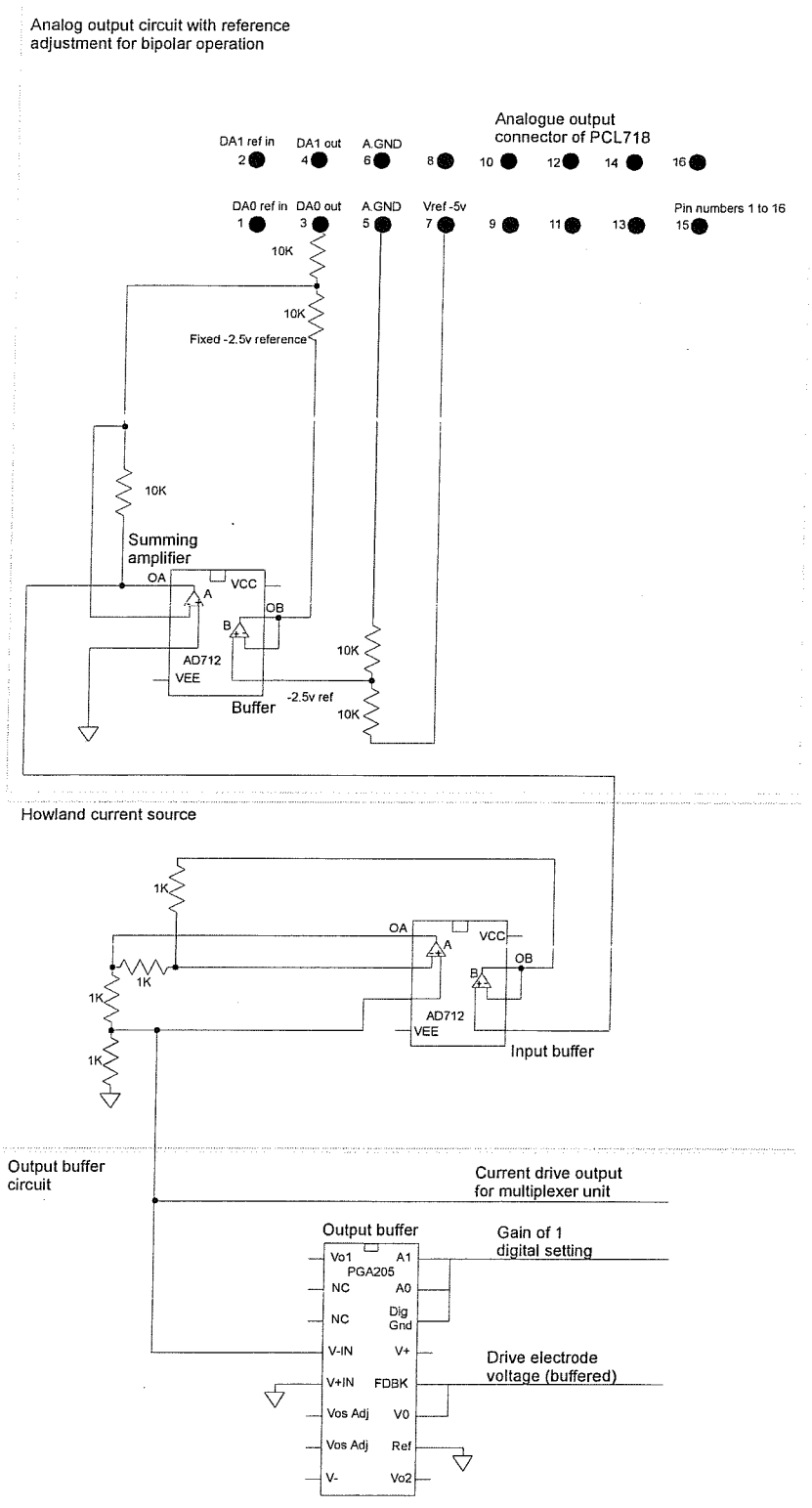

Since a digital device under the control of the host personal computer generated the sequence of square waves, the number, frequency and amplitude of the pulses could be set precisely by software. It was known that the maximum frequency of pulses that could be generated by the PCL718 was 2,500 Hz and so the number of pulses per measurement was dictated by the requirement to remove the maximum amount of 50 Hz noise from the power supply. In this case 2,500 / 50 or 50 pulses, thus the sequence itself was designed with a powerful 50 Hz notch filter. The notch filter worked by averaging the errors introduced by supply line interference over the period of one cycle at 50 Hz.

Testing of the method indicated that the method produced stable and accurate estimates of resistance for the calibration resistances. When connected to the electrodes in the test tank there was still a problem with the resistance estimate gradually increasing. It was thought that this effect was still derived from the capacitance of the electrodes in the tank. Minute differences between the average excitation in either the positive or negative current pulses was thought to be charging up one or other of the electrodes prior to the next measurement.

To address this problem the software that controlled the DAC was modified to vary the size and polarity of the first pulse in the sequence dynamically. An estimate of the direction and degree of offset from steady state conditions was derived from the sum of all of the peak measurements made during the previous measurement. A sum of zero meant that the excitation was balanced and that no correction was necessary. If the sum was nett positive then the first peak was made more negative by a fixed amount.

Figure 25 Arrangement of the six electrode array plate and spatial definitions

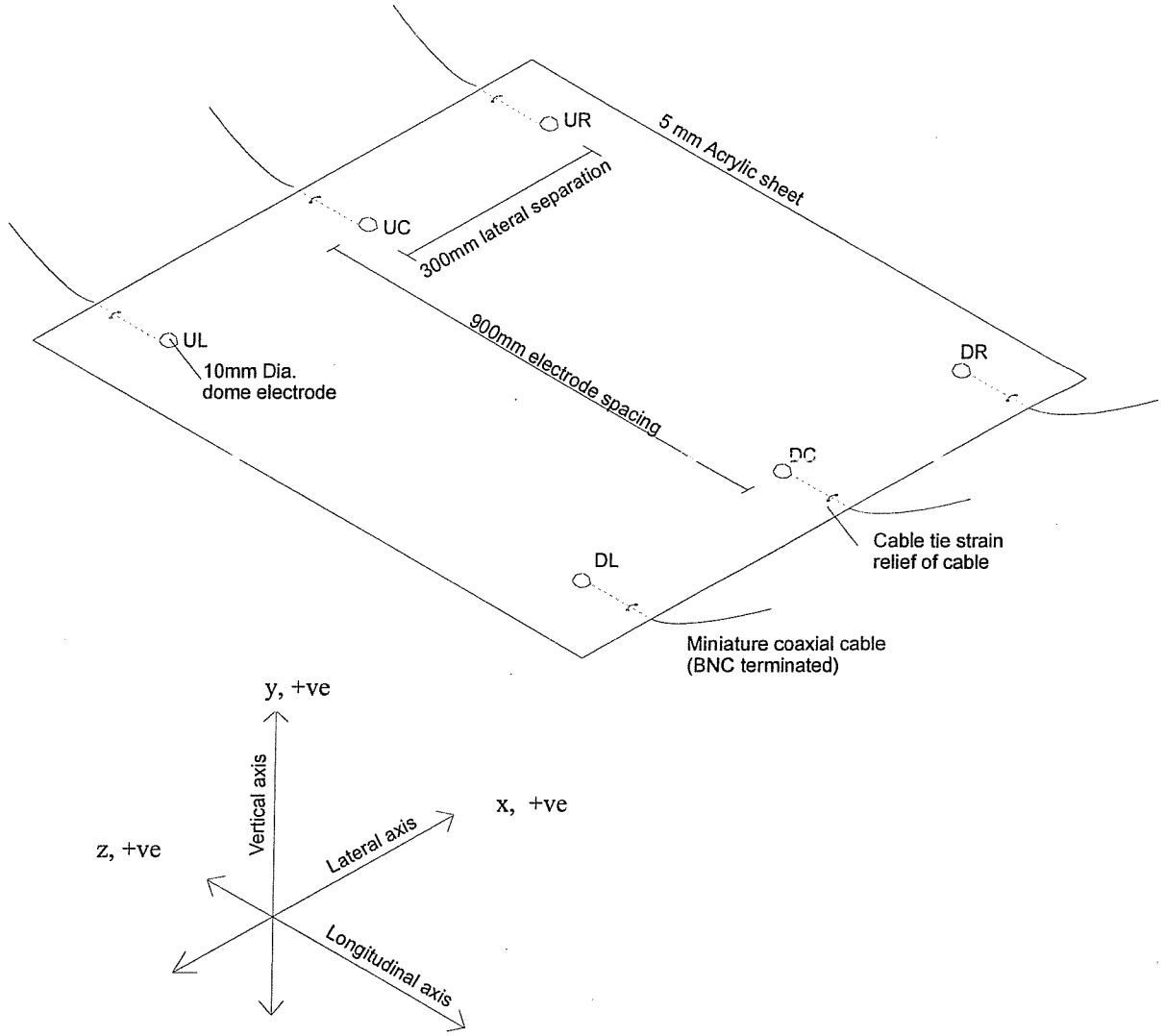

DEFINITIONS

Longitudinal axis	: axis of river channel or z axis, +ve upstream
Lateral axis	: axis across river channel or x axis, +ve to right looking upstream
Vertical axis	: axis from river bed to the water surface, +ve upwards

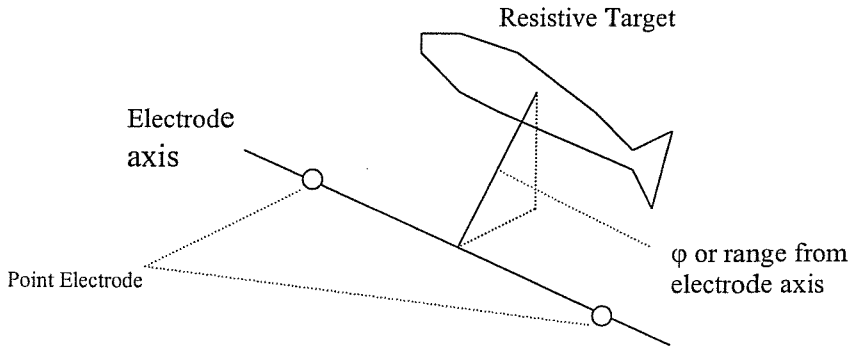

This feedback correction worked well, but if large increments of correction were made, balance was achieved quickly at the expense of substantial fluctuation around the balance point. If a small increment were made then the time to balance was extended. A better method of feedback balance was achieved by making the increment for correction proportional to the degree of imbalance. Thus when the imbalance was large the increment was large but as balance was reached the increment was reduced to a small value. In this case the increment was set at half the imbalance.[α]

After testing and modifying the parameters of the pulse sequence it was found that reducing the number of pulses to 26 was just as effective at removing power supply interference as the 50 pulses. The reasons for this are unclear since the measurements can only average over half of the period of a 50 Hz cycle and so only partial noise removal was expected. The observation did indicate that a higher rate of measurement could be achieved at no apparent cost to resolution.

2.7.3 Incorporation of Multiple Pairs of Electrodes

When three pairs of electrodes were arranged on an acrylic plate using the attachment methods already described and all but the centre pair of electrodes were connected to ground the measurements became even more stable. Figure 25 describes the arrangement of the electrode array. This development led to the incorporation of a more sophisticated multiplexing system in order to allow the connection of any electrode to either the sensor circuit or analogue ground. This multiplexer was implemented using two "PhotoMos" relays per electrode and the digital output port of the PCL718 and is described in detail by Figure 26.

[α] It was later realised that if the other non-sensed electrodes were grounded during the measurement and that all electrodes were grounded between measurements a much simpler and stable solution would have been available at this stage.

Two configurations of grounded electrodes were tested; the first grounded all of the electrodes on the grounded side of the array but none on the sensed side. The alternate configuration grounded all of the electrodes except the electrode used for measurement. No differences were observed in the stability of measurements between the two configurations and so the former was adopted since it was less likely to complicate measurements between adjacent electrodes. Table 6 describes the relay closures required to sense and ground each electrode using 12 digital output lines of the PCL718.

Further control of the sensor interface was exercised using three additional digital outputs of the PCL718. Digital outputs 12, 13 and 14 were designed to control the two calibration resistors and the PGA205 instrumentation amplifier gain respectively. The precise arrangement of the calibration circuit is presented in Figure 27. The layout of the circuit board is shown in Plate 2.

Table 6 Relay closure map for six-electrode array

Bit	0	1	2	3	4	5	6	7	8	9	10	11
Relay	G0	G1	G2	G3	G4	G5	S0	S1	S2	S3	S4	S5
Electrode	UL	DL	UC	DC	UR	DR	UL	DL	UC	DC	UR	DR
Sensed electrode												
UL	1	0	1	0	1	0	0	1	1	1	1	1
DL	0	1	0	1	0	1	1	0	1	1	1	1
UC	1	0	1	0	1	0	1	1	0	1	1	1
DC	0	1	0	1	0	1	1	1	1	0	1	1
UR	1	0	1	0	1	0	1	1	1	1	0	1
DR	0	1	0	1	0	1	1	1	1	1	1	0
NONE	0	0	0	0	0	0	1	1	1	1	1	1

Relays are prefixed with their connection to ground or source (G,S)
Electrodes are described by the prefix upstream or downstream (U,D)
Followed by the lateral position (Left, Centre, Right)
Bit number refers to the bit number in the PCL718 digital output port
NB. Logic 0 closes relay

Figure 26 Six electrode array multiplexer circuit

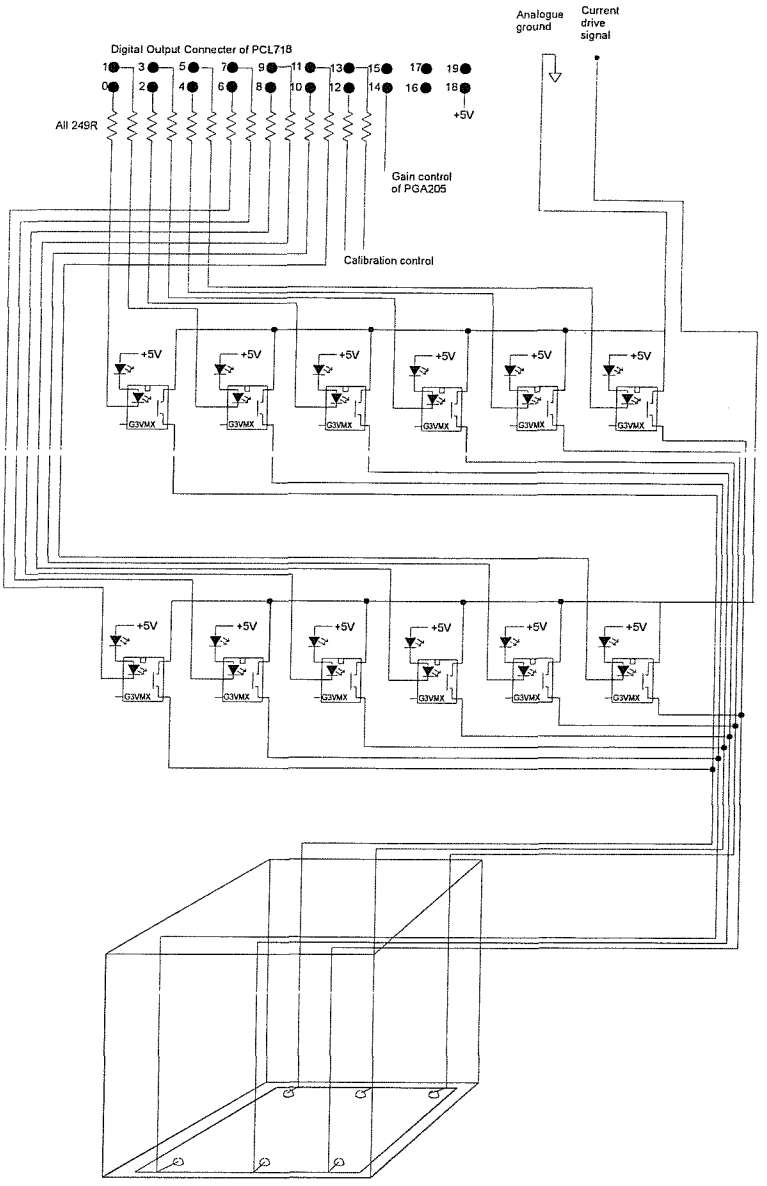

Figure 27 Calibration and instrumentation amplifier control outputs

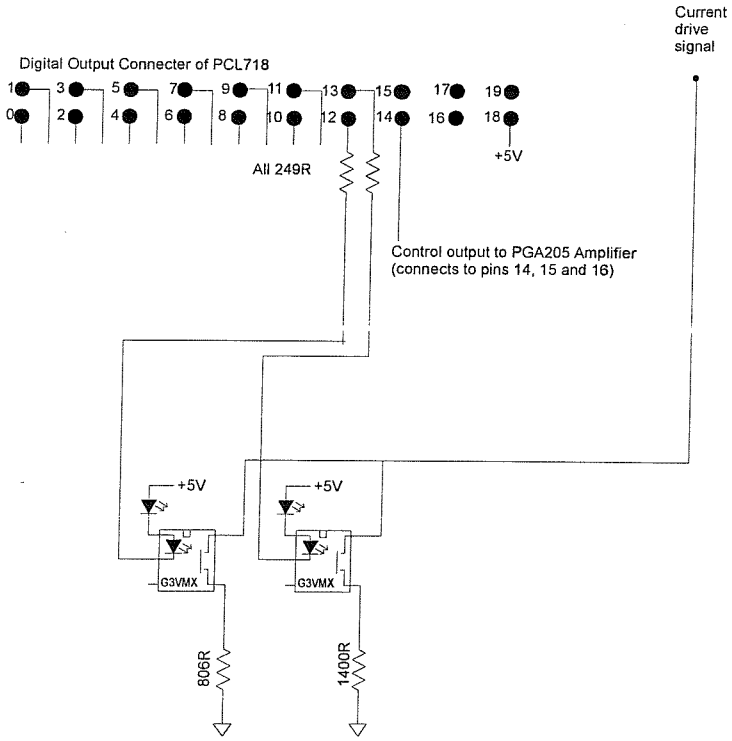

CHAPTER THREE

RESISTANCE SIGNAL SIZE AND RESISTIVE TARGET POSITION

CHAPTER THREE

3 RESISTANCE CHANGE SIGNAL AND RESISTIVE TARGET POSITION

3.1 Test Environment

A test environment was constructed to investigate the effects of fish position and size on the electrical resistance measured between wide spaced point electrodes. The minimum size of water tank that could be used was dictated by the size of resistive targets, which were similar in size to salmon. The height of the tank was specified to allow almost 1 m modification to the range of targets from the plane of the electrodes. The initial electrode spacing was set at 0.9 m and therefore a tank of internal dimensions 1.0 m by 1.0 m by 1.0 m was used. Resistive targets were positioned longitudinally, with respect to the electrode axis, as shown in Figure 19.

3.1.1 Cables and Electrodes

Early experiments used unshielded connections from the resistance sensor to both the drive electrode and the ground electrode. Connection was achieved using "Kynar™" insulated silver plated copper solid wire (0.25 mm diameter., RS stock no. 358-107). It was noticed that operator proximity to the drive cable or the drive side of the test tank influenced sensor measurements. To alleviate this problem two forms of shielding were tested, a grounded shield and a driven shield.

The grounded shield method used coaxial cable to connect the sensor to the point electrodes. The centre core carried signal and the outer sheath was connected to analogue ground in the sensor. Care was taken to prevent electrical connection between the water and the grounded sheath near the connection to the electrode as this could represent a major reduction in the apparent resistance between the electrodes. The driven shield method used the same principle of surrounding the signal cable with a conducting sheath but in this case the sheath was driven by the same voltage signal as the signal core but buffered by an operational amplifier to remove signal loading.

The sheath prevented signal losses by minimising the potential difference between the core and the sheath.

Both methods almost entirely removed the problem of operator induced "noise" but the grounded shield was much simpler. Therefore the grounded shielding method was used for both electrodes on subsequent measurements.

One type of point electrode was used in all of the tank test experiments. These were machined from a rod of stainless steel (type 316) and were of hemispherical shape. The flat underside of the electrode had a central threaded hole (M6 thread) and a square profile recess for the placement of an "O" sealing ring. The domed surface of the electrode was polished during machining to give a smooth surface for contact with the water (see Figure 20).

The electrodes were mounted onto the surface of a 10 mm thick "Perspex™" bar using 316 stainless machine screws (M6). Electrical connection was made with the capture of the cable core under the head of the machine screw recessed into the "Perspex" bar. The thread of the machine screw and the cable ring connector were coated with electrically conductive paint immediately prior to final assembly to provide good electrical connection between components. Clamping of the cable and encapsulation of the connection in the "Perspex" bar recess was achieved using RTV 3160. The purpose of this encapsulation was to prevent water ingress to the connection of copper cable core and stainless screw thus avoiding electrolytic degradation of the connection.

After curing of the encapsulant (48 hrs) the electrode surfaces were cleaned with absolute alcohol and the resistance of the domed surface to the far end core of the electrode cable was measured. For both cables this was found to be 0.4 Ω (ITT model MX50 multimeter uncertified).

3.1.2 Resistive Targets

To measure the effect of resistive target position in the test tank live fish were thought to be unsuitable at the early stages of experimentation. This was due to the difficulties expected in confining the position of such targets and the problem of water contamination by biological targets (Whitney and Pierce, 1957). Therefore a suitable range of resistance targets were made from varying lengths of 6mm diameter stainless steel rod (type 316). Stainless steel targets were selected since the electrical conductivity of the target surface was expected to remain relatively constant due to the prevention of surface corrosion. Such targets were known to have been widely used for the testing of conventional resistivity fish counters (Fewings, 1988). The approximate lengths of the stainless steel targets were 300, 400, 500, 600, 700 and 800 mm with the ends of the targets rounded to remove sharp edges. Targets were cleaned with absolute alcohol prior to each use.

Targets were suspended in the test tank using a polyester twine "yoke" that could be attached to alternate support points above the tank. The support points were in line with the axis of the electrodes and allowed multiple axial positions for the centre of the suspended target. Targets could be raised or lowered using the suspension cord and fixed at a given position using a tie off point or a counterbalance on an inclined track. Targets were prevented from rotating off the electrode axis by the placement of a bar across the top of the test tank so that the yoke cords just touch the edge of the bar.

3.1.3 Software

The voltage output from the sensor interface (d.c.) was measured using a proprietary analogue to digital converter card (PCL 718 interface) used in conjunction with an "IBM" AT personal computer. The interface could sample up to 16 single ended and 8 differential analogue inputs at 12-bit resolution and at rates up to 50,000 samples per second. Two analogue outputs were available at 12-bit resolution as well as 16 digital channels that could be used for digital input or output.

Device drivers were provided to allow control of the interface card from within the "Microsoft™" QuickBasic™ programming language. Control from within a high level language allowed rapid modification of the software during experimentation and access to high-level graphics commands to allow graphic representation of the resistance sensor output.

Specific functions that the software was required to perform are listed below.

- Resistance sensor sampling
- 50 Hz band reject digital filtering
- 1-5 Hz low pass digital filtering
- Display processed data graphically and numerically
- Manual trigger of reference and test measurements
- Automatic calibration of resistance sensor and display of SI units

The control software was under development during tank testing to optimise the digital filters, graphical display, measurement processing and automatic calibration. Due to this continuous development many versions of the software were produced. A listing of each of the key programs is included in Appendix B. Program listing B (i) was used for the initial measurements described below.

Sample rate was 5 kHz with 200 samples averaged giving a capture period of 40 ms. These averages were then placed in an array and a nine-point moving average calculated from this data, effectively a non-recursive digital low-pass filter (finite impulse response filter). Using step changes in test resistance, counting the number of samples made to reach half the maximal resistance change and measurement of the overall sample rate, estimates of the overall frequency response were made.

Measurements of resistance change due to targets in the test tank were made using a manual triggered reference estimate with the target out of the water. Then a manual triggered target measurement was taken with the target lowered into place. The two measurements were taken in quick succession to minimise the impact of low frequency

baseline signal noise. The manual estimates were the average of 50 nine-point moving average samples taken from the point of manual triggering. Both reference and target measurements were taken repeatedly to ensure repeatability of the resistance change measurements.

3.1.4 Test Water

Salmonids migrate through waters of variable electrical conductivity and a range of temperatures, tank tests were organised to evaluate performance of the sensor under a wide variety of these conditions. Initial tests were carried out using water from the domestic supply that had been allowed to stand for one week. The conductivity of this water was initially 390 $\mu S.cm^{-1}$ which decreased to 330 $\mu S.cm^{-1}$ over the course of 15 months as dissolved ions came out of solution. Conductivities were measured with a WTW LF196 conductivity meter.

Low conductivity water (<20 $\mu S.cm^{-1}$) was collected from a plastic coated rooftop into a 1600 *l* black polypropylene storage tank (black to reduce algal growth). This water was to be used for mixing other water conductivities for the test tank. Time constraints prevented using a different water conductivity than that described above.

An air feed to a corner of the test tank provided a circulation of water to ensure a well-mixed test medium. Temperatures were measured using a digital temperature module with a remote probe (accuracy ± 0.2°C, resolution 0.1°C).

3.2 Initial Tests

To establish the form of a relationship between resistance change signal (RCS) and the position of test resistance targets a series of measurements were made with targets of length 704 to 400 mm at ranges of 0 to 600 mm. The targets were centrally placed between the sensor electrodes of 900 mm separation. Table 7 describes the average, and difference between maximum and minimum measurements of RCS for each target and range. Figure 28 and Figure 29 describe these results graphically. These figures indicate that the magnitude of the resistance change signal decreased with increasing

range of the target from the plane of the electrodes. This was particularly evident when the range of the target was greater than 0.1 m. At range less than 0.1 m RCS was reasonably constant and in some cases was actually smaller than at 0.1 m.

When RCS was plotted on a logarithmic axis (see Figure 29) against target range, at ranges greater than 0.1m RCS decreased in a near linear fashion. Each of the plots exhibited a similar slope and primarily differed in their offset on the y-axis.

Table 7 Resistance change signal measurements for stainless steel rod targets at varied range from the plane of the electrodes

Target range (m)	0.704m target Ave (Ω)	+/- (Ω)	0.600m target Ave (Ω)	+/- (Ω)	0.500m target Ave (Ω)	+/- (Ω)	0.400m target Ave (Ω)	+/- (Ω)
0.00	9.859	0.123	5.138	0.065	2.597	0.048	1.149	0.002
0.10	9.042	0.053	5.152	0.022	2.898	0.026	1.306	0.039
0.20	4.683	0.058	2.994	0.099	1.828	0.002	0.858	0.048
0.30	2.481	0.010	1.621	0.031	0.923	0.031	0.542	0.046
0.40	1.120	0.007	0.776	0.024	0.523	0.026	0.359	0.051
0.50	0.687	0.012	0.455	0.031	0.405	0.039	0.229	0.012
0.60	0.405	0.096	0.287	0.060	0.149	0.000	0.116	0.010

Note +/- column denotes the range of values observed (n=2)

Test conditions

General arrangement	Targets placed on axis of dome electrodes 0.9 m apart
Water temperature	13 °C
Water conductivity	380 μScm^{-1}
Water depth	0.814 m
Sensor version	50 kHz sine excitation using amplitude stabilised Wein bridge oscillator with dual buffered current source, buffered active rectifier and low pass filter stages
Digital filter	5 pt moving average digital low pass filter
Sample rate	21.1 Hz
Target type	6 mm diameter stainless steel

Figure 28 Plot of resistance change signal Vs target range for stainless steel targets of 400 to 704 mm in length

Error bars indicate the minimum and maximum measurements observed (n=2)

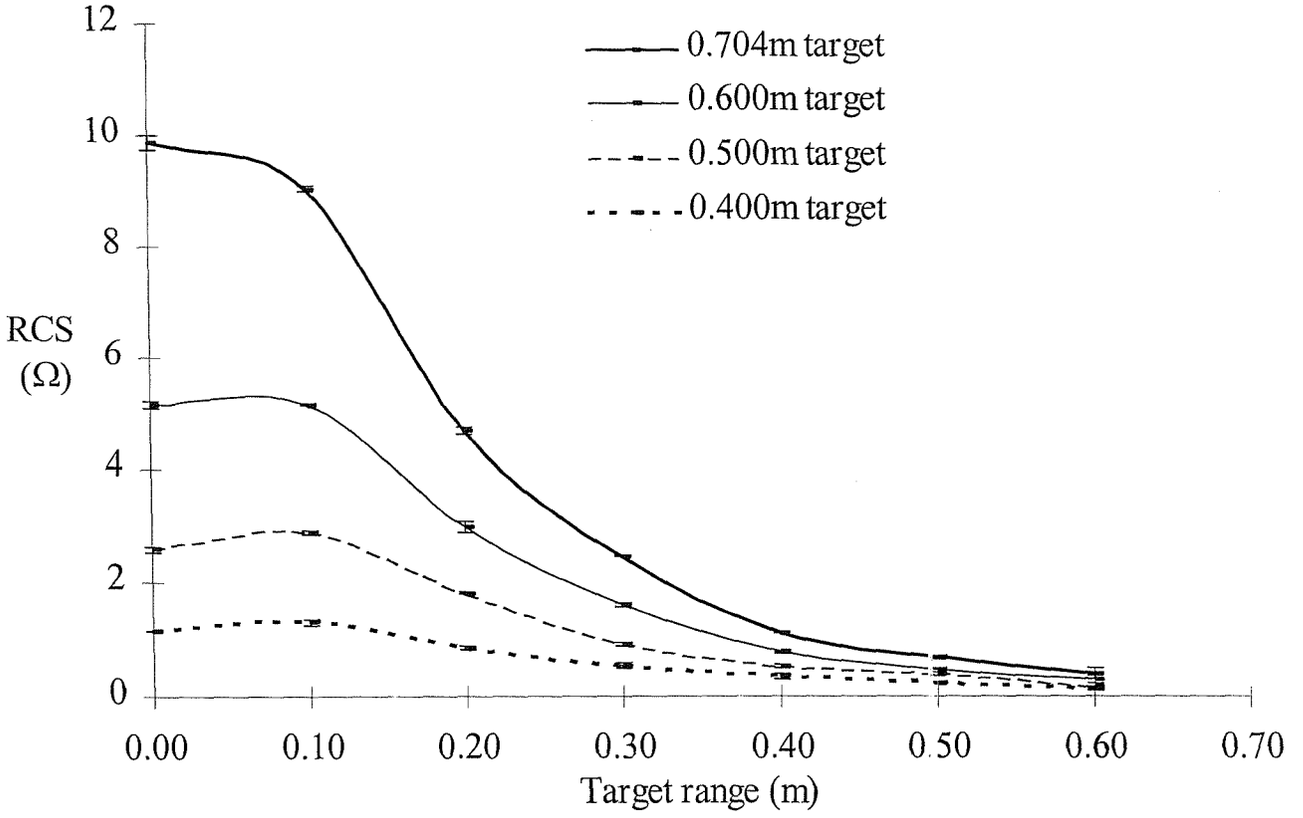

Figure 29 Logarithmic plot of resistance change signal Vs target range for stainless steel targets of 0.400 to 0.704 m in length

Error bars indicate the minimum and maximum measurements observed (n=2)

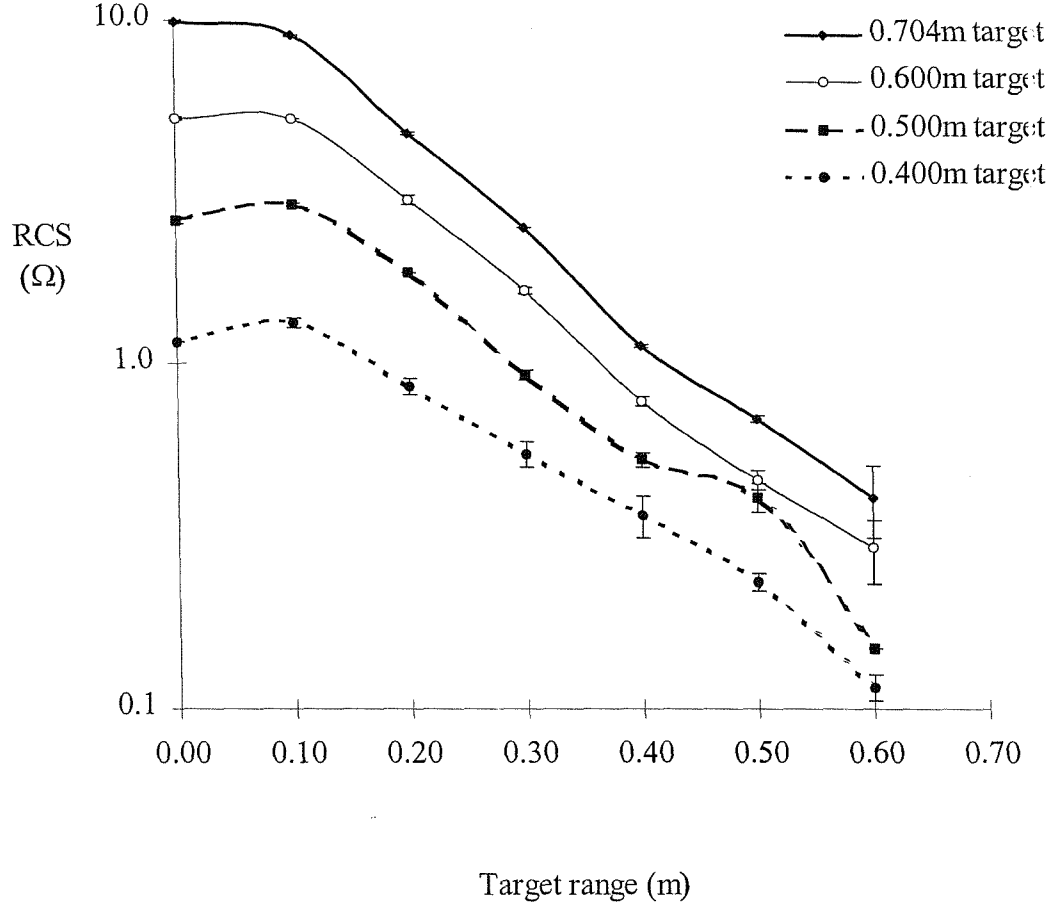

3.2.1 Stainless Steel and Fish Resistive Targets

In order to determine the validity of steel rod targets as an analogue of real fish additional fish targets were suspended in exactly the same manner as the steel targets already described. Two freshly killed migratory trout of 0.36 and 0.58 m were compared with the 0.4 m steel target at ranges of 0.1 to 0.7 m suspended centrally between the two point electrodes (electrode separation 0.9 m). The results of this test are described in Figure 30 and Table 8.

These measurements indicated that the stainless steel rod targets show similar resistive properties to freshly killed fish targets. There does appear to be some difference between the rod target and the larger sea trout but only at range less than 0.1 m. In addition the fish targets provide a smaller RCS for a given length than the rod target. It was therefore concluded that the steel rod targets were a reasonable analogue of the real fish.

Figure 30 Comparison of resistance change signals from stainless steel and freshly killed trout targets

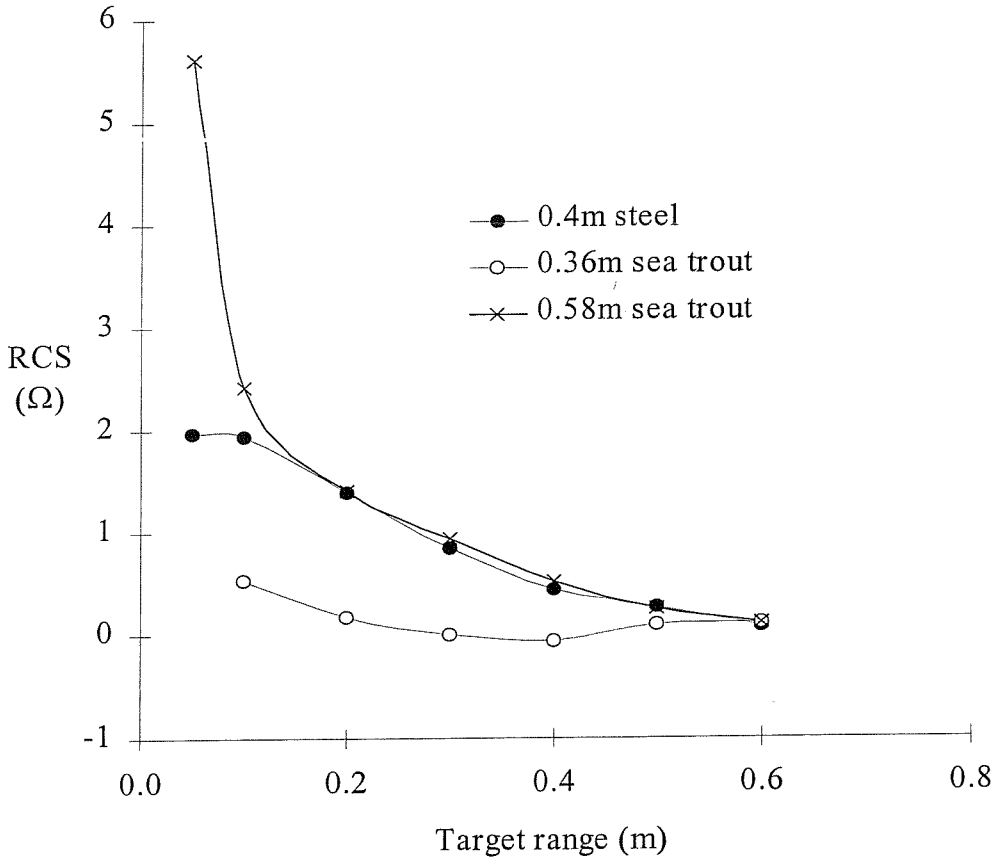

Table 8 Comparison of resistance change signals from stainless steel and freshly killed trout targets

Target range	SSteel target 0.40 m	Trout target 0.36 m	Trout target 0.58 m
(m)	(Ω)	(Ω)	(Ω)
0.05	1.969		5.605
0.10	1.945	0.527	2.429
0.20	1.396	0.173	1.410
0.30	0.849	0.007	0.941
0.40	0.443	-0.066	0.520
0.50	0.273	0.099	0.249
0.60	0.077	0.106	0.112

Test conditions

General arrangement	Targets placed on axis of dome electrodes 0.9m apart
Water temperature	11.8 °C
Water conductivity	340 μScm^{-1}
Water depth	0.75 m
Sensor version	50 kHz sine excitation using amplitude stabilised Wein bridge oscillator with dual buffered current source, AD630 synchronous demodulator and AD624 instrumentation amplifier primary signal buffer
Digital filter	35 pt moving average digital low pass filter
Analogue filter	Two stage LPF both stages -3dB=0.691 Hz
Target type	Targets 6mm diameter stainless steel and freshly killed sea trout (*Salmo trutta*)

3.2.2 Longitudinal Displacement and RCS

In order to investigate the form of a dynamic RCS of a fish swimming longitudinally over the electrodes, static measurements of RCS were made for a range of target lengths, ranges and at varied longitudinal displacement from the central point of the electrode axis. Static tests were necessary since the test tank was not large enough to move the targets into and out of the detection zone in a longitudinal direction. These data are described by Figure 31 and Table 9.

Table 8 includes a measure of the variation in RCS due to the vertical range of each rod target at each longitudinal displacement. This measure is calculated as the difference in RCS between the target at zero range and 0.7 m range. Comparing these measures for each longitudinal displacement it was evident that the least variation due to target range was in the central position. It was therefore concluded that dynamic measurements of RCS for fish swimming over electrodes should be measured in this central position. In order to achieve this a method of detection of longitudinal position fixing was needed.

By plotting the RCS of rod targets by longitudinal position and replicating negative longitudinal displacement an estimation of the likely waveforms of fish passing over the electrodes was possible (see Figure 32). This plot suggested that it might be possible to estimate when a moving target is in the centre of the electrodes based on analysis of the waveform shape. If the waveform was from a target close to the plane of the electrode then the waveform minima corresponded to a central position of the target. A target passing through the detection zone at an intermediate range produced a "flat topped" waveform, the centre of which could provide an estimate of the time when the target was in the centre of the electrodes. If a target passed through the detection zone at a larger range then a good estimate of the central target position was expected to coincide with the peak of the waveform.

3.2.3 The Effect of Electrode Separation on RCS

It was recognised that some method of range estimation was required from measurements of RCS because of the dependence of RCS magnitude on the range of the target from the electrodes and the size of the target. To investigate a potential method of target ranging, a series of RCS measurements were made with two different electrode separations. These data are described by Figure 33 and Table 10.

Figure 31 The effect of longitudinal displacement on RCS for stainless steel targets

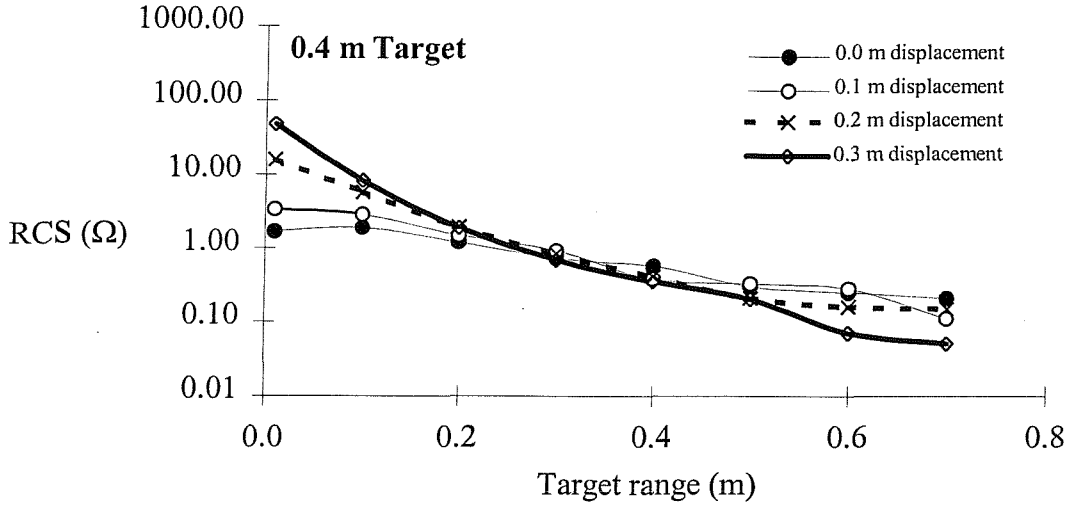

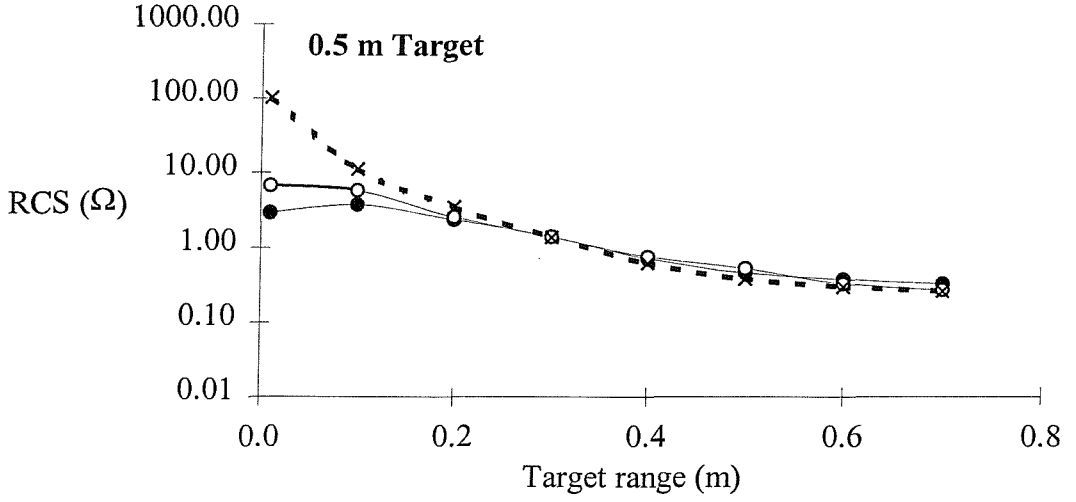

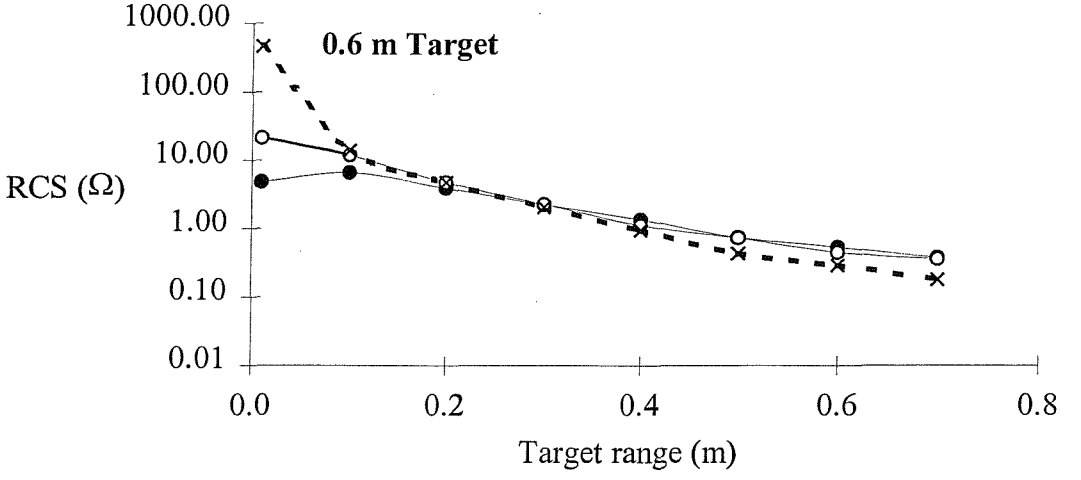

Table 9 The effect of longitudinal displacement on RCS for stainless steel targets

	Target length	Target range	Target longitudinal displacement (relative to centre)			
	(m)	(m)	(0.0 m)	(0.1m)	(0.2m)	(0.3m)
	0.40	0.01	1.67	3.37	15.75	48.06
		0.10	1.89	2.86	5.74	8.26
		0.20	1.19	1.48	1.96	1.88
		0.30	0.72	0.92	0.82	0.69
		0.40	0.57	0.38	0.41	0.35
		0.50	0.30	0.33	0.21	0.20
		0.60	0.25	0.28	0.16	0.07
		0.70	0.21	0.11	0.15	0.05
	0.50	0.01	2.92	6.68	103.02	
		0.10	3.69	5.69	10.95	
		0.20	2.34	2.56	3.42	
		0.30	1.39	1.39	1.38	
		0.40	0.72	0.75	0.62	
		0.50	0.46	0.53	0.38	
		0.60	0.38	0.33	0.30	
		0.70	0.33	0.27	0.26	
	0.60	0.01	4.91	21.46	457.93	
		0.10	6.69	11.99	13.98	
		0.20	3.94	4.73	4.80	
		0.30	2.24	2.29	2.04	
		0.40	1.35	1.12	0.94	
		0.50	0.74	0.72	0.43	
		0.60	0.53	0.45	0.29	
		0.70	0.38	0.36	0.18	
Difference in RCS	0.40		1.46	3.26	15.60	48.01
from 0 to 0.7m	0.50		2.59	6.41	102.76	
range	0.60		4.53	21.10	457.75	

Test conditions

General arrangement	Targets placed on axis of dome electrodes 0.9 m apart
Water temperature	11.8 °C
Water conductivity	340 μScm^{-1}
Water depth	0.75 m
Sensor version	50 kHz sine excitation using amplitude stabilised Wein bridge oscillator with dual buffered current source, AD630 synchronous demodulator and AD624 instrumentation amplifier primary signal buffer
Digital filter	35 pt moving average digital low pass filter
Analogue filter	Two stage LPF both stages -3dB=0.691 Hz
Target type	Targets 6mm diameter stainless steel

Figure 32 Predicted waveform of a traversing rod target at alternate ranges

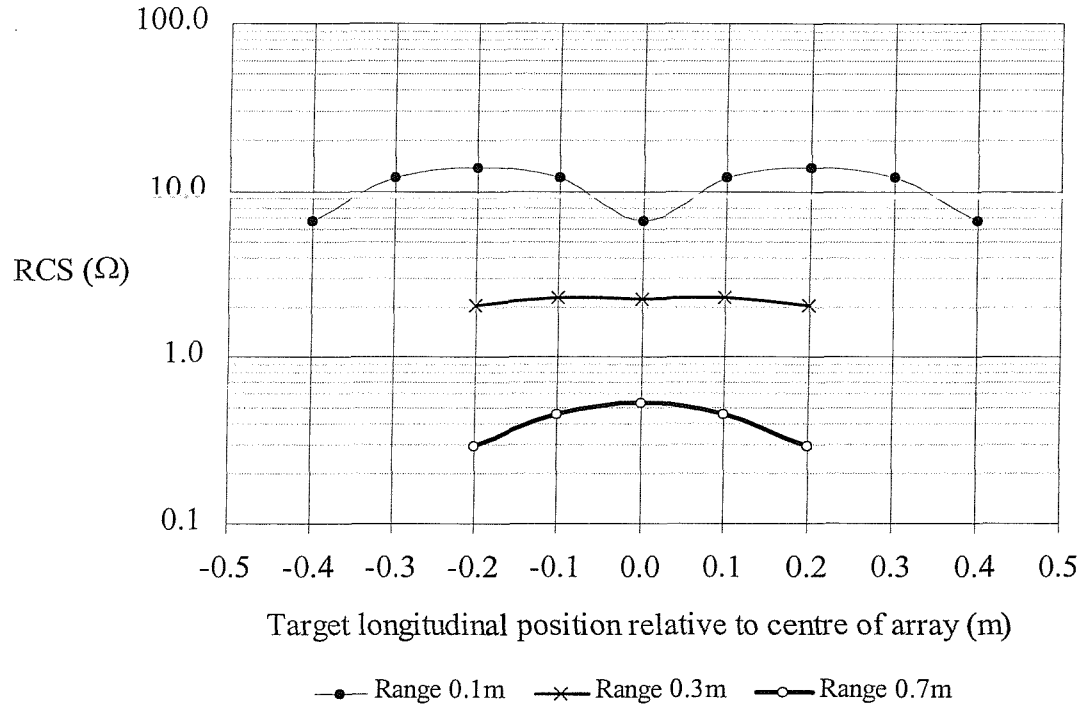

(predicted using point RCS measurements from Table 8, target length 0.6m)

Figure 33 Comparison of RCS measurements for two target lengths and electrode separations

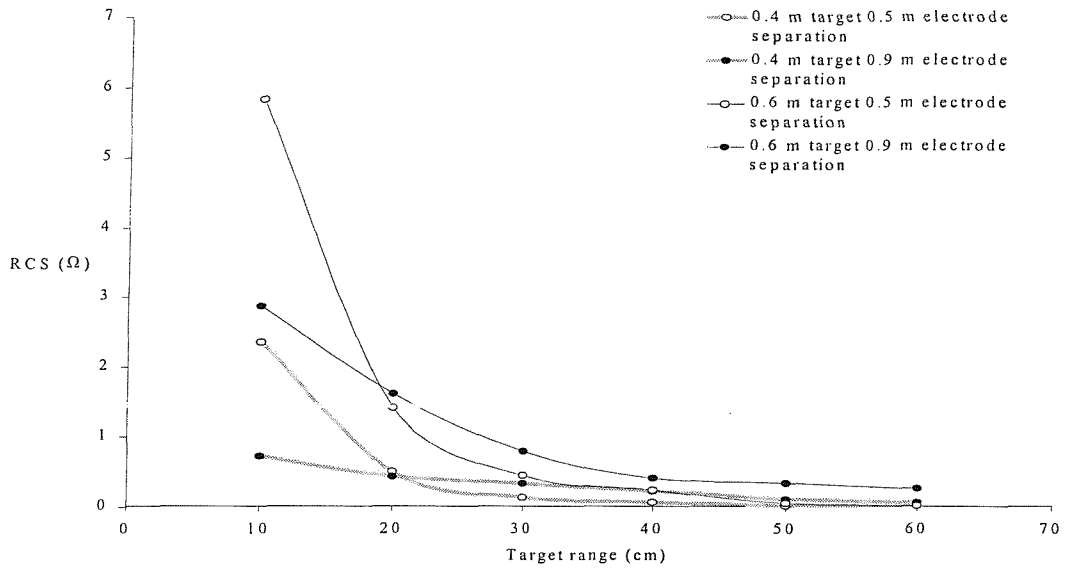

Table 10 Comparison of RCS measurements for two target lengths and electrode separations

Target length (m)	0.4	0.4	0.6	0.6
Electrode separation (m)	0.5	0.9	0.5	0.9
Target range (cm)	(Ω)	(Ω)	(Ω)	(Ω)
0		-0.7334		-3.1906
10	-2.3558	-0.7273	-5.8329	-2.8763
20	-0.5127	-0.4427	-1.4173	-1.6227
30	-0.1383	-0.3302	-0.4484	-0.7913
40	-0.0707	-0.2341	-0.2467	-0.4115
50	-0.0234	-0.1191	-0.0543	-0.3420
60	-0.0264	-0.0732	-0.0275	-0.2672

Note: Absolute values were plotted in Figure 32.

Water temperature 21.1 °C
Water conductivity 342 $\mu S.cm^{-1}$
Digital filter 15 sample moving average
Analogue filter 18.49 Hz
Water depth 0.68 m.

3.3 Further RCS Measurements

In order to form a substantial measurement dataset on which to base further investigation, the measurements of RCS, with respect to target size and range from the plane of electrodes, were repeated with the updated sensor system. The control software was also enhanced in order to include ten replicates of each measurement for statistical analysis in addition to calibration data for each data collection session. The collected data was automatically compiled into an "MSDOS™" compatible text file.

For each rod target, the first set of sample measurements was taken without a target in the test-tank. This enabled a measurement benchmark from which the subsequent samples were subtracted to derive the RCS measurement. Electrodes were sampled with one electrode as the measurement electrode and the opposite three electrodes grounded. All other electrodes were isolated from the interface during the measurement. Electrode pairs were sampled in order from pair 1 to pair 3 (see Figure 34), in each case the notional upstream electrode was sampled first followed by the downstream electrode.

Data was transformed to 10.log RCS as this scaling presented the data in a simpler form prior to the predictive model construction described in Chapter 4. All of the measurements were conducted using water with a measured conductivity of 470 $\mu S.cm^{-1}$ and at a temperature of 14.4 to 14.8 °C. These data are presented below in Figure 34 and Table 11.

Resistance change signal data was also collected for stainless steel targets under the varying conditions of water depth and water conductivity. The water conductivity for these tests ranged from 300 to 470 μScm^{-1} and the water depth from 500 to 900 mm (see Appendix C). On subsequent inspection the data collected for the low water conductivity conditions was found to contain many spurious results. The cause was later identified as a damaged connection to one electrode. This data could not therefore be used.

Table 11 Resistance change signal Vs. target range and target length

Resistance change signal (10·log Ω)						
Target length (mm)	306		400		600	
	Mean	Confidence Interval	Mean	Confidence limits	Mean	Confidence limits
Target Range (mm)	$\bar{x}$	[α=0.025]	$\bar{x}$	[α=0.025]	$\bar{x}$	[α=0.025]
50	-0.7566	0.0749	2.5718	0.0441	8.2740	0.0147
100	-0.9541	0.0909	2.4262	0.0519	8.1234	0.0110
150	-1.4578	0.1238	1.9070	0.0666	7.4655	0.0153
200	-2.2300	0.1428	1.0750	0.0978	6.5139	0.0238
250	-3.0308	0.1756	0.0824	0.1234	5.5393	0.0201
300	-3.7346	0.1634	-0.8879	0.1383	4.4271	0.0294
400	-5.9104	0.3795	-3.2506	0.1926	2.4194	0.0359
500	-7.2450	0.3120	-5.2012	0.3779	0.5594	0.0804
600	-9.4716	0.9660	-6.7532	0.4744	-0.8917	0.0725
700	-9.7105	0.7615	-8.3591	0.2773	-1.8965	0.0968
n=10						
Water Depth (mm)	900					
Water conductivity ($\mu S.cm^{-1}$)	470					
Water temperature (°C)	14.4					

Figure 34 Resistance change signal Vs. target range and target length

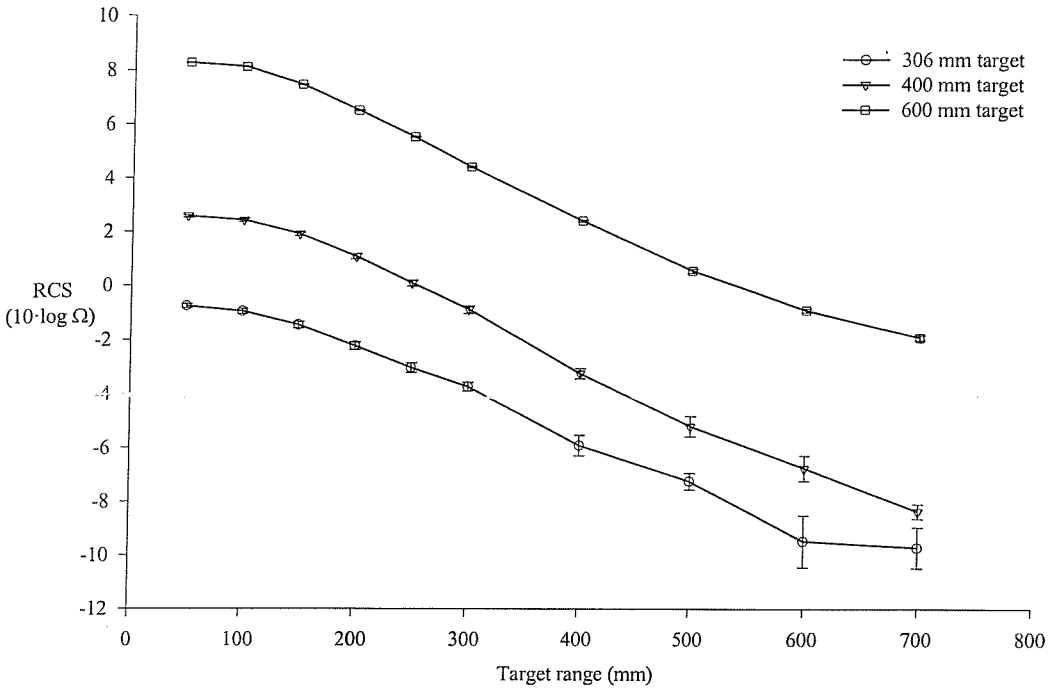

(Error bars indicate confidence interval [α= 0.025, n= 10])

CHAPTER FOUR

MODELLING RCS AND RESISTIVE TARGET POSITION

CHAPTER FOUR

4 MODELLING RCS AND RESISTIVE TARGET POSITION

4.1 Introduction

When stainless steel targets were placed between and above bottom-mounted electrodes the RCS was known to decrease. The logarithmic transform of the resistance change signal was known to exhibit an almost linear relationship with target range (range >200 mm). This linear portion of the curve described a negative slope. Increasing target length increased the intercept with the y-axis. An attempt was therefore made to formulate a mathematical model of this relationship for the purpose of resistance change signal prediction.

4.2 Source Data

The data utilised for the construction of a mathematical model to predict RCS using knowledge of resistive target position is described by Table 11 and Figure 34. Section 3.3 describes the method of data collection. Confidence limits for the data ($\alpha=0.025$, $n=10$) indicated that 95% of RCS measurements lay within 0.96 10·log Ω of the mean estimate in the case of the largest sample spread observed (306 mm target 600 mm range). The majority of sample sets however showed confidence limits of less than 0.2 10·log Ω.

4.3 Measurement Noise

A trend was evident between RCS confidence limits, or sample noise, and RCS mean, as shown in Figure 35. RCS confidence limits were observed to decrease as the magnitude of RCS increased. The graph overleaf was plotted with the y-axis on a logarithmic scale and the relationship appeared linear in nature, similar to the relationship between resistive target range and RCS. If measurement noise was dependent on the magnitude of RCS then this might suggest the cause of the observed trend.

Figure 35 RCS versus confidence limits of RCS

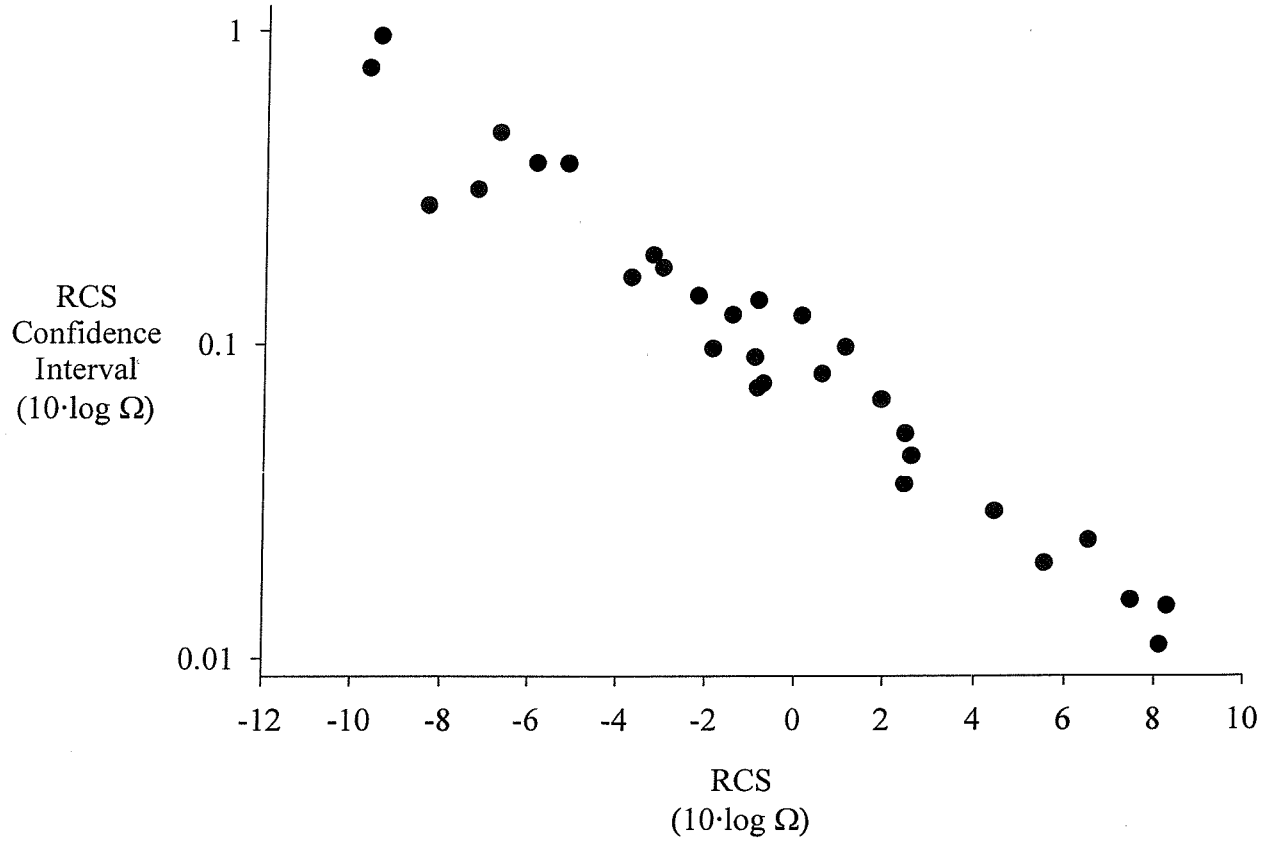

A possible explanation for this trend is that even with the electrode array grounding procedures described in chapters 2 and 3 the grounding in the test tank may still be insufficient to suppress noise. If insufficient grounding paths were available then more measurement noise would be expected with no substantial target present in the test tank. With a substantial target present more conductive paths would be available from the sensor electrode to the grounding electrodes and therefore less opportunity for external noise to enter the sensor system.

4.4 A Sigmoidal Model

Since the curves depicted in Figure 34 were sigmoidal in form a four-parameter logistic model was chosen to describe the relationship between RCS and resistive target position. Below is the general form of the logistic model as described by Fox and Shotton, (1995).

$$\lambda = \lambda_o + \frac{a}{1 + \left(\frac{Tr}{Cr}\right)^b} \qquad \textit{Equation 1}$$

where

λ = 10 log RCS *(10 log Ω)*

λ_0 = 10 log RCS at φ=0 *(10 log Ω)*

T_r = range *(mm)*

C_r = corner range *(mm)*

a = difference in RCS *(10 log Ω)*

b = slope coefficient *(10 log Ω mm^{-1})*

NB. In the context above range is defined as the physical distance from the axis between the measuring electrodes to the centre point of the target. (see Figure 25)

Using estimated values for λ_0, C_r, a and b, in conjunction with values of T_r from 5 to 700 mm values of λ were calculated and compared to the observed values of Table 11. Values of the coefficients were changed to minimise the difference between the observed and calculated estimates of λ for each target. The coefficient values summarised in Table 12 were found to yield the best fit of the models to the observed data.

Since the model curves were approximately parallel to each other, but offset on the λ-axis (y-axis), coefficients a, b and C_r were assumed to be constants. For each parameter the mean was calculated and entered as constants in an attempt to refit the models with λ_0 as the only remaining variable other than T_r, the range of the resistive target from the plane of the electrodes.

Non-linear regression of the revised model used mean values for a, b and C_r and iteration for values of λ_0. Regression fit statistics for the resultant model data compared with the observed measurements is detailed in Table 13. A graphical representation of the model fit is shown in Figure 36.

Table 12 Best fit coefficients of Equation 1

Target length (mm)	306	400	600	$\bar{x}$	
Variable					(Units)
a	12.690	16.338	14.108	14.379	(10·log Ω)
b	2.461	2.317	2.303	2.360	
C_r	469.086	512.608	450.303	477.332	(mm)
λ_0	-13.416	-13.606	-5.658		(10·log Ω)

Table 13 Non-linear regression estimates of λ_o using mean values of a, b and C_r from Table 11

Target length	y_o estimate	$s_{\bar{x}}$	r	r^2	P
(mm)	(10·log Ω)	(10·log Ω)			
306	-14.657	0.1320	0.994	0.988	<0.001
400	-11.846	0.0893	0.997	0.994	<0.001
600	-6.153	0.0445	0.999	0.999	<0.001

Figure 36 Fit of logistic model to source RCS and range data using mean values of a, b and C_r from Table 11

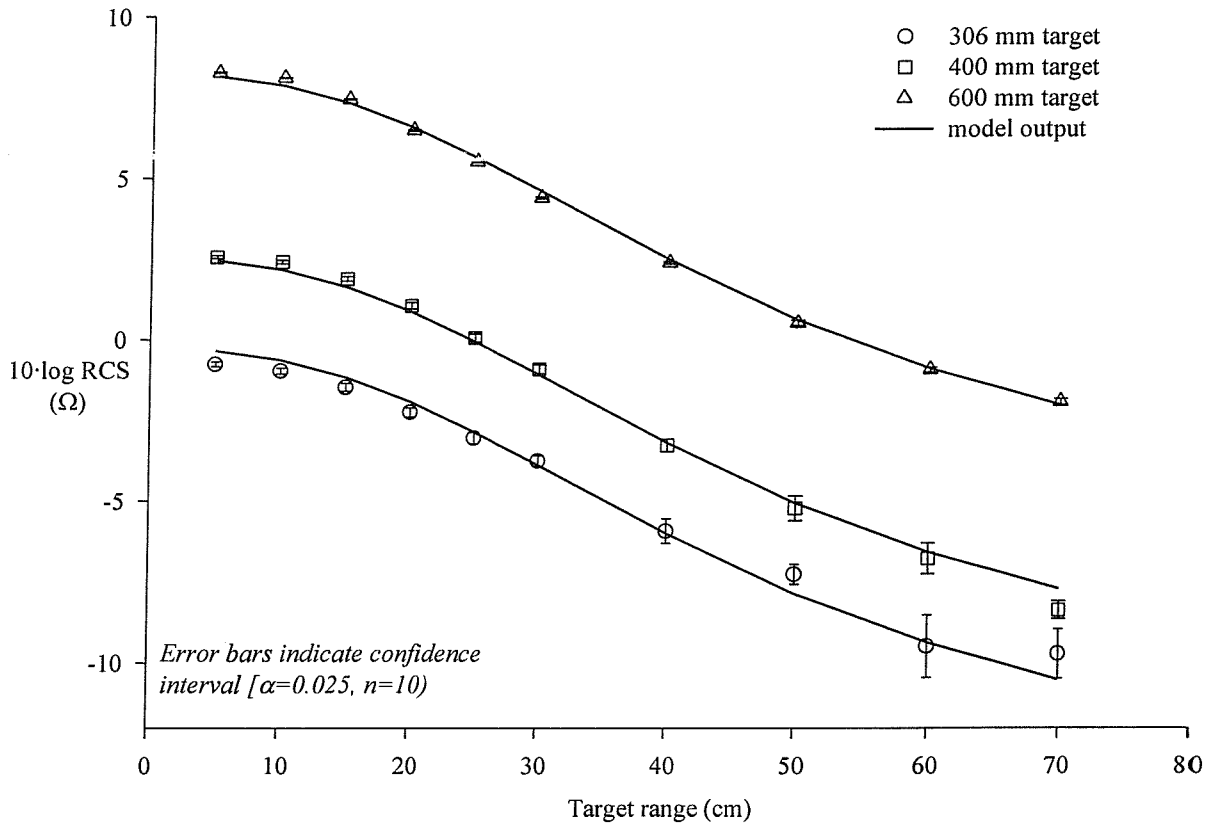

(Error bars indicate confidence interval [α=0.025, n=10])

In order to estimate an RCS measurement given a target range and the logistic model developed so far an estimate of λ_0 was required. A linear model was therefore tested to evaluate if λ_0 could be estimated for known length resistive targets. Figure 37 shows the linear model fit to the estimates of λ_0 presented in Table 13. Regression statistics are presented in Table 14 and estimates of λ_0 from the model are presented in Table 15. The linear model is described by *Equation 2.*

$$\lambda_o = -23.446 + (0.0289\ \gamma) \qquad \textbf{\textit{Equation 2}}$$

where

$\lambda_0 = \lambda_0$ of *Equation 1* ($10 \cdot \log \Omega$)

γ = target length in mm

A test of all of the observed data to the model predictions was possible when the linear model for prediction of λ_0 from target length was incorporated into the general model for prediction of resistance signal using target elevation (*Equation 1,* coefficients Table 12). The results of this test indicated that the logistic model provided a good description of the relationship between the independent variables target elevation and target length and the dependent variable resistance change signal. The goodness of fit is shown by calculation of the correlation coefficient 0.998 (r) and the coefficient of determination 0.997 (r^2).

Table 16 shows an analysis of variance for this regression. The most important figure to note from this table is the *P* value, which indicates the probability of wrongly concluding that there is an association between the independent and dependent variables of the model. In this case, the *P* value was much less than 0.001.

Figure 37 Linear regression model for prediction of λ_o from target length

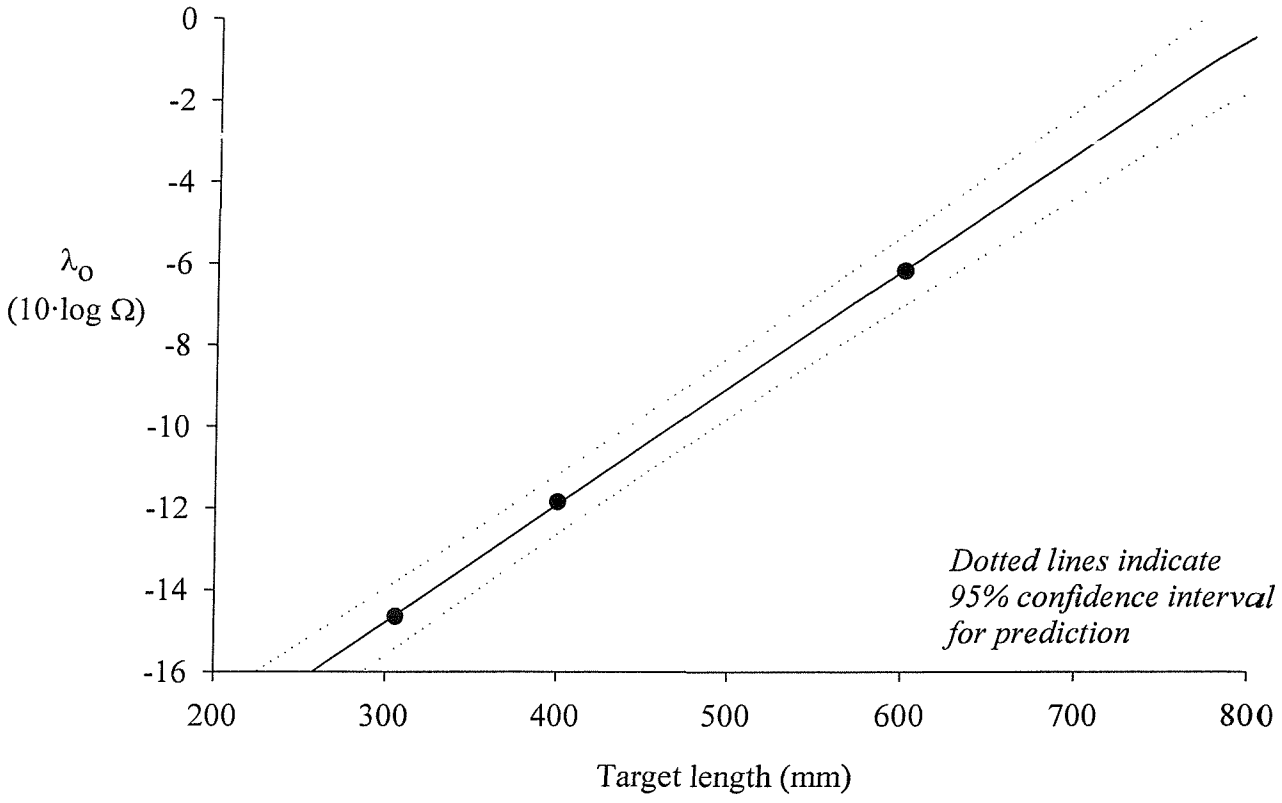

Table 14 Description of linear regression model fit

	Units	Coefficient	Standard error of the mean	*P*
Intercept	(10·log Ω)	-23.446	0.1567	0.0043
Slope	10·log Ω mm^{-1})	0.0289	0.0003	0.0076
r		0.9999		
r^2		0.9999		

Table 15 Estimated values for λ_0 calculated using *Equation2*

Target length	y_0 estimate	Standard error of the mean	r	r^2	P
(mm)	(10·log Ω)	(10·log Ω)			
306 mm	-14.617	0.1325	0.994	0.988	<0.0001
400 mm	-11.902	0.0909	0.997	0.994	<0.0001
600 mm	-6.134	0.0443	0.999	0.999	<0.0001

Table 16 Analysis of variance table for the logistic model

	DF	SS	MS	F	P
Regression	4	751.1373	187.7843	1878.88	<0.0001
Residual	25	2.4986	0.0999		
Total	29	753.6359	25.9874		

4.5 An Exponential Model

In order to investigate a potential method of target ranging another group of models were constructed. The source data described in Table 17 shows the relationship between target length, electrode spacing and target range. This data set consisted of few data points and therefore to extrapolate between observed measurements mathematical models were employed. An initial plot of the absolute[α] RCS measurement indicated linear relationships between RCS and target range when plotted with a logarithmic scale for the y-axis. Since the slope of these relationships was negative, the underlying relationship was considered of the exponential decay form.

$$\lambda = a + e^{-bTr} \qquad \textit{Equation 3}$$

where

a = intercept with the λ-axis or $\lambda_{\varphi=0}$ (NB. Ω)

$e = 2.7183$

b = a slope factor

T_r = the target range (*NB. cm*)

[α] Absolute RCS measurements are unsigned values.

The above model was fitted to each of the four groups of data in Table 17 in order to provide estimates for a and b in each case. Table 18 shows the derived model parameters and presents estimates of r^2, the coefficient of determination, in each case. Figure 38 shows the fit of the model to the data measured data.

Table 17 Source RCS data for rod targets measured with two electrode separations and at varied target range.

Target length (m)	0.4	0.4	0.6	0.6
Electrode separation (m)	0.5	0.9	0.5	0.9
Target range (cm)	(Ω)	(Ω)	(Ω)	(Ω)
0		-0.7334		-3.1906
10	-2.3558	-0.7273	-5.8329	-2.8763
20	-0.5127	-0.4427	-1.4173	-1.6227
30	-0.1383	-0.3302	-0.4484	-0.7913
40	-0.0707	-0.2341	-0.2467	-0.4115
50	-0.0234	-0.1191	-0.0543	-0.3420
60	-0.0264	-0.0732	-0.0275	-0.2672

Table 18 Exponential decay model parameters for rod targets measured with two electrode separations and at varied target range.

Target length (mm)	Electrode separation (mm)	a (Ω)	b (Ωmm^{-1})	r	r^2
400	500	10.4686	-0.1492	0.9995	0.9991
400	900	1.0926	-0.0418	0.9952	0.9905
600	500	22.8376	-0.1367	0.9993	0.9987
600	900	5.2287	-0.0598	0.9532	0.9969

Figure 38 Comparison of observed and model data for rod targets measured with two electrode separations and at varied target range

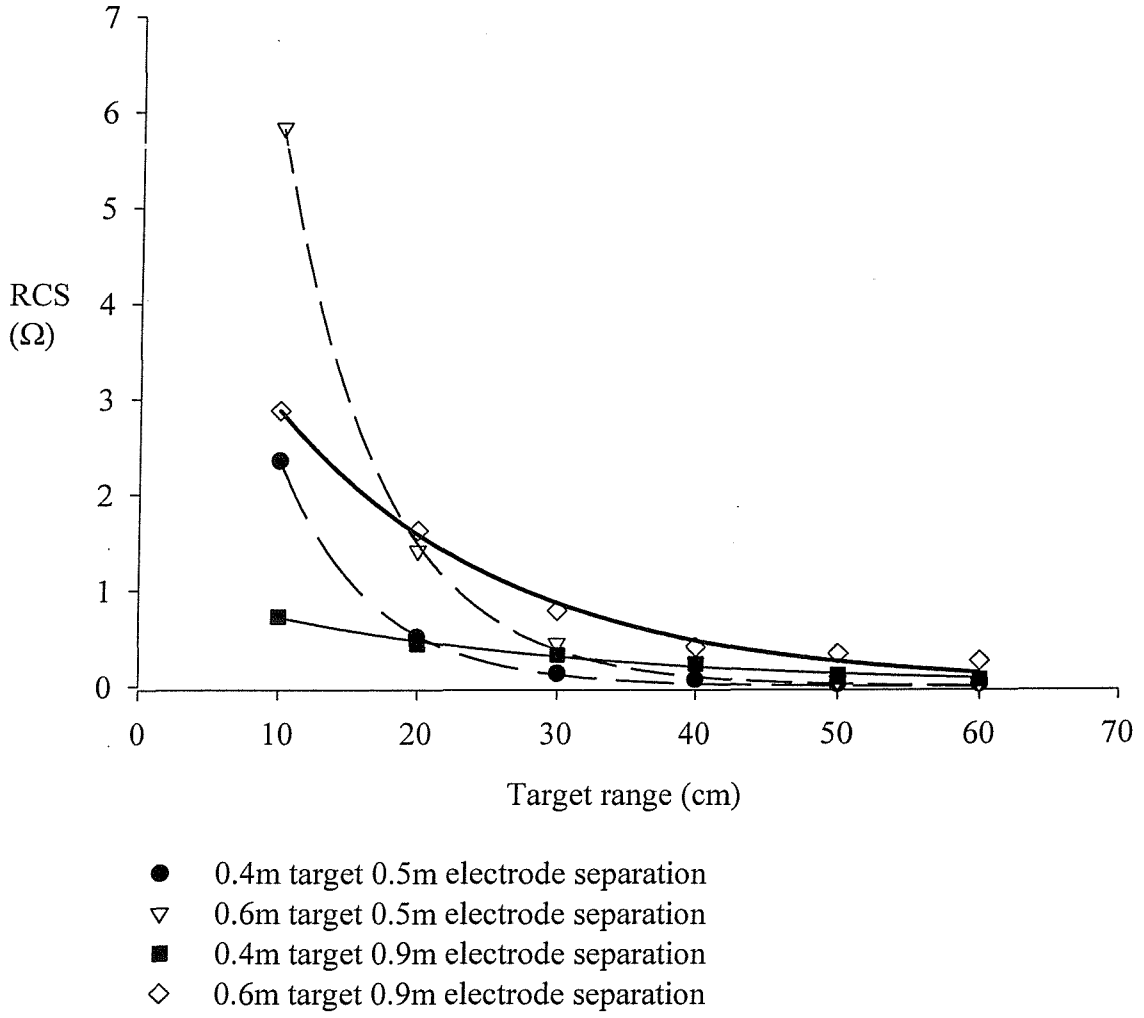

CHAPTER FIVE

TARGET SIZE ESTIMATION USING RESISTANCE CHANGE SIGNAL

CHAPTER FIVE

5 TARGET SIZE ESTIMATION USING RESISTANCE CHANGE SIGNAL

5.1 Background

RCS was known to decrease with increasing resistive target range from the sensor electrodes as described in chapter 3. To accurately estimate the size of resistive targets, or fish in a river, using RCS some compensation was required for the variable range of the target from the sensor electrodes. Two potential methods of target range compensation were investigated. The first used three simultaneous lateral measurements of RCS and the second used two simultaneous longitudinal measurements from electrodes with two different electrode separations.

Figure 39 Trilateral and coaxial methods of target size estimation

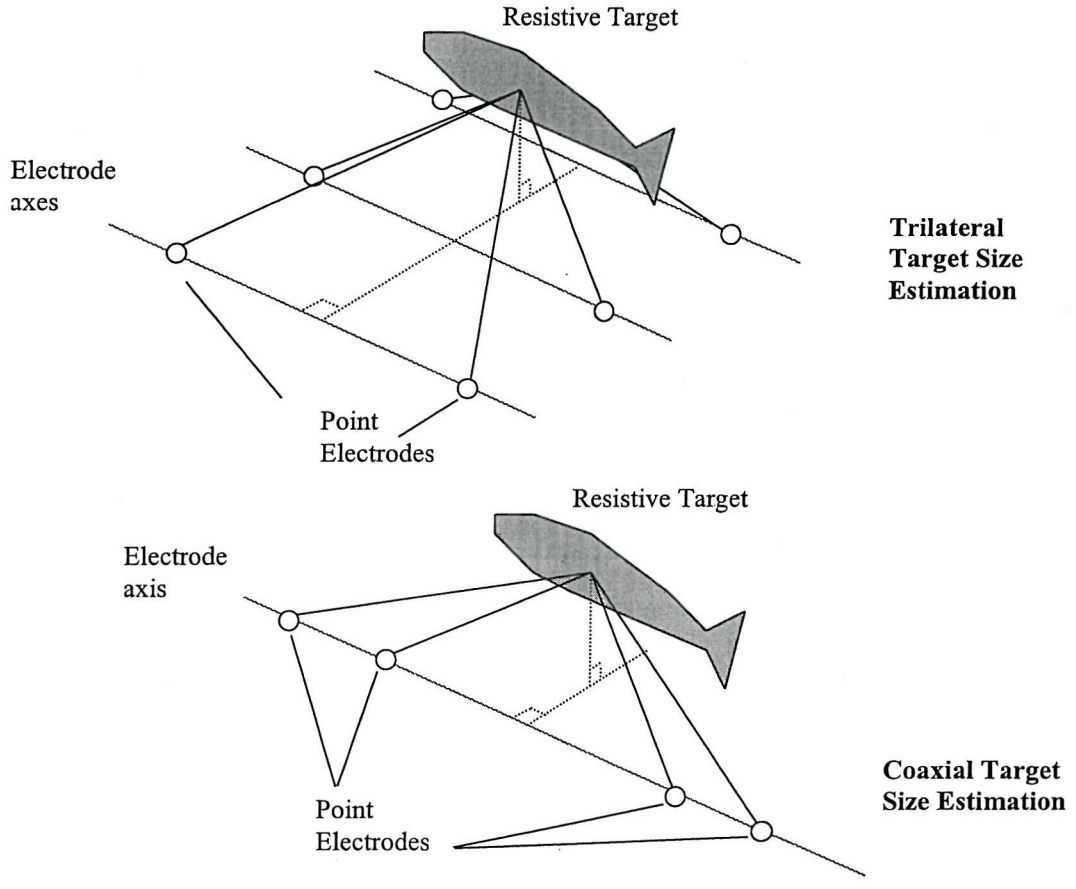

In the first method three pairs of electrodes were arranged in parallel, laterally displaced by a known distance (see Figure 25), and simultaneous measurements made with a centrally located resistive target (trilateral measurement). In such conditions it was expected that there would be few positions where non-unique combinations of RCS could occur. This would allow the determination of target length and perhaps target position using an iterative algorithm. The iterative algorithm was based on calculated RCS estimates for the three pairs of laterally placed electrodes. Such estimates were calculated using the model relationship developed in chapter 4 (section 4.4).

The second method of target range compensation investigated considered the use of two different pairs of electrodes arranged on a longitudinal axis (coaxial measurement). Since each pair of electrodes had different electrode spacing, the relationship between RCS and range to target was expected to be different, as noted by Lawson (1975) with strip electrodes and in section 3.3 using point electrodes. Combination of the two measurements mathematically was expected to provide a measure related to the range of the target but largely independent of target size.

5.2 Trilateral Target Range Compensation

5.2.1 Computer Simulation

A computer simulation was developed to investigate the performance of a trilateral method of target range compensation. The limitations of tank space precluded the testing of a full size array since the proximity of the walls would have distorted the electric fields near the outer electrodes. This would have led to inconsistent measurements being made. To simulate the measurement of RCS the model describing RCS with target range and target length (section 4.4) was incorporated into a "Visual Basic for Applications™" [α] computer program. Centrally placed targets on the

---

[α] "Visual Basic for Applications" is a high level computer language provided with the "Microsoft Office 97™" software suite. In this case the software was written from within "Microsoft Excel 97".

longitudinal axis, were simulated in a range of positions in the vertical and lateral axes. An electrode pair separation of 900 mm and lateral displacement of electrode pairs of 300 mm was assumed. The range of the target from the axis of each pair of electrodes was calculated and used to calculate the RCS as if measured from each electrode pair. To make these simulated measurements realistic, measurement errors were added to the calculated measurements. These measurements were then compared with a series of calculated RCS measurements with no errors added using a signal pattern-matching algorithm.

5.2.2 Measurement Noise

The random error associated with the measurement of RCS was estimated using the standard deviation of repeated measurements without a target in the water. These estimates were collected during the tank test measurements associated with the derivation of the model referred to above and are displayed in Table 19. This estimate of measurement error was incorporated into the simulation by adding random errors to the predicted RCS observed at each of the three pairs of electrodes. This error was assumed Gaussian in distribution with confidence limits of $\pm$ 0.05 Ω (α=0.025).

Table 19 Resistance measurements with no target in the test tank

Control measurement for target length (mm)	306	400	600
Measurement data (Ω)	879.368	879.598	879.282
	879.354	879.526	879.267
	879.325	879.583	879.282
	879.339	879.569	879.296
	879.411	879.483	879.325
	879.296	879.526	879.282
	879.310	879.512	879.339
	879.382	879.569	879.325
	879.339	879.540	879.310
	879.354	879.555	879.296
Mean	879.348	879.546	879.300
Confidence interval (α=0.025, n=10)	0.021	0.022	0.015

Each set of ten measurements was taken immediately prior to the test target entering the test tank to form the control measurement. Subsequent measurements with resistive targets in place were subtracted from the mean of the above in each case to provide the RCS

Figure 40 Error measurement noise added to simulated RCS measurements

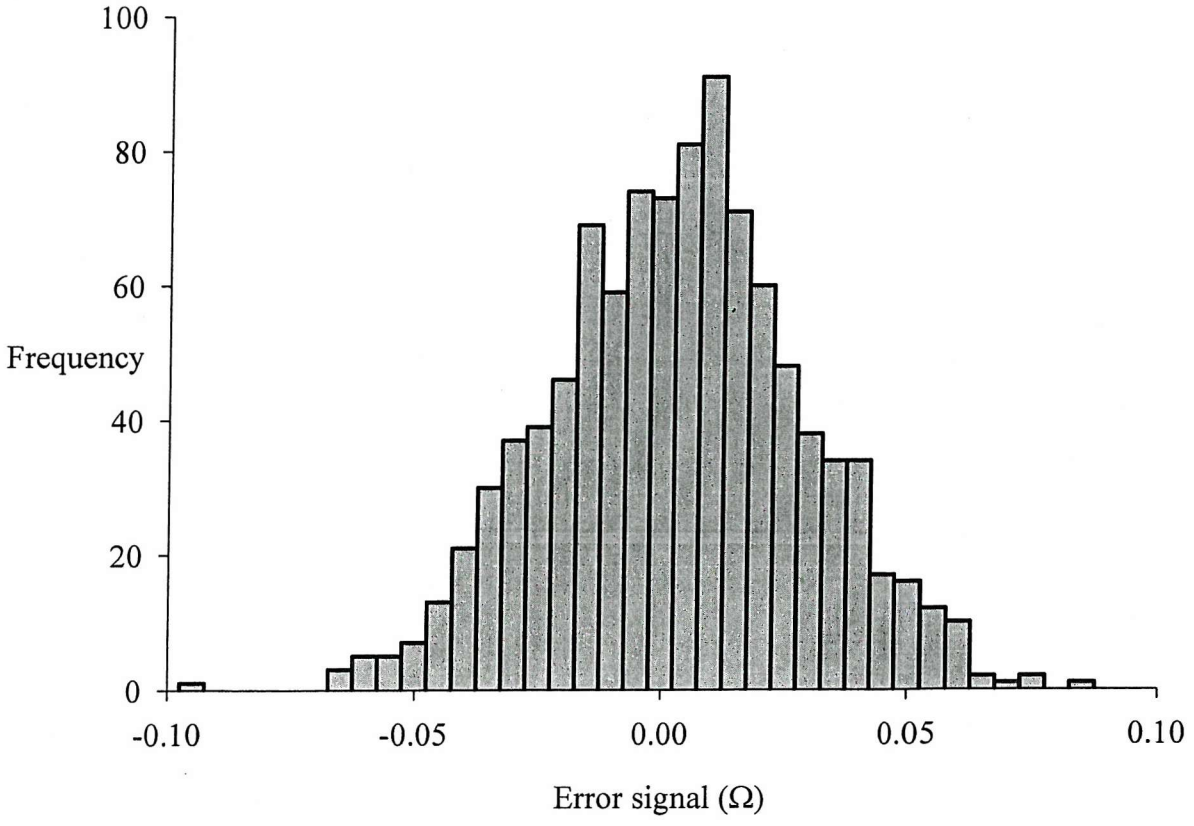

The simulated noise level was chosen since the observed noise[α] of ± 0.022 Ω was obtained under laboratory conditions; this simulation was designed to represent realistic conditions in a noisier operational environment. The noise data set comprised 1,000 error measurements generated by the "Microsoft Excel" random number function. Each error measurement was picked at random[β] from the noise data set. Thus, realistically 'noisy' measurements were simulated for input to a pattern-matching algorithm. Figure 40 describes the frequency distribution of the error measurements used in the simulation.

5.2.3 Pattern Matching

The pattern-matching algorithm calculated estimates of RCS for each notional target length, lateral displacement, target elevation and electrode pair. These estimates of RCS were compared to the simulated 'noisy' measurements and the sum of the absolute differences (SAD) calculated. The combination of target length, target elevation and target displacement with the minimum SAD was selected as the best match pattern of RCS's to the simulated real data. A pseudo-code listing of the algorithm is given in Table 21 and the complete code in Appendix B (iv).

In order to determine the accuracy of this method for estimation of target length and target position, 20 replicates of the test were completed for each target position and

---

[α] It should be noted that the noise measurements described in section 4.2 were derived from confidence limits on 10·log transformed data, the noise measurements above were derived from confidence limits of the untransformed data.

[β] The precise error measurement value picked from the noise data set was selected by a random number generating function for which there was an equal chance, on average, of picking any individual noise measurement.

length. A measure of target length estimate reliability was derived using the confidence[α] intervals for each target position and size.

The limits of the position and length of the simulated "real" targets tested in the simulation are given in Table 20. The limits of the potential target size and position used in the pattern-matching algorithm are also tabled.

[α] The confidence intervals calculated were for the collection of one length estimate ($\pm 1.96 \cdot \sigma$).

Table 20 Simulation and pattern matching algorithm limit parameters

Simulation			
Parameter	Start Value (mm)	End Value (mm)	Increment (mm)
Target Length	300	700	100
Target Displacement	-600	0	50
Target Elevation	20	700	50

Pattern Matching Algorithm			
Parameter	Start Value (mm)	End Value (mm)	Increment (mm)
Target Length	200	850	20
Target Displacement	-600	10	50
Target Elevation	10	800	25

Table 21 Pseudo-code listing of the trilateral pattern-matching algorithm

Start main program

Calculate the number of estimates required in program run

Select a target length, target displacement & target elevation [line 2]

Start a timer

Calculate the range of the target from each electrode pair

Calculate the RCS for the target as if measured from each electrode pair and add a measurement error

Transform each measurement to 10.log form

Write the target position and result data to the spreadsheet

Call Find Target Length function

Set the limits for trying values of target elevation, displacement and target length

For each possible value of target elevation, displacement and target length calculate the signal expected for each electrode pair

Calculate the absolute difference between the simulated measurements and the measurements calculated

If the absolute difference calculated is smaller than the smallest so far then record the target elevation, displacement & target length

Return to main program

Write the target elevation, displacement & target length to the spreadsheet.

Calculate the time taken for one target position and estimate time to complete program

Go to line 2 until all of the possible target positions and lengths requested have been simulated

End main program

For simplicity the repetition of estimation for each simulated target position and target length has been omitted.

5.2.4 Measurement Accuracy

Estimates of target length made using the trilateral pattern-matching algorithm for a range of simulated target sizes, displacements and elevations are given in Appendix C (ii) Tables A to K.

Using confidence limits, calculated from the 20 replicates of target length estimate, as an indicator of length estimation accuracy it was possible to construct contour maps of target lengthing accuracy. The maps describe a planar lateral cross section through the sensor array from –600 mm to 0 mm displacement. The y-coordinate represents the target elevation in the array. Figure 41 to Figure 45 show these accuracy maps. These maps show that reliable target length estimation was achieved outside the perimeter of the array.

The maximum range at which a given target could be distinguished from the next larger test target is displayed in Table 22. To estimate the operational range of such a system Table 23 provides grouped range estimates. These values represent mean values and confidence limits for the range at which a confidence limit of 50 mm was exceeded for each target length at displacements of 0 to –300 mm (see Figure 46).

These data were then re-ordered and plotted to indicate the range at which a given target length could be distinguished from another 100 mm larger target at alternate lateral displacement of the target (see Figure 47). This figure clearly indicates that

reliable target lengthing[α] was achieved at range greater than 500 mm for targets >600 mm length and that targets of 500 mm length were reliably sized at ranges between 300 and 400 mm. Targets of 700 mm length were reliably lengthed at range 670 mm although the real limit may be larger than this figure.

[α] Reliable target length estimation was defined as the ability to distinguish another target 100 mm larger 95% of the time.

Figure 41 Target lengthing accuracy map for a 300 mm target

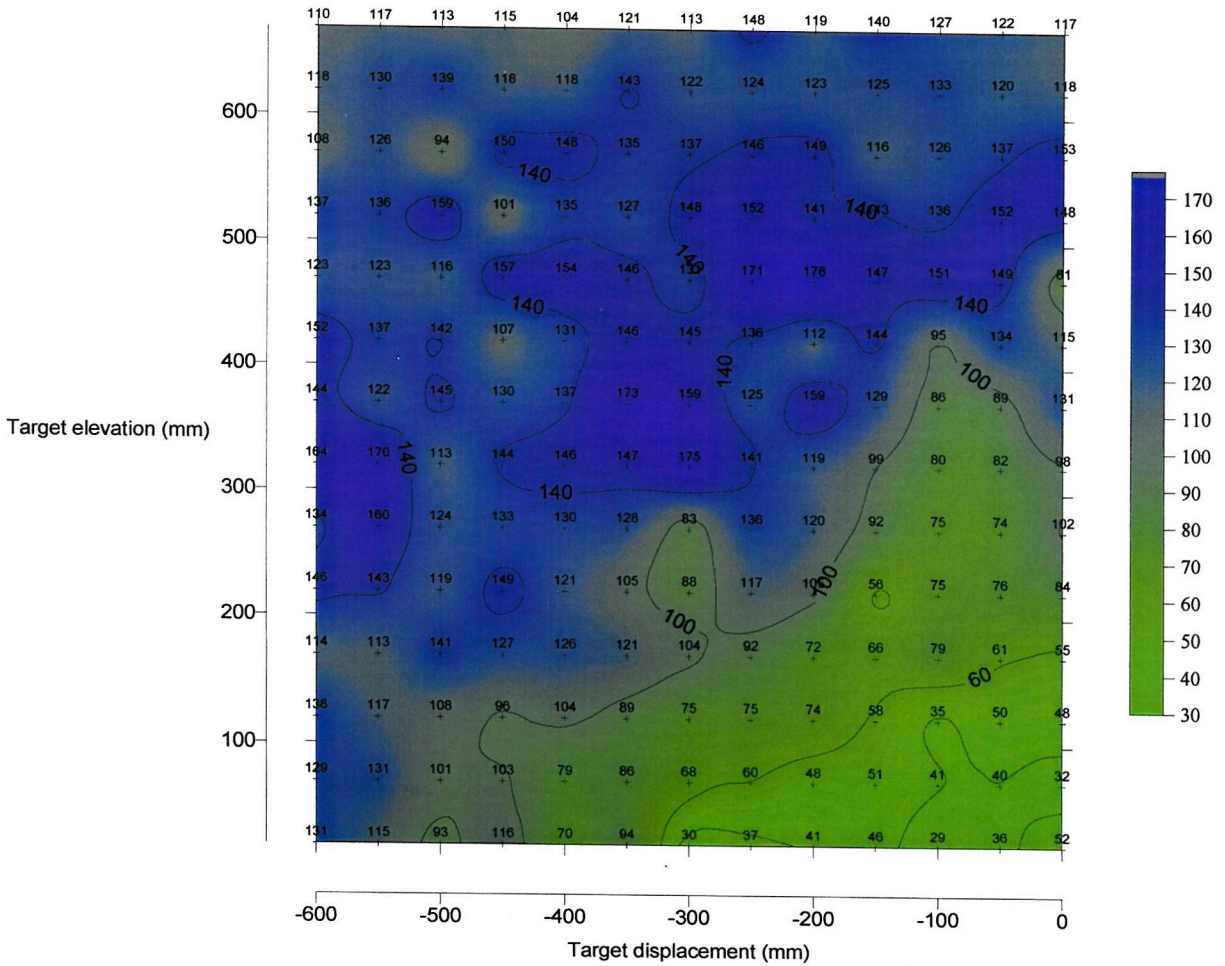

The z-coordinate of the map represents a confidence interval on the 20 length estimates carried out in the simulation

Figure 42 Target lengthing accuracy map for a 400 mm target

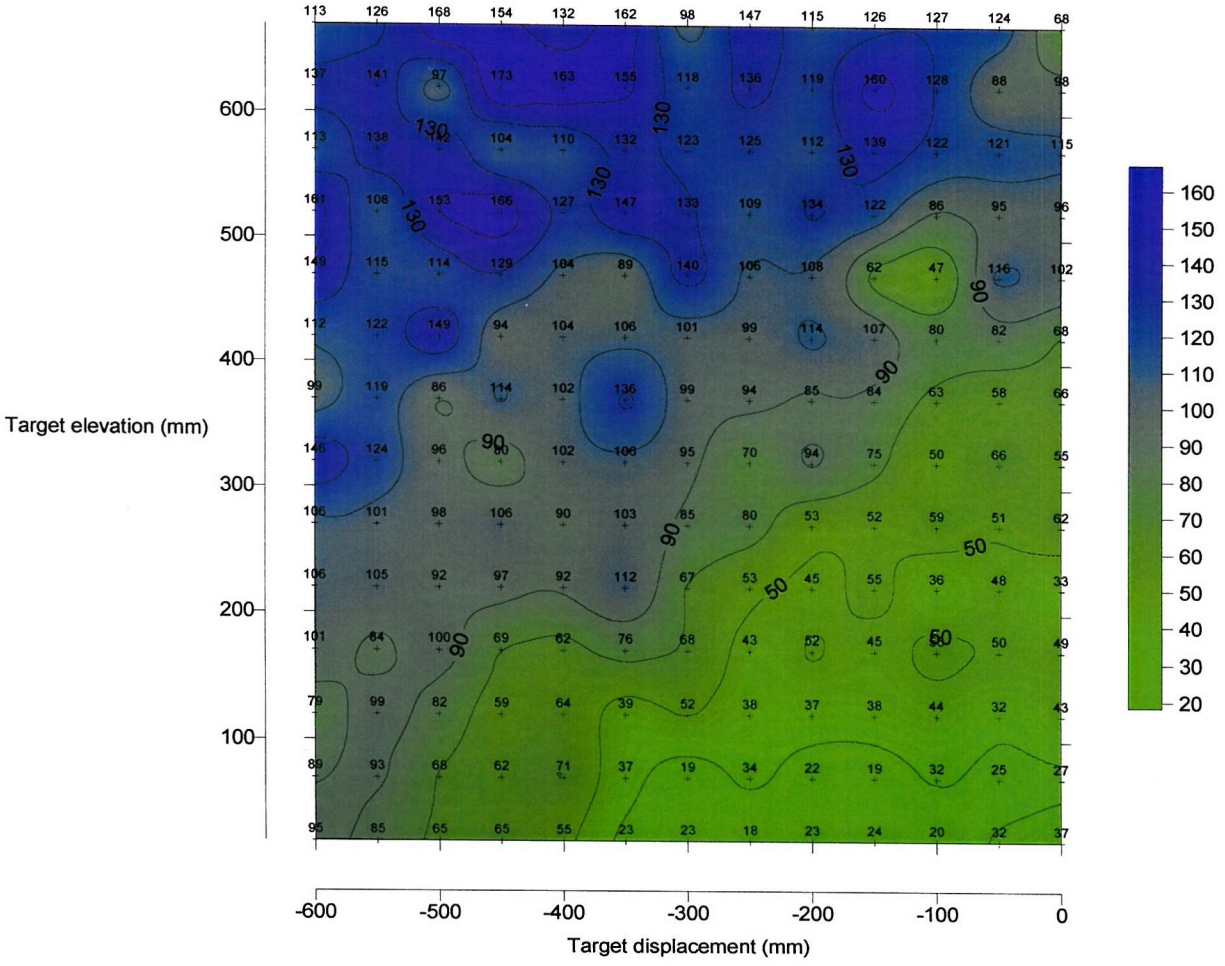

The z-coordinate of the map represents a confidence interval on the 20 length estimates carried out in the simulation

Figure 43 Target lengthing accuracy map for a 500 mm target

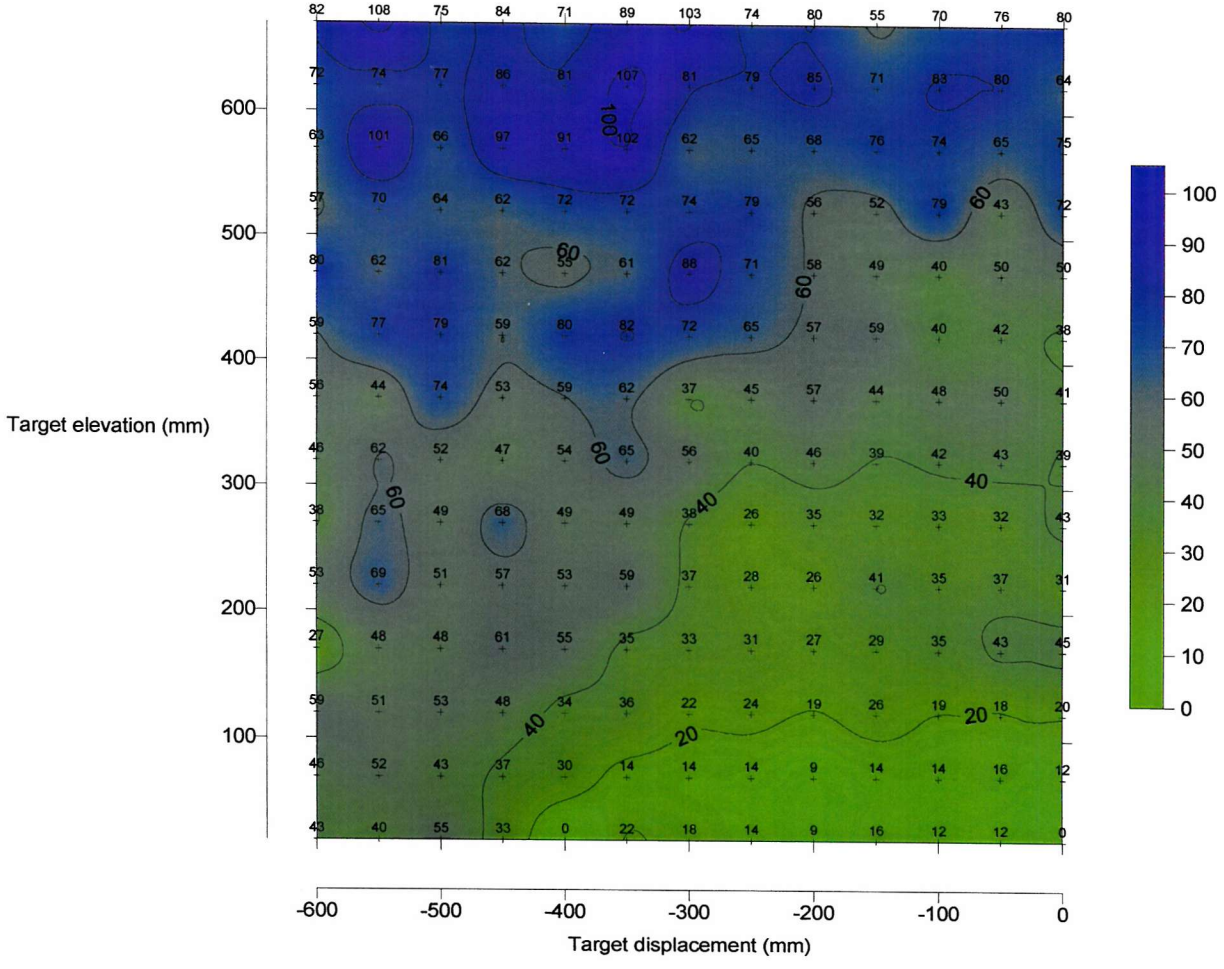

The z-coordinate of the map represents a confidence interval on the 20 length estimates carried out in the simulation

Figure 44 Target lengthing accuracy map for a 600 mm target

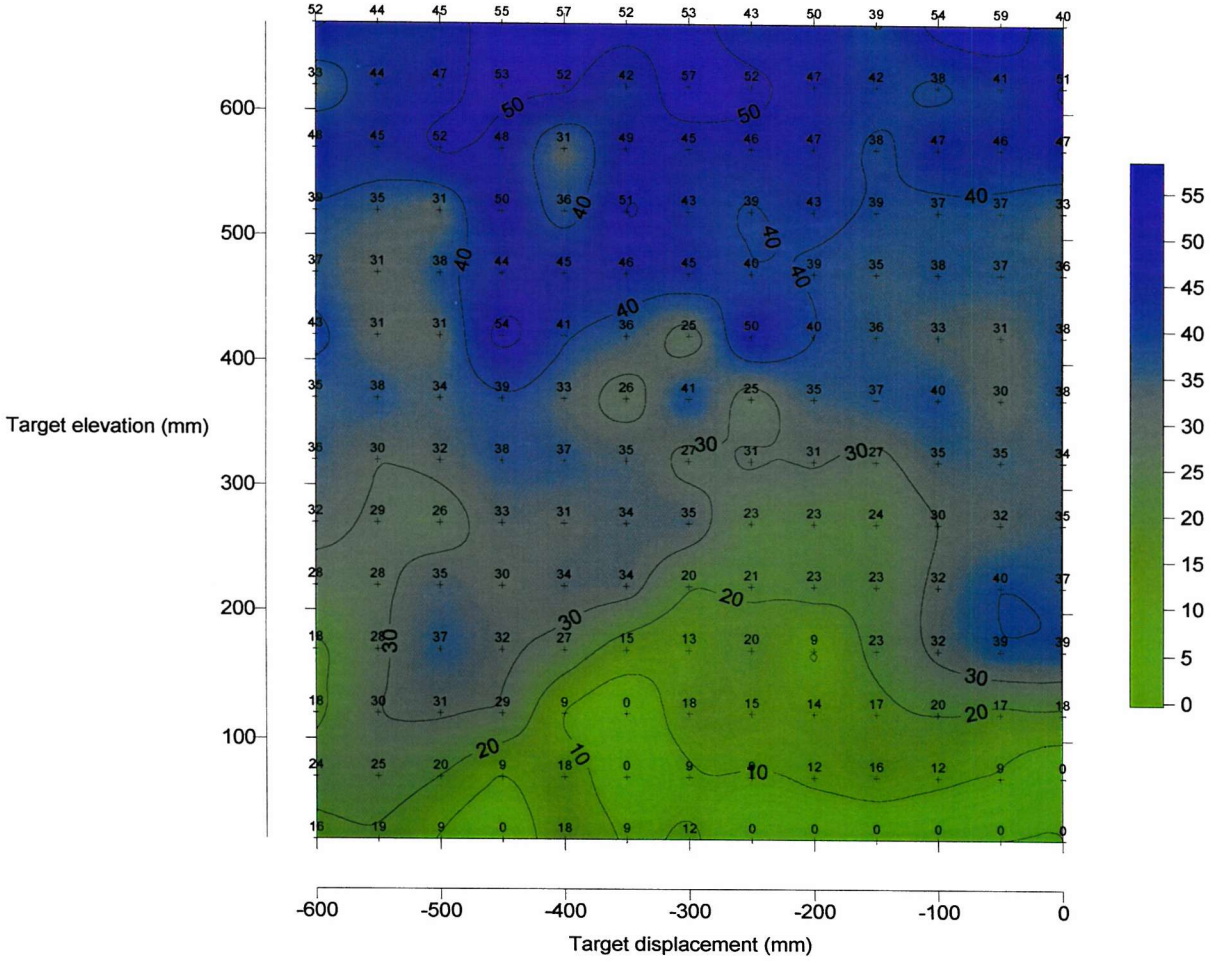

The z-coordinate of the map represents a confidence interval on the 20 length estimates carried out in the simulation

Figure 45 Target lengthing accuracy map for a 700 mm target

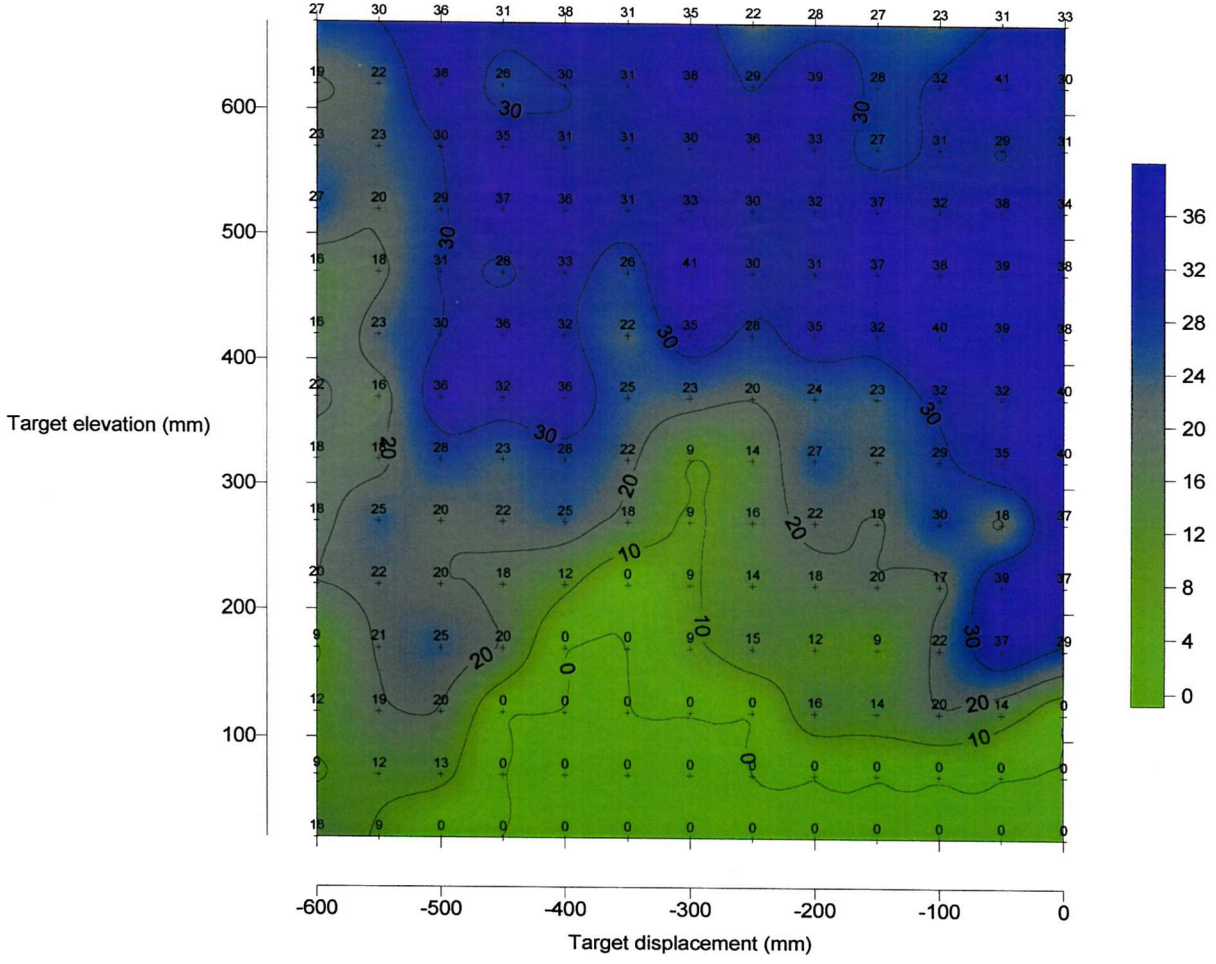

The z-coordinate of the map represents a confidence interval on the 20 length estimates carried out in the simulation

Table 22 Maximum elevation to resolve next larger target [SD of TL estimation <25mm]

	Target Displacement (mm)										
Target length (mm)	**0**	**-50**	**-100**	**-150**	**-200**	**-250**	**-300**	**-350**	**-400**	**-450**	**-500**
300	120	70	120	20	20	20	20				
400	170	120	120	170	120	170	120	120			
500	420	320	320	370	320	370	270	220	120	70	
600	570	620	620	>670	620	420	620	470	570	370	520
700	>670	>670	>670	>670	>670	>670	>670	>670	>670	>670	>670

Table 23 Maximum elevation at which targets could be resolved

Target length (mm)	Range at which targets could be resolved (mm)	Standard deviation (mm)	Confidence interval (mm)
300	56	48	93
400	141	27	52
500	341	49	96
600	578	80	157

(Confidence intervals = 1.96·σ)

Figure 46 Maximum elevation at which targets could be resolved

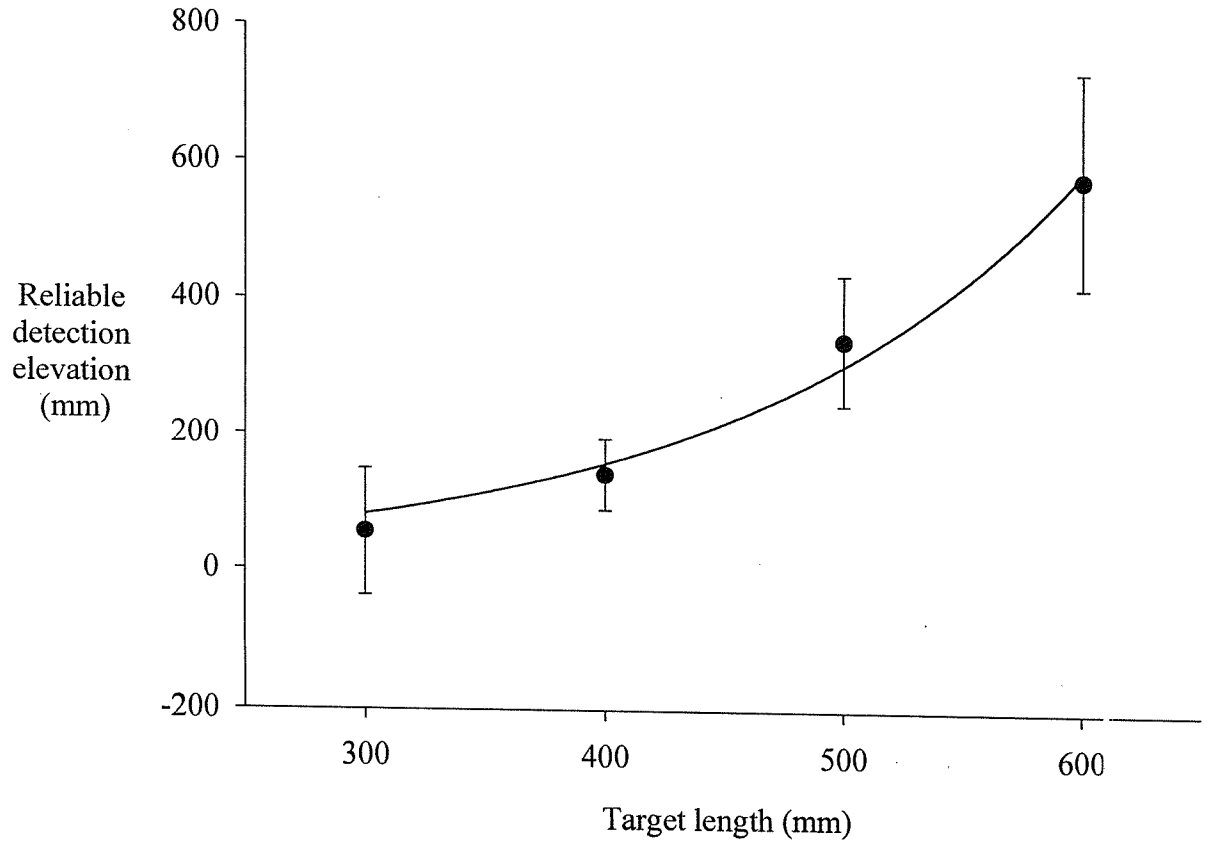

Error bars indicate mean ± 1.96·σ, *n=20*

Figure 47 Map of target elevation at which a given target length could be distinguished reliably from another target 100 mm larger for alternate target lateral displacements.

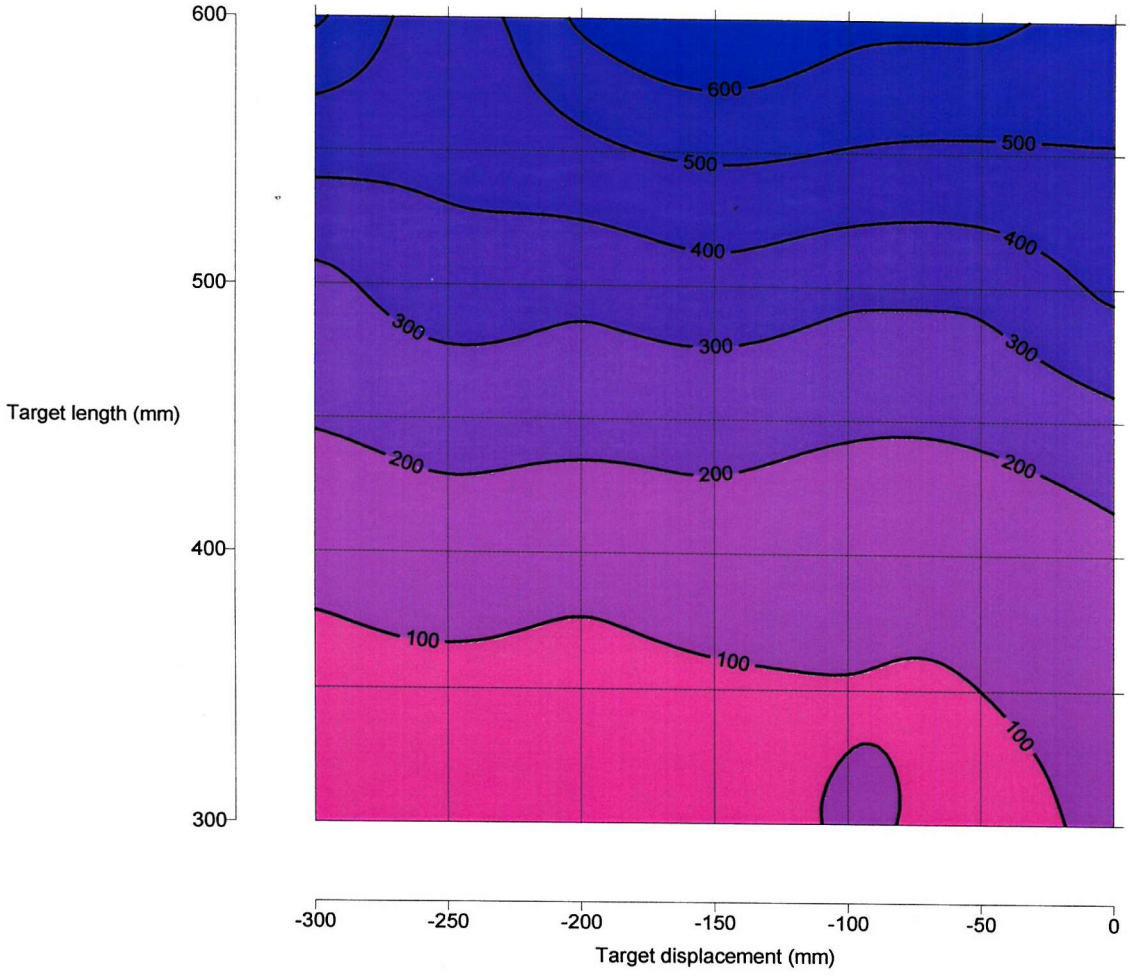

5.3 Coaxial Target Range Compensation

5.3.1 The Principle

The data given in section 3.2.3 indicated that the RCS relationship with target range was different when measured with two different electrode spacings. This observation gave rise to the possibility of target range estimation since the ratio of the RCS measurements from each electrode spacing showed substantial dependence on target range but little dependence on target length as shown in Figure 48.

Using RCS estimates derived from the models constructed in section 4.5, averages of the resistance change ratios for a 400 mm and 600 mm targets were computed for target ranges from 50 mm to 950 mm. These averages were then plotted as resistance change ratio versus target range in order to derive a relationship for the calculation of target range from RCS ratio (Equation 4).

$$T_r = \gamma_0 + \phi . \ln \rho \qquad \textit{Equation 4}$$

Where

T_r = Target range (cm)
γ_0 = 19.936 (cm)
ϕ = -11.53 (dimensionless)
ρ = RCS ratio (dimensionless)

[r=0.999, r^2=0.999, P<0.0001]

This relationship thus yields an estimate of range that was introduced to the target length relationships of section 4.5. Since two estimates of RCS were available for each position of a target then two estimates of target length can be derived.

Figure 48 Ratio of RCS for axial electrodes of 500mm and 900mm separation

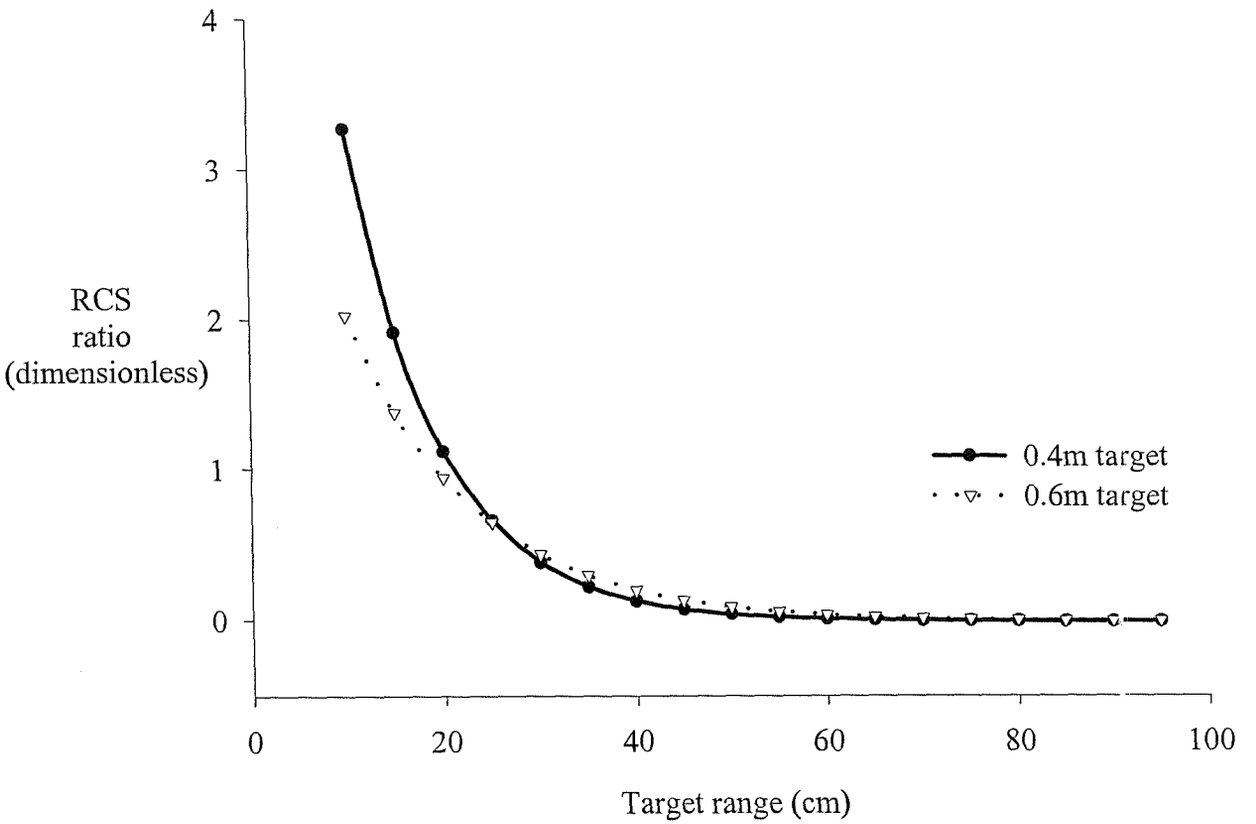

Table 24 Target range estimation using Coaxial RCS measurements

Target Length 400mm				Target Length 600mm		
Target range (cm)	Estimated target range (cm)	Standard deviation of estimated range (cm)	Number of replicates	Estimated target range (cm)	Standard deviation of estimated range (cm)	Number of replicates
5	0.14	0.30	20	7.36	0.09	20
10	6.33	0.50	20	11.78	0.15	20
15	12.56	0.49	20	16.14	0.16	20
20	18.64	0.84	20	20.69	0.15	20
25	24.84	1.65	20	25.12	0.47	20
30	30.83	2.89	20	29.29	1.07	20
35	38.83	5.68	20	33.81	1.30	20
40	42.98	7.71	17	38.24	2.90	20
45	43.61	11.30	16	41.65	3.91	20
50	39.49	10.21	16	45.24	9.59	20
55	48.42	14.77	11	47.03	10.32	15
60	34.44	10.99	13	49.76	8.36	8
65	43.82	17.70	13	40.88	10.88	9
70	33.40	9.66	9	56.74	40.96	5

Figure 49 Estimated target range using Coaxial RCS measurements

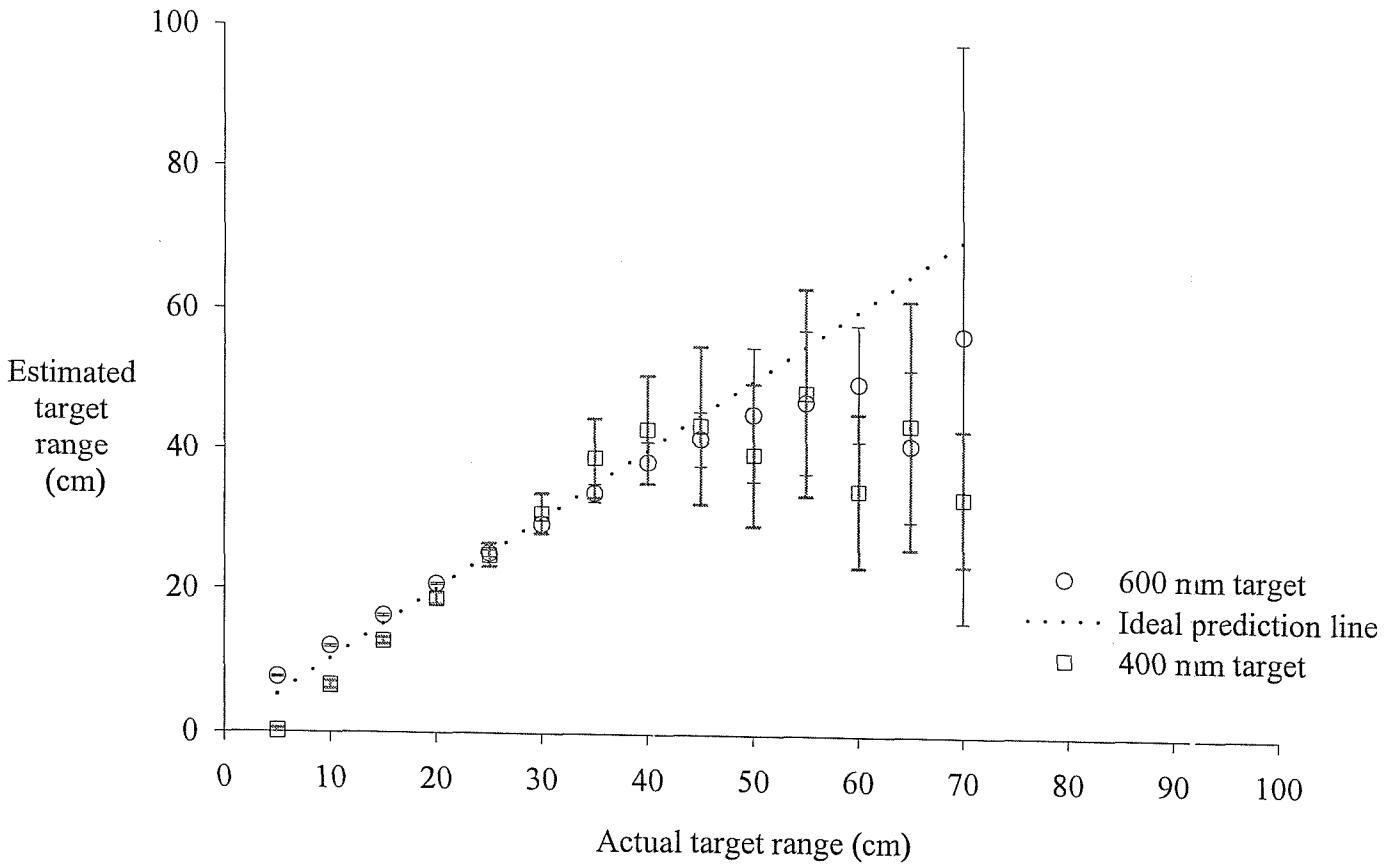

Error bars indicate mean $\pm 1.96 \cdot \sigma$, $n \geq 5$

5.3.2 Computer Simulation

To test the principle of coaxial target range compensation a computer simulation was constructed in an "Excel" spreadsheet. The source data for this simulation were derived from the data given in section 3.2.3 and the models constructed in section 4.5. Simulated RCS measurements were made using the models of section 4.5, the same error data as used for the trilateral target range compensation was then added. An RCS ratio ($RCS_{500\ mm}$/ $RCS_{900\ mm}$) was calculated using the RCS measurements with error signal added. The relationship of equation 4 was used to derive an estimate of target range.

Using this single estimate of target range two estimates of target length were calculated, one from the electrodes with a separation of 500 mm and one from the electrodes with a separation of 900 mm. The mean of these two estimates was calculated and used as the final estimate of target length. For each target range and target length simulated 20 replicates were carried out with the mean and standard deviation calculated for the estimates of target range and target length.

5.3.3 Measurement Accuracy

In some instances the addition of signal noise to the RCS measurements meant that the RCS measurement was less than zero. In such circumstances a target range could not be calculated since the calculation would involve computing the logarithm of a negative number which is not possible. This led to the number of replicates sometimes being less than 20, as shown in Table 24. It was possible to retain enough estimates to plot the results shown in Figure 49.

The results indicate that the method appears to be a good predictor of target range at ranges up to 400 mm. At greater range the presence of signal noise in relation to the signal from the target becomes substantial and the error in range estimation increases rapidly. In this case the errors become substantial when the RCS is smaller in magnitude than that of the confidence limits of the introduced signal noise (see section 5.2.2).

Using the method described above, estimates of target length and the error of estimation were calculated for 400 mm and 600 mm targets at ranges from 50 to 700 mm (see Table 25 and Figure 50).

This plot showing target length estimation against target range suggests that the accuracy of the resultant data is unlikely to be sufficient for operational purposes unless substantial refinement of the technique was possible. A better test of the technique would be possible if more data were available on the effects of target range on RCS for a wider range of electrode separations and target lengths. Under such circumstances an iterative algorithm may provide a more flexible method of target length estimation from coaxial RCS measurements.

Table 25 Target length estimation using coaxial RCS measurements

Target Length 400mm				Target Length 600mm		
Target range (cm)	Estimated target length (mm)	Standard deviation of estimated length (mm)	Number of replicates	Estimated target length (mm)	Standard deviation of estimated length (mm)	Number of replicates
5	352	3	20	692	5	20
10	360	5	20	668	7	20
15	370	6	20	645	7	20
20	381	8	20	629	6	20
25	395	14	20	608	13	20
30	409	26	20	584	23	20
35	445	63	20	571	23	20
40	455	90	17	558	54	20
45	437	109	16	531	57	20
50	381	60	16	540	190	20
55	436	106	11	489	124	15
60	336	35	13	462	86	8
65	377	123	13	370	59	9
70	324	28	9	1141	1738	5

Figure 50 Target length estimation using Coaxial RCS measurements

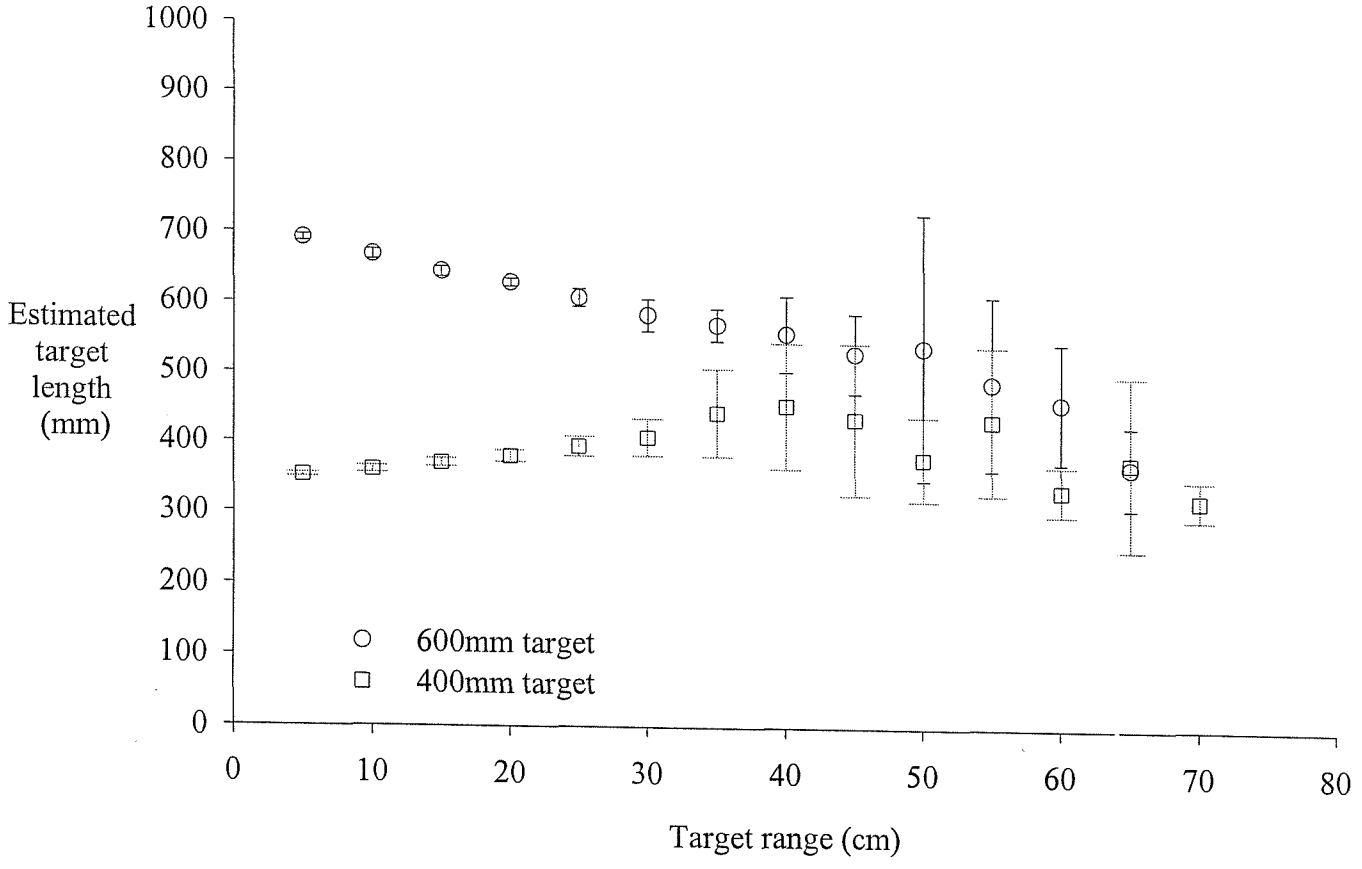

Error bars indicate mean ±1.96·σ, n ≥ 5

CHAPTER SIX

TESTING OF A PROTOTYPE SYSTEM

CHAPTER SIX

6 TESTING OF A PROTOTYPE SYSTEM

6.1 Background

All of the measurements previously described have been made in the confines of an aquarium measuring one metre cube sited within a metal-framed building. This experimental arrangement had several drawbacks including the following:

- Inability to use data from the outer electrode pairs
- Inability to move the target longitudinally through the sensor array
- Uncertainty of how much measurement noise was present in the external environment

To address these points a series of experiments were conducted in larger external tanks. Plans to operate the sensor system in a fish pass on the River Itchen were withdrawn after delays in installation meant that the migration season was missed.

A secondary experiment involved fixture of the sensor array to the bottom of a 10 m diameter circular tank used to hold wild Atlantic salmon adults. This attempt was unsuccessful due to the presence of substantial electrical interference at the site. The most likely sources of the interference were the borehole pumps, that could not be turned off during tests[α].

The concerns listed above were therefore addressed using measurements of stainless steel rod targets moved though the sensor array sited in a 4 m long external tank. This

---

[α] The borehole pumps also fed a hatchery facility that was particularly susceptible to changes in water supply.

was augmented by the collection of RCS measurements of Atlantic salmon allowed to swim over the electrode array.

6.2 Dynamic Stainless Steel Target Measurements

The six-electrode sensor array was set up in a 4 m long fibreglass tank[α] (see Plate 3) and fixed to the floor of the tank by 30 mm diameter rubber suction cups. Stainless steel rod targets were attached to the bottom of vertical fibreglass bars using monofilament nylon line, which allowed the measurement of the targets at varied range from the plane of the sensor array. The complete target positioning assembly was attached to a movable carriage suspended on two parallel 21 mm diameter steel tubes. The carriage allowed the target to move in the longitudinal axis but restricted movement in the lateral axis. Longitudinal motion was effected by manual withdrawal of a monofilament line attached to the carriage.

For each target and vertical position of the target two traverses of the array were carried out. These events were recorded into files as a sequence of 800 sets of six resistance measurements, one measurement per electrode pair and direction of sensor measurement. The order and connection arrangements for the array were as described in Section 2.7.3. For each set of six measurements the time of the measurement was recorded to the nearest 18 ms, the resolution of the computer's system clock.

During earlier tests the water conductivity was 470 $\mu S.cm^{-1}$ and water temperature was 14.4°C, which gave rise to resistance measurements of *circa* 1,300 Ω. These measurements were taken with an electrode excitation current of 1,416 μA and therefore an excitation electrode voltage of *circa* 1.8 V. The tests on moving targets were carried out in water of much lower conductivity (103 $\mu S.cm^{-1}$) and at a lower temperature (3.4°C), which had the effect of increasing the average inter-electrode resistance to *circa* 2,600 Ω. To reduce the electrode excitation to within the range of

---

[α] Dimensions of the tank were 4.0 m by 1.1 m width by 0.6 m deep.

the ADC (±2.5 V) the electrode excitation current was reduced to 708 μA. Measurements were taken for targets of 306, 500 and 700 mm in length at ranges of between 50 and 300 mm. Since RCS measurements were also made using the outer electrode pairs, the range from these electrodes to the target in the central axial position were calculated.

To illustrate a typical set of waveforms collected from the passage of one target, Figure 51 shows the RCS measured from each electrode. For each pair of electrodes a phase difference is evident between the measurements made at the upstream and downstream electrodes. A combination of the two waveforms using the difference of the upstream and downstream RCS measurements allowed estimation of the time when the target was in a central longitudinal position. This was inferred from the waveform as the point when the difference RCS crossed RCS = 0 (see Figure 52). Once the time of central position was known, an estimate of RCS was made from the average of the RCS for each pair of electrodes (see Figure 53).

Plate 3 Test facility used for dynamic RCS measurements

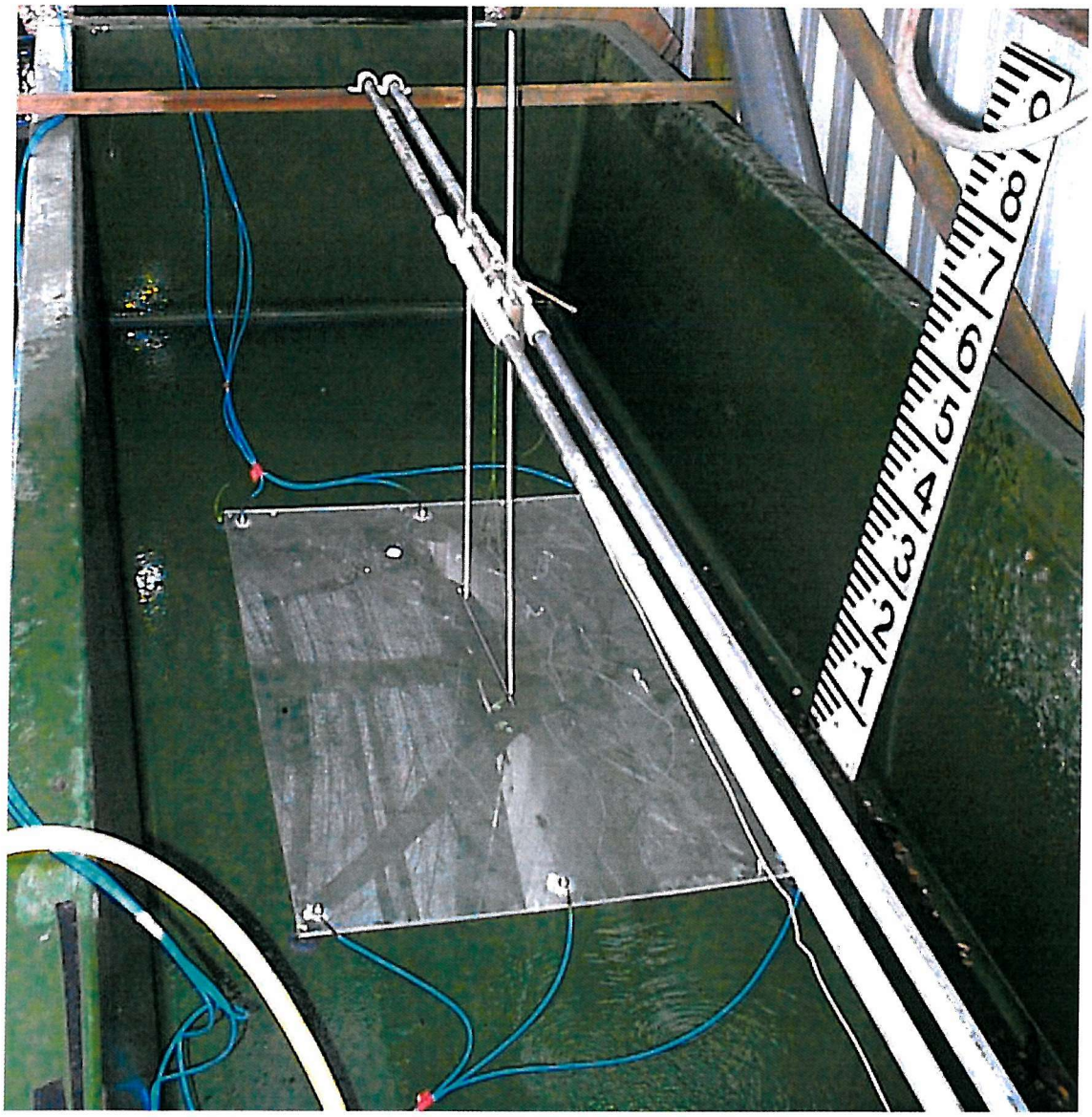

Plate 4 Fish number 2 shown in the lengthing tank

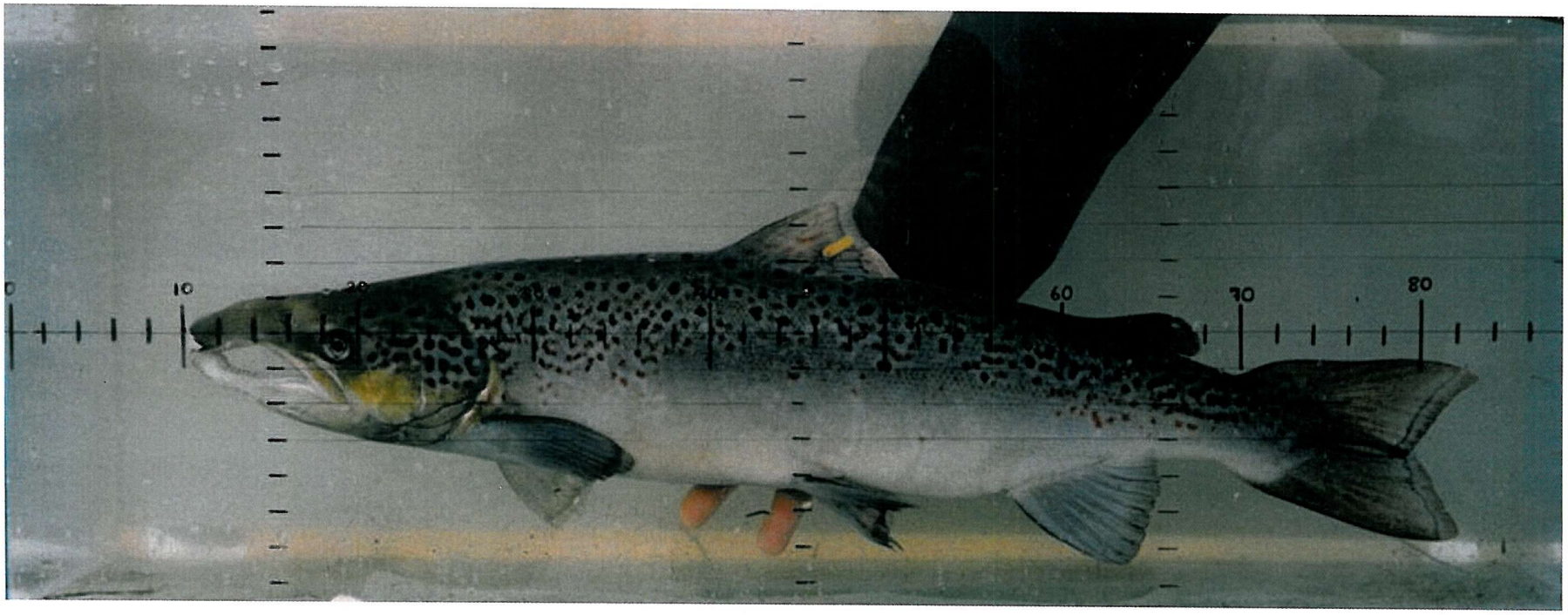

Figure 51 RCS measured at each electrode for a 700 mm rod target at 100 mm from the plane of the array

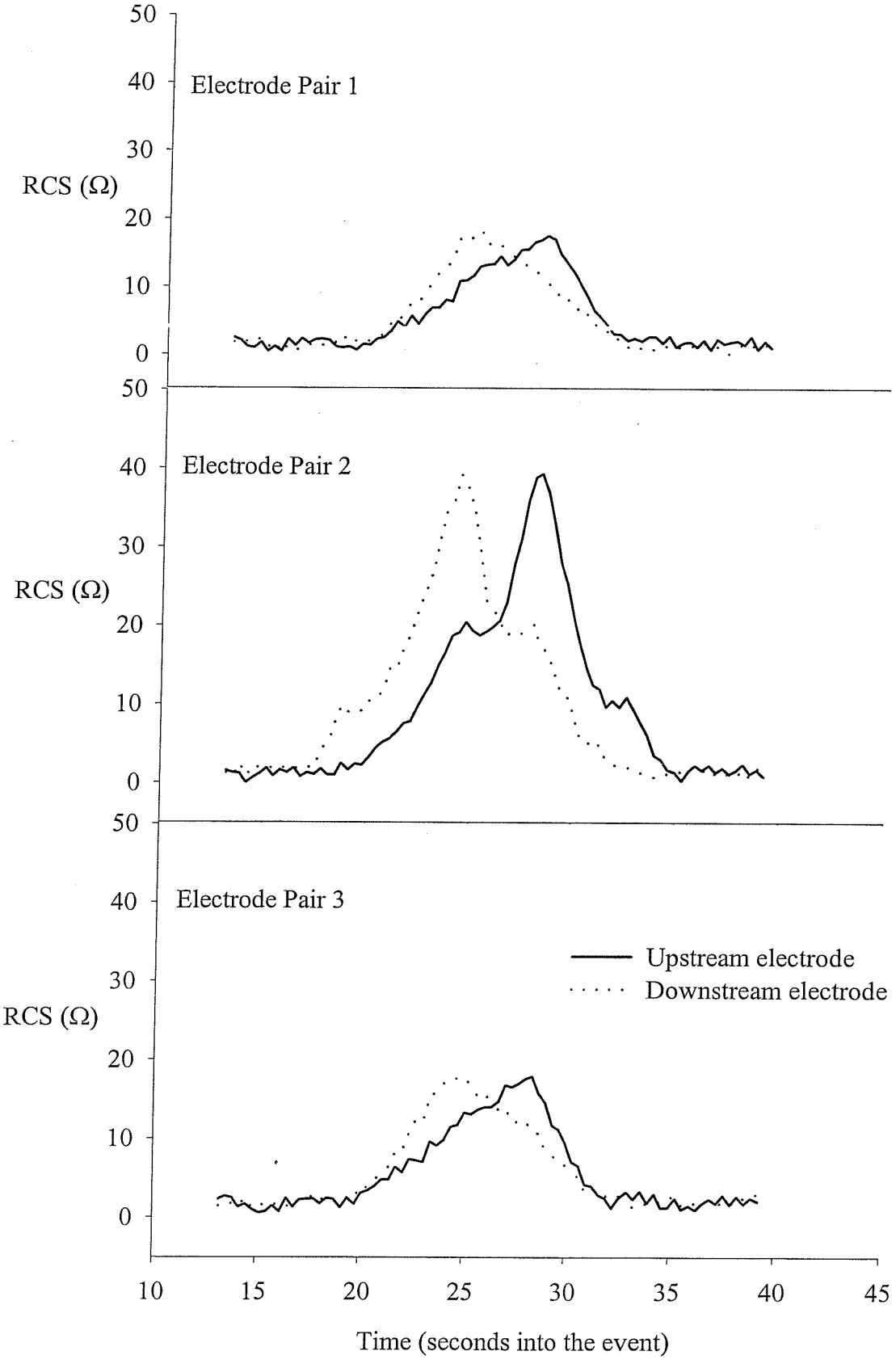

Figure 52 Difference in RCS measurements between upstream and downstream electrode per electrode pair

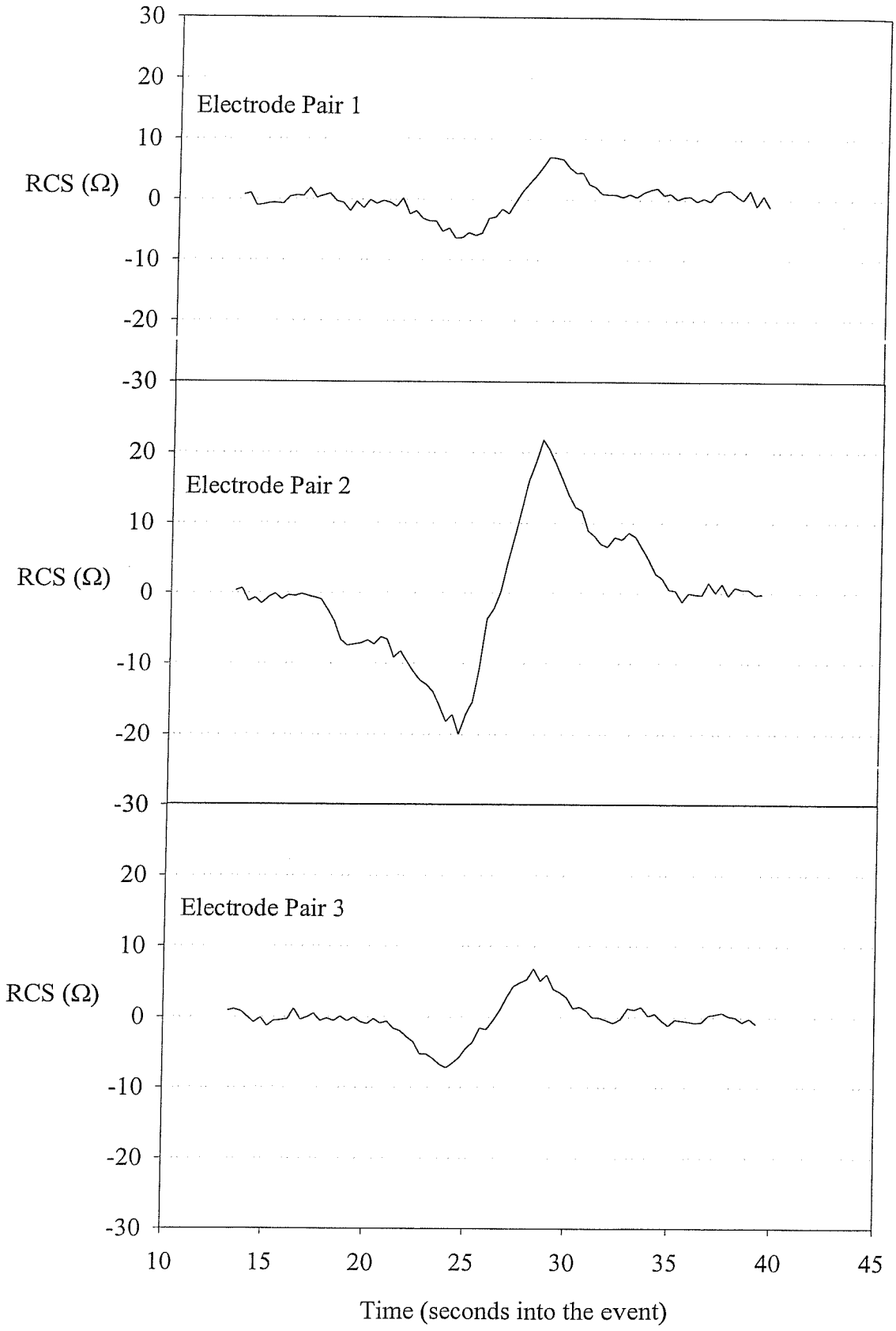

Figure 53 Sum of the RCS measurements made for each pair of electrodes

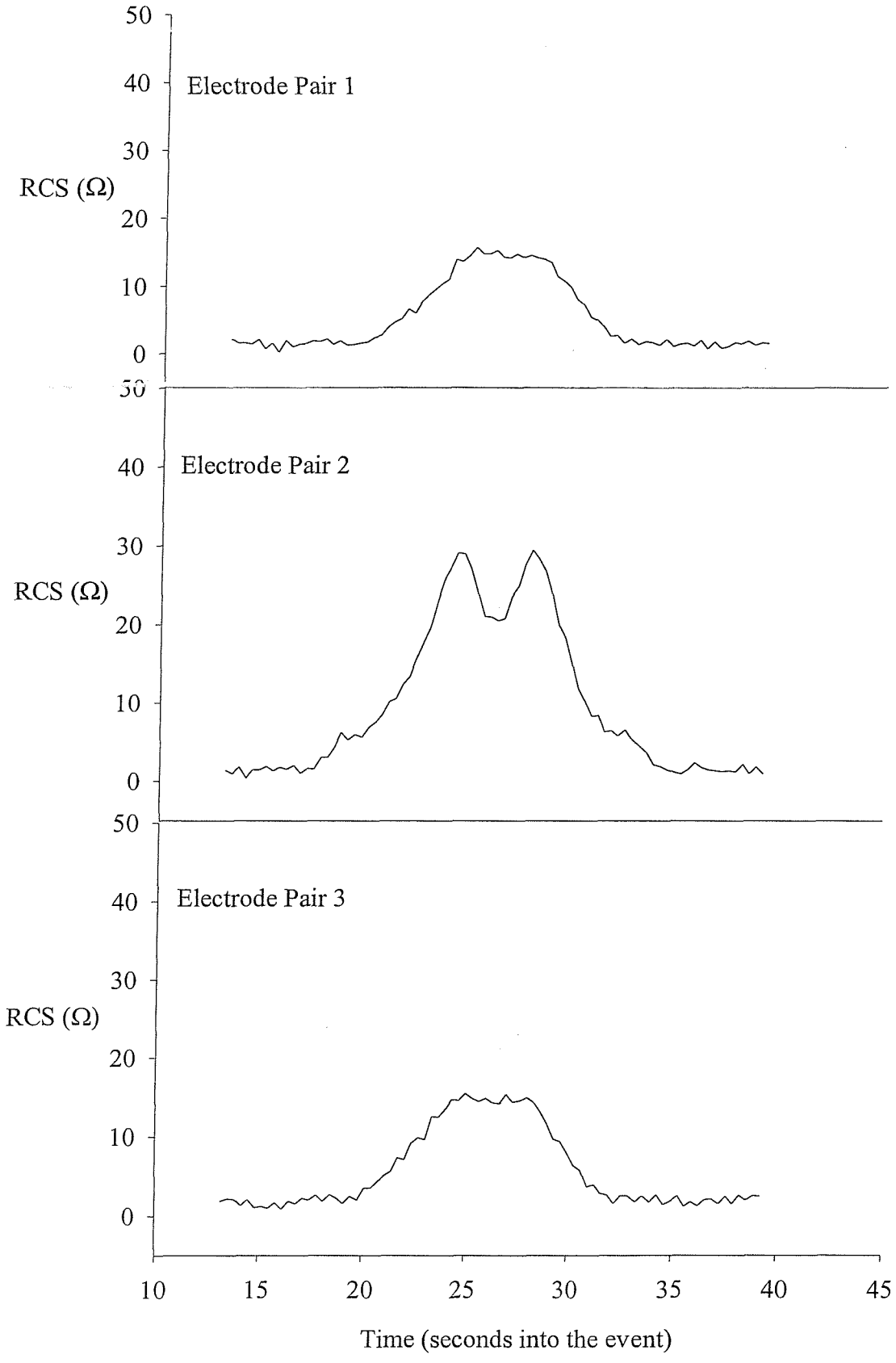

The results of these dynamic tests are presented in Table 26 RCS measurements from all electrodes of moving rod targets, which shows the RCS measurement with the target in the estimated central longitudinal position. A scatter plot of this data suggested a linear relationship between 10.log RCS and target range for each length of rod target (see Figure 54). Linear regression of these data provided the estimates of y intercept and slope tabulated in Table 27[α]. As previously noted in section 4.4, curves of 10·log RCS versus target range for different target lengths show similar slope but were displaced on the RCS (y) axis. An assumption was made that the slope of all of the linear relationships above were the same and that sensor noise had contributed to an error in the estimation of the slope *b* of Table 27 for the 306 mm target.

To test this assumption the slope of the linear model for the 306 mm target was constrained[β] to -0.00754 10·log Ω mm^{-1} and the *y* intercept (*a*) recalculated for maximum fit to a linear model. The product of this recalculation was a revised estimate of $a_{306} = 5.3$. This revised estimate was then plotted on Figure 55, which indicates the confidence limits for each estimate of *a*. The revised estimate of a_{306} was observed to fall within the confidence limits calculated and therefore may be a more accurate estimate for future calculations.

[α] Sigmoidal models were fitted to the data but failed to fit the data better than a simple linear model. The linear model was therefore adopted for simplicity.

[β] The average of the estimated slope *b* for the 700 and 500 mm length targets.

The linear relationship described by Figure 53, using the revised estimate of a_{306} showed a good fit to a linear model and is described below:

$$\lambda_0 = 0.0193\,\varphi \qquad \textit{Equation 5}$$

Where

φ = the length of the target in mm

$[r = 0.97, r^2 = 0.94]$

Using logged measurements of RCS with rod targets of known length at known range from the plane of the sensor array it has been possible to construct similar mathematical models to those calculated from static targets in chapter 4. Such revised models may then be used for estimation of target length from RCS measurements alone in the manner described by chapter 5.

Table 26 RCS measurements from all electrodes of moving rod targets

Target length (mm)	306		500		700	
	Target range (mm)	10.log RCS (10.log Ω)	Target range (mm)	10.log RCS (10.log Ω)	Target range (mm)	10.log RCS (10.log Ω)
	50	3.711	50	10.212	50	13.021
	50	3.892	50	10.414	50	12.967
	100	4.698	100	10.128	100	12.492
	100	5.250	100	10.492	100	12.753
	150	3.522	150	9.638	195	11.477
	150	4.065	150	9.890	195	11.523
	150	4.914	200	8.921	195	11.222
	304	2.041	200	9.269	195	11.430
	304	3.010	304	8.976	245	10.755
	304	3.522	304	8.710	245	11.173
	304	3.222	304	8.513	304	10.969
	316	2.672	304	8.129	304	11.181
	316	2.553	316	9.191	304	11.139
	316	3.424	316	9.085	304	11.399
	316	3.424	316	8.513	316	10.952
	335	3.617	316	8.865	316	10.934
	335	2.672	335	8.633	316	11.089
	335	3.522	335	8.451	316	11.139
	335	4.232	335	8.129	358	10.170
	335	2.672	335	8.028	358	10.170
	335	1.903	361	8.195	358	10.086
			361	7.959	358	10.065
			361	7.782	358	10.334
			361	7.520	358	10.626
					358	10.191
					358	10.212
					387	10.828
					387	10.952
					387	10.414
					387	9.868

Figure 54 Linear regression plots of RCS measurements from all electrodes of moving rod targets

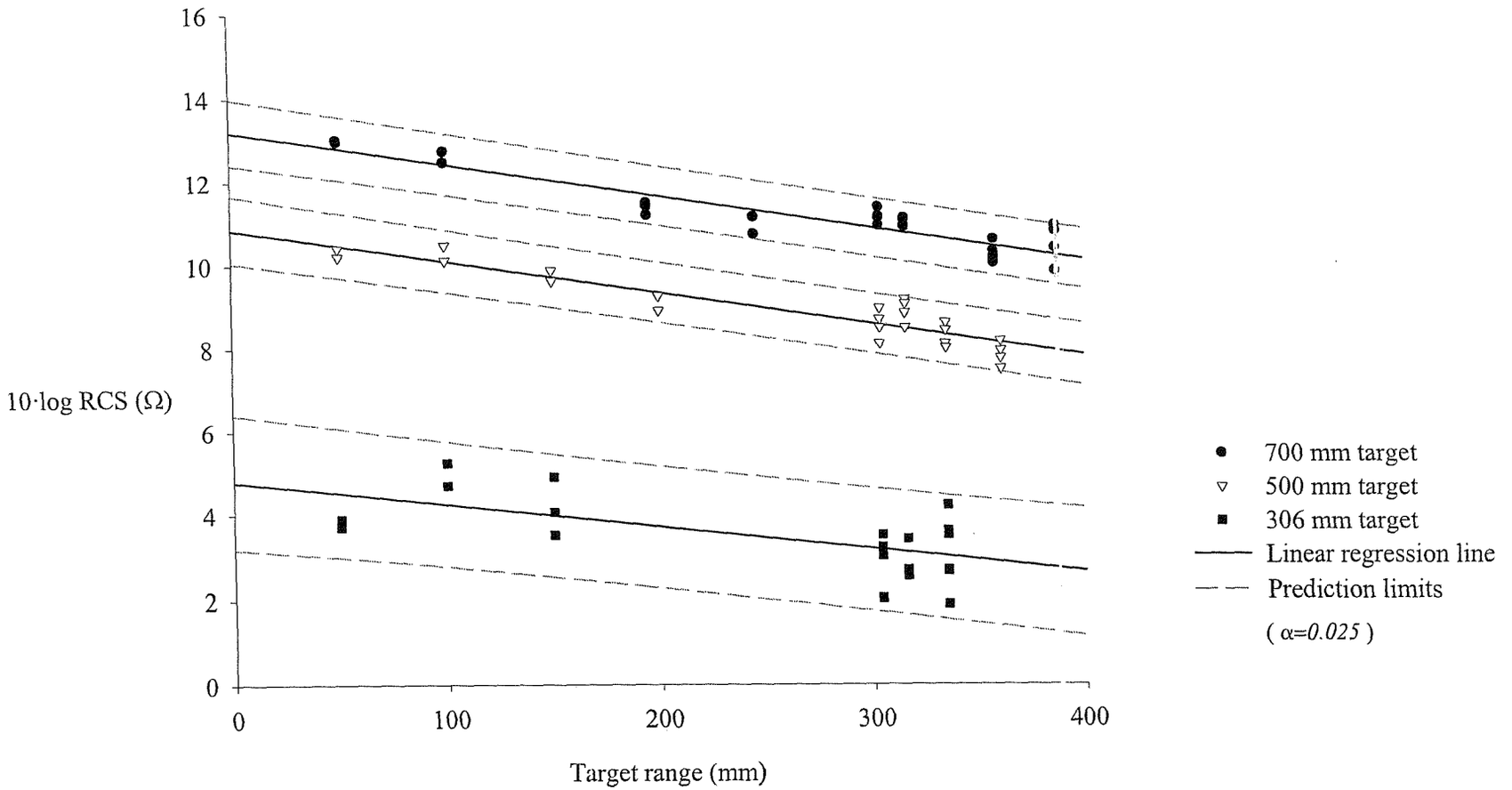

Table 27 Linear regression parameters for target range versus 10·log RCS measurements

Target length (mm)	a 10.log Ω	Standard error of the mean 10.log Ω	Confidence interval (α= 0.025) 10.log Ω	b 10.log Ω mm^{-1}	Standard error of the mean 10.log Ω mm^{-1}	n	r	r^2
700	13.19	0.19	0.3724	-0.00532	0.00144	21	0.65	0.42
500	10.86	0.19	0.3724	-0.00749	0.00069	24	0.92	0.84
306	4.78	0.39	0.7644	-0.00759	0.00062	30	0.92	0.84

Figure 55 Plot of regression intercept against rod target length for moving targets

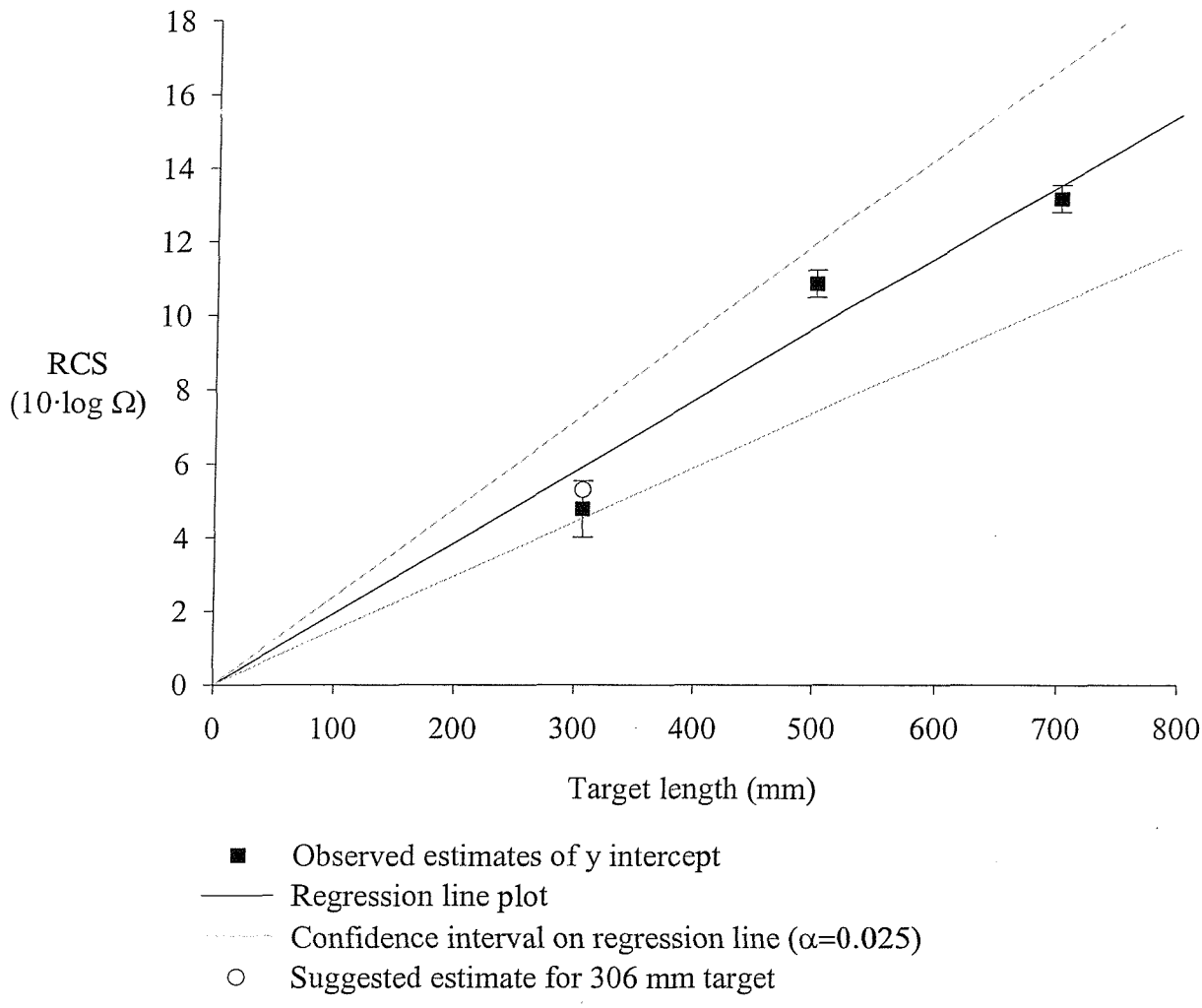

Error bars indicate the standard error of the mean n ≥ 21

6.3 Dynamic Live Fish Measurements

To further establish the suitability of the resistivity sensor system used for the dynamic stainless rod tests (section 6.2) for use as a migratory fish sensor, live Atlantic salmon were allowed to swim over the sensor array. Resistance change signals were recorded from each electrode and stored as described in section 6.2. The water conditions were very similar to those for the previous dynamic RCS measurements[α] and therefore no change was required in the excitation current of the sensor (708 μA).

Two miniature video cameras were positioned to observe the electrode array, one camera from above and the other from side aspect at *circa* 250 mm depth. The video signal from each camera was time division multiplexed using a proprietary video multiplexer and the combined signal recorded by video recorder at 25 frames per second. Two 20 W dichroic security lamps, fixed above the test tank, provided artificial lighting.

The salmon used in the experiment were adult male salmon kelts, which were about to be released to the wild. The males were used since their body mass was less affected by the gamete stripping process that had been carried out prior to their release. To calm the individuals they were partially anaesthetised using 2-phenoxy ethanol (0.2 mg l^{-1}) in a 60 l trough-like tank. Each individual was observed closely for signs of an inability to hold position upright in the trough. Once this point was reached the fish was transferred to the test tank and manually held until signs of sufficient swimming activity were noticed. Fish were positioned at approximately half water depth (250 mm) and in a central lateral position before release. After each release the fish was observed to determine if more anaesthesia were required prior to the next release.

[α] Water temperature 3.1°C, Water conductivity 103 μS.cm^{-1}.

If a successful RCS waveform was collected then the fish was lengthed and photographed in a tank marked for the purpose[α] (see Plate 4).

Two male salmon were allowed to swim over the array; fish 1 was measured at 660 mm and fish 2 at 690 mm (fork length). Considerable difficulty was observed in making the fish swim through the array at a speed consistent with migration in river. The fish were mostly either inactive and sank to the bottom of the tank when released or "sprinted" to the far end of the tank. Four RCS waveform recordings were made where the fish swam through the entire array at a low velocity. The first three waveforms were associated with fish 1 and the last with fish 2. Figure 56 to 59 describe these waveforms and Plate 5 shows video still images of a salmon swimming over the array.

[α] Fish were lengthed and photographed in a tank as part of another study which required additional morphometric measurements.

Figure 56 RCS waveform A

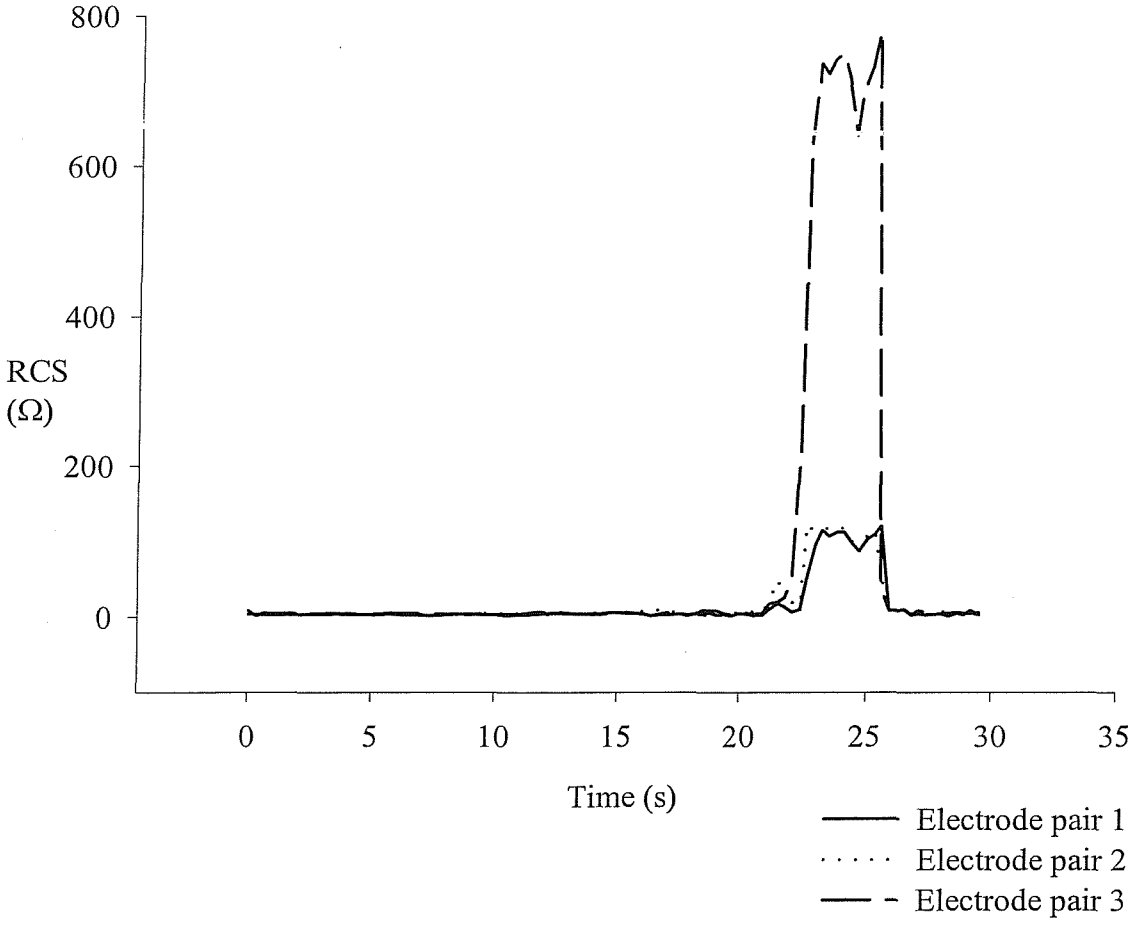

Figure 57 RCS waveform B

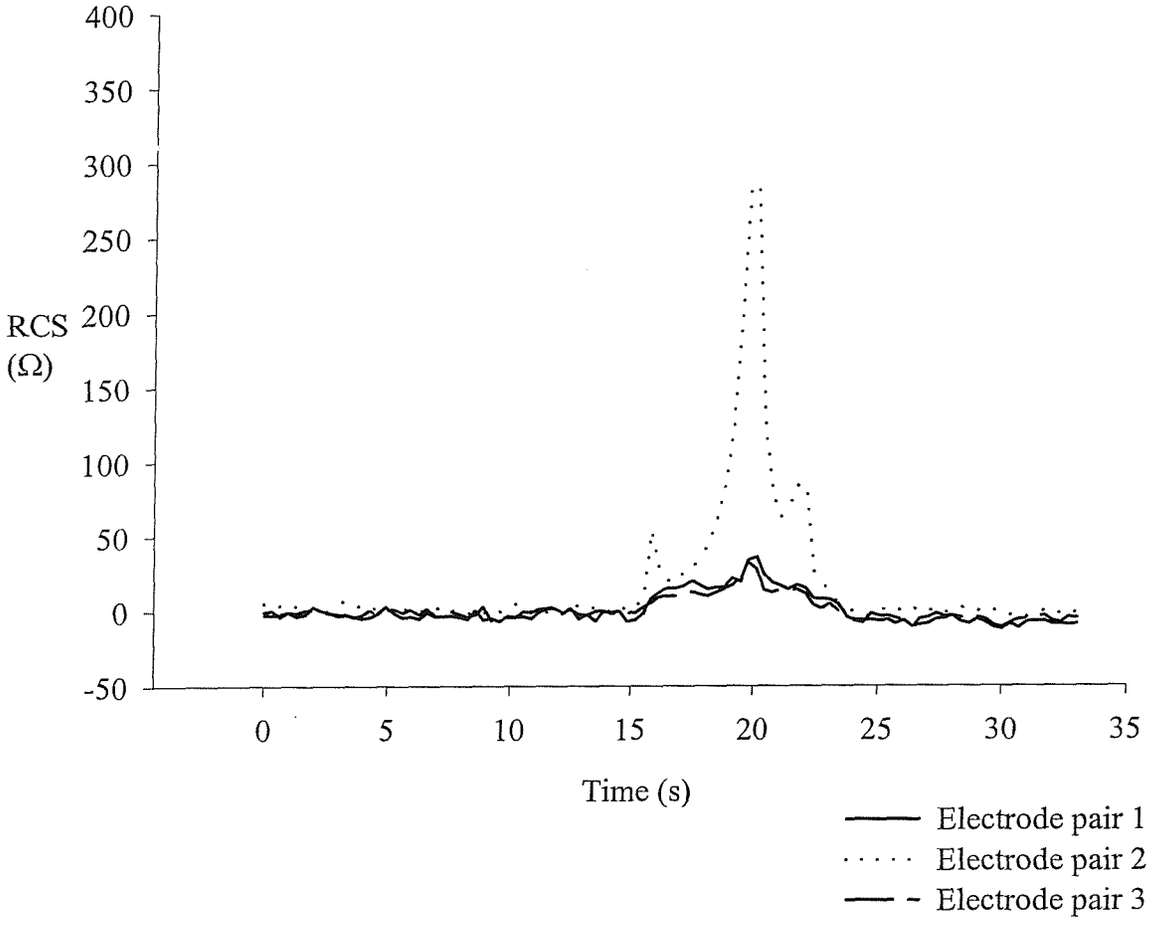

Figure 58 RCS waveform C

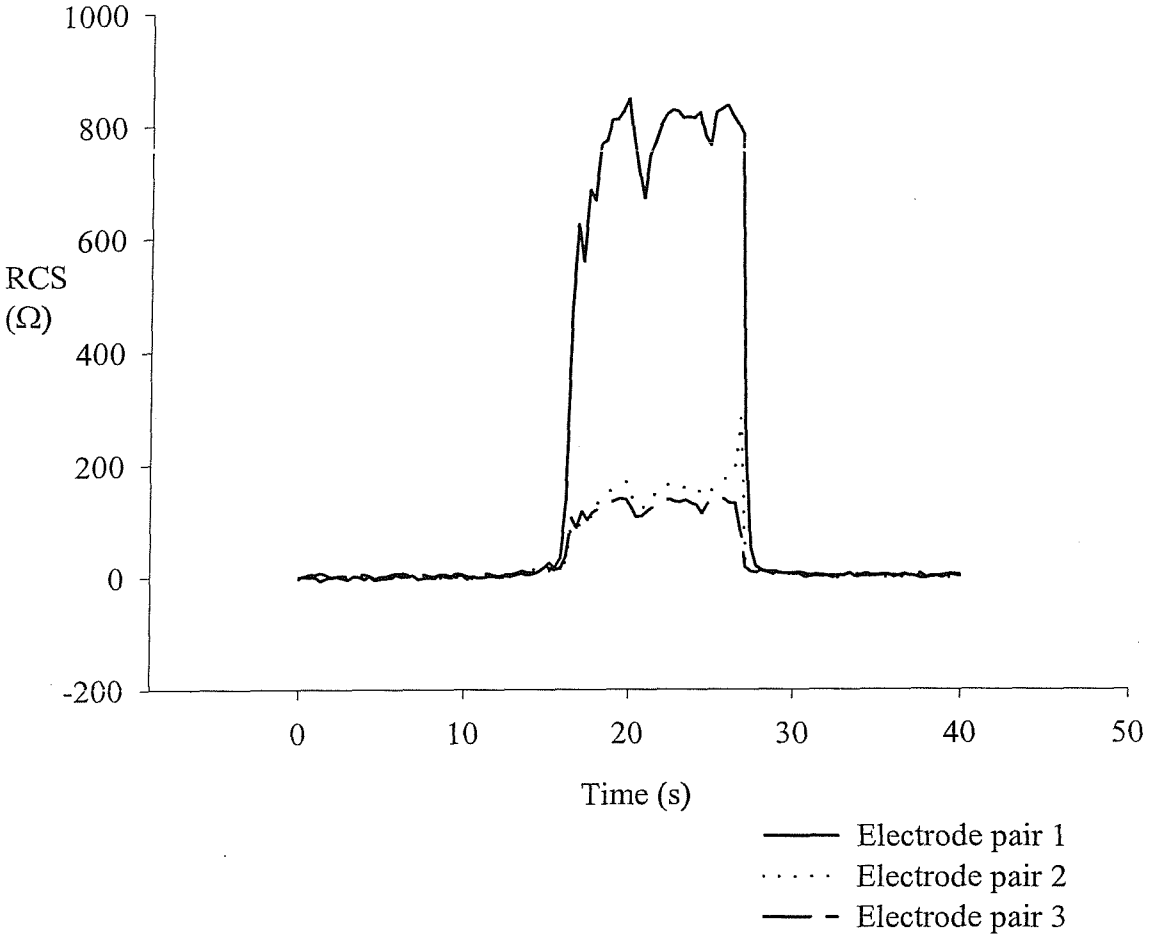

Figure 59 RCS waveform D

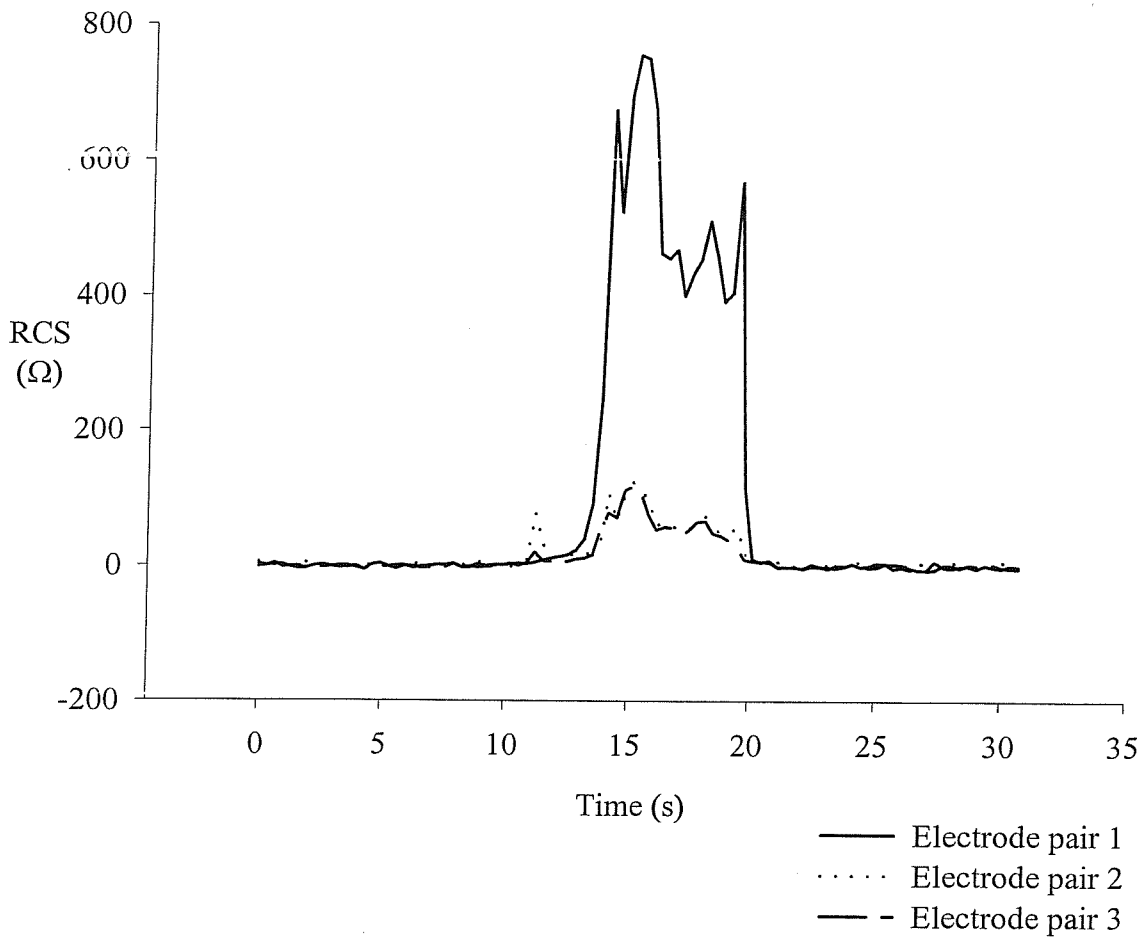

Plate 5 Video still images of fish 1 swimming over the sensor array

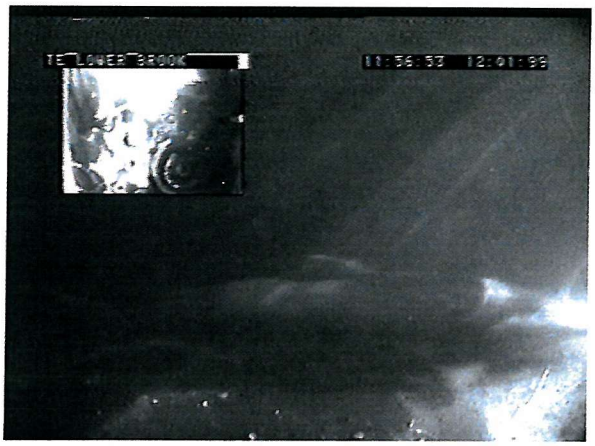

The waveforms presented indicate that salmon size fish can be detected by the sensor array. The magnitude of the peak signals was much larger than anticipated and suggests that earlier tests with freshly killed fish compared with rod targets underestimated the RCS available from live targets. Since the exact position of each fish at the time of each sample was not known it was uncertain if fish had swum into very close proximity to some electrodes. This might explain the observation that, in general, only one of the six electrodes measured the large RCS, all other electrodes showed more consistent measurements.

The electrode that exhibited the large RCS was not consistently the same and therefore it was unlikely that a connection fault was the cause. The largest signals measured were from electrode pairs close to the sidewalls of the test tank. It is possible that the close proximity of the sidewalls confined the field from the outer electrodes and thus made such zones more sensitive to changes in electrical resistance. This effect was not observed with the dynamic stainless rod experiments, possibly due to the central lateral position of the target track.

6.4 Measurement Error

One objective of operating the sensor array in an external test tank was to determine if more measurement noise was expected under field conditions (section 6.1). To investigate this, samples of resistance measurements with no target present over the array were analysed.

Three samples of ten measurements were taken from when the sensor array was in use in the aquarium (section 3.3) the external tank for dynamic rod measurements and the external tank for dynamic fish measurements. The arithmetic mean and standard deviation was calculated for each sample. Since the magnitude of noise was expected to be proportional to the absolute resistance measured, as the measured resistance modulates the voltage measured at the drive electrode, a standardised measure of noise was computed. In this case, the standard deviation of the ten measurements divided by the mean of the measurements. This ratio was expressed in terms of parts per million

(ppm) for ease of description.

Table 28 describes the noise measurements made and includes the arithmetic mean and standard deviation for each set of samples taken. A graphical representation of this data is presented in Figure 60, which indicates that, the estimates of measurement noise have confidence intervals that do not overlap (α=0.025, n=3). A one-way ANOVA to compare the mean measurement error between the aquarium measurements and the external measurements indicates that each of the error estimates were significantly different from each other (α = 0.05, n = 3, P = <0.001).

The measurements made of fish in the external tank preceded those for the rod targets and therefore the most likely cause of the additional noise was an unnoticed experimental defect. Both of the sets of measurements with the sensor array in the external tank exhibited significantly greater measurement noise than when the array was in the aquarium. Continued development of the sensor system should consider the sources of this increased noise and methods to suppress or remove it.

Table 28 Estimates of measurement noise for each group of tests

	Sample 1 (ppm)	Sample 2 (ppm)	Sample 3 (ppm)	Mean (ppm)	Standard deviation (ppm)
Aquarium	49	53	38	46	7.7
External tank stainless rod measurements	257	284	286	275	16.1
External tank live fish measurements	840	988	869	899	78.3

Figure 60 Plot of measurement error for each group of tests

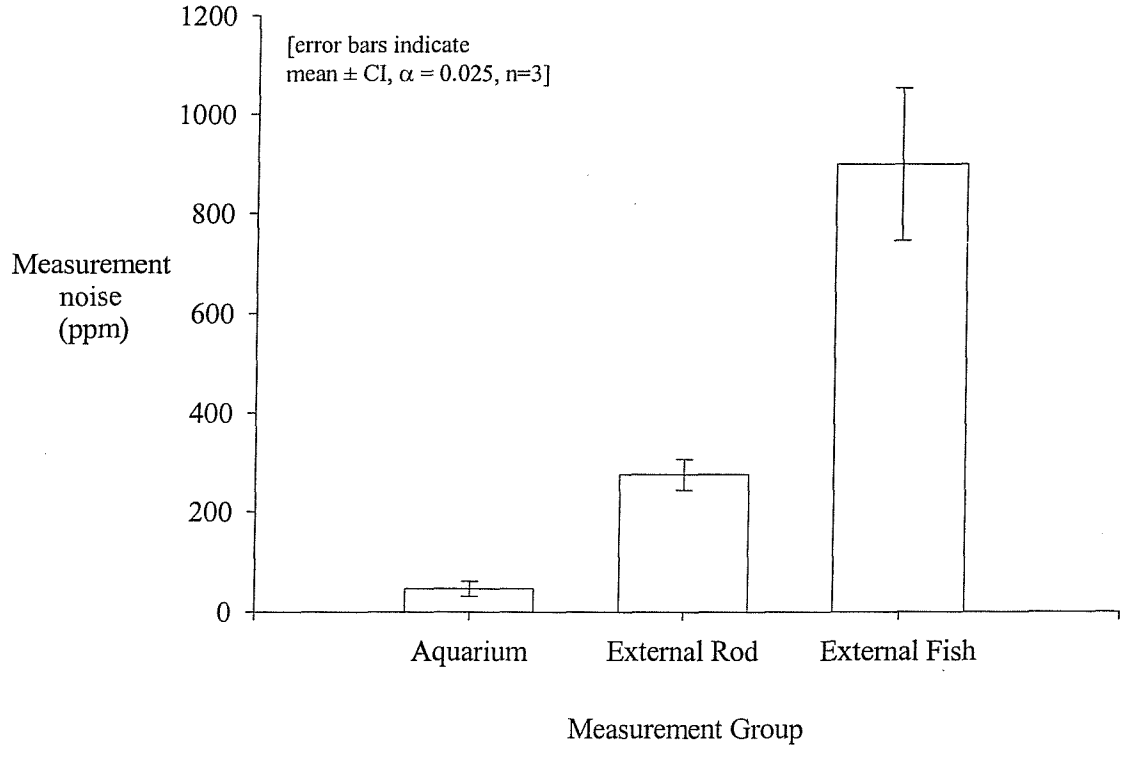

CHAPTER SEVEN

DISCUSSION

CHAPTER SEVEN

7 DISCUSSION

7.1 The Need For High Quality Salmon Stock Assessment

Over the past three decades there has been a substantial decline in the abundance of North Atlantic salmon. Total North Atlantic catches have declined from a peak of *circa* 12,700 t in 1973 to *circa* 2,300 t in 1997 with an especially sharp decline in the late 1980s. Some of this decline in catches may be attributed to increased restrictions on fisheries, which were largely aimed at reducing fishing effort. However, estimates of pre-fishery abundance developed by the International Council for the Exploration of the Sea (ICES) indicate a fall of 46% in the abundance of one-sea-winter stocks and of about 65% in the abundance of multi-sea-winter stocks over a similar period (Hutchinson and Mills, 1999).

In order to effectively manage anadromous stocks under increasing pressure from largely environmental factors, a number of management measures have been taken to reduce fish mortality both in the marine and freshwater environments. In the marine environment, international agreements have removed some fisheries and severely restricted others including West Greenland, the Faroe Islands and northern Norwegian Sea. In the freshwater environment, various factors have been suggested as limiting factors on the success of salmon populations. These include siltation of spawning areas, degradation of river habitat for juveniles, delayed mortality effects of pesticides and commonly discharged chemicals, increased predation and environmental shift due to global warming. To study the effects of any or all of these factors, and to manage stocks under these pressures, high quality stock assessment data is required.

7.2 Salmon Management

In 1994 the North Atlantic Salmon Conservation Organisation (NASCO) recommended that spawning targets be set for all principal rivers in its North East Commission area including England and Wales (NASCO, 1996). Such stock management procedures involve a dynamic approach to the control of fishing effort. Some systems allow a fishery to start only after an agreed spawning escapement has passed through the fishery. In other countries, where the government has less control over fishing access, controls must be set in place long before the fishery starts operating. In England and Wales, controls such as catch and release only fishing before set dates, or the allowance of only certain fishing methods are now related to estimates of a rivers' spawning target. This spawning target is derived from *inter alia* estimates of the carrying capacity of the river in question, survival at sea and the spawning escapement.

Spawning targets can be set based on the catch from recreational fisheries, although the estimation of stock size based on such data can be influenced by a number of seasonal factors. The primary factors include exploitation and reporting rates (Environment Agency, 1996; Davidson *et al.,* 1999). For these reasons, it is recognised that, wherever possible, quality assured independent stock assessment data should be used. This data may be derived from scientific catch data using mark-release methods such as used on the River Dee in North Wales.

7.2.1 Invasive Stock Assessment

In this case a trap is used to examine adult salmon as they enter the non-tidal river. An estimate of catch efficiency is required to convert the number of fish caught to an estimate of the total number of returning fish. This is achieved by releasing some of the fish after the attachment of a recognisable mark, in this case a T-bar anchor tag. Estimates of catch efficiency are then made from the total angler catch and proportion of fish caught with a tag present (Davidson *et al.,* 1999). Quality checks are made using logbooks carried by a group of anglers monitored by the Environment Agency.

Problems associated with this method include some mortality associated with the stress of handling and tagging and some tag loss.

At other trapping sites fish are relocated downstream of the trap and the number of recaptured fish used to estimate trap efficiency. Unfortunately this cannot take account of the problem that fish may subsequently avoid the trap or may be compromised by the stress of handling and relocation.

7.2.2 Non-Invasive Stock Assessment

In contrast, non-invasive methods of stock assessment have little or no effect on the migration or survival of the enumerated individuals. These might include visual counts, optical fish counting, hydro-acoustic survey or resistivity change fish counting. The limitations of the non-invasive methods depend on many factors but it is generally not possible to identify individuals or previously marked fish[α]. Species discrimination by non-invasive automatic fish counting methods is not as accurate as with manual inspection, but in many cases, especially where side-aspect visual images are present, species discrimination may be over 90% (Fewings, 1998).

Another limitation of non-invasive fish counting techniques is the relative lack of resolution and accuracy in the determination of fish size. This aspect of stock assessment can be particularly important for species discrimination and for the assessment of the age structure of the populations of fish in question. In this latter regard, population age structure determination from angler catches is considered unreliable and therefore determination from a less biased source has been recommended (Environment Agency, 1996).

[α] Some tags can be read remotely such as the passive integrated transponding tags but their range is limited. Coded radio tags have a greater range but are larger and more expensive.

A typical error for the estimation of fish length where the fish can be handled is of the order of 2 mm for fish of 250 mm in length, or 0.8%. For fish observed by optical fish counting methods the biomass estimation error has been quoted at <5% for single fish using a counting tube and image analysis software[α] (Fewings, 1994). The "Vaki River Watcher" fish counter uses an array of light beams to achieve a lengthing error at *circa* 10% (Vaki Aquaculture Systems Ltd., *pers comm*[β].). Beach (1978) estimated the error associated with lengthing fish from above using closed circuit video at ≤ ± 14% (95% CI, fish length >381 mm).

Fish size estimation using resistivity change can be considered of intermediate resolution when compared to optical detection methods since estimates of lengthing accuracy vary from ± 12% (Fewings, 1988) to ± 62% (Nicholson *et al.*, 1995) largely dependent on the particular site conditions. Both of these estimates assume a mean length of the fish sampled of 650 mm.

Hydro-acoustic methods of fish sizing are considered to have generally poor accuracy in terms of fish size estimation compared to the former methods. Many relationships exist between the intensity of the backscattered sound from a fish target but these all appear to be based on measurements made of tethered or restrained fish. Researchers in this field (Ransom, *pers comm*[χ]) accept that the estimates obtained in this manner must be treated with caution when translated into estimates of fish length for fish swimming free in a river. More realistic estimates of acoustic target strength are likely to become available as measurements from radio-tagged fish released in the study site and photogrammetric measurements of wild fish are related to observed acoustic target

---

[α] Reson System Ltd. Image processing fish counter.

[β] (1993) Referring to evaluated performance of the "River Watcher" fish counter.

[χ] (2000) Referring to the use of hydro-acoustic fish counters for the estimation of fish length.

strength. At present no estimates of lengthing accuracy are available for hydro-acoustic fish counting.

It is therefore desirable for improvements in the understanding of salmon stock dynamics and salmon management to have available a tool that enables the non-invasive monitoring of such populations. Such a tool would be most useful if it had the ability to operate without an expensive host structure and was able to estimate the size of individual fish with greater accuracy than the non-invasive methods described previously.

7.3 The Present Study

In this study, investigations have been concerned with characterisation and improvement of the electrical resistance change method of fish detection. This method, first described by Lethlean (1953) has been shown to detect fish of adult salmon size with high accuracy (Beach, 1978; Brassington, 1981; Fewings, 1988; Nicholson *et al.*, 1995) but shows poor fish size estimation characteristics. Numerous authors have described the reasons for this poor fish size estimation performance (Kristinsson and Alexandersdóttir, 1978; Lawson, 1975; Nicholson *et al.*, 1995; Dunkley and Shearer, 1982) as a combination of water conductivity changes, the depth of water and the range of the fish from the sensor electrodes.

7.3.1 Water Conductivity

In the case of changes in water conductivity, the magnitude of resistance change that occurs when a resistive target passes over sensor electrodes is inversely related to the conductivity of the water (Dunkley and Shearer, 1982).

The reason for this increase in sensitivity is due to the way in which parallel resistances combine to produce a composite resistance. When two electrical resistances are connected in parallel the combined resistance can be estimated as the reciprocal of the sum of the reciprocals of the constituent resistances (Horowitz and Hill, 1989) (see *Equation 6*). Therefore any effect that increases the water resistance (R_{Water}) between

sensor electrodes has the effect of increasing the change in resistance due to a given large additional parallel resistance, in this case a fish. A reduction in the conductivity of water over the sensor electrodes increases the electrical resistance can cause such an increase in the inter-electrode resistance.

$$\frac{1}{R_{Combined}} = \frac{1}{R_{Fish}} + \frac{1}{R_{Water}}$$

Equation 6

A reduction in river water conductivity often occurs during sudden increases in river discharge due to the contribution of relatively low conductivity rainwater run-off. This is also an important time for the migration of salmon since their spawning migrations are often associated with an increase in river discharge (Banks, 1969).

7.3.2 Water Depth

In contrast to the effect of changes in water conductivity, an increase in water depth causes a reduction in the inter-electrode resistance (R_{Water}) and therefore a decrease in the sensitivity of resistive target detection. At times of increased river discharge, water depth over a fixed fish counting site is often increased, therefore leading to a reduction in detection sensitivity (Nicholson *et al.*, 1995). A combination of these two opposing effects during periods of high migratory activity can therefore lead to variability in the sensitivity of detection. Nicholson *et al.* (1995) observed that 31% of the variability in resistance change measurements were accounted for by the water depth.

Changes in water conductivity and depth cannot be relied upon to maintain a constant sensitivity through fortuitous cancellation since water conductivity and river discharge are often only partially correlated (Fewings, 1988) and variable between river catchments. In addition, the relationship between water depth over fish counter

electrodes and river discharge is variable between counting sites.

7.3.3 Fish Swimming Range

The range of a fish from the fish sensor electrodes has been shown by many to substantially affect the magnitude of the resistance change detected (Kristinsson and Alexandersdóttir, 1978; Lawson, 1975; Simpson *et al.*, 1975; Dunkley and Shearer, 1989). Estimates of the range at which a 50% reduction in the maximum signal for a given fish size vary from 100 mm (Lawson, 1975)[α] to 220 mm (Kristinsson and Alexandersdóttir, 1978)[β]. These authors also indicate that this range dependence of resistance signal magnitude is also dependent on electrode separation. Lawson (1975) presents data that suggests an increase in electrode spacing from 450 mm to 750 mm increased the 50% signal reduction range from 100 mm to 220 mm. The negative aspect of this increase in electrode separation was that small fish were relatively more difficult to detect.

7.3.4 Electrode Length

One other factor that can affect the sensitivity of a resistance detection system is the length of the electrodes (Simpson *et al.*, 1975). Longer electrodes have a similar effect to an increase in water conductivity, the background water resistance decreases. Therefore when a fish passing over the electrodes forms a parallel resistance the resultant change in resistance appears smaller.

[α] Using 450 mm spaced electrodes and a 660 mm fish.

[β] Assumes a 500 mm fish with 500 mm spaced electrodes.

7.3.5 Site Selection

With these limitations in mind most open-channel resistivity change fish counters have been sited on weirs or in fish passes which encourage fish to swim close to the sensor electrodes. Observations of fish swimming depth over Crump weirs (Dunkley and Shearer, 1989) indicate that upstream migrants predominantly swim near the channel bed, Simpson (1978) found that *circa* 87% of fish swam within 160 mm of the channel bed in an available water depth of 700 mm. Similar behaviour was observed by Dunkley and Shearer (1989) and was explained as a behavioural method of conserving energy since lower water velocities were found near the bed of the channel. Downstream migrants were more widely distributed throughout the water column (Hellawell *et al.*, 1974; Dunkley and Shearer, 1989).

When salmon have been observed in open river conditions where the water velocity was lower than on a Crump weir, similar energy conservation behaviours have been noted. Lévesque *et al.* (1996) found that 95% of salmon swam within 350 mm of the river bed even though the water depth was near 3 m. It was concluded that the majority of salmon had selected the swimming depth in order to minimise the velocity of water flowing past them, in this case water velocities <0.8 ms^{-1}. Webb and Hawkins (1989, cited in Lévesque *et al.* (1996)) reported that Atlantic salmon tended to avoid the areas where velocity was greater than 1 ms^{-1} or traversed them by burst swimming. Salmon were also observed to swim closer to shore as river discharge increased ($P = < 0.05$) Lévesque *et al.* (1996).

Such observations therefore suggest that an electrical resistivity fish detection system operated on the bed of a river could have some advantages over existing systems located on weirs and in fish passes. These advantages could include a more stable resistance environment, less water surface noise effects and lower installation costs. The use of existing strip electrode type sensor systems in such locations does create some new challenges. Without any form of fish range compensation, the size estimation capability of the system would probably be compromised by the wide variation in resistance change signal due to fish swimming depth relative to the electrodes. Lawson (1975) suggests that at a range of 350 mm the resistance signal

could be reduced to only 25% of the near electrode signal.

7.4 A Prototype Fish Counting System

7.4.1 Concept

In an effort to address some of these challenges this investigation has attempted to develop a prototype fish detection system that could operate at open river sites and still estimate the size of fish with accuracy at least as good as existing electrical resistivity fish counters. In the first instance, a sensor system was required that could span a range of channel widths without a degradation in sensitivity as experienced with strip electrode type systems. To this end, point electrodes have been investigated instead of strip electrodes. A point electrode system has the advantage that system performance is not degraded as the width of the channel sampled increases. To increase the width of monitored channel more sets of electrodes may be added laterally.

7.4.2 Resistance Sensor

During the course of the investigation two different methods of resistance measurement were designed and tested. The first sensor circuit used circuit designs utilised in the medical field of EIT. In that field, electrical resistance measurements are made by injection of an electrical current, using point electrodes, and the simultaneous measurement of the spatial distribution of voltages on the body. These voltages are then used to construct images that represent the electrical impedence of tissues in the monitored area (Webster, 1990). Damaged or diseased tissues often exhibit different impedence characteristics to healthy tissues thereby aiding diagnosis. The demands of such techniques have led to the development of high performance circuits for the measurement of electrical resistance.

In the particular application of monitoring resistive targets within a body of relatively poor conductivity liquid a more simple approach was adopted to minimise the number of electrodes required. In this case a constant current was injected into the water by a point electrode, other electrodes were used as the ground or return path for the circuit. Under such conditions the voltage required to drive the required current was in linear proportion to the electrical resistance between the electrodes (see section 2.3). In this

type of resistance measurement it is important to maintain a very stable amplitude signal source with which to drive the electrode system, since fluctuations in signal source amplitude cause measurement noise. The circuit utilised was shown to exhibit *circa* 14 bit accuracy or measurement of ± 0.1 Ω in 1,600 Ω.

A significant problem with this method of using a continuous signal source to provide a measurement signal that was then processed using analogue circuitry to provide the resistance signal related output was that the signal could not be switched easily between electrodes. The analogue circuitry required a finite amount of time (*circa* 1.3 s) to settle before stable signals were output that would prevent the rapid scanning of many electrode pair "cells".

To overcome this electrode-switching problem a second resistance sensor was developed that utilised some of the circuits developed for the first sensor. This latter sensor used a sequence of square wave pulses generated by a digital to analog converter to provide the current drive for resistance measurements. Since the pulses were generated digitally it was possible to synchronise voltage measurements to coincide with the peak of the pulses. With synchronised measurement there was no requirement for low-pass filter circuits and therefore electrodes were sampled at a rate of *circa* 18 times a second.

7.4.3 Noise Suppression

Effective suppression of power supply interference was achieved using a digital notch filter as described in section 2.7.2. The digital notch filter was designed to average a precise set of samples that were collected over half of the period of one power supply oscillation. The effect of this averaging was to selectively suppress noise of that frequency. None of the electrical resistance change fish counting systems to date have used such a system of digital current pulse measurements to measure inter-electrode resistance since there has not been a requirement with strip electrode systems to switch electrodes dynamically. The accuracy of this sensor system was estimated at 275 ppm

when used in a large external tank (see Table 26)[α]. Since all of the existing resistance change fish counters measure a differential resistance the two types of systems cannot be compared simply in terms of electronic accuracy.

7.4.4 Measurements of Resistive Targets

When RCS measurements were collected of stainless steel rod targets and freshly killed fish targets a similar relationship between the RCS and target range was observed except at ranges less than 0.1 m. The magnitude of RCS was observed to decrease as the range of the target was increased.

This relationship was similar to that observed by Lawson (1975) and Simpson (1978). One notable difference between the relationships above and that found in this study is that the point at which a 50% reduction in RCS was observed was at the greater range of *circa* 300 mm[β]. This was most probably due to the wider separation of the electrodes compared to that in the previous studies. This is consistent with the observations of Kristinsson and Alexandersdóttir (1978), which includes estimates of relative sensitivity associated with the relative range. Each parameter was measured relative to the electrode spacing and suggests that for a fish length of approximately the separation of the electrodes, the 50% RCS range is equal to *circa* 0.4 times the electrode separation. This estimate of 360 mm using the Kristinsson and Alexandersdóttir (1978) approximation compares favourably with the observed estimate for a freshly killed migratory trout of 300 mm.

The dissimilarity observed between fish and metal rod targets (see section 3.2.1) has not been explained but may be related to the marked differences in resistivity and

---

[α] Table 26 shows another estimate of measurement accuracy substantially poorer than 275 ppm, this alternate estimate was associated but undiagnosed experimental problem.

[β] Minimum target range 100 mm.

surface area of the two types of target. With the metal rod targets, the surface area of the target may become a limiting factor in the mechanism by which electric potentials in the water were coupled to the low resistivity target. Near the plane of the electrodes where the electrical potential gradients were expected to be greatest good electrical coupling may not have been possible with the low surface area rod targets. This hypothesis could be tested using targets more like fish in terms of the volumetric resistivity and surface area. An initial suggestion might be to construct targets from a substrate like graphite or carbon fibre in fusiform shapes like salmon. The development of more realistic resistive targets may provide a means by which existing and future resistance change fish counters could be calibrated.

7.4.5 Resistance Change Signal and Target Range

The relationship between RCS and target range has been shown in four sets of measurements (sections 3.2, 3.2.3, 3.3 and 6.2) to exhibit similar characteristics. The RCS measurements decreased with increasing range from the plane of the sensor electrodes. When the RCS data was transformed using a logarithmic transform the relationship between RCS and target range was substantially linearised.

When curves for each target length tested were plotted as in Figure 33, each curve was offset on the y-axis by a value proportional to the length of the target (see section 4.4). Similar curves were observed when RCS measurements were made using alternate electrode separations. In that case, the slope of the transformed signal was inversely proportional to the electrode separation (see section 4.5). As noted previously, this indicated that the rate of RCS reduction per unit range increase was smaller with larger spaced electrodes.

7.4.6 Environmental Compensation

The effect of water depth on these curves was to shift the curves in a positive direction on the y-axis as water depth was decreased. This pattern of an increase in sensitivity as the depth of water was reduced is also consistent with observations of the performance of strip electrode resistance change fish counters. The nature of the shift has not been

investigated further but appears non-linear as more shift is evident per unit decrease in water depth at lower water depths.

The effects of water conductivity were investigated but experimental faults led to errors in the collection of data at lower water conductivity. The general terms, a similar effect to that caused by changes in water depth was observed. Specifically, the curves were displaced in a positive direction on the y-axis with a decrease in water conductivity. This effect has also been observed using strip electrode resistance change fish counters (Dunkley and Shearer, 1982).

These observations could therefore be used to provide the framework for a mathematical model that relates environmental parameters such as water depth and conductivity to a correction shift for the RCS measurement – target range and target length curves. Since the slope of the curve was proportional to the separation of the electrodes it may be considered a constant for a given installation. This represents a simple approach to environmental compensation that can take into account a number of variables that are not adequately compensated using present fish counting systems. Nicholson *et al.* (1995) describes the performance of the 'Logie' resistivity fish counter at multiple sites with particular reference to the effects of water depth and water conductivity.

The operation of the 'Logie' counter involves a calibration facility during which the fish counter introduces a fixed resistance between pairs of electrodes to simulate the passage of a fish. The signal gain of the fish counter was altered using iteration to provide a constant output signal for the calibration resistance. Nicholson *et al.* (1995) showed that even with this calibration procedure 31% of the variance associated with the RCS output by the fish counter was due to variation in water depth. It was also noted that less than 1% of the variance in RCS was associated with changes in water conductivity and as such it is uncertain if the calibration feature led to the minor influence of water conductivity. Formulation of the models proposed above could solve this problem for existing strip electrode fish counters.

If strip electrodes were placed across a river channel with a variable cross sectional profile then different sensitivity of fish detection could occur dependant on the depth of water over the electrodes nearest the fish. If multiple sets of point electrodes were used then a compensation factor could be applied to each pair of electrodes related to the depth of water above them. Such a scheme could substantially reduce inconsistencies in the detection and size estimation of fish. Another method of limiting the effects of water depth on RCS measurements would be to ensure the water depth was substantial at all times. Under such circumstances, minor fluctuations in water depth would be unlikely to affect RCS measurements since the proportional change in water depth is minimised.

7.4.7 Target Range Compensation

For any river-bed mounted sensor system to function adequately it is likely that some form of target range compensation would be required. If sensor systems similar to that used previously (Kristinsson and Alexandersdóttir, 1978; Lawson, 1975; Simpson *et al.,* 1975; Dunkley and Shearer, 1989) were used, with their 50% loss of signal over a range of ≤ 200 mm, then it is likely that a fixed threshold detection criterion would exclude substantial proportions of fish. In particular, fish swimming downstream have been shown to be counted less accurately because of this effect (Dunkley and Shearer, 1989; Smith *et al.,* 1996). Upstream migrants have been observed to predominantly swim near the channel bottom when ascending weir structures but downstream migrants showed a different vertical distribution. Downstream migrants were distributed more randomly in the vertical plane, which led to a greater probability of an ascending fish that then drops downstream being counted up but not down.

In some cases, a potential solution would be to increase the sensitivity of the counting system. This could only improve the count accuracy under conditions of low background noise and where only fish of the target species were present that were of sufficient size to be counted. A likely consequence of this approach would also be to degrade the performance of length estimation from RCS due to an acceptance of a greater range of RCS sizes for a given fish size.

A better solution to the problem would be the inclusion of a scheme to scale the RCS signals according to their range from the sensor array. Under such a scheme the difference in counting accuracy between upstream and downstream migrants would be reduced since the swimming depth bias could be substantially removed.

This study has attempted to develop and evaluate potential methods for undertaking such target range compensation. Chapter 5 considers two potential methods of target range compensation. The first and simplest method called coaxial range compensation measurement utilised the different RCS with range relationship between electrode separations of 500 mm and 900 mm to calculate a range to the target. The alternate method uses measurements from three parallel pairs of electrodes to estimate the best match with model predictions. The combination of position and target length with the best match was then used as the estimated target length. This method was called trilateral range compensation.

Coaxial target range compensation was shown to provide reasonable estimates of target range for 400 and 600 mm targets up to a range of approximately 400 mm. At ranges greater than this the background noise contributed to substantial errors in target range estimation. When such range information was used to calculate the target length some improvement in target length estimation was evident. For the 400 mm target the average length estimation error was 47 mm with target range compensation and 58 mm without. When simulated with the 600 mm target the average length estimation error was 92 mm with target range compensation and 247 mm without. These tests considered the two targets at ranges between 50 and 950 mm.

The method does show some potential for target range compensation but is limited by the magnitude of RCS measured by the smallest electrode separation used. The rate of signal reduction with range was inversely proportional to the separation of the electrodes (see section 4.5), therefore the signal measured by the smallest separation electrodes can become obscured by noise at relatively small range. This is likely to be a primary limiting factor for the technique unless experimentation indicates that the difference in electrode separation required for useful target range determination can be

reduced from 400 mm. Thus the minimum electrode separation could increase to 700 or 800 mm with a resultant increase in the maximum detection range.

The specific method tested in this study used a mathematical transform of the RCS measurements to calculate the range of the target. This approach may have been too prescriptive and therefore may have contributed to the poor performance of the tests. An alternate approach, which may prove more reliable, could use an iterative method to test a range of simulated targets, generated by the model relationships of section 4.5, at different positions away from the electrodes. This method has the potential to operate in a more flexible fashion than the mathematical method tested.

Trilateral target range compensation involves the use of an iterative algorithm combined with a model that describes RCS for varied target length at range from the plane of three pairs of sensor electrodes (see section 5.2). Repeated comparisons of measured RCS signals were compared to those derived from a model in a simulation that introduced realistic levels of measurement noise. The results of these tests showed that reliable estimates of target size were achievable even outside the confines of the array.

The error associated with estimation of target length was influenced by a number of factors including the length of the target, the lateral displacement of the target, the elevation of the target from the plane of the electrodes and the underlying level of measurement noise.

Smaller targets gave rise to greater uncertainty of target length probably due to the proportional influence of measurement noise in relation to the magnitude of the RCS measured. As a result, targets of 300, 500 and 600 mm exhibited length error confidence intervals of 29 to 170 mm, 0 to 108 mm and 0 and 38 mm respectively ($\alpha = 0.025$, $n = 20$). The targets were simulated at displacements of up to 600 mm from the centre pair of electrodes and 700 mm from the plane of the electrodes. Since the imposed measurement noise introduced measurement variability into the data the measurement accuracy maps did not exhibit regular patterns (see Figures 39 to 43) and

numerous points of unusually high accuracy and unusually poor accuracy were evident. For comparison with conventional resistance change fish counting systems this represents a substantial increase in lengthing accuracy. The smallest length estimation errors reported for strip electrode systems are *circa* ± 100 mm (Fewings, 1988, [1.96·σ]) and ± 250 mm (Nicholson *et al.,* 1995, [1.96·σ]) where fish were normally constrained to swim within 500 mm of the electrodes.

In general terms, the greatest accuracy was observed between the centre pair of electrodes and the outer pair. When larger targets were considered (600 and 700 mm) sub-optimal length estimation was observed when the targets were near the central axis of the array. A possible explanation for this observation is that with large targets the ratio of measurement noise to the real measurement was small and therefore a target on the central axis produced two measurements that were very similar and a third relatively large signal. This may have represented an ambiguous set of measurements that was replicated by adjacent target positions in the iterative algorithm thus leading to an additional source of target length estimation error.

When the target elevation at which another target 100 mm larger could still be resolved was plotted against target length it was noted that these parameters were not independent; longer targets were resolved at greater range. The variability in this reliable detection range also increased with the length of the target. The reasons for this observation are unclear.

One further measure of the effects of range compensation was to compare the lengthing error associated with the RCS measurements used in the trilateral target range compensation simulation for range compensated and uncompensated estimates. As a benchmark, a target length of 500 mm was tested at simulated ranges of 20 to 670 mm on the central axis of the sensor array. Without target range compensation the mean estimated target length was 553 mm (CI, 408 to 698 mm) and with trilateral range compensation the estimated target length was 498 mm (CI, 449 to 548 mm). The incorporation of trilateral target range compensation therefore decreased the error associated with target length estimation by a factor of 2.93. It was therefore considered

that the method was highly successful and could represent a useful operational technique for future development.

7.4.8 Tests with Moving Resistive Targets

The final set of experimental tests were carried out to determine if the system developed during the course of this study could operate in field or near-field conditions. The experiments involved the measurement of RCS from a six-electrode array placed on the bottom of a large external water tank. Stainless steel rod targets were moved over the array using a carriage and track as described in section 6.2 to determine if RCS measurements were possible for moving resistive targets.

These tests showed that dynamic RCS measurements were possible using the resistance sensor described in chapter 2. The RCS waveforms collected showed similar characteristics to that described in section 3.1.5 (Figure 32). Targets close to the plane of the electrodes exhibited a waveform with two peaks separated by a minimum that was coincident with the target in a central longitudinal position between the electrodes. Targets that passed over the sensor array at greater range exhibited either a 'flat topped' waveform or single central peak waveform dependant on target range.

Combination of two waveforms using subtraction of the waveform measured at the notional upstream electrode from the waveform measured at the notional downstream electrode produced a bipolar waveform similar to that reported for conventional fish counting systems (Fewings, 1994). The point in time at which the waveform passed through the zero difference RCS indicated the point at which the target was in a central longitudinal position. The RCS measurement indicated for this time was then used as the measurement with which to compile an updated RCS , target range and target length model. These measurements were found to exhibit very similar characteristics to those collected using static targets (see section 3.1.6 and 6.2). When models were constructed from these data, a sigmoidal model did not fit the data any better than a simple linear relationship. Linear models were therefore constructed and presented in section 6.2. This evaluation demonstrated that such a system could capture the RCS of moving resistive targets and be used to formulate model relationships as were utilised

for the target range compensation tests.

In addition to the tests on moving stainless steel targets some live salmon were allowed to swim freely over the electrodes during which RCS measurements were collected. Although significant difficulties were experienced in making the fish swim over the electrode array in a manner similar to that expected in the wild, some RCS waveforms were collected. When the waveforms were inspected, major similarities were found between the waveforms derived from live targets and those from stainless targets. Dual-aspect video recording was carried out of the dynamic fish tests but lighting conditions and turbidity of the water in the test tank meant that fish position was not estimated. Some anomalies in the RCS waveforms were observed that were not consistent with a fault in the electrode connections and the cause has not been identified. Some RCS signals observed were much larger than expected from previous observations of RCS and fish position. Without further experimentation the source of these unexpected results cannot be identified.

7.5 Summary

In summary, problems experienced with conventional resistance change fish counters has meant that new concepts for the enumeration and characterisation of adult migratory salmonids have been investigated. These new methods were designed for operation in open river systems without the need for expensive weir structures. To remove the effects of electrode length on the sensitivity of a fish counting system, the measurements undertaken were carried out using multiple point electrodes and not strip electrodes, as used in previous systems. The development of an absolute resistance measurement system not only improved non-fish object discrimination but also had the potential to compensate for changes in water conductivity and water

depth. Tests of the accuracy of this sensor indicated a laboratory accuracy of 0.022 Ω in 880 Ω or 25 ppm[α].

The sensor system was used to measure the effects of resistive target position on RCS and, using these data, models were constructed which related resistive target position to RCS. These models were of a form that could readily incorporate factors such as water conductivity and depth to allow improved environmental compensation of resistive target length estimation. Tests that compared the RCS from stainless steel rods and freshly killed fish indicated that the stainless rods were a close analogue of the freshly killed fish.

Previous studies of the performance of resistivity fish counters had identified a limitation of conventional systems because of the RCS measured with fish targets at varied range from the plane of the sensor electrodes. To compensate for this deficiency, two methods of target range compensation were devised and investigated using computer simulations. Both systems provided some reduction in the error associated with the estimation of target length although the more complex method, called trilateral target range compensation, showed the best performance overall. When compared with no target range compensation, as found in conventional systems, an almost three-fold improvement in the accuracy of target length estimation was observed.

To evaluate the capabilities of the system developed to measure RCS waveforms of moving resistive targets and live fish, experiments were carried out in a large exterior tank using stainless steel rods and adult Atlantic salmon. The results of these tests indicated that RCS waveforms could be collected from moving targets and that signal processing techniques could be used to identify the longitudinal position of the resistive target.

[α] The accuracy of the sensor system was defined as the confidence interval of the resistance measurements when no targets were present in the test tank (α= 0.025, n = 10) (see section 5.2.2).

The major achievements of this study are summarised below

1) A review of present fish counting methods indicated that electrical resistance change detection could fulfil an important stock assessment role if some technical limits were overcome.

2) A concept of a "cellular" approach to fish counting was developed to overcome some of the limitations of existing fish counting systems.

3) An electrical resistance sensor was developed, capable of 25 ppm accuracy, which was controlled by a host personal computer and included a self-calibration facility.

4) RCS measurements were made of freshly killed sea trout and stainless steel rods at a range of positions in a test tank, the rods were found to be a good analogue of real fish.

5) RCS measurements of stainless steel rods were repeated under varied conditions of water depth and water conductivity.

6) Using the RCS measurements mathematical models were formulated to describe the RCS of resistive targets of varied length and position with two different electrode separations.

7) Simulations were constructed to test the performance of two target range compensation methods under simulated measurement noise conditions.

8) The target range compensation methods tested were shown to improve the target length estimation capability of the system by up to 66% compared with no length compensation as with existing systems.

9) Tests of the sensor system in a large external tank showed that dynamic measurements of moving targets were possible and that calibration model relationships could be derived from such measurements.

10) Further tests of the sensor system with live salmon showed that the required measurements were achievable and that the signals from live fish were substantially larger than those from the stainless steel rods used.

7.6 Proposals for Future Research

During this investigation substantial advances have been made in the field of measurement electronics and micro controller design. These advances mean that improvements in the analogue to digital conversion of a signal proportional to a resistance between electrodes could be achieved at a greater accuracy and reduced cost compared to the methods described in chapter 2. Of the two methods that are particularly suitable for this task, one uses an integration technique that is inherently less susceptible to electrical noise than those used to date. The other method uses the same technique employed in this study to selectively remove power supply interference but is technically far more capable of this noise reduction function. Both alternatives are now available on a single integrated circuit with an interface suitable for control by a contemporary micro controller.

The sample rate achieved during the dynamic tests of chapter 6 was *circa* 3[α] samples per second. For an operational system a sample rate of nearer 30 samples per second is required to observe the passage of the faster migrating fish. The latter ADC suggested above uses internal high speed sampling with digital filtering to remove power supply

---

[α] This sample rate includes the rate at which all six electrodes were sampled therefore the sample rate for each electrode was 18 samples per second.

50 Hz noise. The data sheets for the device suggest that high resolution sample conversions (16 bit) were available at speeds of 100 samples per second. This approach could therefore achieve much of the sample rate required.

The integration of a micro controller to the system as near to the electrode array as possible could confer a number of advantages. These include the generation of less endogenous noise since the measurement unit could be powered by a d.c. power source and the transfer of the measurement data achieved using digital methods to enable a larger distance between recording equipment and the sensor without adding noise. Micro controllers also offer the possibility of low power operation that could be useful for sites where no mains power supply was available.

All of the tests carried out in this study used one type of point electrode that was hemi-spherical with a diameter of 10 mm. There may be an advantage in the use of electrodes of different size and shape to those tested. In particular, larger electrodes may overcome some of the grounding problems that were encountered.

The only method used in this study to measure electrical resistance was the injection of a fixed current and the measurement of the electrode voltage required to drive that current. The alternate scheme of using a fixed voltage on the drive electrode and measurement of the current in the circuit may produce more consistent results since the electrical potential field near the drive electrode may be more consistent. Another measurement scheme, as used in EIT, includes the injection of a fixed current by different electrodes to those used for measurement. The advantage with such a scheme is that fluctuations in the contact resistance between the injection electrodes and the water do not affect the measurement electrodes. Each of these schemes could be tested for its application to fish detection and length estimation.

The methods of resistive target range compensation tested in this study are likely to be only the start of attempts to improve target range compensation. No attempt has been made to optimise the performance of the methods used and therefore significant opportunities exist for tests of the effects of alternate electrode separation, both in the longitudinal and lateral planes, on the performance of target length compensation.

Other improvements in target range compensation could arise from a more highly optimised algorithm for matching the observed RCS measurements to measurements calculated from the models.

The coaxial target range compensation method was shown to provide only a modest improvement in the estimation of target length. Alternate electrode separations and the use of an iterative algorithm to compensate for target range could be tested to determine if this system could be made more effective.

Few measurements of the RCS of live fish were recorded in this study, to improve this aspect of the research, anaesthetised live fish could be passed over the sensor array using the track and carriage used for stainless steel rod targets. Analysis of the body shape and composition for fish of different reproductive status and species may indicate that more information may be available from RCS measurements than thought at present. Such a study could also indicate a limit to the resolution of fish size estimates due to the natural range in body resistivity. Methods are now available to estimate the body composition of fish without the destruction of fish (Brown *et al.*, 1993; Gillooly and Baylis, 1999). This could enable the measurement of RCS over an extended period of time to examine changes in measurements for the same fish. In addition, a laboratory version of the resistance sensor could be constructed to measure body electrical conductivity as an alternative to the methods used by Brown *et al* (1993) and Gillooly and Baylis (1999).

Once the restricted fish tests above were completed, trials of a prototype sensor system could be undertaken in a flat bottomed channel that could be observed by video for fish position fixing and sizing. Under such conditions the models constructed from the fish test could be validated under near-field conditions prior to full field trials.

A range of tests carried out in a large tank to determine the effects of water conductivity and water depth on RCS, target length and target range relationships could provide a method of environmental compensation that is not available at present.

CHAPTER EIGHT

CONCLUSIONS

CHAPTER EIGHT

8 CONCLUSIONS

8.1 Concept

One of the major limitations of existing electrical resistivity detection systems is the requirement for siting the sensor electrodes on a weir or confined channel. This siting is necessary to encourage favourable swimming behaviour of the fish to be counted. A key objective of this study was the development of a new method of non-invasive migratory fish stock monitoring. This objective was achieved using the concept of an array of small sensor units or cells. This array system was expected to provide the capability to count and estimate fish size when used on the bed of a river channel without the need for a costly structure that could affect fish migration.

8.2 Sensor Development

To investigate the feasibility of the electrode array concept a resistance sensor was required that was capable of sufficient resolution to detect resistive targets similar to those of small adult salmon. In addition the sensor was required to perform calibrations in order to allow consistent measurements. Through the combination of sub-circuits from the medical field of EIT and other general electronic applications a sensor was constructed with a measured accuracy of 25 ppm (see section 5.2.2). This accuracy was sufficient to detect 306 mm targets at 700 mm range. Subsequent developments of the sensor included electrode switching of up to six electrodes and automatic calibration. Output data was expressed in terms of SI (Ω) units and recorded in real time to a computer disk at a rate of 18 measurements per second.

8.3 Measurements

Measurements of resistance change signal (RCS) were made of freshly killed sea trout and stainless steel rod targets at a range of elevations from the plane of the electrode array. A comparison of the RCS measurements indicated that the stainless steel rod

targets were a good analogue of the freshly killed trout for the purpose of this study. Further measurements of stainless steel rod targets at alternate range from the electrodes, separation of electrodes, depth of water and water conductivity were carried out.

The log transform of RCS was observed to reduce in linear proportion with increasing range from the plane of the electrodes at range greater than 0.1 m. The rate of reduction in log RCS was dependent on the separation of the electrodes. Smaller electrode separation was associated with a greater reduction in RCS per unit increase in target range. The depth of water modified the RCS and target range relationship by effecting a shift in the whole curve. The curves were displaced positively on the log RCS axis as water depth was reduced. Conclusions could not be drawn on the effects of water conductivity because of faults in the collection of the data.

8.4 Mathematical Models

Using measurements of RCS described in section 8.3 mathematical models were constructed for the prediction of RCS using the parameters of target length and target range. In the case of the logistic model, the fit of the model to the data was described by the correlation coefficient and the coefficient of determination, 0.998 (r) and 0.997 (r^2) respectively. For the exponential model the coefficient of determination ranged from 0.930 to 0.987.

8.5 Target Range Compensation

In order that an array of resistance sensors could be used across a river channel of substantial water depth some means of compensation for the range of the target from the plane of the electrodes was required. Using the models developed in section 8.4, two methods of target range compensation were evaluated using a computer simulation. In the tests, measurement noise was introduced equivalent to twice the measured noise levels to provide realistic conditions for the simulation. The first method called trilateral target range compensation was shown to exhibit substantial target range compensation at ranges over 500 mm from the plane of the electrodes for targets of 600 mm length. A 66% reduction in the error associated with target

length estimation compared to no target range compensation was indicated for a target of 500 mm length. In addition, the target range compensation capabilities extended laterally outside the confines of the array.

The second method of target range compensation showed some useful target range compensation capabilities. For targets of 400 mm and 600 mm length the average length estimation accuracy was increased by 19% and 63% respectively at target ranges of between 50 mm and 950 mm.

8.6 Tests with Moving Resistive Targets

To test a prototype system in semi-field conditions, the sensor array was tested in a large external tank with moving resistive targets. These resistive targets consisted of stainless steel rods and adult Atlantic salmon.

Using the measurements derived from moving rod targets alone, model relationships were constructed similar to those of chapter 4. The goodness of fit, as indicated by correlation coefficient, was not as high as for static tests and ranged from 0.65 to 0.92 (see Table 25). This exercise demonstrated that it was possible to construct operational models using measurements from moving resistive targets.

Key target position information was derived from digital signal processing of the RCS measurements recorded as the rod targets passed over the sensor array. This positional information enabled the selection of the RCS measurement that was considered the most suitable for target length estimation.

Free-swimming salmon exhibited very variable behaviour on release in a large external test tank. Measurements of RCS were recorded when fish swam through the sensor array and were recorded to a computer disk. Analysis of these RCS measurements showed that salmon sized fish could be detected using the prototype sensor system. The magnitude of the RCS measurements was larger than that expected from tests with freshly killed fish in earlier experiments.

8.7 Overview

The developments described in this study exhibit most of the capabilities required by the concept of an array of point electrodes that could be deployed as a mat across the bottom of a river channel. Using models to compensate for changes in water depth and water conductivity it is possible for such a system to achieve accuracies of fish length estimation similar to that achieved at present without the need for an expensive counting structure. This technique therefore represents a means by which accurate non-invasive stock assessment could be carried out at locations that were not previously feasible at substantially reduced cost with no potential impact on the migration of the fish.

LITERATURE CITED

Banks, J.W. (1969). A review of the literature on the upstream migration of adult salmonids. *Journal of Fish Biology*, **1**, 85-136.

Beach, M.H. (1978). Determination of the accuracy of two types of fish counter employing the principles of (i) conductivity change and (ii) acoustic reflection. In Bussell, R. B. (ed): *Fish Counting Stations: Notes For Guidance In Their Design And Use.* Appendix B pp. 1-27. Department of the Environment, London. 70 pp.

Bleckmann, H. (1986) Role of the lateral line in fish behaviour. In *The behaviour of teleost fishes.* Ed. Pitcher, T.J. ISBN 0-7099-2070-9

Blonder, B.I. and W.S. Alevizon (1988). Prey discrimination and electroreception in the stingray *(Dasyatis sabina). Copeia*, **1**, 33-36.

Brassington, R.A. (1981). Afon Seiont fish counter evaluation. Welsh Water Authority Area Technical Fisheries Unit (North) Report No. 81/7, 10 pp.

Brown, M.L., Gatlin III, D.M. and Murphy, B.R. (1993) Non-destructive measurement of sunshine bass, *Morone chrysops* (Rafinesque) × *Morone saxatilis* (Walbaum), body composition using electrical conductivity. *Aquaculture and Fisheries Management,* **24**, 585-592.

Crump, E. S., (1952) A new method of gauging stream flow with little afflux by means of a submerged weir of triangular profile. Proceedings of the Institute of Engineering. Part 1, **1**, 223-242.

Davidson, I.C., Cove, R.J. and Milner, N.J. (1999). The effectiveness of rod and net fishery bye-laws in reducing exploitation of spring salmon on the Welsh Dee. In Cowx, I.G. (ed) *Management and Ecology of River Fisheries*. pp. 373-387.

Dunkley, D.A. and Shearer, W.M. (1982). An assessment of the performance of a resistivity fish counter. *Journal of Fish Biology*, **20,** 717-737.

Dunkley, D.A. and Shearer, W.M. (1989). Swimming height of Atlantic salmon, *Salmo salar* L. crossing a Crump weir. *Aquaculture and Fisheries Management*. **20**, 193-198.

Emde, G. von der (1993). The sensing of electric capacitances by weakly electric mormyrid fish: Effects of water conductivity. *Journal of Experimental Biology,* **181**, 157-173.

Environment Agency (1996). Salmon Action Plan Guidelines, version 1, 11/96. *Fisheries Technical Manual series*, No. **3.** 125 pp.

Fewings, G.A. (1988). Fish counter validation. MSc. Thesis, University College of North Wales, Bangor.

Fewings, G.A. (1993). NRA Hampshire salmon seminar. *National Rivers Authority Publication, Winchester Guildhall.*

Fewings, G.A. (1994). Automatic salmon counting technologies, a contemporary review. Bensinger-Liddel Fellowship. *Atlantic Salmon Trust, Moulin, Pitlochry, Scotland.*, pp. 66.

Fewings, G.A. (1998). Recent fish counter developments in England and Wales. In Holden, A. V. and Struthers, G. (eds) *Fish Counters – the proceedings of a seminar held in Perth on 4 April 1997 by the Atlantic Salmon Trust and the Institute of Fisheries Management (Scottish Branch)*, pp. 82-91.

Fox, E. and Shotton, K. (1995). *Transforms and nonlinear regressions.* Sigmaplot 4.0 Reference manual. Published by Jandel Corporation, pp. A-4.

Gillooly, J.F. and Baylis, J.R. (1999). Reproductive success and the energetic cost of parental care in male smallmouth bass. Journal of Fish Biology, 54, 573-584.

Gough, P. (1989). A fresh start for Thames salmon? *Salmon, Trout, and Sea-Trout.* October 1989, 14-38.

Gough, P. (1990). Rebirth of the Thames salmon? *Salmon, Trout, and Sea-Trout.* August 1990, 60-79.

Gough, P. (1991). What future for Thames salmon? *Salmon, Trout, and Sea-Trout.* March 1991, 20-107.

Gregory J. (1987). *Water schemes- The safeguarding of fisheries.* Atlantic Salmon Trust, Moulin, Pitlochry, Perthshire. 117 pp.

Gray, D. (1995). *The Aquantic Logie 2100 fish counter operations manual.* Aquantic Ltd, Dingwall Scotland. 37 pp.

Harte, M. K. (1993). *Final report of 1992 Hydroacoustic study of the Atlantic salmon spawning run on the Moisie River, Quebec, Canada.* Report by Biosonics Inc., 39 pp.

Hellawell, J.M. (1973). *Automatic methods of monitoring salmon populations.* Special publication of the Atlantic Salmon Foundation. **4**, 317-337.

Hellawell, J.M., Leatham, H. and Williams, G. I. (1974) The upstream migratory behaviour of salmonids in the River Frome in Dorset. *Journal of Fish Biology*, **6,** 729-744.

Horowitz, P. and W. Hill. (1989). *The Art of Electronics.* 2nd. Ed. Cambridge University Press. 1125 pp.

Hutchinson, P. and Mills, D.H. (1999). Executive summary. In Mills, D.H. (ed): *The Ocean Life of Salmon – Environmental and Biological Factors Influencing Survival*. pp. 7-18. Blackwell Science Ltd.

Johnson, F. and Clarke, A. M., (1987) Specification, development, experience and performance of fish counters in the North of Scotland Hydro Electric Board. In The automatic counter – a tool for the management of salmon fisheries. Report of a workshop held at Montrose, Scotland. Sept. 1987. Atlantic Salmon Trust, Pitlochry

Johnson, I.K., Beaumont, W.R.C. and Welton, S. (1988). Automated video fish counting. *Personal communication. Unpublished.*

Johnston, S.V., B.H. Ransom and K.K. Kumagai (1993) Hydroacoustic evaluation of adult chinook and chum salmon migrations in the Yukon River during 1992 *Report prepared for US Fish and Wildlife Service by Hydroacoustic Technology Inc.*

Knudsen, F.R., P.S. Enger and O. Sand (1992) Awareness reactions and avoidance responses to sound in juvenile Atlantic Salmon, *Salmo salar* L. Journal of Fish Biology, **40**, 523-534.

Kristinsson, B. and Alexandersdóttir, M. (1978) Design and calibration of a salmon counter. *Journal of Agricultural Research Iceland,* **10**, 57-66.

Kaljmin, A.J. (1982). Electric and magnetic field detection in elasmobranch fishes. *Science.*, **218**, 916-918.

Lannoo, M.J. and Lannoo, S.J. (1993) Why do electric fishes swim backwards? An hypothesis based on gymnotiform foraging behaviour interpreted through sensory constraints. *Environmental Biology of Fishes.*, **36**, 157-165.

Larinier, M. and Travade, F., (1992) Inspection techniques for fishways. In *Aquatic resource management.* French Journal Of Fishing And Fish Breeding. Nos. 326-327, 142-153.

Lawson, K., (1975). The electronic monitoring of salmon in Lancashire, England. In Symposium on The Methodology for the Survey, Monitoring and Appraisal of Fishery Resources In Lakes And Large Rivers. European Inland Fisheries Advisory Commission, Book 1 No. 23 Supplement 1 Vol. 1. pp. 388 – 399.

Lethlean, N.G. (1953). An investigation into the design and performance of an electric fish screen and an electric fish counter. *Transactions of the Royal Society of Edinburgh*, **62,** 479-526.

Lévesque, F., Proulx, M. and Corfa, G. (1996). Effect of hydraulic variables on migratory behaviour of Atlantic salmon (*Salmo salar*) in the Moisie River, Quebec. In Leclerc, M., Boudreault, A., Capra, H., Cõté, Y. and Valentin, S. (eds): *2nd International Symposium on Habitat Hydraulics*. Proceedings Volume B, pp. 81-93. Publishers INRS-EAU.

Lissmann, H.W. (1963). Electric location by fishes. *Scientific American,* Reprint No. **152**, 11.

Marston, R.M. (1990). *Timer generator circuits manual.* Heinemann Newnes, Oxford. 269 pp.

Mills, D.H. (1989). *The Ecology and Management of Atlantic Salmon*. Chapman and Hall,London. 351 pp.

Moller, P. (1995). Active Electrolocation In *Electric Fishes, History and Behaviour.* Chapman and Hall. pp. 111-132.

Monan, G.E. and Engstrom, D.E. (1963). Development of a mathematical relationship between electric-field parameters and the electrical characteristics of fish. *Fisheries Bulletin,* **63,** 123-136.

North Atlantic Salmon Conservation Organisation (1996). *Report of the ICES Advisory Committee on Fishery Management.* NASCO CNL (96). **15**, 30 pp.

Nicholson, S.A., Aprahamian M W., Best P. M., Shaw R.A. and Karr E.T. (1995). *Design and use of fish counters.* National Rivers Authority R&D Note 382, 204 pp.

Northrop, R.B. (1989). Autobalancing Impedence Measurement In *Analog Electronic Circuits.* pp. 455-459. Addison-Wesley Series in Electrical and Computer Engineering.

Radford, A.F., Hatcher, A.C., and Whitmarsh, D.J. (1991). *An Economic Evaluation of Salmon Fisheries in Great Britain.* Summary of a report prepared for the Ministry of Agriculture, Fisheries and Food. Portsmouth Polytechnic. 32 pp.

Simpson, D., Clark, A. M., Slessor, M.D. and Dudgeon, I.D. (1975). Conception and development of electrical resistivity fish counters. In *Symposium on the Methodology for the Survey, Monitoring and Appraisal of Fishery Resources in Lakes and Large Rivers.* European Inland Fisheries Advisory Commission, Book 1 No. 23 Supplement 1 Vol. 1, pp. 414 – 435.

Simpson, D. (1978) Electrical resistivity fish counters. In Thorpe, J. E. (ed): *Rhythmic Activity of Fishes.* pp. 259-268. London Academic Press.

Smith, I. P., Johnstone, A.D.F. and Dunkley, D.A. (1996). Evaluation of a portable electrode array for a resistivity fish counter. *Fisheries Management and Ecology*, **3**, 129-141.

Sund, O. (1935) Echo sounding in fishery research. *Nature,* **135**, 953.

Solomon. D.J. and Potter E.C.E (1992). *The measurement and evaluation of the exploitation of Atlantic Salmon*. Report of a workshop organised by the Atlantic Salmon Trust and the Royal Irish Academy in Dublin, April 8-10, 1991, Atlantic Salmon Trust, Pitlochry, Perthshire.

Travade, F., (1990) Monitoring techniques for fish passes recently used in France. Proceedings of the International Symposium on Fishways, Gifu, Japan, 119-126.

Van der Walt. (1981). A Wein-bridge oscillator with high-amplitude stability. *IEEE Transactions Instrumentation and Measurement.* IM-30, 292-294.

Webster, J.G. (1990). *Electrical Impedance Tomography*, 240 pp., Adam Hilger, Bristol.

Whitney, L.V. and Pearce, R.L. (1957). Factors controlling the input of electrical energy into a fish (*Cyprinus carpio* L.) in an electric field. *Limnology and Oceanography,* **2**, 55-61.

Woods, R. (1995). *Quality review of fish counter data from the Rivers Itchen and Test.* Internal report for the National Rivers Authority by Fawley Aquatic Research Laboratory, Southampton.

APPENDICES

9 APPENDIX A SEMICONDUCTOR DATA SHEETS

9.1 A (i) AD536A True RMS-to-DC Converter

Integrated Circuit, True RMS-to-DC Converter

AD536A

FEATURES

True RMS-to-DC Conversion
Laser-Trimmed to High Accuracy
  0.2% max Error (AD536AK)
  0.5% max Error (AD536AJ)
Wide Response Capability:
  Computes RMS of AC and DC Signals
  450 kHz Bandwidth: V rms > 100 mV
  2 MHz Bandwidth: V rms > 1 V
  Signal Crest Factor of 7 for 1% Error
dB Output with 60 dB Range
Low Power: 1.2 mA Quiescent Current
Single or Dual Supply Operation
Monolithic Integrated Circuit
-55°C to +125°C Operation (AD536AS)

PIN CONFIGURATIONS AND FUNCTIONAL BLOCK DIAGRAMS

TO-116 (D-14) and Q-14 Package

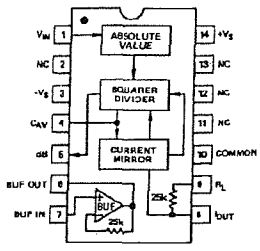

TO-100 (H-10A) Package

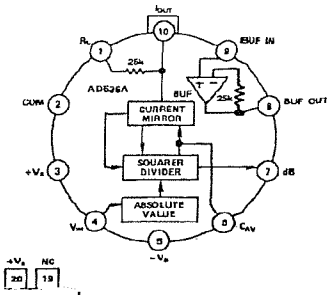

LCC (E-20A) Package

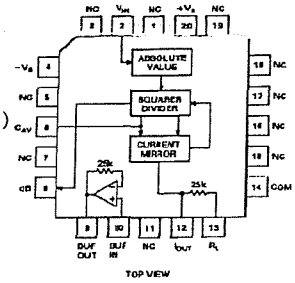

PRODUCT DESCRIPTION

The AD536A is a complete monolithic integrated circuit which performs true rms-to-dc conversion. It offers performance which is comparable or superior to that of hybrid or modular units costing much more. The AD536A directly computes the true rms value of any complex input waveform containing ac and dc components. It has a crest factor compensation scheme which allows measurements with 1% error at crest factors up to 7. The wide bandwidth of the device extends the measurement capability to 300 kHz with 3 dB error for signal levels above 100 mV.

An important feature of the AD536A not previously available in rms converters is an auxiliary dB output. The logarithm of the rms output signal is brought out to a separate pin to allow the dB conversion, with a useful dynamic range of 60 dB. Using an externally supplied reference current, the 0 dB level can be conveniently set by the user to correspond to any input level from 0.1 to 2 volts rms.

The AD536A is laser trimmed at the wafer level for input and output offset, positive and negative waveform symmetry (dc reversal error), and full-scale accuracy at 7 V rms. As a result, no external trims are required to achieve the rated accuracy of the unit.

There is full protection for both inputs and outputs. The input circuitry can take overload voltages well beyond the supply levels. Loss of supply voltage with inputs connected will not cause unit failure. The output is short-circuit protected.

The AD536A is available in two accuracy grades (J, K) for commercial temperature range (0°C to +70°C) applications, and one grade (S) rated for the −55°C to +125°C extended range. The AD536AK offers a maximum total error of ± 2 mV ± 0.2% of reading, and the AD536AJ and AD536AS have maximum errors of ± 5 mV ± 0.5% of reading. All three versions are available in either a hermetically sealed 14-pin DIP or 10-pin TO-100 metal can. The AD536AS is also available in a 20-pin hermetically sealed ceramic leadless chip carrier.

PRODUCT HIGHLIGHTS

1. The AD536A computes the true root-mean-square level of a complex ac (or ac plus dc) input signal and gives an equivalent dc output level. The true rms value of a waveform is a more useful quantity than the average rectified value since it relates directly to the power of the signal. The rms value of a statistical signal also relates to its standard deviation.
2. The crest factor of a waveform is the ratio of the peak signal swing to the rms value. The crest factor compensation scheme of the AD536A allows measurement of highly complex signals with wide dynamic range.
3. The only external component required to perform measurements to the fully specified accuracy is the capacitor which sets the averaging period. The value of this capacitor determines the low frequency ac accuracy, ripple level and settling time.
4. The AD536A will operate equally well from split supplies or a single supply with total supply levels from 5 to 36 volts. The one milliampere quiescent supply current makes the device well-suited for a wide variety of remote controllers and battery powered instruments.
5. The AD536A directly replaces the AD536 and provides improved bandwidth and temperature drift specifications.

REV. A

One Technology Way, P.O. Box 9106, Norwood, MA 02062-9106, U.S.A.
Tel: 617/329-4700 Fax: 617/326-8703

AD536A—SPECIFICATIONS (@ +25°C, and ±15 V dc unless otherwise noted)

Model	AD536AJ Min	AD536AJ Typ	AD536AJ Max	AD536AK Min	AD536AK Typ	AD536AK Max	AD536AS Min	AD536AS Typ	AD536AS Max	Units
TRANSFER FUNCTION		$V_{OUT} = \sqrt{avg.(V_{IN})^2}$			$V_{OUT} = \sqrt{avg.(V_{IN})^2}$			$V_{OUT} = \sqrt{avg.(V_{IN})^2}$		
CONVERSION ACCURACY										
Total Error, Internal Trim[1] (Figure 1)			±5 ±0.5			±2 ±0.2			±5 ±0.5	mV ± % of Reading
vs. Temperature, T_{MIN} to +70°C			±0.1 ±0.01			±0.05 ±0.005			±0.1 ±0.005	mV ± % of Reading/°C
+70°C to +125°C									±0.3 ±0.005	mV ± % of Reading/°C
vs. Supply Voltage		±0.1 ±0.01			±0.1 ±0.01			±0.1 ±0.01		mV ± % of Reading/V
dc Reversal Error		±0.2			±0.1			±0.2		± % of Reading
Total Error, External Trim[1] (Figure 2)		±3 ±0.3			±2 ±0.1			±3 ±0.3		mV ± % of Reading
ERROR VS. CREST FACTOR[2]										
Crest Factor 1 to 2		Specified Accuracy			Specified Accuracy			Specified Accuracy		
Crest Factor = 3		−0.1			−0.1			−0.1		% of Reading
Crest Factor = 7		−1.0			−1.0			−1.0		% of Reading
FREQUENCY RESPONSE[3]										
Bandwidth for 1% Additional Error (0.09 dB)										
V_{IN} = 10 mV		5			5			5		kHz
V_{IN} = 100 mV		45			45			45		kHz
V_{IN} = 1 V		120			120			120		kHz
±3 dB Bandwidth										
V_{IN} = 10 mV		90			90			90		kHz
V_{IN} = 100 mV		450			450			450		kHz
V_{IN} = 1 V		2.3			2.3			2.3		MHz
AVERAGING TIME CONSTANT (Figure 5)		25			25			25		ms/μF CAV
INPUT CHARACTERISTICS										
Signal Range, ±15 V Supplies										
Continuous rms Level		0 to 7			0 to 7			0 to 7		V rms
Peak Transient Input			±20			±20			±20	V peak
Continuous rms Level, ±5 V Supplies		0 to 2			0 to 2			0 to 2		V rms
Peak Transient Input, ±5 V Supplies			±7			±7			±7	V peak
Maximum Continuous Nondestructive Input Level (All Supply Voltages)			±25			±25			±25	V peak
Input Resistance	13.33	16.67	20	13.33	16.67	20	13.33	16.67	20	kΩ
Input Offset Voltage		0.8	±2		0.5	±1		0.8	±2	mV
OUTPUT CHARACTERISTICS										
Offset Voltage, V_{IN} = COM (Figure 1)		±1	±2		±0.5	±1			+2	mV
vs. Temperature		±0.1			±0.1				±0.2	mV/°C
vs. Supply Voltage		±0.1			±0.1			±0.2		mV/V
Voltage Swing, ±15 V Supplies	0 to +11	+12.5		0 to +11	+12.5		0 to +11	+12.5		V
±5 V Supply	0 to +2			0 to +2			0 to +2			V
dB OUTPUT (Figure 13)										
Error, V_{IN} 7 mV to 7 V rms, 0 dB = 1 V rms		±0.4	±0.6		±0.2	±0.3		±0.5	±0.6	dB
Scale Factor		−3			−3			−3		mV/dB
Scale Factor TC (Uncompensated, see Figure 1 for Temperature Compensation		−0.033 +0.33			−0.033 +0.33			−0.033 +0.33		dB/°C % of Reading/°C
I_{REF} for 0 dB = 1 V rms	5	20	80	5	20	80	5	20	80	μA
I_{REF} Range	1		100	1		100	1		100	μA
I_{OUT} TERMINAL										
I_{OUT} Scale Factor		40			40			40		μA/V rms
I_{OUT} Scale Factor Tolerance		±10	±20		±10	±20		±10	±20	%
Output Resistance	20	25	30	20	25	30	20	25	30	kΩ
Voltage Compliance		$-V_S$ to ($+V_S$ −2.5 V)			$-V_S$ to ($+V_S$ −2.5 V)			$-V_S$ to ($+V_S$ −2.5 V)		V
BUFFER AMPLIFIER										
Input and Output Voltage Range	$-V_S$ to ($+V_S$ −2.5 V)			$-V_S$ to ($+V_S$ −2.5 V)			$-V_S$ to ($+V_S$ −2.5 V)			V
Input Offset Voltage, R_S = 25 k		±0.5	±4		±0.5	±4		±0.5	±4	mV
Input Bias Current		20	60		20	60		20	60	nA
Input Resistance		10^8			10^8			10^8		Ω
Output Current	(+5 mA, −130 μA)			(+5 mA, −130 μA)			(+5 mA, −130 μA)			
Short Circuit Current		20			20			20		mA
Output Resistance			0.5			0.5			0.5	Ω
Small Signal Bandwidth		1			1			1		MHz
Slew Rate[4]		5			5			5		V/μs
POWER SUPPLY										
Voltage Rated Performance		±15			±15			±15		V
Dual Supply	±3.0		±18	±3.0		±18	±3.0		±18	V
Single Supply	+5		+36	+5		+36	+5		+36	V
Quiescent Current										
Total V_S, 5 V to 36 V, T_{MIN} to T_{MAX}		1.2	2		1.2	2		1.2	2	mA
TEMPERATURE RANGE										
Rated Performance	0		+70	0		+70	−55		+125	°C
Storage	−55		+150	−55		+150	−55		+150	°C
NUMBER OF TRANSISTORS		65			65			65		
PACKAGE OPTIONS										
Ceramic DIP (D-14)		AD536AJD			AD536AKD			AD536ASH		
Metal Can TO-100 (H-10A)		AD5536AJH			AD536AKH			AD536ASH		
LCC (E-20A)								AD536ASE		

NOTES

[1]Accuracy is specified for 0 V to 7 V rms, dc or 1 kHz sine wave input with the AD536A connected as in the figure referenced.

[2]Error vs. crest factor is specified as an additional error for 1 V rms rectangular pulse input, pulse width = 200μs.

[3]Input voltages are expressed in volts rms, and error is percent of reading.

[4]With 2k external pull-down resistor.

Specifications subject to change without notice.

Specifications shown in boldface are tested on all production units at final electrical test. Results from those tests are used to calculate outgoing quality levels. All min and max specifications are guaranteed, although only those shown in boldface are tested on all production units.

ABSOLUTE MAXIMUM RATINGS[1]

Supply Voltage
- Dual Supply ..... ±18 V
- Single Supply ..... +36 V

Internal Power Dissipation[2] ..... 500 mW
Maximum Input Voltage ..... ±25 V Peak
Buffer Maximum Input Voltage ..... $\pm V_S$
Maximum Input Voltage ..... ±25 V Peak
Storage Temperature Range ..... –55°C to +150°C
Operating Temperature Range
- AD536AJ/K ..... 0°C to +70°C
- AD536AS ..... –55°C to +125°C

Lead Temperature Range
(Soldering 60 sec) ..... +300°C
ESD Rating ..... 1000 V

NOTES
[1]Stresses above those listed under "Absolute Maximum Ratings" may cause permanent damage to the device. This is a stress rating only and functional operation of the device at these or any other conditions above those indicated in the operational section of this specification is not implied. Exposure to absolute maximum rating conditions for extended periods may affect device reliability.
[illegible]
20-Pin LCC: θ_{JA} = 95°C/W
14-Pin Size Brazed Ceramic DIP: θ_{JA} = 95°C/W.

CHIP DIMENSIONS AND PAD LAYOUT

Dimensions shown in inches and (mm).

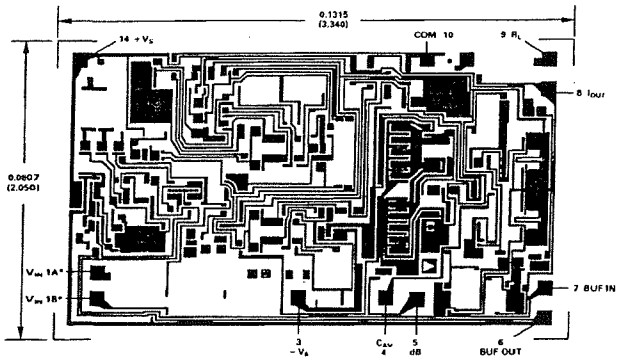

PAD NUMBERS CORRESPOND TO PIN NUMBERS FOR THE TO-116 14-PIN CERAMIC DIP PACKAGE.

NOTE
*BOTH PADS SHOWN MUST BE CONNECTED TO V_{IN}.
THE AD536A IS AVAILABLE IN LASER TRIMMED CHIP FORM.
SUBSTRATE CONNECTED TO $-V_S$.

ORDERING GUIDE

Model[1]	Temperature Range	Package Description	Package Option
AD536AJD	0°C to +70°C	Side Brazed Ceramic DIP	D-14
AD536AKD	0°C to +70°C	Side Brazed Ceramic DIP	D-14
AD536AJH	0°C to +70°C	Header	H-10A
AD536AKH	0°C to +70°C	Header	H-10A
AD536AJQ	0°C to +70°C	Cerdip	Q-14
AD536AKQ	0°C to +70°C	Cerdip	Q-14
AD536ASD	–55°C to +125°C	Side Brazed Ceramic DIP	D-14
AD536ASD/883B	–55°C to +125°C	Side Brazed Ceramic DIP	D-14
AD536ASE	–55°C to +125°C	LCC	E-20A
AD536ASE/883B	–55°C to +125°C	LCC	E-20A
AD536ASH	–55°C to +125°C	Header	H-10A
AD536ASH/883B	–55°C to +125°C	Header	H-10A

NOTE
[1]"S" grade chips are available tested at +25°C and +125°C. "J" grade chips are also available.

STANDARD CONNECTION

The AD536A is simple to connect for the majority of high accuracy rms measurements, requiring only an external capacitor to set the averaging time constant. The standard connection is shown in Figure 1. In this configuration, the AD536A will measure the rms of the ac and dc level present at the input, but will show an error for low frequency inputs as a function of the filter capacitor, C_{AV}, as shown in Figure 5. Thus, if a 4 µF capacitor is used, the additional average error at 10 Hz will be 0.1%, at 3 Hz it will be 1%. The accuracy at higher frequencies will be according to specification. If it is desired to reject the dc input, a capacitor is added in series with the input, as shown in Figure 3, the capacitor must be nonpolar. If the AD536A is driven with power supplies with a considerable amount of high frequency ripple, it is advisable to bypass both supplies to ground with 0.1 µF ceramic discs as near the device as possible.

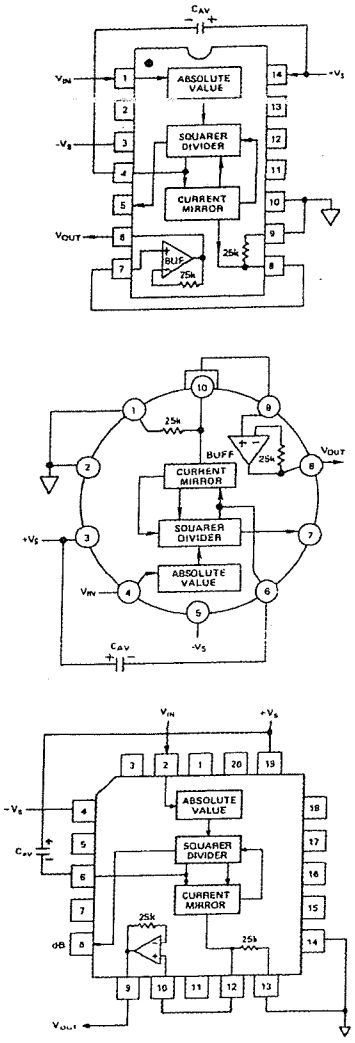

Figure 1. Standard RMS Connection

The input and output signal ranges are a function of the supply voltages; these ranges are shown in Figure 14. The AD536A can also be used in an unbuffered voltage output mode by disconnecting the input to the buffer. The output then appears unbuffered across the 25k resistor. The buffer amplifier can then be used for other purposes. Further the AD536A can be used in a current output mode by disconnecting the 25k resistor from ground. The output current is available at Pin 8 (Pin 10 on the "H" package) with a nominal scale of 40 μA per volt rms input positive out.

OPTIONAL EXTERNAL TRIMS FOR HIGH ACCURACY

If it is desired to improve the accuracy of the AD536A, the external trims shown in Figure 2 can be added. R4 is used to trim the offset. Note that the offset trim circuit adds 365 Ω in series with the internal 25 kΩ resistor. This will cause a 1.5% increase in scale factor, which is trimmed out by using R1 as shown. Range of scale factor adjustment is ± 1.5%.

The trimming procedure is as follows:

1. Ground the input signal, V_{IN}, and adjust R4 to give zero volts output from Pin 6. Alternatively, R4 can be adjusted to give the correct output with the lowest expected value of V_{IN}.
2. Connect the desired full scale input level to V_{IN}, either dc or a calibrated ac signal (1 kHz is the optimum frequency); then trim R1, to give the correct output from Pin 6, i.e., 1000 V dc input should give 1.000 V dc output. Of course, a ± 1.000 V peak-to-peak sine wave should give a 0.707 V dc output. The remaining errors, as given in the specifications are due to the nonlinearity.

The major advantage of external trimming is to optimize device performance for a reduced signal range; the AD536A is internally trimmed for a 7 V rms full-scale range.

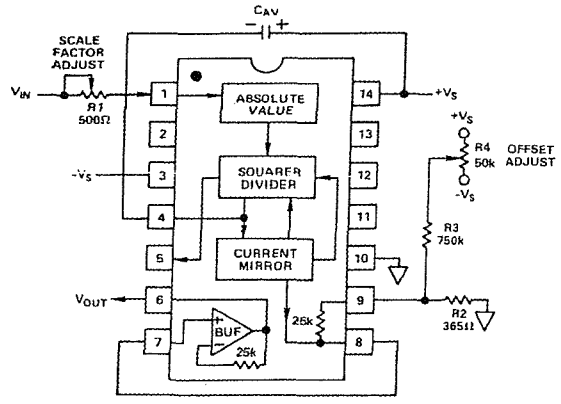

Figure 2. Optional External Gain and Output Offset Trims

SINGLE SUPPLY CONNECTION

The applications in Figures 1 and 2 require the use of approximately symmetrical dual supplies. The AD536A can also be used with only a single positive supply down to +5 volts, as shown in Figure 3. The major limitation of this connection is that only ac signals can be measured since the differential input stage must be biased off ground for proper operation. This biasing is done at Pin 10; thus it is critical that no extraneous signals be coupled into this point. Biasing can be accomplished by using a resistive divider between $+V_S$ and ground. The values of the resistors can be increased in the interest of lowered power consumption, since only 5 mA of current flows into Pin 10 (Pin 2 on the "H" package). AC input coupling requires only capacitor C2 as shown; a dc return is not necessary as it is provided internally. C2 is selected for the proper low frequency break point with the input resistance of 16.7 kΩ; for a cutoff at 10 Hz, C2 should be 1 μF. The signal ranges in this connection are slightly more restricted than in the dual supply connection. The input and output signal ranges are shown in Figure 14. The load resistor, R_L, is necessary to provide output sink current.

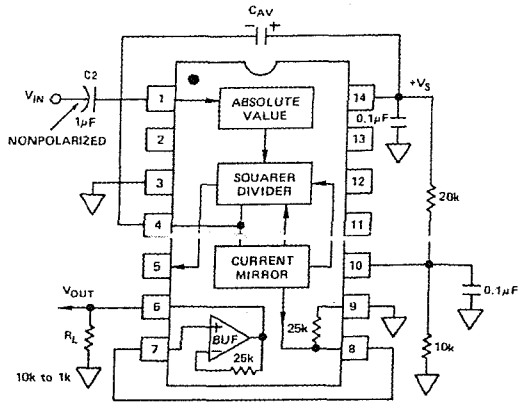

Figure 3. Single Supply Connection

CHOOSING THE AVERAGING TIME CONSTANT

The AD536A will compute the rms of both ac and dc signals. If the input is a slowly-varying dc signal, the output of the AD536A will track the input exactly. At higher frequencies, the average output of the AD536A will approach the rms value of the input signal. The actual output of the AD536A will differ from the ideal output by a dc (or average) error and some amount of ripple, as demonstrated in Figure 4.

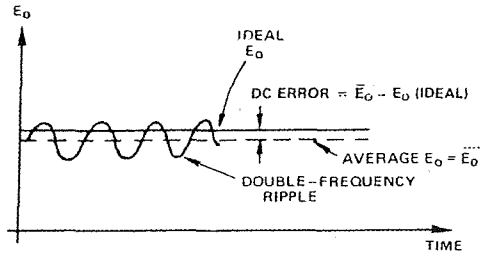

Figure 4. Typical Output Waveform for Sinusoidal Input

The dc error is dependent on the input signal frequency and the value of C_{AV}. Figure 5 can be used to determine the minimum value of C_{AV} which will yield a given percent dc error above a given frequency using the standard rms connection.

The ac component of the output signal is the ripple. There are two ways to reduce the ripple. The first method involves using a large value of C_{AV}. Since the ripple is inversely proportional to C_{AV}, a tenfold increase in this capacitance will affect a tenfold reduction in ripple. When measuring waveforms with high crest

factors, (such as low duty cycle pulse trains), the averaging time constant should be at least ten times the signal period. For example, a 100 Hz pulse rate requires a 100 ms time constant, which corresponds to a 4 µF capacitor (time constant = 25 ms per µF).

The primary disadvantage in using a large C_{AV} to remove ripple is that the settling time for a step change in input level is increased proportionately. Figure 5 shows that the relationship between C_{AV} and 1% settling time is 115 milliseconds for each microfarad of C_{AV}. The settling time is twice as great for decreasing signals as for increasing signals (the values in Figure 5 are for decreasing signals). Settling time also increases for low signal levels, as shown in Figure 6.

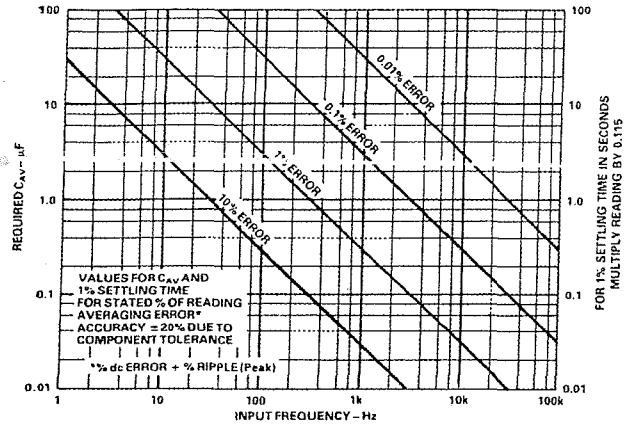

Figure 5. Error/Settling Time Graph for Use with the Standard rms Connection in Figure 1

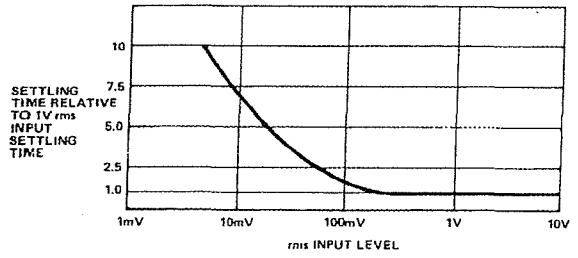

Figure 6. Settling Time vs. Input Level

A better method for reducing output ripple is the use of a "post-filter." Figure 7 shows a suggested circuit. If a single-pole filter is used (C3 removed, R_X shorted), and C2 is approximately twice the value of C_{AV}, the ripple is reduced as shown in Figure 8 and settling time is increased. For example, with C_{AV} = 1 µF and C2 = 2.2 µF, the ripple for a 60 Hz input is reduced from 10% of reading to approximately 0.3% of reading. The settling time, however, is increased by approximately a factor of 3. The values of C_{AV} and C2, can, therefore, be reduced to permit faster settling times while still providing substantial ripple reduction.

The two-pole post-filter uses an active filter stage to provide even greater ripple reduction without substantially increasing the settling times over a circuit with a one-pole filter. The values of C_{AV}, C2, and C3 can then be reduced to allow extremely fast settling times for a constant amount of ripple. Caution should be exercised in choosing the value of C_{AV}, since the dc error is dependent upon this value and is independent of the post filter.

For a more detailed explanation of these topics refer to the *RMS to DC Conversion Application Guide 2nd Edition*, available from Analog Devices.

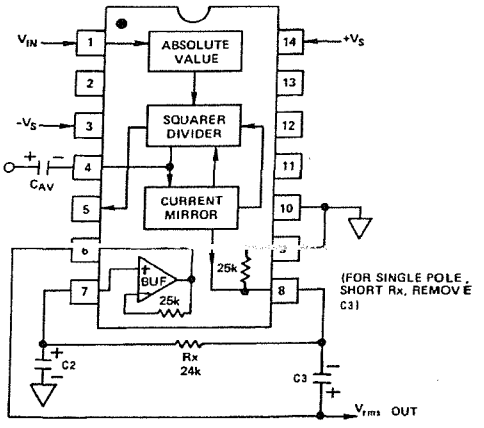

Figure 7. 2-Pole "Post" Filter

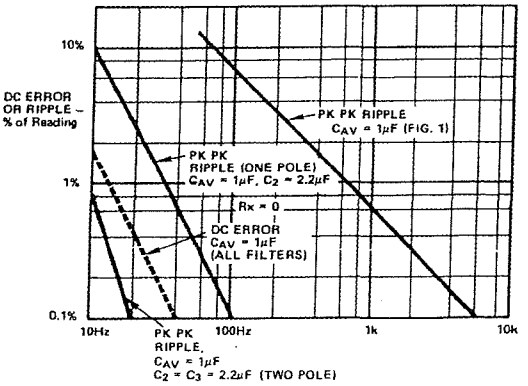

Figure 8. Performance Features of Various Filter Types

AD536A PRINCIPLE OF OPERATION

The AD536A embodies an implicit solution of the rms equation that overcomes the dynamic range as well as other limitations inherent in a straightforward computation of rms. The actual computation performed by the AD536A follows the equation:

$$V\,rms = Avg.\left[\frac{V_{IN}^{\,2}}{V\,rms}\right]$$

Figure 9 is a simplified schematic of the AD536A; it is subdivided into four major sections: absolute value circuit (active rectifier), squarer/divider, current mirror, and buffer amplifier. The input voltage, V_{IN}, which can be ac or dc, is converted to a unipolar current I_1, by the active rectifier A_1, A_2. I_1 drives one input of the squarer/divider, which has the transfer function:

$$I_4 = I_1^2/I_3$$

The output current, I_4, of the squarer/divider drives the current mirror through a low-pass filter formed by R1 and the externally connected capacitor, C_{AV}. If the R1, C_{AV} time constant is much greater than the longest period of the input signal, then I_4 is effectively averaged. The current mirror returns a current I_3, which equals Avg. $[I_4]$, back to the squarer/divider to complete the implicit rms computation. Thus:

$$I_4 = Avg.\left[I_1^2/I_4\right] = I_1\ rms$$

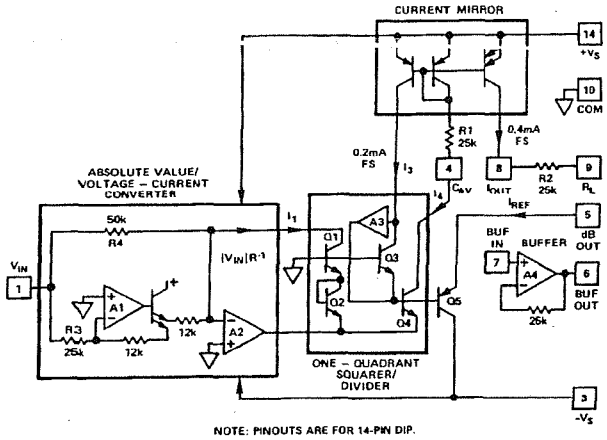

Figure 9. Simplified Schematic

The current mirror also produces the output current, I_{OUT}, which equals $2I_4$. I_{OUT} can be used directly or converted to a voltage with R2 and buffered by A4 to provide a low impedance voltage output. The transfer function of the AD536A thus results:

$$V_{OUT} = 2R2\ I\ rms = V_{IN}\ rms$$

The dB output is derived from the emitter of Q3, since the voltage at this point is proportional to –log V_{IN}. Emitter follower, Q5, buffers and level shifts this voltage, so that the dB output voltage is zero when the externally supplied emitter current (I_{REF}) to Q5 approximates I_3.

CONNECTIONS FOR dB OPERATION

A powerful feature added to the AD536A is the logarithmic or decibel output. The internal circuit computing dB works accurately over a 60 dB range. The connections for dB measurements are shown in Figure 10. The user selects the 0 dB level by adjusting R1, for the proper 0 dB reference current (which is set to exactly cancel the log output current from the squarer-divider at the desired 0 dB point). The external op amp is used to provide a more convenient scale and to allow compensation of the +0.33%/°C scale factor drift of the dB output pin. The special T.C. resistor, R2, is available from Tel Labs in Londonderry, N.H. (model Q-81) or from Precision Resistor Inc., Hillside, N.J. (model PT146). The averaged temperature coefficients of resistors R2 and R3 develop the +3300 ppm needed to reverse compensate the dB output. The linear rms output is available at Pin 8 on DIP or Pin 10 on header device with an output impedance of 25 kΩ; thus some applications may require an additional buffer amplifier if this output is desired.

dB Calibration:

1. Set V_{IN} = 1.00 V dc or 1.00 V rms
2. Adjust R1 for dB out = 0.00 V
3. Set V_{IN} = +0.1 V dc or 0.10 V rms
4. Adjust R5 for dB out = –2.00 V

Any other desired 0 dB reference level can be used by setting V_{IN} and adjusting R1, accordingly. Note that adjusting R5 for the proper gain automatically gives the correct temperature compensation.

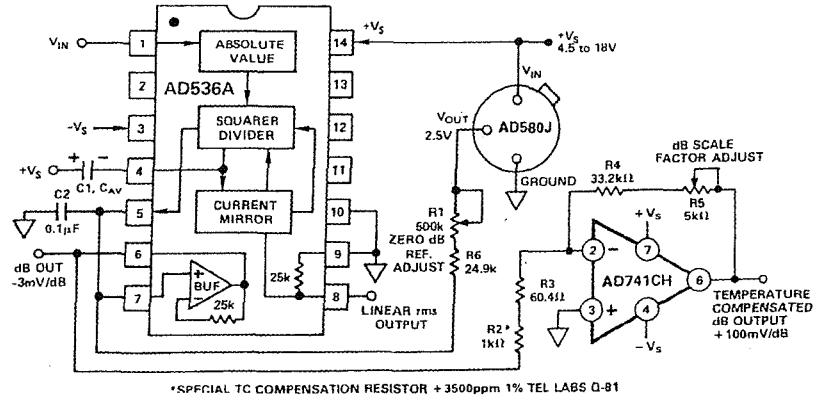

Figure 10. dB Connection

FREQUENCY RESPONSE

The AD536A utilizes a logarithmic circuit in performing the implicit rms computation. As with any log circuit, bandwidth is proportional to signal level. The solid lines in the graph below represent the frequency response of the AD536A at input levels from 10 millivolts to 7 volts rms. The dashed lines indicate the upper frequency limits for 1%, 10%, and 3 dB of reading additional error. For example, note that a 1 volt rms signal will produce less than 1% of reading additional error up to 120 kHz. A 10 millivolt signal can be measured with 1% of reading additional error (100 µV) up to only 5 kHz.

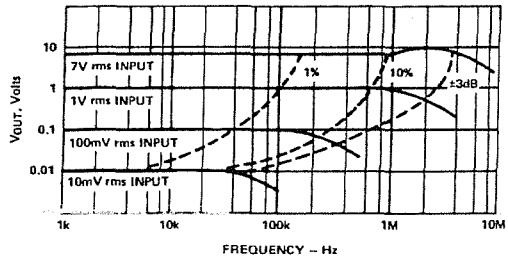

Figure 11. High Frequency Response

AC MEASUREMENT ACCURACY AND CREST FACTOR

Crest factor is often overlooked in determining the accuracy of an ac measurement. Crest factor is defined as the ratio of the peak signal amplitude to the rms value of the signal (CF = V_P/V rms). Most common waveforms, such as sine and triangle waves, have relatively low crest factors (<2). Waveforms which resemble low duty cycle pulse trains, such as those occurring in switching power supplies and SCR circuits, have high crest factors. For example, a rectangular pulse train with a 1% duty cycle has a crest factor of 10 (CF = $1/\sqrt{\eta}$).

Figure 12 is a curve of reading error for the AD536A for a 1 volt rms input signal with crest factors from 1 to 11. A rectangular pulse train (pulse width 100 µs) was used for this test since it is the worst-case waveform for rms measurement (all the energy is contained in the peaks). The duty cycle and peak amplitude were varied to produce crest factors from 1 to 11 while maintaining a constant 1 volt rms input amplitude.

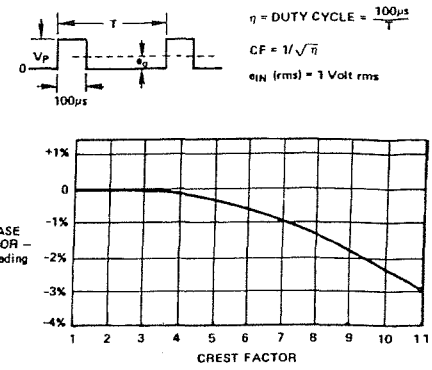

Figure 12. Error vs. Crest Factor

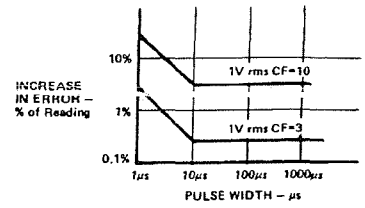

Figure 13. AD536A Error vs. Pulse Width Rectangular Pulse

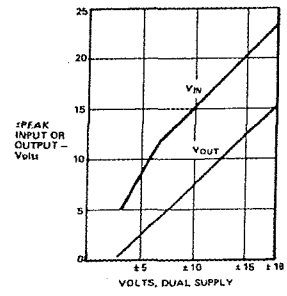

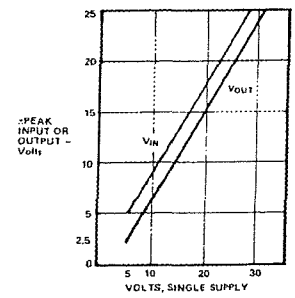

Figure 14. AD536A Input and Output Voltage Ranges vs. Supply

OUTLINE DIMENSIONS

Dimensions shown in inches and (mm).

D-14 Package
TO-116

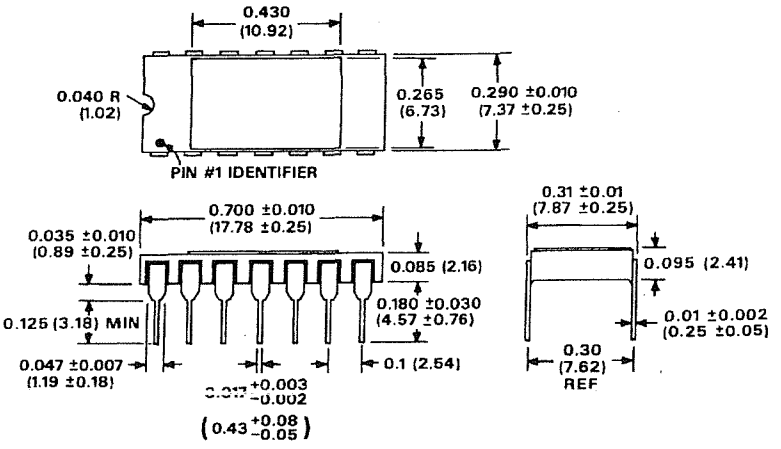

H-10A Package
TO-100

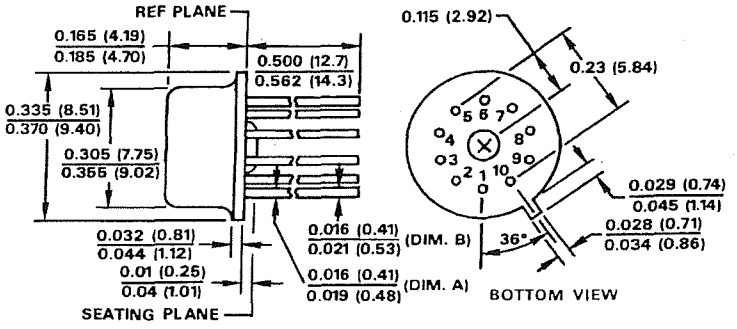

E-20A Package
LCC

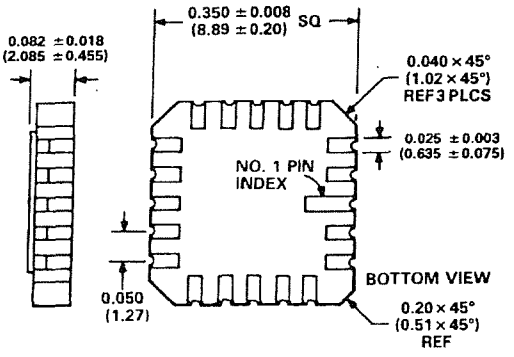

9.2 A (ii) AD636 Low Level True RMS-to-DC Convertor

Low Level, True RMS-to-DC Converter

AD636

FEATURES

True RMS-to-DC Conversion
200 mV Full Scale
Laser-Trimmed to High Accuracy
  0.5% max Error (AD636K)
  1.0% max Error (AD636J)
Wide Response Capability:
  Computes RMS of AC and DC Signals
  1 MHz -3 dB Bandwidth: V RMS>100 mV
  Signal Crest Factor of 6 for 0.5% Error
dB Output with 50 dB Range
Low Power: 800 µA Quiescent Current
Single or Dual Supply Operation
Monolithic Integrated Circuit
Low Cost
Available in Chip Form

PIN CONNECTIONS & FUNCTIONAL BLOCK DIAGRAM

"D" Package (TO-116)

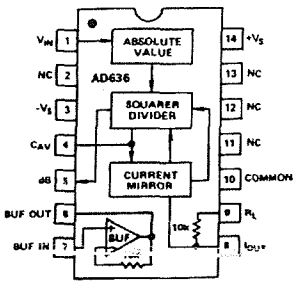

"H" Package (TO-100)

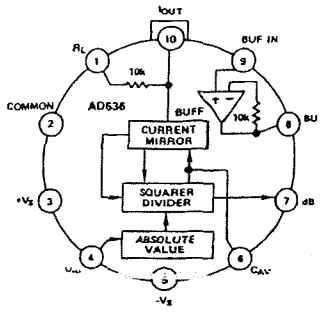

PRODUCT DESCRIPTION

The AD636 is a low power monolithic IC which performs true rms-to-dc conversion on low level signals. It offers performance which is comparable or superior to that of hybrid and modular converters costing much more. The AD636 is specified for a signal range of 0 mV to 200 mV rms. Crest factors up to 6 can be accommodated with less than 0.5% additional error, allowing accurate measurement of complex input waveforms.

The low power supply current requirement of the AD636, typically 800 µA, allows it to be used in battery-powered portable instruments. A wide range of power supplies can be used, from ±2.5 V to ±16.5 V or a single +5 V to +24 V supply. The input and output terminals are fully protected; the input signal can exceed the power supply with no damage to the device (allowing the presence of input signals in the absence of supply voltage) and the output buffer amplifier is short-circuit protected.

The AD636 includes an auxiliary dB output. This signal is derived from an internal circuit point which represents the logarithm of the rms output. The 0 dB reference level is set by an externally supplied current and can be selected by the user to correspond to any input level from 0 dBm (774.6 mV) to −20 dBm (77.46 mV). Frequency response ranges from 1.2 MHz at a 0 dBm level to over 10 kHz at −50 dBm.

The AD636 is designed for ease of use. The device is factory-rimmed at the wafer level for input and output offset, positive and negative waveform symmetry (dc reversal error), and full-scale accuracy at 200 mV rms. Thus no external trims are required to achieve full-rated accuracy.

AD636 is available in two accuracy grades; the AD636J total error of ±0.5 mV ±0.06% of reading, and the AD636K is accurate within ±0.2 mV to ±0.3% of reading. Both versions are specified for the 0°C to +70°C temperature range, and are offered in either a hermetically sealed 14-pin DIP or a 10-pin TO-100 metal can. Chips are also available.

PRODUCT HIGHLIGHTS

1. The AD636 computes the true root-mean-square of a complex ac (or ac plus dc) input signal and gives an equivalent dc output level. The true rms value of a waveform is a more useful quantity than the average rectified value since it is a measure of the power in the signal. The rms value of an ac-coupled signal is also its standard deviation.
2. The 200 millivolt full-scale range of the AD636 is compatible with many popular display-oriented analog-to-digital converters. The low power supply current requirement permits use in battery powered hand-held instruments.
3. The only external component required to perform measurements to the fully specified accuracy is the averaging capacitor. The value of this capacitor can be selected for the desired trade-off of low frequency accuracy, ripple, and settling time.
4. The on-chip buffer amplifier can be used to buffer either the input or the output. Used as an input buffer, it provides accurate performance from standard 10 MΩ input attenuators. As an output buffer, it can supply up to 5 milliamps of output current.
5. The AD636 will operate over a wide range of power supply voltages, including single +5 V to + 24 V or split ±2.5 V to ±16.5 V sources. A standard 9 V battery will provide several hundred hours of continuous operation.

REV. A

One Technology Way, P.O. Box 9106, Norwood, MA 02062-9106, U.S.A.
Tel: 617/329-4700 Fax: 617/326-8703

AD636—SPECIFICATIONS (@ +25°C, and $+V_S$ = +3 V, $-V_S$ = −5 V, unless otherwise noted)

Model	AD636J Min	AD636J Typ	AD636J Max	AD636K Min	AD636K Typ	AD636K Max	Units
TRANSFER FUNCTION		$V_{OUT} = \sqrt{avg.(V_{IN})^2}$			$V_{OUT} = \sqrt{avg.(V_{IN})^2}$		
CONVERSION ACCURACY							
Total Error, Internal Trim[1, 2]			±0.5 ±1.0			±0.2 ±0.5	mV ± % of Reading
vs. Temperature, 0°C to +70°C			±0.1 ±0.01			±0.1 ±0.005	mV ± % of Reading/°C
vs. Supply Voltage		±0.1 ±0.01			±0.1 ±0.01		mV ± % of Reading/V
dc Reversal Error at 200 mV		±0.2			±0.1		% of Reading
Total Error, External Trim[1]		±0.3 ±0.3			±0.1 ±0.2		mV ± % of Reading
ERROR VS. CREST FACTOR[3]							
Crest Factor 1 to 2		Specified Accuracy			Specified Accuracy		
Crest Factor = 3		−0.2			−0.2		% of Reading
Crest Factor = 6		−0.5			−0.5		% of Reading
AVERAGING TIME CONSTANT		25			25		ms/μF CAV
INPUT CHARACTERISTICS							
Signal Range, All Supplies							
Continuous rms Level		0 to 200			0 to 200		mV rms
Peak Transient Inputs							
+3 V, −5 V Supply			±2.8			±2.8	V pk
±2.5 V Supply			±2.0			±2.0	V pk
±5 V Supply			±5.0			±5.0	V pk
Maximum Continuous Nondestructive							
Input Level (All Supply Voltages)			±12			±12	V pk
Input Resistance	5.33	6.67	8	5.33	6.67	8	kΩ
Input Offset Voltage			±0.5			±0.2	mV
FREQUENCY RESPONSE[2, 4]							
Bandwidth for 1% Additional Error (0.09 dB)							
V_{IN} = 10 mV		14			14		kHz
V_{IN} = 100 mV		90			90		kHz
V_{IN} = 200 mV		130			130		kHz
±3 dB Bandwidth							
V_{IN} = 10 mV		100			100		kHz
V_{IN} = 100 mV		900			900		MHz
V_{IN} = 200 mV		1.5			1.5		MHz
OUTPUT CHARACTERISTICS[2]							
Offset Voltage, V_{IN} = COM			±0.5			±0.2	mV
vs. Temperature		±10			±10		μV/°C
vs. Supply		±0.1			±0.1		mV/V
Voltage Swing							
+3 V, −5 V Supply	0.3	0 to +1.0		0.3	0 to +1.0		V
±5 V to ±16.5 V Supply	0.3	0 to +1.0		0.3	0 to +1.0		V
Output Impedance	8	10	12	8	10	12	kΩ
dB OUTPUT							
Error, V_{IN} = 7 mV to 300 mV rms		±0.3	±0.5		±0.1	±0.2	dB
Scale Factor		−3.0			−3.0		mV/dB
Scale Factor Temperature Coefficient		+0.33			+0.33		% of Reading/°C
		−0.033			−0.033		dB/°C
I_{REF} for 0 dB = 0.1 V rms	2	4	8	2	4	8	μA
I_{REF} Range	1		50	1		50	μA
I_{OUT} TERMINAL							
I_{OUT} Scale Factor		100			100		μA/V rms
I_{OUT} Scale Factor Tolerance	−20	±10	+20	−20	±10	+20	%
Output Resistance	8	10	12	8	10	12	kΩ
Voltage Compliance		$-V_S$ to ($+V_S$ −2 V)			$-V_S$ to ($+V_S$ −2 V)		V
BUFFER AMPLIFIER							
Input and Output Voltage Range	$-V_S$ to ($+V_S$ −2 V)			$-V_S$ to ($+V_S$ −2 V)			V
Input Offset Voltage, R_S = 10k		±0.8	±2		±0.5	±1	mV
Input Bias Current		100	300		100	300	nA
Input Resistance		10^8			10^8		Ω
Output Current	(+5 mA, −130 μA)			(+5 mA, −130 μA)			
Short Circuit Current		20			20		mA
Small Signal Bandwidth		1			1		MHz
Slew Rate[5]		5			5		V/μs
POWER SUPPLY							
Voltage, Rated Performance		+3, −5			+3, −5		V
Dual Supply	+2, −2.5		±16.5	+2, −2.5		±16.5	V
Single Supply	+5		+24	+5		+24	V
Quiescent Current[6]		0.80	1.00		0.80	1.00	mA

Model	AD636J Min	AD636J Typ	AD636J Max	AD636K Min	AD636K Typ	AD636K Max	Units
TEMPERATURE RANGE							
Rated Performance	0		+70	0		+70	°C
Storage	–55		+150	–55		+150	°C
TRANSISTOR COUNT		62			62		

NOTES
[1]Accuracy specified for 0 mV to 200 mV rms, dc or 1 kHz sine wave input. Accuracy is degraded at higher rms signal levels.
[2]Measured at Pin 8 of DIP (I_{OUT}), with Pin 9 tied to common.
[3]Error vs. crest factor is specified as additional error for a 200 mV rms rectangular pulse trim, pulse width = 200 µs.
[4]Input voltages are expressed in volts rms.
[5]With 10 kΩ pull down resistor from Pin 6 (BUF OUT) to $-V_S$.
[6]With BUF input tied to Common.

Specifications subject to change without notice.

All min and max specifications are guaranteed. Specifications shown in **boldface** are tested on all production units at final electrical test and are used to calculate outgoing quality levels.

ABSOLUTE MAXIMUM RATINGS[1]

Supply Voltage
Dual Supply ..... ±16.5 V
Single Supply ..... +24 V
Internal Power Dissipation[2] ..... 500 mW
Maximum Input Voltage ..... ±12 V Peak
Storage Temperature Range N, R ..... –55°C to +150°C
Operating Temperature Range
AD636J/K ..... 0°C to +70°C
Lead Temperature Range (Soldering 60 sec) ..... +300°C
ESD Rating ..... 1000 V

NOTES
[1]Stresses above those listed under "Absolute Maximum Ratings" may cause permanent damage to the device. This is a stress rating only and functional operation of the device at these or any other conditions above those indicated in the operational section of this specification is not implied. Exposure to absolute maximum rating conditions for extended periods may affect device reliability.
[2]10-Pin Header: θ_{JA} = 150°C/Watt.
14-Pin Side Brazed Ceramic DIP: θ_{JA} = 95°C/Watt.

METALIZATION PHOTOGRAPH

Contact factory for latest dimensions.
Dimensions shown in inches and (mm).

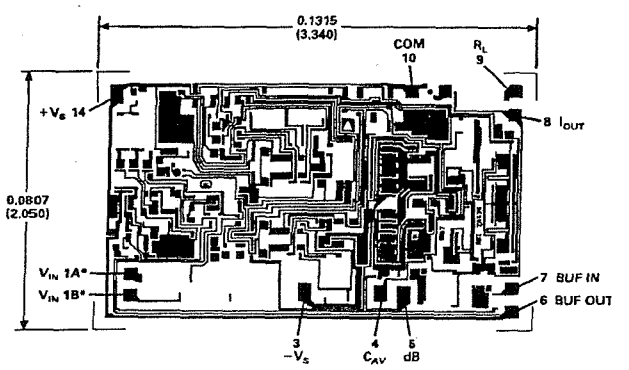

PAD NUMBERS CORRESPOND TO PIN NUMBERS FOR THE TO-116 14-PIN CERAMIC DIP PACKAGE.

NOTE
*BOTH PADS SHOWN MUST BE CONNECTED TO V_{IN}.

ORDERING GUIDE

Model	Temperature Range	Package Description	Package Option
AD636JD	0°C to +70°C	Side Brazed Ceramic DIP	D-14
AD636KD	0°C to +70°C	Side Brazed Ceramic DIP	D-14
AD636JH	0°C to +70°C	Header	H-10A
AD636KH	0°C to +70°C	Header	H-10A
AD636J Chip	0°C to +70°C	Chip	
AD636K Chip	0°C to +70°C	Chip	

STANDARD CONNECTION

The AD636 is simple to connect for the majority of high accuracy rms measurements, requiring only an external capacitor to set the averaging time constant. The standard connection is shown in Figure 1. In this configuration, the AD636 will measure the rms of the ac and dc level present at the input, but will show an error for low frequency inputs as a function of the filter capacitor, C_{AV}, as shown in Figure 5. Thus, if a 4 µF capacitor is used, the additional average error at 10 Hz will be 0.1%, at 3 Hz it will be 1%. The accuracy at higher frequencies will be according to specification. If it is desired to reject the dc input, a capacitor is added in series with the input, as shown in Figure 3; the capacitor must be nonpolar. If the AD636 is driven with power supplies with a considerable amount of high frequency ripple, it is advisable to bypass both supplies to ground with 0.1 µF ceramic discs as near the device as possible. C_F is an optional output ripple filter, as discussed elsewhere in this data sheet.

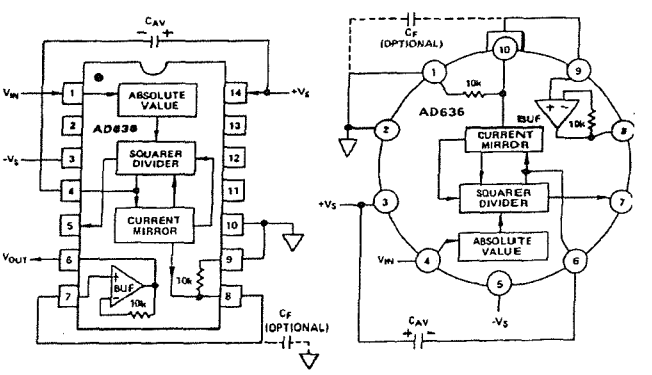

Figure 1. Standard RMS Connection

Applying the AD636

The input and output signal ranges are a function of the supply voltages as detailed in the specifications. The AD636 can also be used in an unbuffered voltage output mode by disconnecting the input to the buffer. The output then appears unbuffered across the 10k resistor. The buffer amplifier can then be used for other purposes. Further, the AD636 can be used in a current output mode by disconnecting the 10k resistor from the ground. The output current is available at Pin 8 (Pin 10 on the "H" package) with a nominal scale of 100 µA per volt rms input, positive out.

OPTIONAL TRIMS FOR HIGH ACCURACY

If it is desired to improve the accuracy of the AD636, the external trims shown in Figure 2 can be added. R4 is used to trim the offset. The scale factor is trimmed by using R1 as shown. The insertion of R2 allows R1 to either increase or decrease the scale factor by ±1.5%.

The trimming procedure is as follows:

1. Ground the input signal, V_{IN}, and adjust R4 to give zero volts output from Pin 6. Alternatively, R4 can be adjusted to give the correct output with the lowest expected value of V_{IN}.
2. Connect the desired full-scale input level to V_{IN}, either dc or a calibrated ac signal (1 kHz is the optimum frequency); then trim R1 to give the correct output from Pin 6, i.e., 200 mV dc input should give 200 mV dc output. Of course, a ±200 mV peak-to-peak sine wave should give a 141.4 mV dc output. The remaining errors, as given in the specifications, are due to the nonlinearity.

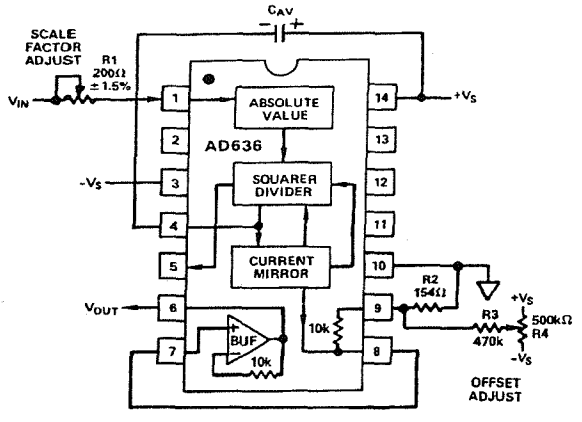

Figure 2. Optional External Gain and Output Offset Trims

SINGLE SUPPLY CONNECTION

The applications in Figures 1 and 2 assume the use of dual power supplies. The AD636 can also be used with only a single positive supply down to +5 volts, as shown in Figure 3. Figure 3 is optimized for use with a 9 volt battery. The major limitation of this connection is that only ac signals can be measured since the input stage must be biased off ground for proper operation. This biasing is done at Pin 10; thus it is critical that no extraneous signals be coupled into this point. Biasing can be accomplished by using a resistive divider between $+V_S$ and ground. The values of the resistors can be increased in the interest of lowered power consumption, since only 1 microamp of current flows into Pin 10 (Pin 2 on the "H" package). Alternately, the COM pin of some CMOS ADCs provides a suitable artificial ground for the AD636. AC input coupling requires only capacitor C2 as shown; a dc return is not necessary as it is provided internally. C2 is selected for the proper low frequency break point with the input resistance of 6.7 kΩ; for a cut-off at 10 Hz, C2 should be 3.3 µF. The signal ranges in this connection are slightly more restricted than in the dual supply connection. The load resistor, R_L, is necessary to provide current sinking capability.

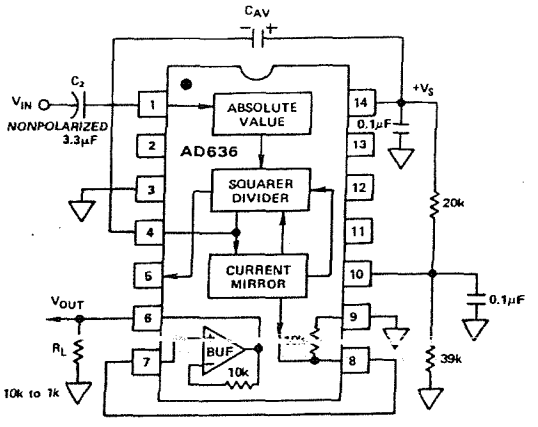

Figure 3. Single Supply Connection

CHOOSING THE AVERAGING TIME CONSTANT

The AD636 will compute the rms of both ac and dc signals. If the input is a slowly-varying dc voltage, the output of the AD636 will track the input exactly. At higher frequencies, the average output of the AD636 will approach the rms value of the input signal. The actual output of the AD636 will differ from the ideal output by a dc (or average) error and some amount of ripple, as demonstrated in Figure 4.

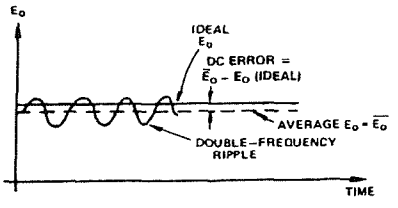

Figure 4. Typical Output Waveform for Sinusoidal Input

The dc error is dependent on the input signal frequency and the value of C_{AV}. Figure 5 can be used to determine the minimum value of C_{AV} which will yield a given % dc error above a given frequency using the standard rms connection.

The ac component of the output signal is the ripple. There are two ways to reduce the ripple. The first method involves using a large value of C_{AV}. Since the ripple is inversely proportional to C_{AV}, a tenfold increase in this capacitance will effect a tenfold reduction in ripple. When measuring waveforms with high crest factors, (such as low duty cycle pulse trains), the averaging time constant should be at least ten times the signal period. For example, a 100 Hz pulse rate requires a 100 ms time constant, which corresponds to a 4 µF capacitor (time constant = 25 ms per µF).

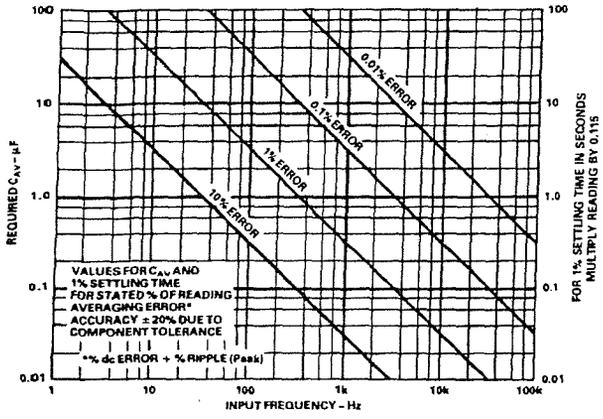

Figure 5. Error/Settling Time Graph for Use with the Standard rms Connection

The primary disadvantage in using a large C_{AV} to remove ripple is that the settling time for a step change in input level is increased proportionately. Figure 5 shows the relationship between C_{AV} and 1% settling time is 115 milliseconds for each microfarad of C_{AV}. The settling time is twice as great for decreasing signals as for increasing signals (the values in Figure 5 are for decreasing signals). Settling time also increases for low signal levels, as shown in Figure 6.

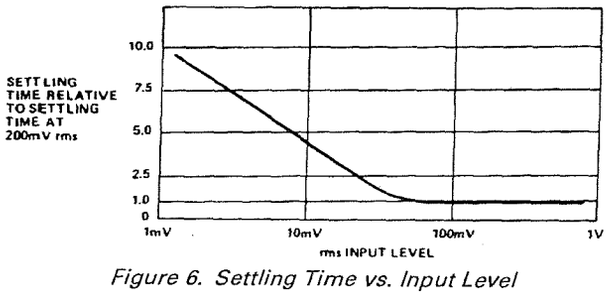

Figure 6. Settling Time vs. Input Level

A better method for reducing output ripple is the use of a "post-filter." Figure 7 shows a suggested circuit. If a single pole filter is used (C3 removed, R_X shorted), and C2 is approximately 5 times the value of C_{AV}, the ripple is reduced as shown in Figure 8, and settling time is increased. For example, with C_{AV} = 1 µF and C2 = 4.7 µF, the ripple for a 60 Hz input is reduced from 10% of reading to approximately 0.3% of reading. The settling time, however, is increased by approximately a factor of 3. The values of C_{AV} and C2 can therefore be reduced to permit faster settling times while still providing substantial ripple reduction.

The two-pole post-filter uses an active filter stage to provide even greater ripple reduction without substantially increasing the settling times over a circuit with a one-pole filter. The values of C_{AV}, C2, and C3 can then be reduced to allow extremely fast settling times for a constant amount of ripple. Caution should be exercised in choosing the value of C_{AV}, since the dc error is dependent upon this value and is independent of the post filter.

For a more detailed explanation of these topics refer to the *RMS-to-DC Conversion Application Guide, 2nd Edition,* available from Analog Devices.

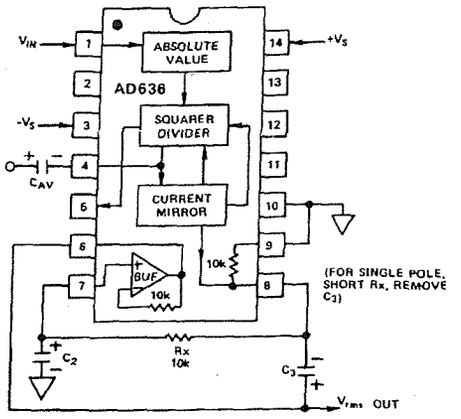

Figure 7. 2 Pole "Post" Filter

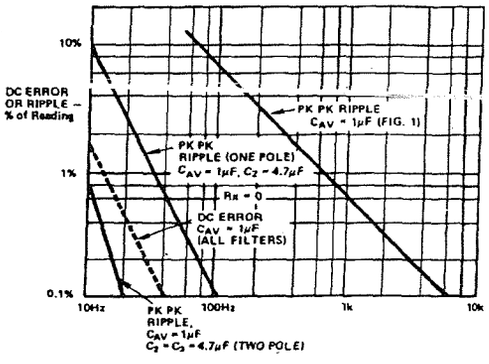

Figure 8. Performance Features of Various Filter Types

RMS MEASUREMENTS

AD636 PRINCIPLE OF OPERATION

The AD636 embodies an implicit solution of the rms equation that overcomes the dynamic range as well as other limitations inherent in a straightforward computation of rms. The actual computation performed by the AD636 follows the equation:

$$V\ rms = Avg.\left[\frac{V_{IN}^{\ 2}}{V\ rms}\right]$$

Figure 9 is a simplified schematic of the AD636; it is subdivided into four major sections: absolute value circuit (active rectifier), squarer/divider, current mirror, and buffer amplifier. The input voltage, V_{IN}, which can be ac or dc, is converted to a unipolar current I_1, by the active rectifier A_1, A_2. I_1 drives one input of the squarer/divider, which has the transfer function:

$$I_4 = \frac{I_1^{\ 2}}{I_3}$$

The output current, I_4, of the squarer/divider drives the current mirror through a low-pass filter formed by R1 and the externally connected capacitor, C_{AV}. If the R1, C_{AV} time constant is much greater than the longest period of the input signal, then I_4 is effectively averaged. The current mirror returns a current I_3, which equals Avg. [I_4], back to the squarer/divider to complete the implicit rms computation. Thus:

$$I_4 = Avg.\left[\frac{I_1^{\ 2}}{I_4}\right] = I_1\ rms$$

The current mirror also produces the output current, I_{OUT}, which equals $2I_4$. I_{OUT} can be used directly or converted to a voltage with R2 and buffered by A_4 to provide a low impedance voltage output. The transfer function of the AD636 thus results:

$$V_{OUT} = 2\ R2\ I\ rms = V_{IN}\ rms$$

The dB output is derived from the emitter of Q_3, since the voltage at this point is proportional to $-\log V_{IN}$. Emitter follower, Q_5, buffers and level shifts this voltage, so that the dB output voltage is zero when the externally supplied emitter current (I_{REF}) to Q_5 approximates I_3.

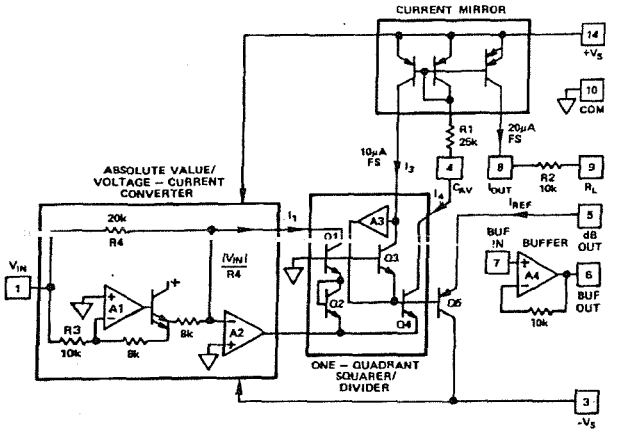

Figure 9. Simplified Schematic

THE AD636 BUFFER AMPLIFIER

The buffer amplifier included in the AD636 offers the user additional application flexibility. It is important to understand some of the characteristics of this amplifier to obtain optimum performance. Figure 10 shows a simplified schematic of the buffer.

Since the output of an rms-to-dc converter is always positive, it is not necessary to use a traditional complementary Class AB output stage. In the AD636 buffer, a Class A emitter follower is used instead. In addition to excellent positive output voltage swing, this configuration allows the output to swing fully down to ground in single-supply applications without the problems associated with most IC operational amplifiers.

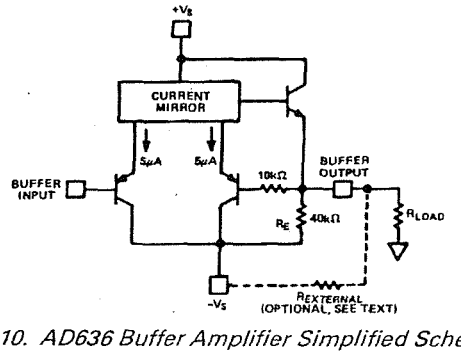

Figure 10. AD636 Buffer Amplifier Simplified Schematic

When this amplifier is used in dual-supply applications as an input buffer amplifier driving a load resistance referred to ground, steps must be taken to insure an adequate negative voltage swing. For negative outputs, current will flow from the load resistor through the 40 kΩ emitter resistor, setting up a voltage divider between $-V_S$ and ground. This reduced effective $-V_S$, will limit the available negative output swing of the buffer. Addition of an external resistor in parallel with R_E alters this voltage divider such that increased negative swing is possible.

Figure 11 shows the value of $R_{EXTERNAL}$ for a particular ratio of V_{PEAK} to $-V_S$ for several values of R_{LOAD}. Addition, of $R_{EXTERNAL}$ increases the quiescent current of the buffer amplifier by an amount equal to $R_{EXT}/-V_S$. Nominal buffer quiescent current with no $R_{EXTERNAL}$ is 30 μA at $-V_S = -5$ V.

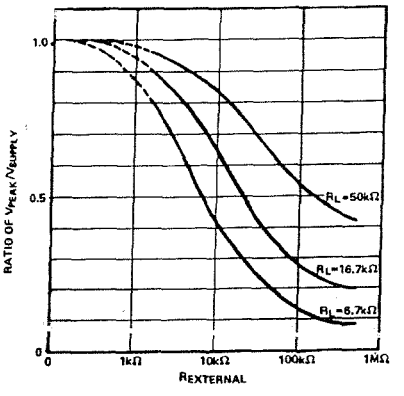

Figure 11. Ratio of Peak Negative Swing to $-V_S$ vs. $R_{EXTERNAL}$ for Several/Load Resistances

FREQUENCY RESPONSE

The AD636 utilizes a logarithmic circuit in performing the implicit rms computation. As with any log circuit, bandwidth is proportional to signal level. The solid lines in the graph below represent the frequency response of the AD636 at input levels from 1 millivolt to 1 volt rms. The dashed lines indicate the upper frequency limits for 1%, 10%, and ±3 dB of reading additional error. For example, note that a 1 volt rms signal will produce less than 1% of reading additional error up to 220 kHz. A 10 millivolt signal can be measured with 1% of reading additional error (100 μV) up to 14 kHz.

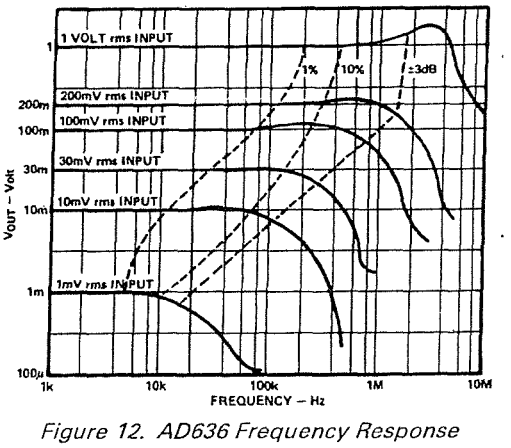

Figure 12. AD636 Frequency Response

AC MEASUREMENT ACCURACY AND CREST FACTOR

Crest factor is often overlooked in determining the accuracy of an ac measurement. Crest factor is defined as the ratio of the peak signal amplitude to the rms value of the signal (C.F. = V_P/V rms) Most common waveforms, such as sine and triangle waves, have relatively low crest factors (<2). Waveforms which

resemble low duty cycle pulse trains, such as those occurring in switching power supplies and SCR circuits, have high crest factors. For example, a rectangular pulse train with a 1% duty cycle has a crest factor of 10 (C.F. = $1\sqrt{\eta}$).

Figure 13 is a curve of reading error for the AD636 for a 200 mV rms input signal with crest factors from 1 to 7. A rectangular pulse train (pulse width 200 µs) was used for this test since it is the worst-case waveform for rms measurement (all the energy is contained in the peaks). The duty cycle and peak amplitude were varied to produce crest factors from 1 to 7 while maintaining a constant 200 mV rms input amplitude.

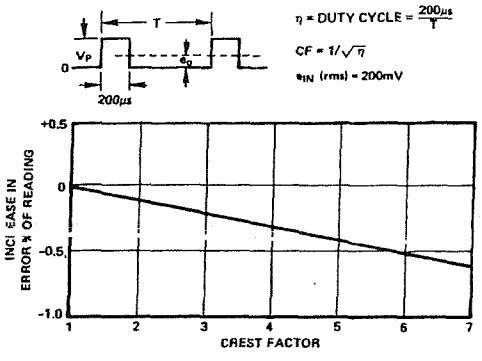

Figure 13. Error vs. Crest Factor

A COMPLETE AC DIGITAL VOLTMETER

Figure 14 shows a design for a complete low power ac digital voltmeter circuit based on the AD636. The 10 MΩ input attenuator allows full-scale ranges of 200 mV, 2 V, 20 V and 200 V rms. Signals are capacitively coupled to the AD636 buffer amplifier, which is connected in an ac bootstrapped configuration to minimize loading. The buffer then drives the 6.7 kΩ input impedance of the AD636. The COM terminal of the ADC chip provides the false ground required by the AD636 for single supply operation. An AD589 1.2 volt reference diode is used to provide a stable 100 millivolt reference for the ADC in the linear rms mode; in the dB mode, a 1N4148 diode is inserted in series to provide correction for the temperature coefficient of the dB scale factor. Calibration of the meter is done by first adjusting offset pot R17 for a proper zero reading, then adjusting the R13 for an accurate readout at full scale.

Calibration of the dB range is accomplished by adjusting R9 for the desired 0 dB reference point, then adjusting R14 for the desired dB scale factor (a scale of 10 counts per dB is convenient).

Total power supply current for this circuit is typically 2.8 mA using a 7106-type ADC.

A LOW POWER, HIGH INPUT IMPEDANCE dB METER

Introduction

The portable dB meter circuit featured here combines the functions of the AD636 rms converter, the AD589 voltage reference, and a µA776 low power operational amplifier. This meter offers excellent bandwidth and superior high and low level accuracy while consuming minimal power from a standard 9 volt transistor radio battery.

In this circuit, the built-in buffer amplifier of the AD636 is used as a "bootstrapped" input stage increasing the normal 6.7 kΩ input Z to an input impedance of approximately $10^{10}\Omega$.

Circuit Description

The input voltage, V_{IN}, is ac coupled by C4 while resistor R8, together with diodes D1, and D2, provide high input voltage protection.

The buffer's output, Pin 6, is ac coupled to the rms converter's input (Pin 1) by capacitor C2. Resistor, R9, is connected between the buffer's output, a Class A output stage, and the negative output swing. Resistor R1, is the amplifier's "bootstrapping" resistor.

With this circuit, single supply operation is made possible by setting "ground" at a point between the positive and negative sides of the battery. This is accomplished by sending 250 µA from the positive battery terminal through resistor R2, then through the 1.2 volt AD589 bandgap reference, and finally back to the negative side of the battery via resistor R10. This sets ground at 1.2 volts +3.18 volts (250 µA × 12.7 kΩ) = 4.4 volts below the positive battery terminal and 5.0 volts (250µA × 20 kΩ) above the negative battery terminal. Bypass capacitors C3 and C5 keep both sides of the battery at a low ac impedance to ground. The AD589 bandgap reference establishes the 1.2 volt regulated reference voltage which together with resistor R3 and trimming potentiometer R4 set the zero dB reference current I_{REF}.

Performance Data

0 dB Reference Range = 0 dBm (770 mV) to -20 dBm (77 mV) rms
0 dBm = 1 milliwatt in 600 Ω
Input Range (at I_{REF} = 770 mV) = 50 dBm
Input Impedance = approximately 10^{10} Ω
V_{SUPPLY} Operating Range +5 V dc to +20 V dc
$I_{QUIESCENT}$ = 1. 8 mA typical

Accuracy with 1 kHz sine wave and 9 volt dc supply:
0 dB to -40 dBm ± 0.1 dBm
0 dBm to -50 dBm ± 0.15 dBm
+10 dBm to -50 dBm ± 0.5 dBm

Frequency Response ±3 dBm:

Input
0 dBm = 5 Hz to 380 kHz
-10 dBm = 5 Hz to 370 kHz
-20 dBm = 5 Hz to 240 kHz
-30 dBm = 5 Hz to 100 kHz
-40 dBm = 5 Hz to 45 kHz
-50 dBm = 5 Hz to 17 kHz

Calibration

1. First calibrate the zero dB reference level by applying a 1 kHz sine wave from an audio oscillator at the desired zero dB amplitude. This may be anywhere from zero dBm (770 mV rms - 2.2 volts p-p) to -20 dBm (77 mV rms 220 mV - p-p). Adjust the I_{REF} cal trimmer for a zero indication on the analog meter.
2. The final step is to calibrate the meter scale factor or gain. Apply an input signal -40 dB below the set zero dB reference and adjust the scale factor calibration trimmer for a 40 µA reading on the analog meter.

The temperature compensation resistors for this circuit may be purchased from: *Tel Labs Inc.*, 154 Harvey Road, P.O. Box 375, Londonderry, NH 03053, Part #Q332A 2 kΩ 1% +3500 ppm/°C or from *Precision Resistor Company*, 109 U.S. Highway 22, Hillside, NJ 07205, Part #PT146 2 kΩ 1% +3500 ppm/°C.

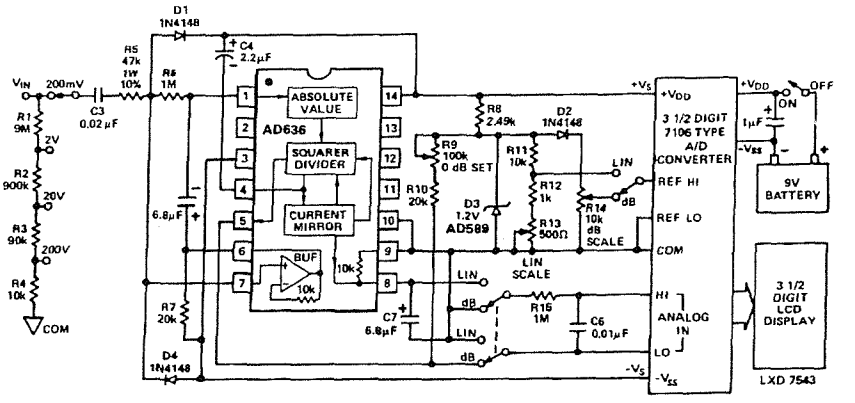

Figure 14. A Portable, High Z Input, RMS DPM and dB Meter Circuit

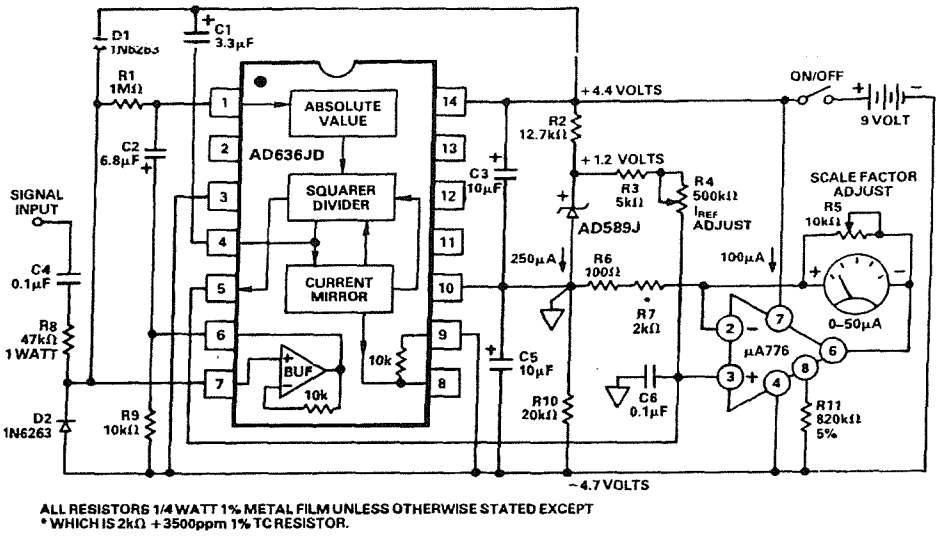

ALL RESISTORS 1/4 WATT 1% METAL FILM UNLESS OTHERWISE STATED EXCEPT
* WHICH IS 2kΩ + 3500ppm 1% TC RESISTOR.

Figure 15. A Low Power, High Input Impedance dB Meter

OUTLINE DIMENSIONS

Dimensions shown in inches and (mm).

D Package (TO-116)

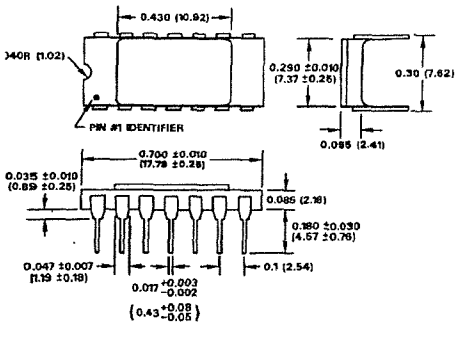

H Package (TO-100)

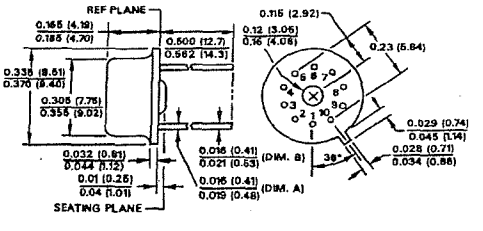

9.3 A (iii) AD637 Wide-Band RMS-to-DC Convertor

High Precision, Wide-Band RMS-to-DC Converter

AD637

FEATURES

High Accuracy
- 0.02% Max Nonlinearity, 0 V to 2 V RMS Input
- 0.10% Additional Error to Crest Factor of 3

Wide Bandwidth
- 8 MHz at 2 V RMS Input
- 600 kHz at 100 mV RMS

Computes:
- True RMS
- Square
- Mean Square
- Absolute Value

dB Output (60 dB Range)

Chip Select-Power Down Feature Allows:
- Analog "3-State" Operation
- Quiescent Current Reduction from 2.2 mA to 350 µA

Side-Brazed DIP, Low Cost Cerdip and SOIC

FUNCTIONAL BLOCK DIAGRAMS

Ceramic DIP (D) and Cerdip (Q) Packages

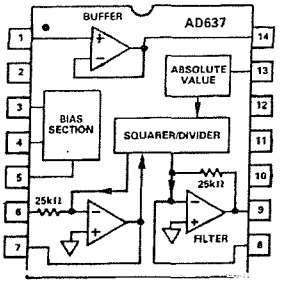

SOIC (R) Package

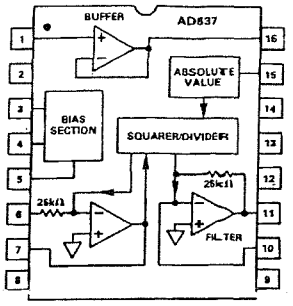

PRODUCT DESCRIPTION

The AD637 is a complete high accuracy monolithic rms-to-dc converter that computes the true rms value of any complex waveform. It offers performance that is unprecedented in integrated circuit rms-to-dc converters and comparable to discrete and modular techniques in accuracy, bandwidth and dynamic range. A crest factor compensation scheme in the AD637 permits measurements of signals with crest factors of up to 10 with less than 1% additional error. The circuit's wide bandwidth permits the measurement of signals up to 600 kHz with inputs of 200 mV rms and up to 8 MHz when the input levels are above 1 V rms.

As with previous monolithic rms converters from Analog Devices, the AD637 has an auxiliary dB output available to the user. The logarithm of the rms output signal is brought out to a separate pin allowing direct dB measurement with a useful range of 60 dB. An externally programmed reference current allows the user to select the 0 dB reference voltage to correspond to any level between 0.1 V and 2.0 V rms.

A chip select connection on the AD637 permits the user to decrease the supply current from 2.2 mA to 350 µA during periods when the rms function is not in use. This feature facilitates the addition of precision rms measurement to remote or hand-held applications where minimum power consumption is critical. In addition when the AD637 is powered down the output goes to a high impedance state. This allows several AD637s to be tied together to form a wide-band true rms multiplexer.

The input circuitry of the AD637 is protected from overload voltages that are in excess of the supply levels. The inputs will not be damaged by input signals if the supply voltages are lost.

The AD637 is available in two accuracy grades (J, K) for commercial (0°C to +70°C) temperature range applications; two accuracy grades (A, B) for industrial (–40°C to +85°C) applications; and one (S) rated over the –55°C to + 125°C temperature range. All versions are available in hermetically-sealed, 14-pin side-brazed ceramic DIPs as well as low cost cerdip packages. A 16-pin SOIC package is also available.

PRODUCT HIGHLIGHTS

1. The AD637 computes the true root-mean-square, mean square, or absolute value of any complex ac (or ac plus dc) input waveform and gives an equivalent dc output voltage. The true rms value of a waveform is more useful than an average rectified signal since it relates directly to the power of the signal. The rms value of a statistical signal is also related to the standard deviation of the signal.
2. The AD637 is laser wafer trimmed to achieve rated performance without external trimming. The only external component required is a capacitor which sets the averaging time period. The value of this capacitor also determines low frequency accuracy, ripple level and settling time.
3. The chip select feature of the AD637 permits the user to power down the device down during periods of nonuse, thereby, decreasing battery drain in remote or hand-held applications.
4. The on-chip buffer amplifier can be used as either an input buffer or in an active filter configuration. The filter can be used to reduce the amount of ac ripple, thereby, increasing the accuracy of the measurement.

REV. C

One Technology Way, P.O. Box 9106, Norwood, MA 02062-9106, U.S.A.
Tel: 617/329-4700 Fax: 617/326-8703

AD637–SPECIFICATIONS (@ + 25°C, and ±15 V dc unless otherwise noted)

Model	AD637J/A Min	AD637J/A Typ	AD637J/A Max	AD637K/B Min	AD637K/B Typ	AD637K/B Max	AD637S Min	AD637S Typ	AD637S Max	Units
TRANSFER FUNCTION		$V_{OUT} = \sqrt{avg.(V_{IN})^2}$			$V_{OUT} = \sqrt{avg.(V_{IN})^2}$			$V_{OUT} = \sqrt{avg.(V_{IN})^2}$		
CONVERSION ACCURACY										
Total Error, Internal Trim[1] (Fig. 2)			±1 ± 0.5			±0.5 ± 0.2			±1 ± 0.5	mV ± % of Reading
T_{MIN} to T_{MAX}			±3.0 ± 0.6			±2.0 ± 0.3			±6 ± 0.7	mV ± % of Reading
vs. Supply, + V_{IN} = +300 mV		30	150		30	150		30	150	µV/V
vs. Supply, - V_{IN} = -300 mV		100	300		100	300		100	300	µV/V
DC Reversal Error at 2 V			0.25			0.1			0.25	% of Reading
Nonlinearity 2 V Full Scale[2]			0.04			0.02			0.04	% of FSR
Nonlinearity 7 V Full Scale			0.05			0.05			0.05	% of FSR
Total Error, External Trim		±0.5 ± 0.1			±0.25 ± 0.05			±0.5 ± 0.1		mV ± % of Reading
ERROR VS. CREST FACTOR[3]										
Crest Factor 1 to 2		*Specified Accuracy*			*Specified Accuracy*			*Specified Accuracy*		
Crest Factor = 3		±0.1			±0.1			±0.1		% of Reading
Crest Factor = 10		±1.0			±1.0			±1.0		% of Reading
AVERAGING TIME CONSTANT		25			25			25		ms/µF C_{AV}
INPUT CHARACTERISTICS										
Signal Range, ±15 V Supply										
Continuous RMS Level		0 to 7			0 to 7			0 to 7		V rms
Peak Transient Input			±15			±15			±15	V p-p
Signal Range, ±5 V Supply										
Continuous rms Level		0 to 4			0 to 4			0 to 4		V rms
Peak Transient Input			±6			±6			±6	V p-p
Maximum Continuous Nondestructive Input Level (All Supply Voltages)			±15			±15			±15	V p-p
Input Resistance	6.4	8	9.6	6.4	8	9.6	6.4	8	9.6	kΩ
Input Offset Voltage			±0.5			±0.2			±0.5	mV
FREQUENCY RESPONSE[4]										
Bandwidth for 1% Additional Error (0.09 dB)										
V_{IN} = 20 mV		11			11			11		kHz
V_{IN} = 200 mV		66			66			66		kHz
V_{IN} = 2 V		200			200			200		kHz
±3 dB Bandwidth										
V_{IN} = 20 mV		150			150			150		kHz
V_{IN} = 200 mV		1			1			1		MHz
V_{IN} = 2 V		8			8			8		MHz
OUTPUT CHARACTERISTICS										
Offset Voltage			±1			±0.5			±1	mV
vs. Temperature		±0.05	±0.089		±0.04	±0.056		±0.04	±0.07	mV/°C
Voltage Swing, ±15 V Supply, 2 kΩ Load	0 to +12.0	+13.5		0 to +12.0	+13.5		0 to +12.0	+13.5		V
Voltage Swing, ±3 V Supply, 2 kΩ Load	0 to +2	+2.2		0 to +2	+2.2		0 to +2	+2.2		V
Output Current	6			6			6			mA
Short Circuit Current		20			20			20		mA
Resistance, Chip Select "High"		0.5			0.5			0.5		Ω
Resistance, Chip Select "Low"		100			100			100		kΩ
dB OUTPUT										
Error, V_{IN} 7 mV to 7 V rms, 0 dB = 1 V rms		±0.5			±0.3			±0.5		dB
Scale Factor		-3			-3			-3		mV/dB
Scale Factor Temperature Coefficient		+0.33			+0.33			+0.33		% of Reading/°C
		-0.033			-0.033			-0.033		dB/°C
I_{REF} for 0 dB = 1 V rms	5	20	80	5	20	80	5	20	80	µA
I_{REF} Range	1		100	1		100	1		100	µA
BUFFER AMPLIFIER										
Input Output Voltage Range	$-V_S$ to ($+V_S$ - 2.5 V)			$-V_S$ to ($+V_S$ - 2.5 V)			$-V_S$ to ($+V_S$ - 2.5 V)			V
Input Offset Voltage		±0.8	±2		±0.5	±1		±0.8	±2	mV
Input Current		±2	±10		±2	±5		±2	±10	nA
Input Resistance		10^8			10^8			10^8		Ω
Output Current	(+5 mA, -130 µA)			(+5 mA, -130 µA)			(+5 mA, -130 µA)			
Short Circuit Current		20			20			20		mA
Small Signal Bandwidth		1			1			1		MHz
Slew Rate[5]		5			5			5		V/µs
DENOMINATOR INPUT										
Input Range		0 to +10			0 to +10			0 to +10		V
Input Resistance	20	25	30	20	25	30	20	25	30	kΩ
Offset Voltage		±0.2	±0.5		±0.2	±0.5		±0.2	±0.5	mV
CHIP SELECT PROVISION (CS)										
RMS "ON" Level	Open or +2.4 V < V_C < $+V_S$			Open or +2.4 V < V_C < $+V_S$			Open or +2.4 V < V_C < $+V_S$			
RMS "OFF" Level	V_C < +0.2 V			V_C < +0.2 V			V_C < +0.2 V			
I_{OUT} of Chip Select										
CS "LOW"	10			10			10			µA
CS "HIGH"	Zero			Zero			Zero			
On Time Constant	10 µs + ((25 kΩ) x C_{AV})			10 µs + ((25 kΩ) x C_{AV})			10 µs + ((25 kΩ) x C_{AV})			
Off Time Constant	10 µs + ((25 kΩ) x C_{AV})			10 µs + ((25 kΩ) x C_{AV})			10 µs + ((25 kΩ) x C_{AV})			
POWER SUPPLY										
Operating Voltage Range	±3.0		±18	±3.0		±18	±3.0		±18	V
Quiescent Current		2.2	3		2.2	3		2.2	3	mA
Standby Current		350	450		350	450		350	450	µA
TRANSISTOR COUNT		107			107			107		

NOTES
[1]Accuracy specified 0-7 V rms dc with AD637 connected as shown in Figure 2.
[2]Nonlinearity is defined as the maximum deviation from the straight line connecting the readings at 10 mV and 2 V.
[3]Error vs. crest factor is specified as additional error for 1 V rms.
[4]Input voltages are expressed in volts rms. % are in % of reading.
[5]With external 2 kΩ pull down resistor tied to $-V_S$.

Specifications subject to change without notice.

Specifications shown in **boldface** are tested on all production units at final electrical test. Results from those tests are used to calculate outgoing quality levels. All min and max specifications are guaranteed, although only those shown in boldface are tested on all production units.

ABSOLUTE MAXIMUM RATINGS

ESD Rating	500 V
Supply Voltage	±18 V dc
Internal Quiescent Power Dissipation	108 mW
Output Short-Circuit Duration	Indefinite
Storage Temperature Range	-65°C to +150°C
Lead Temperature Range (Soldering 10 secs)	+300°C
Rated Operating Temperature Range	
AD637J, K	0°C to +70°C
AD637A, B	-40°C to +85°C
AD637S, 5962-8963701CA	-55°C to +125°C

ORDERING GUIDE

Model[1, 2]	Temperature Range	Package Description	Package Option
AD637AR	-40°C to +85°C	SOIC	R-16
AD637BR	-40°C to +85°C	SOIC	R-16
AD637AQ	-40°C to +85°C	Cerdip	Q-14
AD637BQ	-40°C to +85°C	Cerdip	Q-14
AD637JD	0°C to +70°C	Side Brazed Ceramic DIP	D-14
AD637KD	0°C to +70°C	Side Brazed Ceramic DIP	D-14
AD637JQ	0°C to +70°C	Cerdip	Q-14
AD637KQ	0°C to +70°C	Cerdip	Q-14
AD637JR	0°C to +70°C	SOIC	R-16
AD637JR-REEL	0°C to +70°C	SOIC	R-16
AD637JR-REEL7	0°C to +70°C	SOIC	R-16
AD637KR	0°C to +70°C	SOIC	R-16
AD637SD	-55°C to +125°C	Side Brazed Ceramic DIP	D-14
AD637SD/883B	-55°C to +125°C	Side Brazed Ceramic DIP	D-14
AD637SQ/883B	-55°C to +125°C	Cerdip	Q-14

NOTES
[1]"S" grade chips are also available.
[2]A Standard Microcircuit Drawing, 5962-8963701CA, is also available.

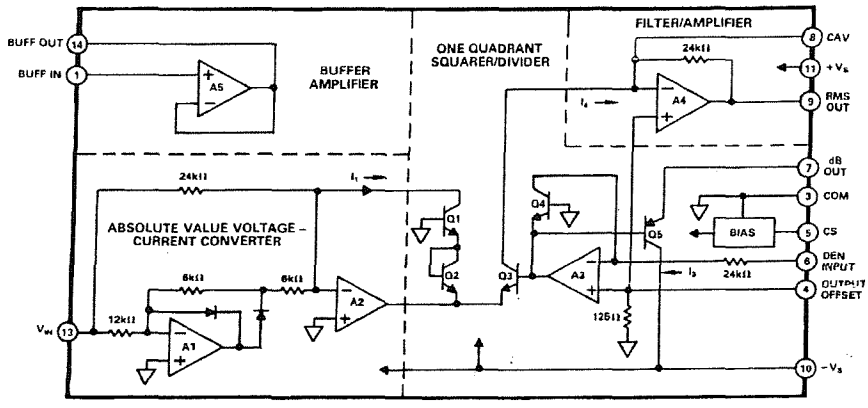

Figure 1. Simplified Schematic

CAUTION

ESD (electrostatic discharge) sensitive device. Electrostatic charges as high as 4000 V readily accumulate on the human body and test equipment and can discharge without detection. Although the AD637 features proprietary ESD protection circuitry, permanent damage may occur on devices subjected to high energy electrostatic discharges. Therefore, proper ESD precautions are recommended to avoid performance degradation or loss of functionality.

FUNCTIONAL DESCRIPTION

The AD637 embodies an implicit solution of the rms equation that overcomes the inherent limitations of straightforward rms computation. The actual computation performed by the AD637 follows the equation

$$V\ rms = Avg\left[\frac{V_{IN}^2}{V\ rms}\right]$$

Figure 1 is a simplified schematic of the AD637, it is subdivided into four major sections; absolute value circuit (active rectifier), square/divider, filter circuit and buffer amplifier. The input voltage V_{IN} which can be ac or dc is converted to a unipolar current I1 by the active rectifier A1, A2. I1 drives one input of the squarer divider which has the transfer function

$$I_4 = \frac{I_1^2}{I_3}$$

The output current of the squarer/divider, I4 drives A4 which forms a low-pass filter with the external averaging capacitor. If the RC time constant of the filter is much greater than the longest period of the input signal than A4s output will be proportional to the average of I4. The output of this filter amplifier is used by A3 to provide the denominator current I3 which equals Avg. I4 and is returned to the squarer/divider to complete the implicit rms computation.

$$I_4 = Avg\left[\frac{I_1^2}{I_4}\right] = I_1\ rms$$

and

$$V_{OUT} = V_{IN}\ rms$$

If the averaging capacitor is omitted, the AD637 will compute the absolute value of the input signal. A nominal 5 pF capacitor should be used to insure stability. The circuit operates identically to that of the rms configuration except that I3 is now equal to I4 giving

$$I_4 = \frac{I_1^2}{I_4}$$

$$I_4 = |I_1|$$

The denominator current can also be supplied externally by providing a reference voltage, V_{REF}, to Pin 6. The circuit operates identically to the rms case except that I3 is now proportional to V_{REF}. Thus:

$$I_4 = Avg\frac{I_1^2}{I_3}$$

and

$$V_O = \frac{V_{IN}^2}{V_{DEN}}$$

This is the mean square of the input signal.

STANDARD CONNECTION

The AD637 is simple to connect for a majority of rms measurements. In the standard rms connection shown in Figure 2, only a single external capacitor is required to set the averaging time constant. In this configuration, the AD637 will compute the true rms of any input signal. An averaging error, the magnitude of which will be dependent on the value of the averaging capacitor, will be present at low frequencies. For example, if the filter capacitor C_{AV}, is 4 µF this error will be 0.1% at 10 Hz and increases to 1% at 3 Hz. If it is desired to measure only ac signals, the AD637 can be ac coupled through the addition of a nonpolar capacitor in series with the input as shown in Figure 2.

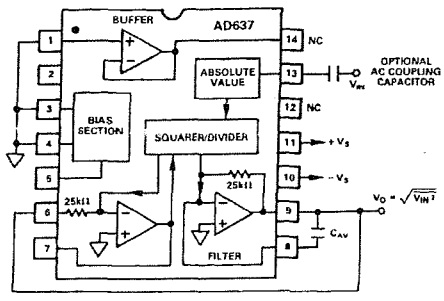

Figure 2. Standard RMS Connection

The performance of the AD637 is tolerant of minor variations in the power supply voltages, however, if the supplies being used exhibit a considerable amount of high frequency ripple it is advisable to bypass both supplies to ground through a 0.1 µF ceramic disc capacitor placed as close to the device as possible.

The output signal range of the AD637 is a function of the supply voltages, as shown in Figure 3. The output signal can be used buffered or nonbuffered depending on the characteristics of the load. If no buffer is needed, tie buffer input (Pin 1) to common. The output of the AD637 is capable of driving 5 mA into a 2 kΩ load without degrading the accuracy of the device.

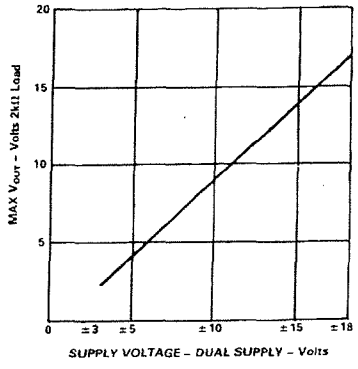

Figure 3. AD637 max V_{OUT} vs. Supply Voltage

CHIP SELECT

The AD637 includes a chip select feature which allows the user to decrease the quiescent current of the device from 2.2 mA to 350 µA. This is done by driving the CS, Pin 5, to below 0.2 V dc. Under these conditions, the output will go into a high impedance state. In addition to lowering power consumption, this feature permits bussing the outputs of a number of AD637s to form a wide bandwidth rms multiplexer. If the chip select is not being used, Pin 5 should be tied high.

OPTIONAL TRIMS FOR HIGH ACCURACY

The AD637 includes provisions to allow the user to trim out both output offset and scale factor errors. These trims will result in significant reduction in the maximum total error as shown in Figure 4. This remaining error is due to a nontrimmable input offset in the absolute value circuit and the irreducible nonlinearity of the device.

The trimming procedure on the AD637 is as follows:

1. Ground the input signal, V_{IN} and adjust R1 to give 0 V output from Pin 9. Alternatively R1 can be adjusted to give the correct output with the lowest expected value of V_{IN}.

2. Connect the desired full scale input to V_{IN}, using either a dc or a calibrated ac signal, trim R3 to give the correct output at Pin 9, i.e., 1 V dc should give 1.000 V dc output. Of course, a 2 V peak-to-peak sine wave should give 0.707 V dc output. Remaining errors are due to the nonlinearity.

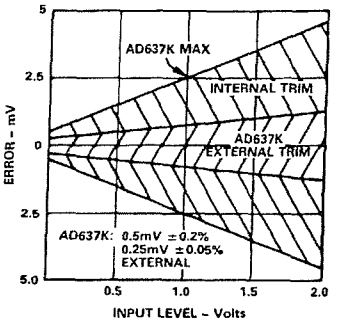

Figure 4. Max Total Error vs. Input Level AD637K Internal and External Trims

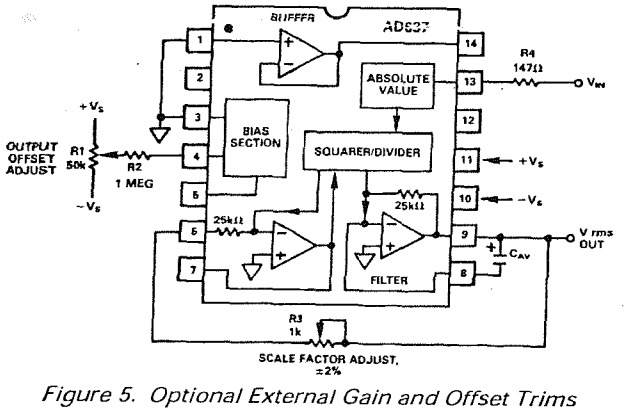

Figure 5. Optional External Gain and Offset Trims

CHOOSING THE AVERAGING TIME CONSTANT

The AD637 will compute the true rms value of both dc and ac input signals. At dc the output will track the absolute value of the input exactly; with ac signals the AD637's output will approach the true rms value of the input. The deviation from the ideal rms value is due to an averaging error. The averaging error is comprised of an ac and dc component. Both components are functions of input signal frequency *f*, and the averaging time constant τ (τ: 25 ms/μF of averaging capacitance). As shown in Figure 6, the averaging error is defined as the peak value of the ac component, ripple, plus the value of the dc error.

The peak value of the ac ripple component of the averaging error is defined approximately by the relationship:

$$\frac{50}{6.3\,\tau f} \text{ in \% of reading where } (t > 1/f)$$

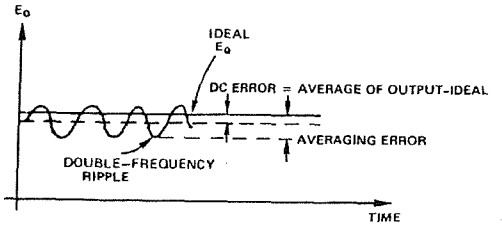

Figure 6. Typical Output Waveform for a Sinusoidal Input

This ripple can add a significant amount of uncertainty to the accuracy of the measurement being made. The uncertainty can be significantly reduced through the use of a post filtering network or by increasing the value of the averaging capacitor.

The dc error appears as a frequency dependent offset at the output of the AD637 and follows the equation:

$$\frac{1}{0.16 + 6.4\tau^2 f^2} \text{ in \% of reading}$$

Since the averaging time constant, set by C_{AV}, directly sets the time that the rms converter "holds" the input signal during computation, the magnitude of the dc error is determined only by C_{AV} and will not be affected by post filtering.

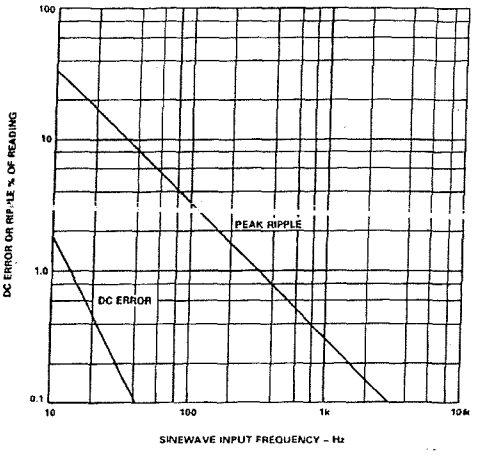

Figure 7. Comparison of Percent DC Error to the Percent Peak Ripple over Frequency Using the AD637 in the Standard RMS Connection with a 1 × μF C_{AV}

The ac ripple component of averaging error can be greatly reduced by increasing the value of the averaging capacitor. There are two major disadvantages to this: first, the value of the averaging capacitor will become extremely large and second, the settling time of the AD637 increases in direct proportion to the value of the averaging capacitor (Ts = 115 ms/μF of averaging capacitance). A preferable method of reducing the ripple is through the use of the post filter network, shown in Figure 8. This network can be used in either a one or two pole configuration. For most applications the single pole filter will give the best overall compromise between ripple and settling time.

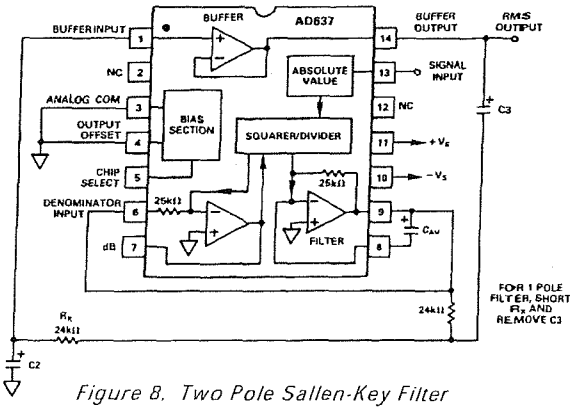

Figure 8. Two Pole Sallen-Key Filter

Figure 9a shows values of C_{AV} and the corresponding averaging error as a function of sine-wave frequency for the standard rms connection. The 1% settling time is shown on the right side of the graph.

Figure 9b shows the relationship between averaging error, signal frequency settling time and averaging capacitor value. This graph is drawn for filter capacitor values of 3.3 times the averaging capacitor value. This ratio sets the magnitude of the ac and dc errors equal at 50 Hz. As an example, by using a 1 µF averaging capacitor and a 3.3 µF filter capacitor, the ripple for a 60 Hz input signal will be reduced from 5.3% of reading using the averaging capacitor alone to 0.15% using the single pole filter. This gives a factor of thirty reduction in ripple and yet the settling time would only increase by a factor of three. The values of C_{AV} and C_2, the filter capacitor, can be calculated for the desired value of averaging error and settling time by using Figure 9b.

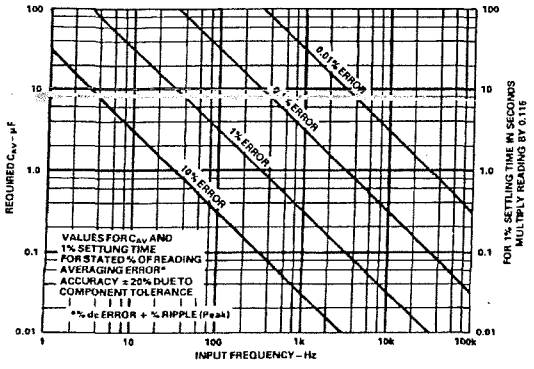

Figure 9a.

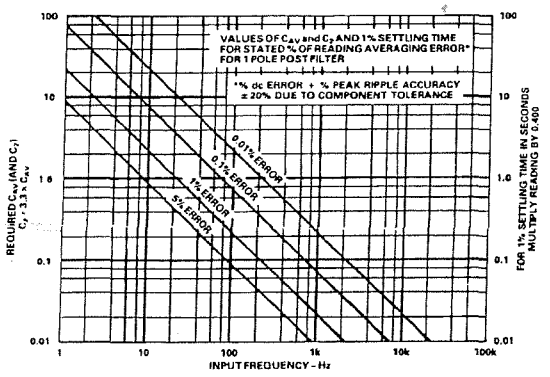

Figure 9b.

The symmetry of the input signal also has an effect on the magnitude of the averaging error. Table I gives practical component values for various types of 60 Hz input signals. These capacitor values can be directly scaled for frequencies other than 60 Hz, i.e., for 30 Hz double these values, for 120 Hz they are halved.

For applications that are extremely sensitive to ripple, the two pole configuration is suggested. This configuration will minimize capacitor values and settling time while maximizing performance.

Figure 9c can be used to determine the required value of C_{AV}, C_2 and C_3 for the desired level of ripple and settling time.

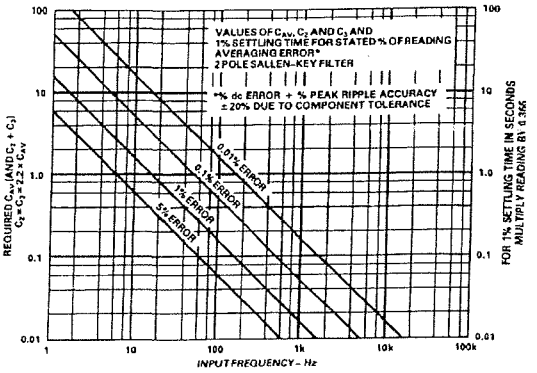

Figure 9c.

Table I. Practical Values of C_{AV} and C2 for Various Input Waveforms

	Input Waveform and Period	Absolute Value Circuit Waveform and Period	Minimum R × C_{AV} Time Constant	Recommended C_{AV} and C2 Values for 1% Averaging Error in 60Hz with T = 16.6ms		1% Settling Time
				Recommended Standard	Recommended Standard	
A	Symmetrical Sine Wave	1/2T	1/2T	0.47µF	1.5µF	181ms
B	Sine Wave with dc Offset	T	T	0.82µF	2.7µF	325ms
C	Pulse Train Waveform	T, T_2	$10(T - T_2)$	6.8µF	22µF	2.67sec
D	T, T_2	T, T_2	$10(T - 2T_2)$	5.6µF	18µF	2.17sec

FREQUENCY RESPONSE

The frequency response of the AD637 at various signal levels is shown in Figure 10. The dashed lines show the upper frequency limits for 1%, 10% and ± 3 dB of additional error. For example, note that for 1% additional error with a 2 V rms input the highest frequency allowable is 200 kHz. A 200 mV signal can be measured with 1% error at signal frequencies up to 100 kHz.

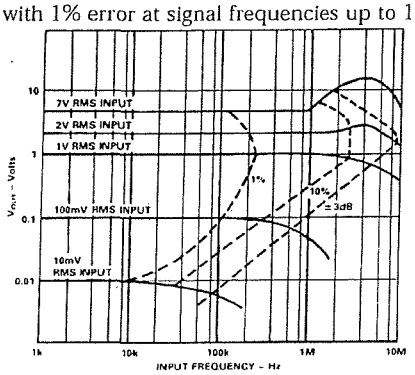

Figure 10. Frequency Response

To take full advantage of the wide bandwidth of the AD637 care must be taken in the selection of the input buffer amplifier. To insure that the input signal is accurately presented to the converter, the input buffer must have a -3 dB bandwidth that is

wider than that of the AD637. A point that should not be overlooked is the importance of slew rate in this application. For example, the minimum slew rate required for a 1 V rms 5 MHz sine-wave input signal is 44 V/µs. The user is cautioned that this is the minimum rising or falling slew rate and that care must be exercised in the selection of the buffer amplifier as some amplifiers exhibit a two-to-one difference between rising and falling slew rates. The AD845 is recommended as a precision input buffer.

AC MEASUREMENT ACCURACY AND CREST FACTOR

Crest factor is often overlooked in determining the accuracy of an ac measurement. Crest factor is defined as the ratio of the peak signal amplitude to the rms value of the signal (C.F. = Vp/V rms). Most common waveforms, such as sine and triangle waves, have relatively low crest factors (≤2). Waveforms which resemble low duty cycle pulse trains, such as those occurring in switching power supplies and SCR circuits, have high crest factors. For example, a rectangular pulse train with a 1% duty cycle has a crest factor of 10 (C.F. = $1/\sqrt{\eta}$).

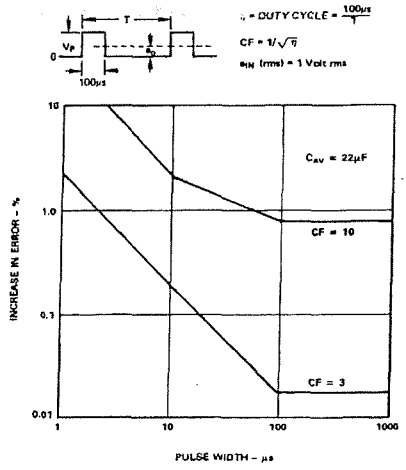

Figure 11. AD637 Error vs. Pulse Width Rectangular Pulse

Figure 12 is a curve of additional reading error for the AD637 for a 1 volt rms input signal with crest factors from 1 to 11. A rectangular pulse train (pulse width 100 µs) was used for this test since it is the worst-case waveform for rms measurement (all

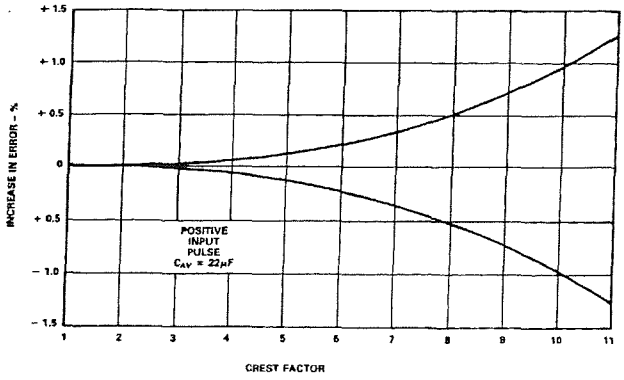

Figure 12. Additional Error vs. Crest Factor

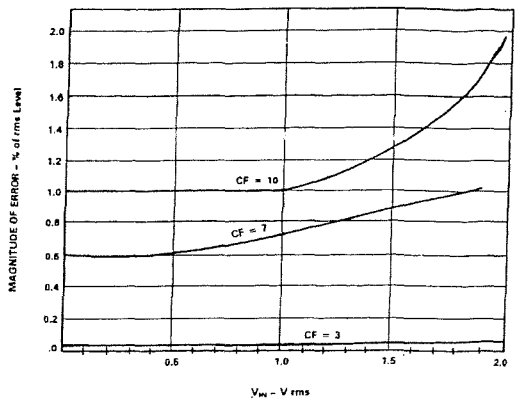

Figure 13. Error vs. RMS Input Level for Three Common Crest Factors

the energy is contained in the peaks). The duty cycle and peak amplitude were varied to produce crest factors from 1 to 10 while maintaining a constant 1 volt rms input amplitude.

CONNECTION FOR dB OUTPUT

Another feature of the AD637 is the logarithmic or decibel output. The internal circuit which computes dB works well over a 60 dB range. The connection for dB measurement is shown in Figure 14. The user selects the 0 dB level by setting R1 for the proper 0 dB reference current (which is set to exactly cancel the log output current from the squarer/divider circuit at the desired 0 dB point). The external op amp is used to provide a more convenient scale and to allow compensation of the +0.33%/°C temperature drift of the dB circuit. The special T.C. resistor R3 is available from Tel Labs in Londenderry, New Hampshire (model Q-81) and from Precision Resistor Inc., Hillside, N.J. (model PT146).

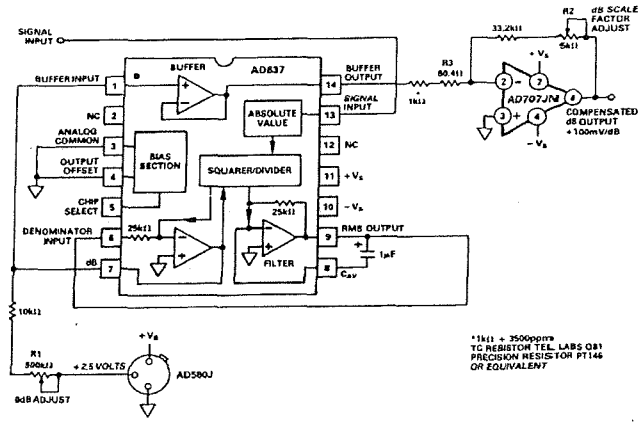

Figure 14. dB Connection

DB CALIBRATION

1. Set V_{IN} = 1.00 V dc or 1.00 V rms
2. Adjust R1 for 0 dB out = 0.00 V
3. Set V_{IN} = 0.1 V dc or 0.10 V rms
4. Adjust R2 for dB out = – 2.00 V

Any other dB reference can be used by setting V_{IN} and R1 accordingly.

LOW FREQUENCY MEASUREMENTS

If the frequencies of the signals to be measured are below 10 Hz, the value of the averaging capacitor required to deliver even 1% averaging error in the standard rms connection becomes extremely large. The circuit shown in Figure 15 shows an alternative method of obtaining low frequency rms measurements. The averaging time constant is determined by the product of R and C_{AV1}, in this circuit 0.5 s/μF of C_{AV}. This circuit permits a 20:1 reduction in the value of the averaging capacitor, permitting the use of high quality tantalum capacitors. It is suggested that the two pole Sallen-Key filter shown in the diagram be used to obtain a low ripple level and minimize the value of the averaging capacitor.

If the frequency of interest is below 1 Hz, or if the value of the averaging capacitor is still too large, the 20:1 ratio can be increased. This is accomplished by increasing the value of R. If this is done it is suggested that a low input current, low offset voltage amplifier like the AD548 be used instead of the internal buffer amplifier. This is necessary to minimize the offset error introduced by the combination of amplifier input currents and the larger resistance.

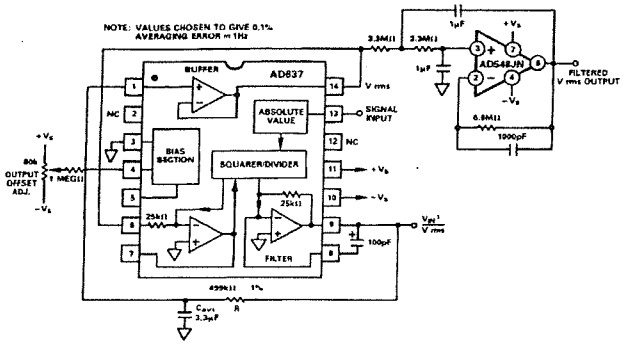

Figure 15. AD637 as a Low Frequency RMS Converter

VECTOR SUMMATION

Vector summation can be accomplished through the use of two AD637s as shown in Figure 16. Here the averaging capacitors are omitted (nominal 100 pF capacitors are used to insure stability of the filter amplifier), and the outputs are summed as shown. The output of the circuit is

$$V_O = \sqrt{V_X^2 + V_Y^2}$$

This concept can be expanded to include additional terms by feeding the signal from Pin 9 of each additional AD637 through a 10 kΩ resistor to the summing junction of the AD711, and tying all of the denominator inputs (Pin 6) together.

If C_{AV} is added to IC1 in this configuration, the output is $\sqrt{V_X^2 + V_Y^2}$. If the averaging capacitor is included on both IC1 and IC2, the output will be $\sqrt{\sqrt{V_X^2 + V_Y^2}}$.

This circuit has a dynamic range of 10 V to 10 mV and is limited only by the 0.5 mV offset voltage of the AD637. The useful bandwidth is 100 kHz.

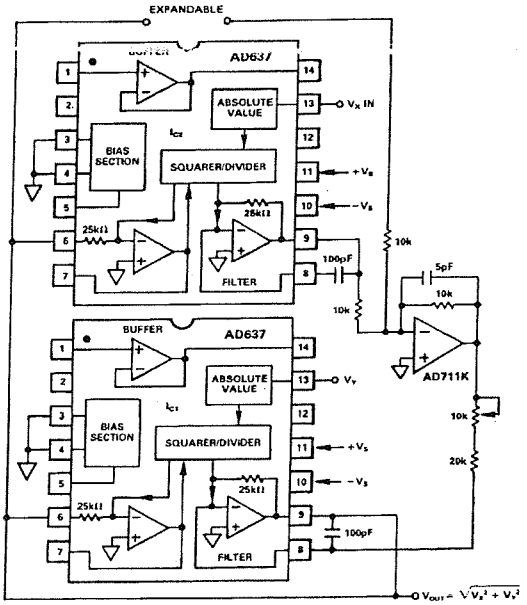

Figure 16. AD637 Vector Sum Configuration

OUTLINE DIMENSIONS

Dimensions shown in inches and (mm).

TO-116 (D) Package

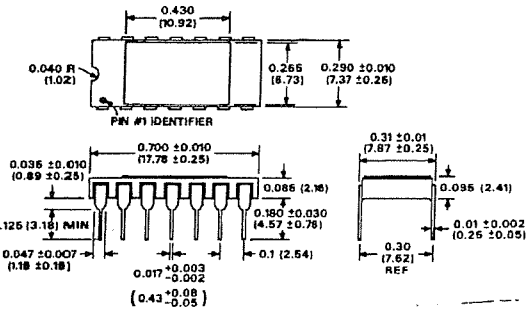

Cerdip (Q) Package

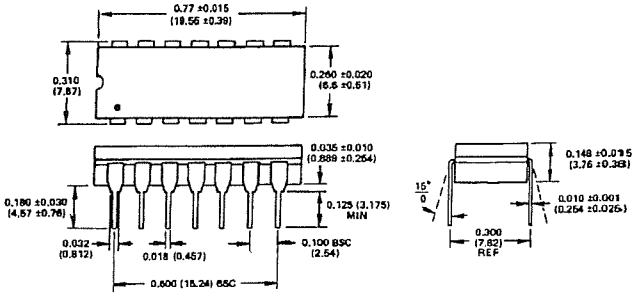

9.4 A (iv) AD624 Instrumentation Amplifier

ANALOG DEVICES

Precision Instrumentation Amplifier

AD624

FEATURES

Low Noise: 0.2 μV p-p 0.1 Hz to 10 Hz
Low Gain TC: 5 ppm max (G = 1)
Low Nonlinearity: 0.001% max (G = 1 to 200)
High CMRR: 130 dB min (G = 500 to 1000)
Low Input Offset Voltage: 25 μV, max
Low Input Offset Voltage Drift: 0.25 μV/°C max
Gain Bandwidth Product: 25 MHz
Pin Programmable Gains of 1, 100, 200, 500, 1000
No External Components Required
Internally Compensated

CONNECTION DIAGRAM

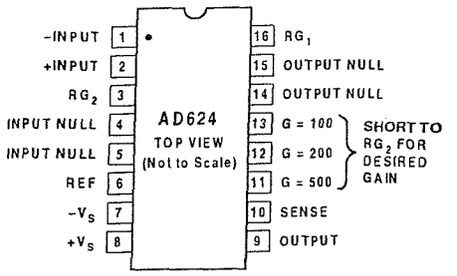

FOR GAINS OF 1000 SHORT RG_1 TO PIN 12 AND PINS 11 AND 13 TO RG_2

PRODUCT DESCRIPTION

The AD624 is a high precision, low noise, instrumentation amplifier designed primarily for use with low level transducers, including load cells, strain gauges and pressure transducers. An outstanding combination of low noise, high gain accuracy, low gain temperature coefficient and high linearity make the AD624 ideal for use in high resolution data acquisition systems.

The AD624C has an input offset voltage drift of less than 0.25 μV/°C, output offset voltage drift of less than 10 μV/°C, CMRR above 80 dB at unity gain (130 dB at G = 500) and a maximum nonlinearity of 0.001% at G = 1. In addition to these outstanding dc specifications, the AD624 exhibits superior ac performance as well. A 25 MHz gain bandwidth product, 5 V/μs slew rate and 15 μs settling time permit the use of the AD624 in high speed data acquisition applications.

The AD624 does not need any external components for pretrimmed gains of 1, 100, 200, 500 and 1000. Additional gains such as 250 and 333 can be programmed within one percent accuracy with external jumpers. A single external resistor can also be used to set the 624's gain to any value in the range of 1 to 10,000.

PRODUCT HIGHLIGHTS

1. The AD624 offers outstanding noise performance. Input noise is typically less than 4 nV/$\sqrt{\text{Hz}}$ at 1 kHz.
2. The AD624 is a functionally complete instrumentation amplifier. Pin programmable gains of 1, 100, 200, 500 and 1000 are provided on the chip. Other gains are achieved through the use of a single external resistor.
3. The offset voltage, offset voltage drift, gain accuracy and gain temperature coefficients are guaranteed for all pretrimmed gains.
4. The AD624 provides totally independent input and output offset nulling terminals for high precision applications. This minimizes the effect of offset voltage in gain ranging applications.
5. A sense terminal is provided to enable the user to minimize the errors induced through long leads. A reference terminal is also provided to permit level shifting at the output.

REV. B

One Technology Way, P.O. Box 9106, Norwood, MA 02062-9106, U.S.A.
Tel: 617/329-4700 Fax: 617/326-8703

AD624–SPECIFICATIONS (@ V_S = ±15 V, R_L = 2 kΩ and T_A = +25°C, unless otherwise noted)

Model	AD624A Min	AD624A Typ	AD624A Max	AD624B Min	AD624B Typ	AD624B Max	AD624C Min	AD624C Typ	AD624C Max	AD624S Min	AD624S Typ	AD624S Max	Units
GAIN													
Gain Equation (External Resistor Gain Programming)		$\left[\frac{40,000}{R_G}+1\right]\pm 20\%$			$\left[\frac{40,000}{R_G}+1\right]\pm 20\%$			$\left[\frac{40,000}{R_G}+1\right]\pm 20\%$			$\left[\frac{40,000}{R_G}+1\right]\pm 20\%$		
Gain Range (Pin Programmable)	1 to 1000			1 to 1000			1 to 1000			1 to 1000			
Gain Error													
G = 1			±0.05			±0.03			±0.02			±0.05	%
G = 100			±0.25			±0.15			±0.1			±0.25	%
G = 200, 500			±0.5			±0.35			±0.25			±0.5	%
Nonlinearity													
G = 1			±0.005			±0.003			±0.001			±0.005	%
G = 100, 200			±0.005			±0.003			±0.001			±0.005	%
G = 500			±0.005			±0.005			±0.005			±0.005	%
Gain vs. Temperature													
G = 1			5			5			5			5	ppm/°C
G = 100, 200			10			10			10			10	ppm/°C
G = 500			25			15			15			15	ppm/°C
VOLTAGE OFFSET (May be Nulled)													
Input Offset Voltage			200			75			25			75	µV
vs. Temperature			2			0.5			0.25			2.0	µV/°C
Output Offset Voltage			5			3			2			3	mV
vs. Temperature			50			25			10			50	µV/°C
Offset Referred to the Input vs. Supply													
G = 1	70			75			80			75			dB
G = 100, 200	95			105			110			105			dB
G = 500	100			110			115			110			dB
INPUT CURRENT													
Input Bias Current			±50			±25			±15			±50	nA
vs. Temperature		±50			±50			±50			±50		pA/°C
Input Offset Current			±35			±15			±10			±35	nA
vs. Temperature		±20			±20			±20			±20		pA/°C
INPUT													
Input Impedance													
Differential Resistance		10^9			10^9			10^9			10^9		Ω
Differential Capacitance		10			10			10			10		pF
Common-Mode Resistance		10^9			10^9			10^9			10^9		Ω
Common-Mode Capacitance		10			10			10			10		pF
Input Voltage Range[1]													
Max Differ. Input Linear (V_{DL})	±10			±10			±10			±10			V
Max Common-Mode Linear (V_{CM})	$12\ V-\left(\frac{G}{2}\times V_D\right)$			$12\ V-\left(\frac{G}{2}\times V_D\right)$			$12\ V-\left(\frac{G}{2}\times V_D\right)$			$12\ V-\left(\frac{G}{2}\times V_D\right)$			V
Common-Mode Rejection dc to 60 Hz with 1 kΩ Source Imbalance													
G = 1	70			75			80			70			dB
G = 100, 200	100			105			110			100			dB
G = 500	110			120			130			110			dB
OUTPUT RATING													
V_{OUT}, R_L = 2 kΩ		±10			±10			±10			±10		V
DYNAMIC RESPONSE													
Small Signal -3 dB													
G = 1		1			1			1			1		MHz
G = 100		150			150			150			150		kHz
G = 200		100			100			100			100		kHz
G = 500		50			50			50			50		kHz
G = 1000		25			25			25			25		kHz
Slew Rate		5.0			5.0			5.0			5.0		V/µs
Settling Time to 0.01%, 20 V Step													
G = 1 to 200		15			15			15			15		µs
G = 500		35			35			35			35		µs
G = 1000		75			75			75			75		µs
NOISE													
Voltage Noise, 1 kHz													
R.T.I.		4			4			4			4		$nV/\sqrt{Hz}$
R.T.O.		75			75			75			75		$nV/\sqrt{Hz}$
R.T.I., 0.1 Hz to 10 Hz													
G = 1		10			10			10			10		µV p-p
G = 100		0.3			0.3			0.3			0.3		µV p-p
G = 200, 500, 1000		0.2			0.2			0.2			0.2		µV p-p
Current Noise													
0.1 Hz to 10 Hz		60			60			60			60		pA p-p
SENSE INPUT													
R_{IN}	8	10	12	8	10	12	8	10	12	8	10	12	kΩ
I_{IN}		30			30			30			30		µA
Voltage Range	±10			±10			±10			±10			V
Gain to Output		1			1			1			1		%

Model	AD624A Min	AD624A Typ	AD624A Max	AD624B Min	AD624B Typ	AD624B Max	AD624C Min	AD624C Typ	AD624C Max	AD624S Min	AD624S Typ	AD624S Max	Units
REFERENCE INPUT													
R_{IN}	16	20	24	16	20	24	16	20	24	16	20	24	kΩ
I_{IN}		30			30			30			30		μA
Voltage Range	±10			±10			±10			±10			V
Gain to Output		1			1			1			1		%
TEMPERATURE RANGE													
Specified Performance	-25		+85	-25		+85	-25		+85	-55		+125	°C
Storage	-65		+150	-65		+150	-65		+150	-65		+150	°C
POWER SUPPLY													
Power Supply range	±6	±15	±18	±6	±15	±18	±6	±15	±18	±6	±15	±18	V
Quiescent Current		3.5	5		3.5	5		3.5	5		3.5	5	mA

NOTES

[1] V_{DL} is the maximum differential input voltage at G = 1 for specified nonlinearity, V_{DL} at other gains = 10 V/G. V_D = actual differential input voltage. Example: G = 10, V_D = 0.50. V_{CM} = 12 V - (10/2 x 0.50 V) = 9.5 V.

Specifications subject to change without notice.

Specifications shown in **boldface** are tested on all production unit at final electrical test. Results from those tests are used to calculate outgoing quality levels. All min and max specifications are guaranteed, although only those shown in boldface are tested on all production units.

ABSOLUTE MAXIMUM RATINGS*

Supply Voltage ..... ±18 V
Internal Power Dissipation ..... 420 mW
Input Voltage ..... $\pm V_S$
Differential Input Voltage ..... $\pm V_S$
Output Short Circuit Duration ..... Indefinite
Storage Temperature Range ..... -65°C to +150°C
Operating Temperature Range
AD624A/B/C ..... -25°C to +85°C
AD624S ..... -55°C to +125°C
Lead Temperature (Soldering, 60 secs) ..... +300°C

*Stresses above those listed under *"Absolute Maximum Ratings"* may cause permanent damage to the device. This is a stress rating only and functional operation of the device at these or any other conditions above those indicated in the operational sections of this specification is not implied. Exposure to absolute maximum rating conditions for extended periods may affect device reliability.

ORDERING GUIDE

Model	Temperature Range	Package Description	Package Option
AD624AD	-25°C to +85°C	16-Pin Ceramic DIP	D-16
AD624BD	-25°C to +85°C	16-Pin Ceramic DIP	D-16
AD624CD	-25°C to +85°C	16-Pin Ceramic DIP	D-16
AD624SD	-55°C to +125°C	16-Pin Ceramic DIP	D-16
AD624SD/883B*	-55°C to +125°C	16-Pin Ceramic DIP	D-16
AD624SChips	-25°C to +85°C	Die	

*See Analog Devices' military data sheet for 883B specifications.

METALIZATION PHOTOGRAPH

Contact factory for latest dimensions
Dimensions shown in inches and (mm).

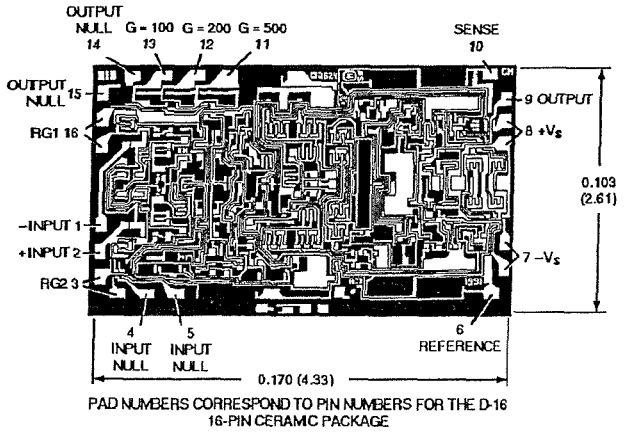

PAD NUMBERS CORRESPOND TO PIN NUMBERS FOR THE D-16 16-PIN CERAMIC PACKAGE

FUNCTIONAL BLOCK DIAGRAM

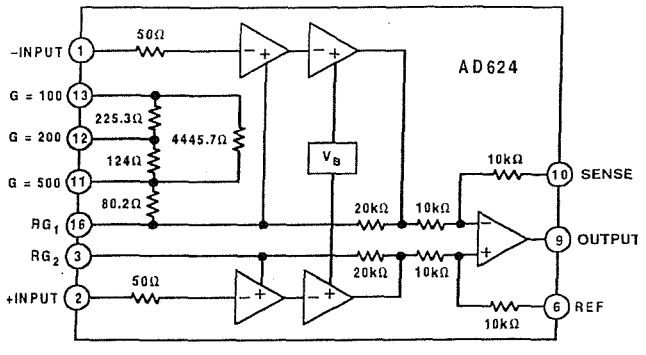

OUTLINE DIMENSIONS

Dimensions shown in inches and (mm).

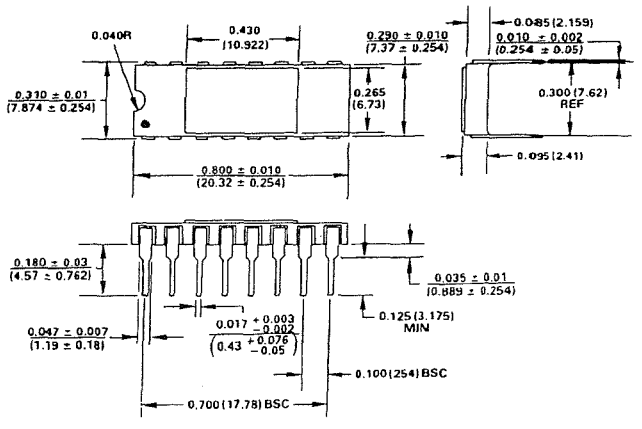

AD624–Typical Characteristics

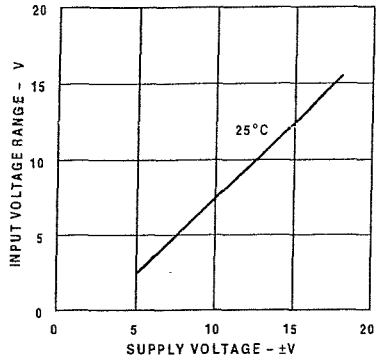

Figure 1. Input Voltage Range vs. Supply Voltage, G = 1

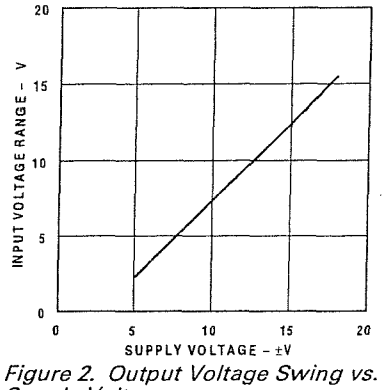

Figure 2. Output Voltage Swing vs. Supply Voltage

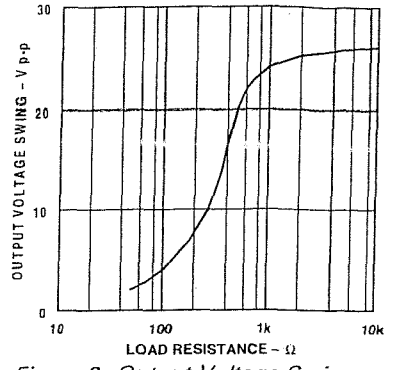

Figure 3. Output Voltage Swing vs. Load Resistance

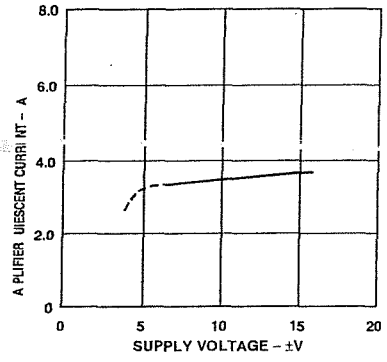

Figure 4. Quiescent Current vs. Supply Voltage

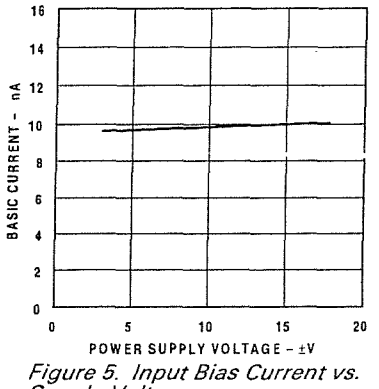

Figure 5. Input Bias Current vs. Supply Voltage

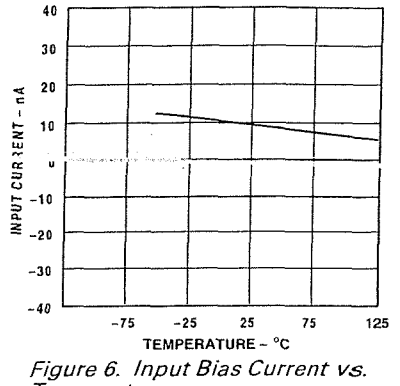

Figure 6. Input Bias Current vs. Temperature

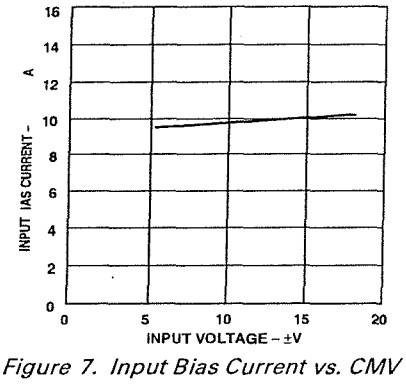

Figure 7. Input Bias Current vs. CMV

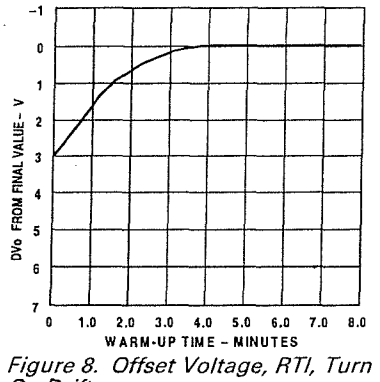

Figure 8. Offset Voltage, RTI, Turn On Drift

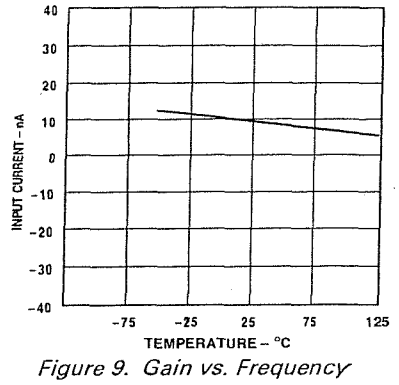

Figure 9. Gain vs. Frequency

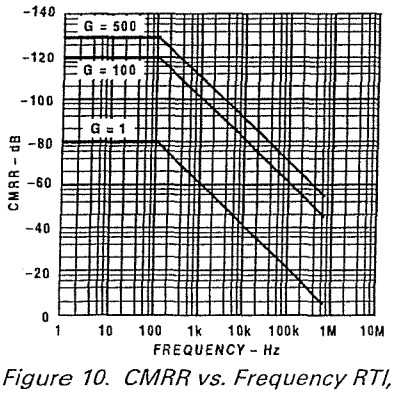

Figure 10. CMRR vs. Frequency RTI, Zero to 1k Source Imbalance

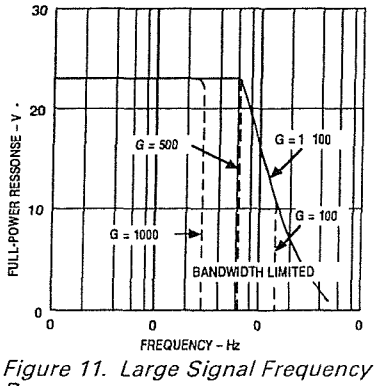

Figure 11. Large Signal Frequency Response

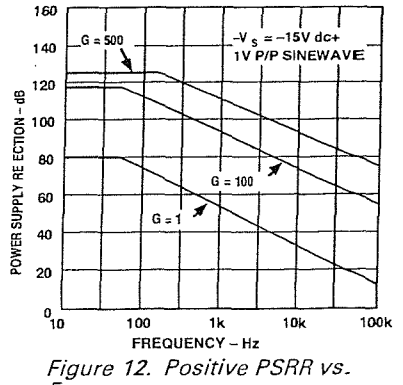

Figure 12. Positive PSRR vs. Frequency

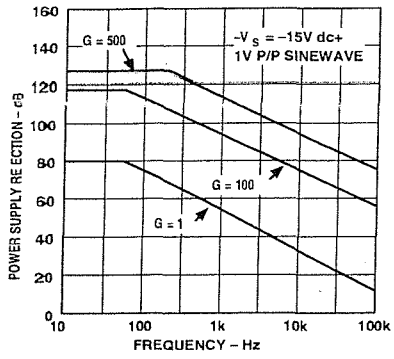

Figure 13. Negative PSRR vs. Frequency

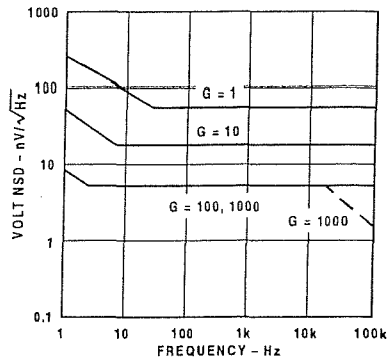

Figure 14. RTI Noise Spectral Density vs. Gain

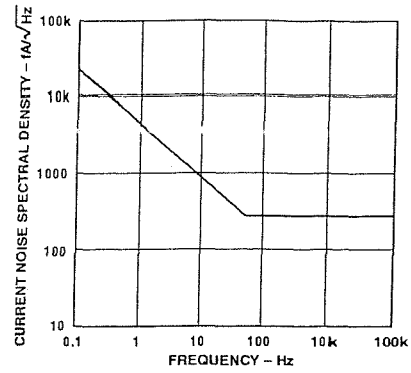

Figure 15. Input Current Noise

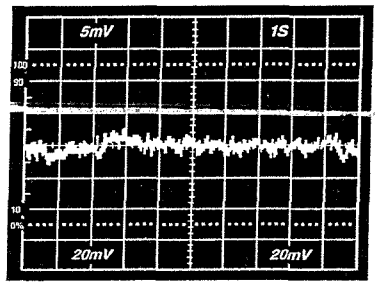

Figure 16. Low Frequency Voltage Noise, G = 1 (System Gain = 1000)

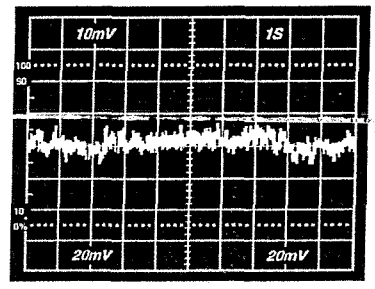

Figure 17. Low Frequency Voltage Noise, G = 1000 (System Gain = 100,000)

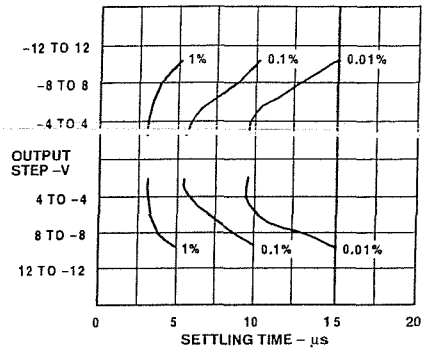

Figure 18. Settling Time, Gain = 1

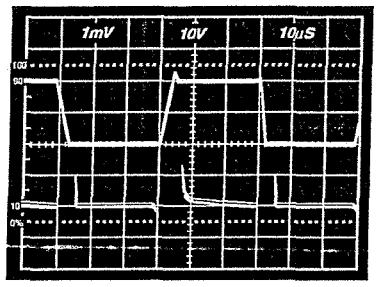

Figure 19. Large Signal Pulse Response and Settling Time, G = 1

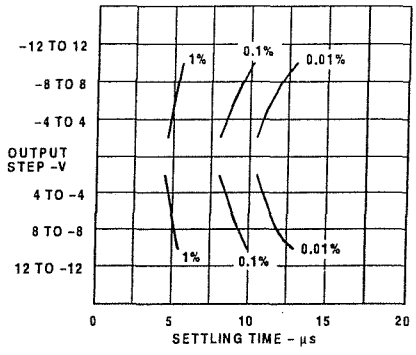

Figure 20. Settling Time Gain = 100

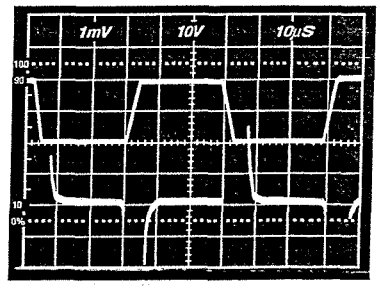

Figure 21. Large Signal Pulse Response and Settling Time, G = 100

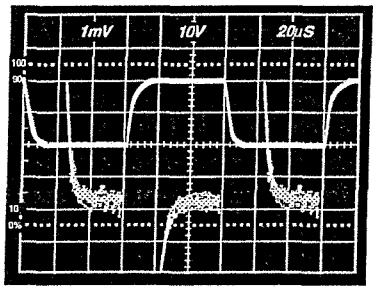

Figure 22. Range Signal Pulse Response and Settling Time, G = 500

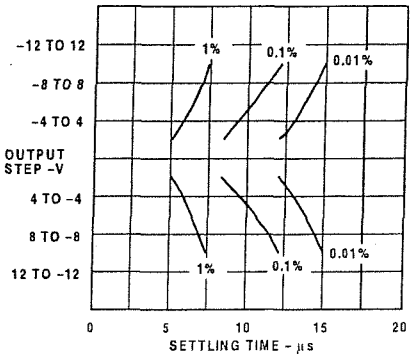

Figure 23. Settling Time Gain = 1000

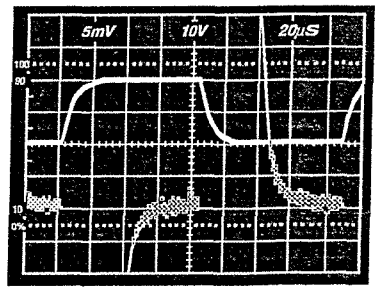

Figure 24. Large Signal Pulse Response and Settling Time, G = 1000

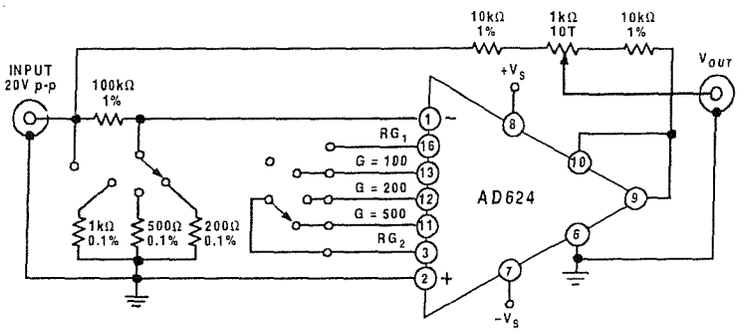

Figure 25. Settling Time Test Circuit

THEORY OF OPERATION

The AD624 is a monolithic instrumentation amplifier based on a modification of the classic three-op-amp instrumentation amplifier. Monolithic construction and laser-wafer-trimming allow the tight matching and tracking of circuit components and the high level of performance that this circuit architecture is capable of.

A preamp section (Q1–Q4) develops the programmed gain by the use of feedback concepts. Feedback from the outputs of A1 and A2 forces the collector currents of Q1–Q4 to be constant thereby impressing the input voltage across R_G.

The gain is set by choosing the value of R_G from the equation, Gain = $\frac{40\,k}{R_G}$ + 1. The value of R_G also sets the transconductance of the input preamp stage increasing it asymptotically to the transconductance of the input transistors as R_G is reduced for larger gains. This has three important advantages. First, this approach allows the circuit to achieve a very high open loop gain of 3×10^8 at a programmed gain of 1000 thus reducing gain related errors to a negligible 3 ppm. Second, the gain bandwidth product which is determined by C3 or C4 and the input transconductance, reaches 25 MHz. Third, the input voltage noise reduces to a value determined by the collector current of the input transistors for an RTI noise of 4 nV/$\sqrt{\text{Hz}}$ at G ≥ 500.

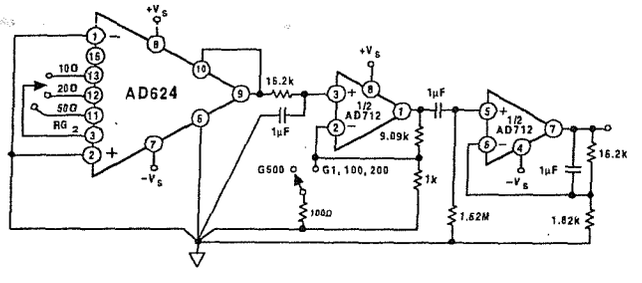

Figure 26. Noise Test Circuit

INPUT CONSIDERATIONS

Under input overload conditions the user will see R_G + 100 Ω and two diode drops (~1.2 V) between the plus and minus inputs, in either direction. If safe overload current under all conditions is assumed to be 10 mA, the maximum overload voltage is ~ ±2.5 V. While the AD624 can withstand this continuously, momentary overloads of ±10 V will not harm the device. On the other hand the inputs should never exceed the supply voltage.

The AD524 should be considered in applications that require protection from severe input overload. If this is not possible, external protection resistors can be put in series with the inputs of the AD624 to augment the internal (50 Ω) protection resistors. This will most seriously degrade the noise performance. For this reason the value of these resistors should be chosen to be as low as possible and still provide 10 mA of current limiting under maximum continuous overload conditions. In selecting the value of these resistors, the internal gain setting resistor and the 1.2 volt drop need to be considered. For example, to protect the device from a continuous differential overload of 20 V at a gain of 100, 1.9 kΩ of resistance is required. The internal gain resistor is 404 Ω; the internal protect resistor is 100 Ω. There is a 1.2 V drop across D1 or D2 and the base-emitter junction of either Q1 and Q3 or Q2 and Q4 as shown in Figure 27, 1400 Ω of external resistance would be required (700 Ω in series with each input). The RTI noise in this case would be

$$\sqrt{4\,KTR_{ext} + (4\,nV/\sqrt{Hz})^2} = 6.2\,nV/\sqrt{Hz}$$

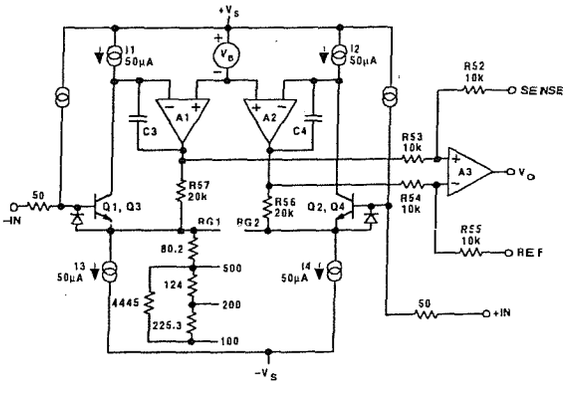

Figure 27. Simplified Circuit of Amplifier; Gain Is Defined as (R56 + R57)/(R_G) + 1. For a Gain of 1, R_G Is an Open Circuit.

INPUT OFFSET AND OUTPUT OFFSET

Voltage offset specifications are often considered a figure of merit for instrumentation amplifiers. While initial offset may be adjusted to zero, shifts in offset voltage due to temperature variations will cause errors. Intelligent systems can often correct for this factor with an auto-zero cycle, but there are many small-signal high-gain applications that don't have this capability.

Voltage offset and offset drift each have two components; input and output. Input offset is that component of offset that is

directly proportional to gain i.e., input offset as measured at the output at G = 100 is 100 times greater than at G = 1. Output offset is independent of gain. At low gains, output offset drift is dominant, while at high gains input offset drift dominates. Therefore, the output offset voltage drift is normally specified as drift at G = 1 (where input effects are insignificant), while input offset voltage drift is given by drift specification at a high gain (where output offset effects are negligible). All input-related numbers are referred to the input (RTI) which is to say that the effect on the output is "G" times larger. Voltage offset vs. power supply is also specified at one or more gain settings and is also RTI.

By separating these errors, one can evaluate the total error independent of the gain setting used. In a given gain configuration both errors can be combined to give a total error referred to the input (R.T.I.) or output (R.T.O.) by the following formula:

Total Error R.T.I. = input error + (output error/gain)

Total Error R.T.O. = (Gain x input error) + output error

As an illustration, a typical AD624 might have a +250 µV output offset and a -50 µV input offset. In a unity gain configuration, the *total* output offset would be 200 µV or the sum of the two. At a gain of 100, the output offset would be -4.75 mV or: +250 µV + 100 (-50 µV) = -4.75 mV.

The AD624 provides for both input and output offset adjustment. This optimizes nulling in very high precision applications and minimizes offset voltage effects in switched gain applications. In such applications the input offset is adjusted first at the highest programmed gain, then the output offset is adjusted at G = 1.

GAIN

The AD624 includes high accuracy pretrimmed internal gain resistors. These allow for single connection programming of gains of 1, 100, 200 and 500. Additionally, a variety of gains including a pretrimmed gain of 1000 can be achieved through series and parallel combinations of the internal resistors. Table I shows the available gains and the appropriate pin connections and gain temperature coefficients.

The gain values achieved via the combination of internal resistors are extremely useful. The temperature coefficient of the gain is dependent primarily on the mismatch of the temperature coefficients of the various internal resistors. Tracking of these resistors is extremely tight resulting in the low gain TCs shown in Table I.

If the desired value of gain is not attainable using the internal resistors, a single external resistor can be used to achieve any gain between 1 and 10,000. This resistor connected between

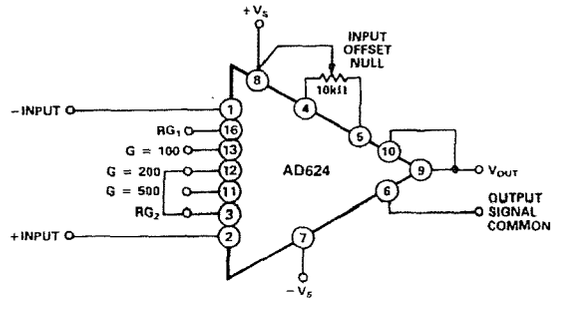

Figure 28. Operating Connections for G = 200

Table I.

Gain (Nominal)	Temperature Coefficient (Nominal)	Pin 3 to Pin	Connect Pins
1	-0 ppm/C	-	-
100	-1.5 ppm/°C	13	-
125	-5 ppm/°C	13	11 to 16
137	-5.5 ppm/°C	13	11 to 12
186.5	-6.5 ppm/°C	13	11 to 12 to 16
200	-3.5 ppm/°C	12	-
250	-5.5 ppm/°C	12	11 to 13
333	-15 ppm/°C	12	11 to 16
375	-0.5 ppm/°C	12	13 to 16
500	-10 ppm/°C	11	-
624	-5 ppm/°C	11	13 to 16
688	-1.5 ppm/°C	11	11 to 12; 13 to 16
831	+4 ppm/°C	11	16 to 12
1000	0 ppm/°C	11	16 to 12; 13 to 11

Pins 3 and 16 programs the gain according to the formula $R_G = \frac{40k}{G-1}$ (see Figure 29). For best results R_G should be a precision resistor with a low temperature coefficient. An external R_G affects both gain accuracy and gain drift due to the mismatch between it and the internal thin-film resistors R56 and R57. Gain accuracy is determined by the tolerance of the external R_G and the absolute accuracy of the internal resistors (±20%). Gain drift is determined by the mismatch of the temperature coefficient of R_G and the temperature coefficient of the internal resistors (-15 ppm/°C typ), and the temperature coefficient of the internal interconnections .

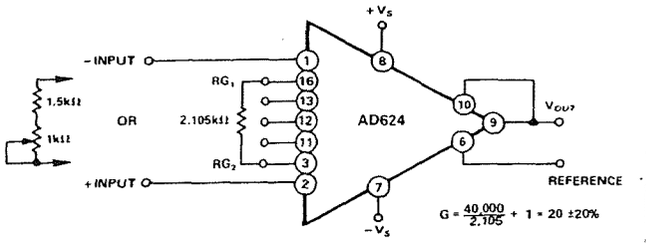

Figure 29. Operating Connections for G = 20

The AD624 may also be configured to provide gain in the output stage. Figure 30 shows an H pad attenuator connected to the reference and sense lines of the AD624. The values of R1, R2 and R3 should be selected to be as low as possible to minimize the gain variation and reduction of CMRR. Varying R2 will precisely set the gain without affecting CMRR. CMRR is determined by the match of R1 and R3.

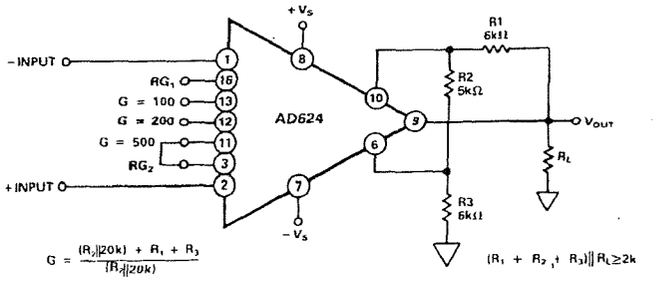

Figure 30. Gain of 2500

NOISE

The AD624 is designed to provide noise performance near the theoretical noise floor. This is an extremely important design criteria as the front end noise of an instrumentation amplifier is the ultimate limitation on the resolution of the data acquisition system it is being used in. There are two sources of noise in an instrument amplifier, the input noise, predominantly generated by the differential input stage, and the output noise, generated by the output amplifier. Both of these components are present at the input (and output) of the instrumentation amplifier. At the input, the input noise will appear unaltered; the output noise will be attenuated by the closed loop gain (at the output, the output noise will be unaltered; the input noise will be amplified by the closed loop gain). Those two noise sources must be root sum squared to determine the total noise level expected at the input (or output).

The low frequency (0.1 Hz to 10 Hz) voltage noise due to the output stage is 10 µV p-p, the contribution of the input stage is 0.2 µV p-p. At a gain of 10, the RTI voltage noise would be 1 µV p-p, $\sqrt{\left(\frac{10}{G}\right)^2 + (0.2)^2}$. The RTO voltage noise would be 10.2 µV p-p, $\sqrt{10^2 + (0.2(G))^2}$. These calculations hold for applications using either internal or external gain resistors.

INPUT BIAS CURRENTS

Input bias currents are those currents necessary to bias the input transistors of a dc amplifier. Bias currents are an additional source of input error and must be considered in a total error budget. The bias currents when multiplied by the source resistance imbalance appear as an additional offset voltage. (What is of concern in calculating bias current errors is the change in bias current with respect to signal voltage and temperature.) Input offset current is the difference between the two input bias currents. The effect of offset current is an input offset voltage whose magnitude is the offset current times the source resistance.

Although instrumentation amplifiers have differential inputs, there must be a return path for the bias currents. If this is not provided, those currents will charge stray capacitances, causing the output to drift uncontrollably or to saturate. Therefore,

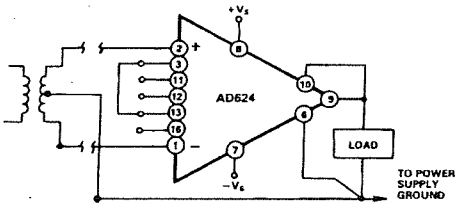

a. Transformer Coupled

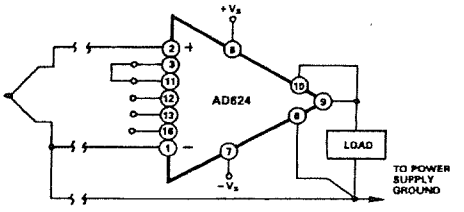

b. Thermocouple

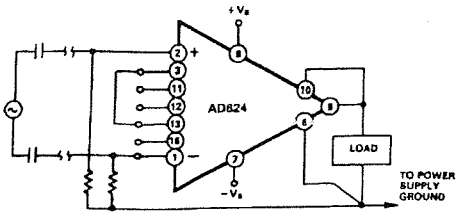

c. AC Coupled

Figure 31. Indirect Ground Returns for Bias Currents

when amplifying "floating" input sources such as transformers and thermocouples, as well as ac-coupled sources, there must still be a dc path from each input to ground, (see Figure 31).

COMMON-MODE REJECTION

Common-mode rejection is a measure of the change in output voltage when both inputs are changed by equal amounts. These specifications are usually given for a full-range input voltage change and a specified source imbalance. "Common-Mode Rejection Ratio" (CMRR) is a ratio expression while "Common-Mode Rejection" (CMR) is the logarithm of that ratio. For example, a CMRR of 10,000 corresponds to a CMR of 80 dB.

In an instrumentation amplifier, ac common-mode rejection is only as good as the differential phase shift. Degradation of ac common-mode rejection is caused by unequal drops across differing track resistances and a differential phase shift due to varied stray capacitances or cable capacitances. In many applications shielded cables are used to minimize noise. This technique can create common-mode rejection errors unless the shield is properly driven. Figures 32 and 33 shows active data guards which are configured to improve ac common-mode rejection by "bootstrapping" the capacitances of the input cabling, thus minimizing differential phase shift.

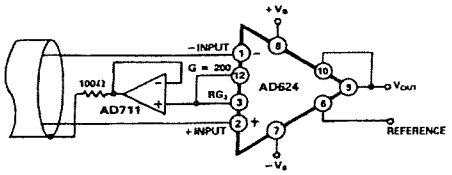

Figure 32. Shield Driver, G ≥ 100

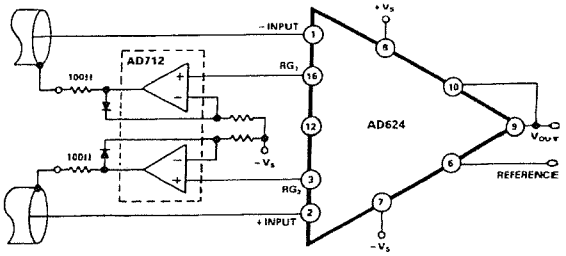

Figure 33. Differential Shield Driver

GROUNDING

Many data-acquisition components have two or more ground pins which are not connected together within the device. These grounds must be tied together at one point, usually at the system power supply ground. Ideally, a single solid ground would be desirable. However, since current flows through the ground wires and etch stripes of the circuit cards, and since these paths

have resistance and inductance, hundreds of millivolts can be generated between the system ground point and the data acquisition components. Separate ground returns should be provided to minimize the current flow in the path from the most sensitive points to the system ground point. In this way supply currents and logic-gate return currents are not summed into the same return path as analog signals where they would cause measurement errors (see Figure 34).

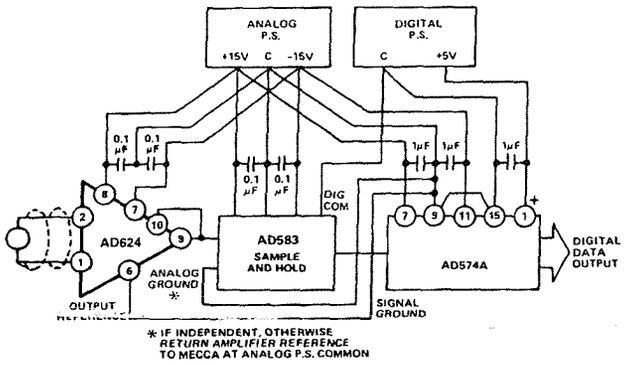

Figure 34. Basic Grounding Practice

Since the output voltage is developed with respect to the potential on the reference terminal an instrumentation amplifier can solve many grounding problems.

SENSE TERMINAL

The sense terminal is the feedback point for the instrument amplifier's output amplifier. Normally it is connected to the instrument amplifier output. If heavy load currents are to be drawn through long leads, voltage drops due to current flowing through lead resistance can cause errors. The sense terminal can be wired to the instrument amplifier at the load thus putting the IxR drops "inside the loop" and virtually eliminating this error source.

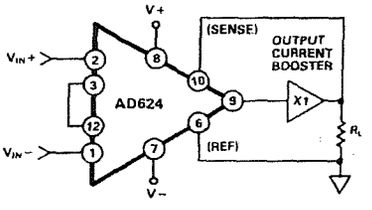

Figure 35. AD624 Instrumentation Amplifier with Output Current Booster

Typically, IC instrumentation amplifiers are rated for a full ±10 volt output swing into 2 kΩ. In some applications, however, the need exists to drive more current into heavier loads. Figure 35 shows how a current booster may be connected "inside the loop" of an instrumentation amplifier to provide the required current without significantly degrading overall performance. The effects of nonlinearities, offset and gain inaccuracies of the buffer are reduced by the loop gain of the IA output amplifier. Offset drift of the buffer is similarly reduced.

REFERENCE TERMINAL

The reference terminal may be used to offset the output by up to ±10 V. This is useful when the load is "floating" or does not share a ground with the rest of the system. It also provides a direct means of injecting a precise offset. It must be remembered that the total output swing is ±10 volts, from ground, to be shared between signal and reference offset.

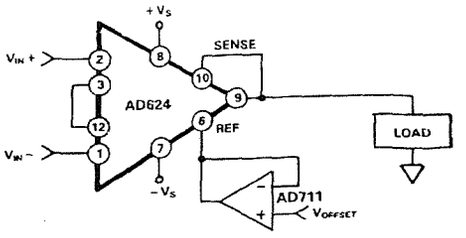

Figure 36. Use of Reference Terminal to Provide Output Offset

When the IA is of the three-amplifier configuration it is necessary that nearly zero impedance be presented to the reference terminal. Any significant resistance, including those caused by PC layouts or other connection techniques, which appears between the reference pin and ground will increase the gain of the noninverting signal path, thereby upsetting the common-mode rejection of the IA. Inadvertent thermocouple connections created in the sense and reference lines should also be avoided as they will directly affect the output offset voltage and output offset voltage drift.

In the AD624 a reference source resistance will unbalance the CMR trim by the ratio of 10 kΩ/R_{REF}. For example, if the reference source impedance is 1 Ω, CMR will be reduced to 80 dB (10 kΩ/1 Ω = 80 dB). An operational amplifier may be used to provide that low impedance reference point as shown in Figure 36. The input offset voltage characteristics of that amplifier will add directly to the output offset voltage performance of the instrumentation amplifier.

An instrumentation amplifier can be turned into a voltage-to-current converter by taking advantage of the sense and reference terminals as shown in Figure 37.

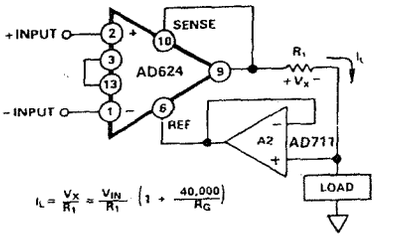

Figure 37. Voltage-to-Current Converter

By establishing a reference at the "low" side of a current setting resistor, an output current may be defined as a function of input voltage, gain and the value of that resistor. Since only a small current is demanded at the input of the buffer amplifier A_2, the forced current I_L will largely flow through the load. Offset and drift specifications of A_2 must be added to the output offset and drift specifications of the IA.

PROGRAMMABLE GAIN

Figure 38 shows the AD624 being used as a software programmable gain amplifier. Gain switching can be accomplished with mechanical switches such as DIP switches or reed relays. It should be noted that the "on" resistance of the switch in series

with the internal gain resistor becomes part of the gain equation and will have an effect on gain accuracy.

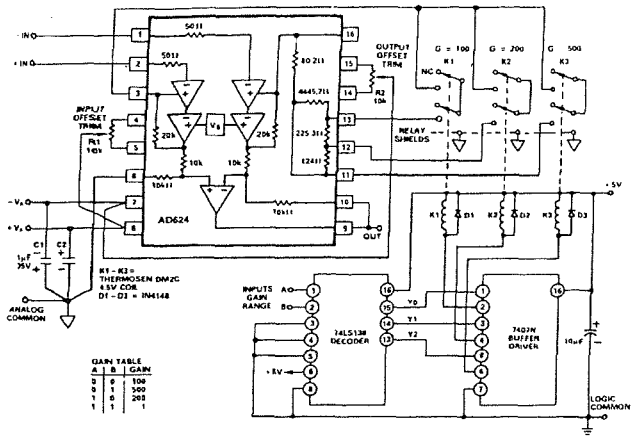

Figure 38. Gain Programmable Amplifier

A significant advantage in using the internal gain resistors in a programmable gain configuration is the minimization of thermocouple signals which are often present in multiplexed data acquisition systems.

If the full performance of the AD624 is to be achieved, the user must be extremely careful in designing and laying out his circuit to minimize the remaining thermocouple signals.

The AD624 can also be connected for gain in the output stage. Figure 39 shows an AD547 used as an active attenuator in the output amplifier's feedback loop. The active attenuation presents a very low impedance to the feedback resistors therefore minimizing the common-mode rejection ratio degradation.

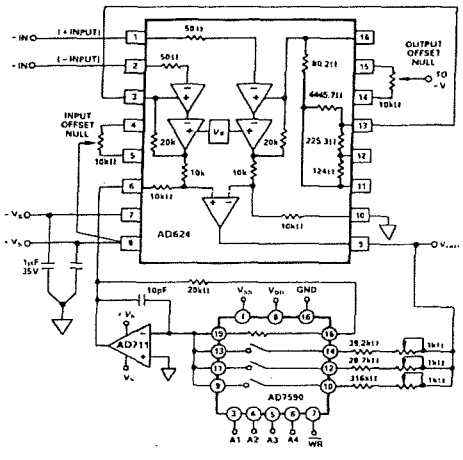

Figure 39. Programmable Output Gain

Another method for developing the switching scheme is to use a DAC. The AD7528 dual DAC which acts essentially as a pair of switched resistive attenuators having high analog linearity and symmetrical bipolar transmission is ideal in this application. The multiplying DAC's advantage is that it can handle inputs of either polarity or zero without affecting the programmed gain. The circuit shown uses an AD7528 to set the gain (DAC A) and to perform a fine adjustment (DAC B).

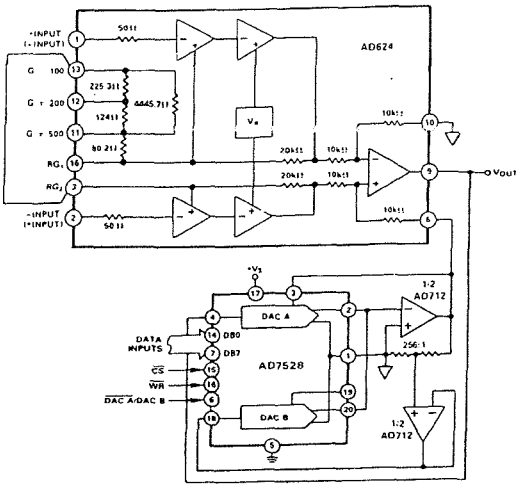

Figure 40. Programmable Output Gain Using a DAC

AUTO-ZERO CIRCUITS

In many applications it is necessary to provide very accurate data in high gain configurations. At room temperature the offset effects can be nulled by the use of offset trimpots. Over the operating temperature range, however, offset nulling becomes a problem. The circuit of Figure 41 shows a CMOS DAC operating in the bipolar mode and connected to the reference terminal to provide software controllable offset adjustments.

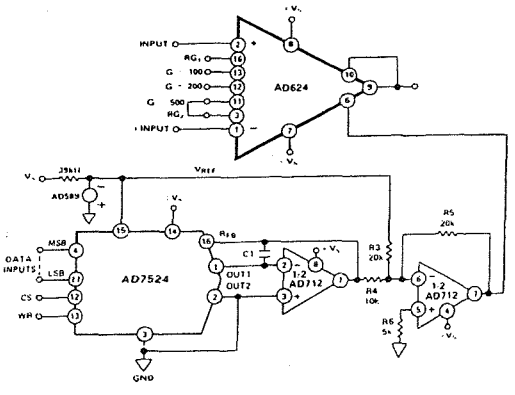

Figure 41. Software Controllable Offset

In many applications complex software algorithms for auto-zero applications are not available. For these applications Figure 42 provides a hardware solution.

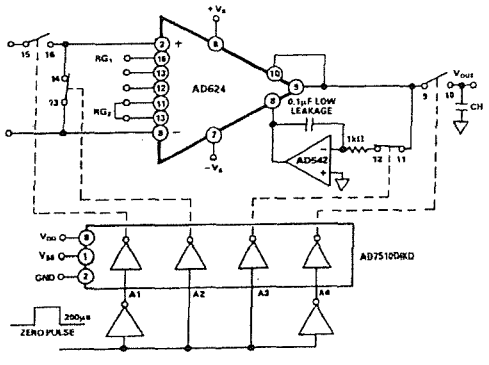

Figure 42. Auto-Zero Circuit

The microprocessor controlled data acquisition system shown in Figure 43 includes includes both auto-zero and auto-gain capability. By dedicating two of the differential inputs, one to ground and one to the A/D reference, the proper program calibration cycles can eliminate both initial accuracy errors and accuracy errors over temperature. The auto-zero cycle, in this application, converts a number that appears to be ground and then writes that same number (8 bit) to the AD7524 which eliminates the zero error since its output has an inverted scale. The auto-gain cycle converts the A/D reference and compares it with full scale. A multiplicative correction factor is then computed and applied to subsequent readings.

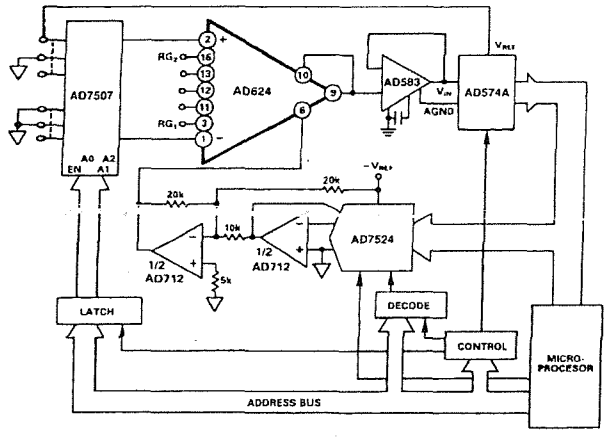

Figure 43. Microprocessor Controlled Data Acquisition System

WEIGH SCALE

Figure 44 shows an example of how an AD624 can be used to condition the differential output voltage from a load cell. The 10% reference voltage adjustment range is required to accommodate the 10% transducer sensitivity tolerance. The high linearity and low noise of the AD624 make it ideal for use in applications of this type particularly where it is desirable to measure small changes in weight as opposed to the absolute value. The addition of an auto gain/auto tare cycle will enable the system to remove offsets, gain errors, and drifts making possible true 14-bit performance.

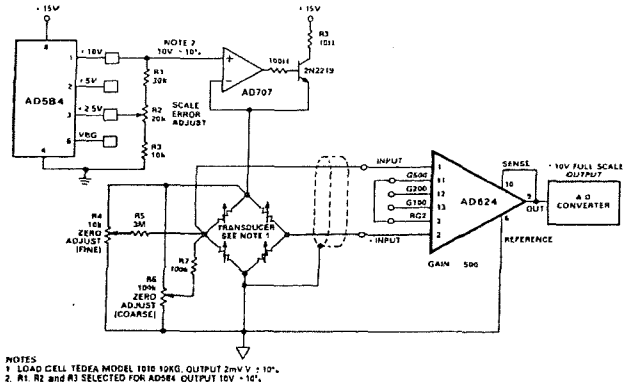

Figure 44. AD624 Weigh Scale Application

AC BRIDGE

Bridge circuits which use dc excitation are often plagued by errors caused by thermocouple effects, 1/f noise, dc drifts in the electronics, and line noise pickup. One way to get around these problems is to excite the bridge with an ac waveform, amplify the bridge output with an ac amplifier, and synchronously demodulate the resulting signal. The ac phase and amplitude information from the bridge is recovered as a dc signal at the output of the synchronous demodulator. The low frequency system noise, dc drifts, and demodulator noise all get mixed to the carrier frequency and can be removed by means of a low-pass filter. Dynamic response of the bridge must be traded off against the amount of attenuation required to adequately suppress these residual carrier components in the selection of the filter.

Figure 45 is an example of an ac bridge system with the AD630 used as a synchronous demodulator. The oscilloscope photograph shows the results of a 0.05% bridge imbalance caused by the 1 Meg resistor in parallel with one leg of the bridge. The top trace represents the bridge excitation, the upper middle trace is the amplified bridge output, the lower-middle trace is the output of the synchronous demodulator and the bottom trace is the filtered dc system output.

This system can easily resolve a 0.5 ppm change in bridge impedance. Such a change will produce a 6.3 mV change in the low-pass filtered dc output, well above the RTO drifts and noise.

The AC-CMRR of the AD624 decreases with the frequency of the input signal. This is due mainly to the package-pin capacitance associated with the AD624's internal gain resistors. If AC-CMRR is not sufficient for a given application, it can be trimmed by using a variable capacitor connected to the amplifier's RG_2 pin as shown in Figure 45.

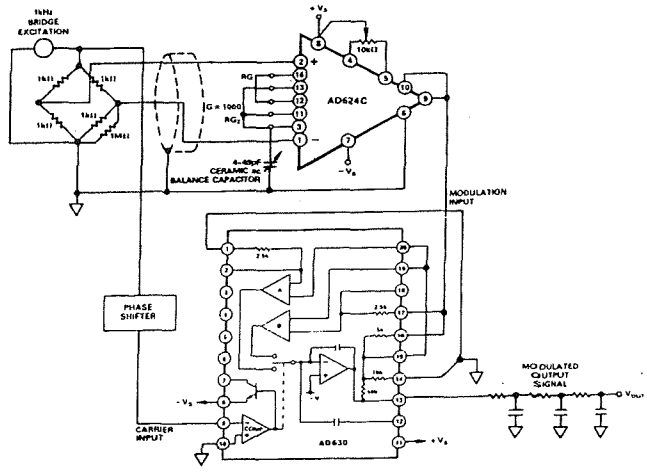

Figure 45. AC Bridge

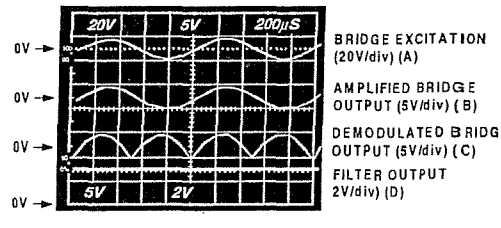

Figure 46. AC Bridge Waveforms

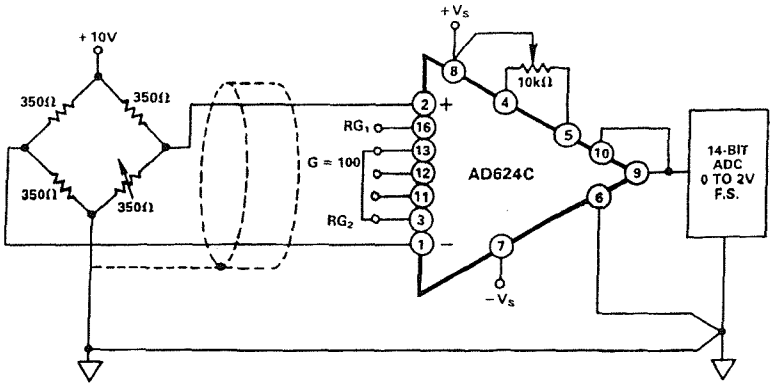

Figure 47. Typical Bridge Application

ERROR BUDGET ANALYSIS

To illustrate how instrumentation amplifier specifications are applied, we will now examine a typical case where an AD624 is required to amplify the output of an unbalanced transducer. Figure 47 shows a differential transducer, unbalanced by 5 Ω, supplying a 0 to 20 mV signal to an AD624C. The output of the IA feeds a 14-bit A to D converter with a 0 to 2 volt input voltage range. The operating temperature range is –25°C to +85°C. Therefore, the largest change in temperature ΔT within the operating range is from ambient to + 85°C (85°C – 25°C = 60°C.)

In many applications, differential linearity and resolution are of prime importance. This would be so in cases where the absolute value of a variable is less important than changes in value. In these applications, only the irreducible errors (20 ppm = 0.002%) are significant. Furthermore, if a system has an intelligent processor monitoring the A to D output, the addition of an auto-gain/auto-zero cycle will remove all reducible errors and may eliminate the requirement for initial calibration. This will also reduce errors to 0.002%.

Table II. Error Budget Analysis of AD624CD in Bridge Application

Error Source	AD624C Specifications	Calculation	Effect on Absolute Accuracy at T_A = 25°C	Effect on Absolute Accuracy at T_A = 85°C	Effect on Resolution
Gain Error	±0.1%	±0.1% = 1000 ppm	1000 ppm	1000 ppm	–
Gain Instability	10 ppm	(10 ppm/°C) (60°C) = 600 ppm	–	600 ppm	–
Gain Nonlinearity	±0.001%	±0.001% = 10 ppm	–	–	10 ppm
Input Offset Voltage	±25 μV, RTI	±25 μV/20 mV = ±1250 ppm	1250 ppm	1250 ppm	–
Input Offset Voltage Drift	±0.25 μV/°C	(±0.25 μV/°C) (60°C)= 15 μV 15 μV/20 mV = 750 ppm	–	750 ppm	–
Output Offset Voltage[1]	±2.0 mV	±2.0 mV/20 mV = 1000 ppm	1000 ppm	1000 ppm	–
Output Offset Voltage Drift[1]	±10 μV/°C	(±10 μV/°C) (60°C) = 600 μV 600 μV/20 mV = 300 ppm	–	300 ppm	–
Bias Current–Source Imbalance Error	±15 nA	(±15 nA)(5 Ω) = 0.075 μV 0.075 μV/20mV = 3.75 ppm	3.75 ppm	3.75 ppm	–
Offset Current–Source Imbalance Error	±10 nA	(±10 nA)(5 Ω) = 0.050 μV 0.050 μV/20 mV = 2.5 ppm	2.5 ppm	2.5 ppm	–
Offset Current–Source Resistance Error	±10 nA	(10 nA) (175 Ω) = 1.75 μV 1.75 μV/20 mV = 87.5 ppm	87.5 ppm	87.5 ppm	–
Offset Current–Source Resistance–Drift	±100 pA/°C	(100 pA/°C) (175 Ω) (60°C) = 1 μV 1 μV/20 mV = 50 ppm	–	50 ppm	–
Common-Mode Rejection 5 V dc	115 dB	115 dB = 1.8 ppm × 5 V = 9 μV 9 μV/20 mV = 444 ppm	450 ppm	450 ppm	–
Noise, RTI (0.1 Hz–10 Hz)	0.22 μV p-p	0.22 μV p-p/20 mV = 10 ppm	–	–	10 ppm
		Total Error	3793.75 ppm	5493.75 ppm	20 ppm

[1]Output offset voltage and output offset voltage drift are given as RTI figures.

For a comprehensive study of instrumentation amplifier design and applications, refer to the *Instrumentation Amplifier Application Guide*, available free from Analog Devices.

9.5 A (v) "PhotoMos" MOS FET Relay

OMRON

MOS FET Relay

G3VM-X/4

SSR for Switching Analog Signals, with an Insulation Value of 2.5 kVAC between Input and Output Terminals

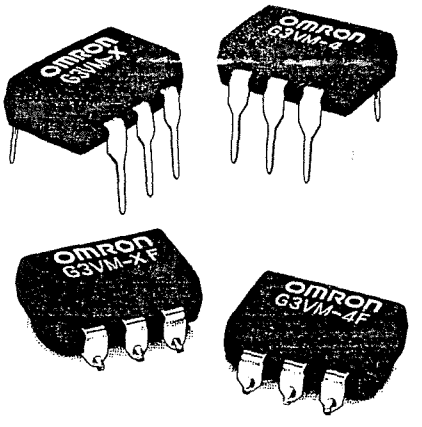

- Switching minute analog signals.
- Linear voltage and current characteristics.
- Switching AC and DC.
- Ultra-highly sensitive and subminiature SSR assuring long life.
- Low ON-resistance.
- Low current leakage between output terminals when they are open.
- Surface-mounting-type models are also available.
- Conforms to UL/CSA file# E41515/LR7486.

Ordering Information

Model Number Legend:

G3VM - □ □
1 2

1. Load Voltage
X: A load voltage of 60 VDC or 60 VAC (peak value)
4: A load voltage of 400 VDC or 400 VAC (peak value)

2. Terminal
None: PCB terminals
F: Surface-mounting terminals

Contact form	Terminals	Load voltage (peak value)	Model
SPST-NO	PCB terminals	60 VAC	G3VM-X
		400 VAC	G3VM-4
	Surface-mounting terminals	60 VAC	G3VM-XF
		400 VAC	G3VM-4F

Specifications

■ Absolute Maximum Ratings (Ta = 25°C)

Item		Symbol	G3VM-X/-XF	G3VM-4/-4F	Conditions
Input	LED forward current	I_F	20 mA		---
	Repetitive peak LED forward current	I_{FP}	40 mA		Duty: 50% max.; pulse width: 100 ms max.
	Excessive peak LED forward current	I_{FT}	100 mA		Duty: 1% max.; pulse width: 0.2 ms max.
	LED reverse voltage	V_R	3 V		---
Output	Output dielectric strength (load voltage)	V_{BO}	–60 to 60 V	–400 to 400 V	DC or AC peak value; AC connection (see note 1)
			0 to 60 V	0 to 400 V	DC; DC parallel connection (see note 2)
	Continuous load current (see note)	I_O	500 mA	150 mA	AC connection (see note 1)
			650 mA	200 mA	DC parallel connection (see note 2)
	Peak load current	I_{OP}	3.5 A	1.0 A	Pulse width: 100 ms max. per shot
	Output permissible loss	P_O	425 mW		–5 mW/°C 40°C min.
Dielectric strength between I/O terminals		V_{I-O}	2,500 VAC		1 min
Ambient temperature		Ta	Operating: –40°C to 85°C		With no icing and condensation
Storage temperature		Tstg	Storage: –55°C to 125°C		With no icing and condensation
Max. soldering temperature and time		---	260°C		5 s

Note: The output load current varies depending on the ambient temperature. Refer to *Engineering Data*.

■ Characteristics (Ta = 25°C)

Item	Symbol	G3VM-X/-XF	G3VM-4/-4F	Conditions
Output ON resistance	R_{ON}	0.7 Ω max.	10.0 Ω max.	AC connection I_F = 10 mA, I_O = 500/150 mA (see note 1)
		0.18 Ω max.	2.5 Ω max.	DC parallel connection I_F = 10 mA, I_O = 650/200 mA (see note 2)
Switching current leakage	I_{LEAK}	1.0 μA		V_F = 0.8 V, V_O = 60/400 V
LED forward current	V_F	1.3 V min., 1.85 V max.		I_F = 10 mA
Capacity between input and output terminals	C_{I-O}	Approx. 1.0 pF		1 MHz
Insulation resistance between input and output	R_{I-O}	1,000 MΩ min.		500 VDC
Operating time	t_{ON}	1.4 ms max.	0.95 ms max.	I_F = 10 mA (see note 3)
Release time	t_{OFF}	0.1 ms max.		I_F = 10 mA (see note 3)

Note: 1. AC Connection

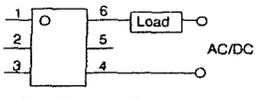

2. DC Parallel Connection

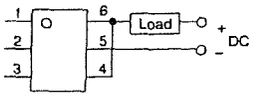

3.

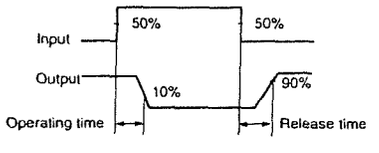

Engineering Data

■ Reference Data

Load Current vs. Ambient Temperature Characteristics

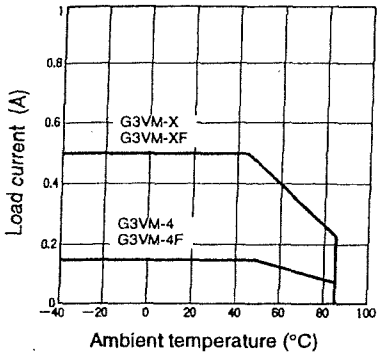

Distribution of ON-resistance (AC Connection)

G3VM-X

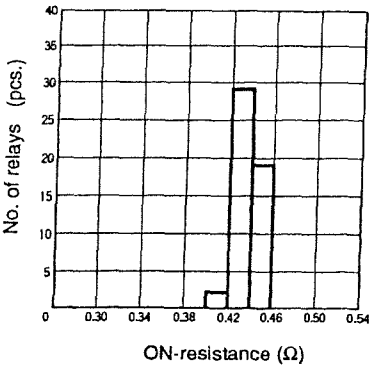

G3VM-4

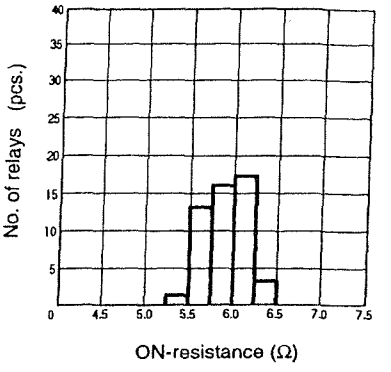

Distribution of ON-resistance (DC Parallel Connection)

G3VM-X

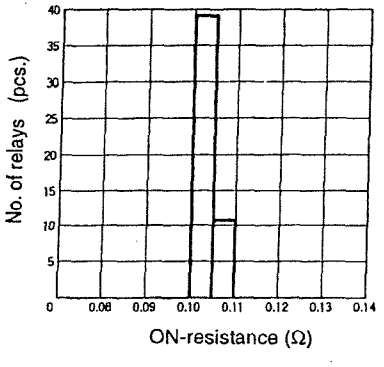

G3VM-4

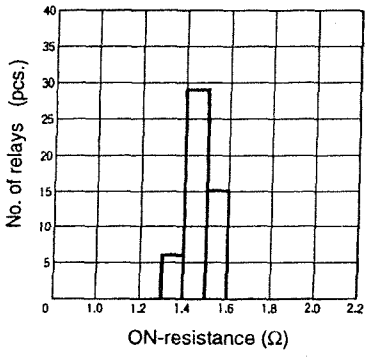

Operating Time vs. LED Forward Current

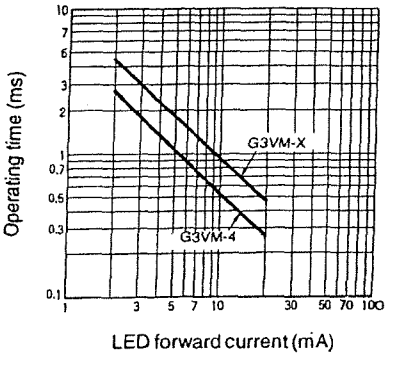

Distribution of Operating Time

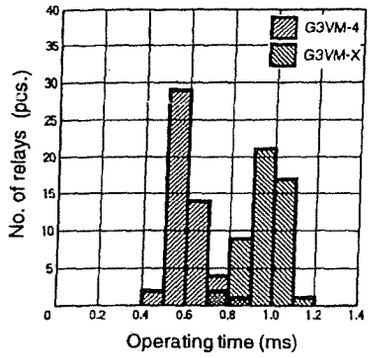

Distribution of Release Time

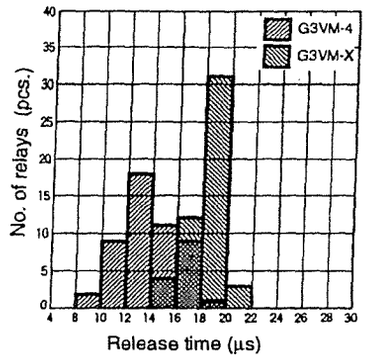

Output Voltage vs. Current Characteristics

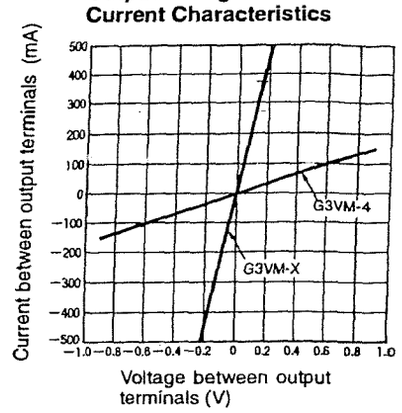

ON-resistance vs. Ambient Temperature

G3VM-X

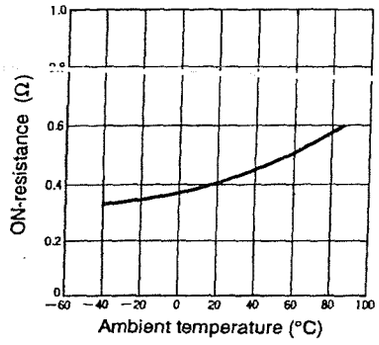

G3VM-4

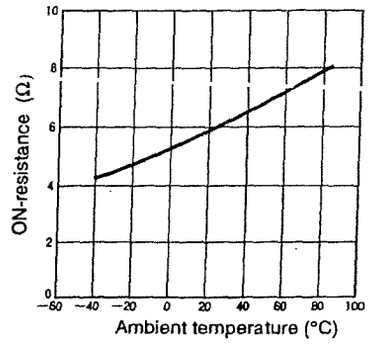

Dimensions

Note: All units are in millimeters unless otherwise indicated.

G3VM-X
G3VM-4

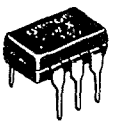

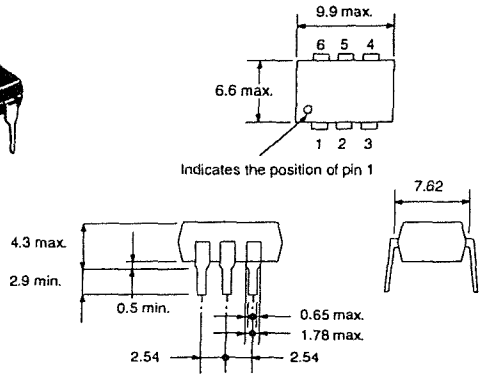

Terminal Arrangement/ Internal Connections (Top View)

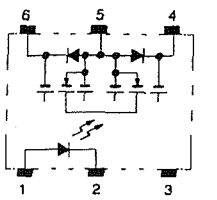

PCB Dimensions (Bottom View)

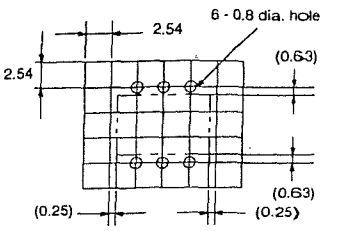

G3VM-XF
G3VM-4F

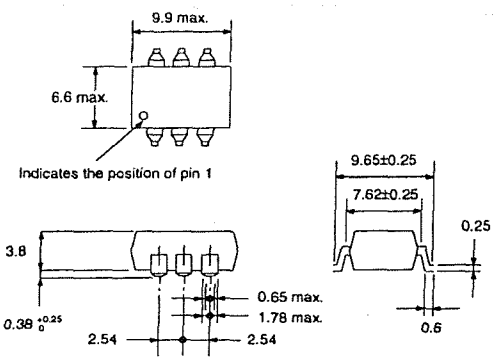

Terminal Arrangement/ Internal Connections (Top View)

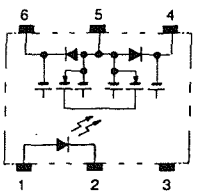

Actual Mounting Pad Dimensions (Recommended Value, Top View)

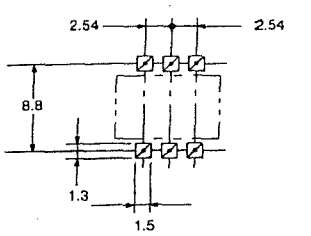

Note: Mounting pad dimensions shown are a top view.

Precautions

■ Correct Use

Recommended Operating Conditions

Use the G3VM under the following conditions so that the Relay will *operate properly.*

Item	Min.	Type	Max.
Operating LED forward current	5 mA	10 mA	20 mA
Releasing LED forward current	0 V	---	0.8 V

Note: Refer to page 35 for precautions common to all G3VM models.

10 APPENDIX B SENSOR SYSTEM PROGRAM LISTINGS

10.1 B (i) Analogue sensor

"MICROSOFT QUICKBASIC 4.5"

```
    PROGRAM DMASCOPE
    PCL718 CONTROL OF CALIBRATION FUNCTIONS ON RESISTANCE INTERFACE
    USES TTL CONTROL OF MERCURY WETTED RELAYS FOR SELECTION OF CALIBRATION RESISTANCES
    DMA TRANSFER OF DATA FROM ADC CARD TO PC


'INITIAL CALIBRATION ESTIMATES
slope = 2.744
intc = 4.85

n% = 200 'NUMBER OF SAMPLES TO AVERAGE IN 50HZ REJECT FILTER
cal = 0                                          'INITIAL RELAY SETTING
r = 10                                           '?
df% = 15                                         'MOVING AVERAGE SAMPLE SIZE
df2% = df%
ow% = df%
ch% = 0                                          'ADC CHANNEL TO USE

DIM DAT%(4), ARY1%(n%), ARY2%(n%), est(1000, 3), caldat(4)      'PREPARE ARRAYS FOR USE

GOSUB setad                                      'SETUP ADC

outp = 4                                         'CONFIGURE CODE FOR CONTROL OF RELAYS
GOSUB setoutp                                    'RELAY CONTROL ROUTINE

SCREEN 10                                        'PREPARE SCREEN FOOR GRAPHICAL OUTPUT

I = 0                                            'DRAWING COLOUR
my = 0                                           'SCREEN WINDOW SETTINGS
mx = 4095                                        'SCREEN WINDOW SETTINGS

WINDOW (0, my)-(500, mx)                         'SCREEN WINDOW SETTINGS
VIEW (1, 1)-(500, 348), 1, 3                     'SCREEN WINDOW SETTINGS
LOCATE 1, 64: PRINT USING "####.###"; mx         'MAX WINDOW Y
LOCATE 23, 64: PRINT USING "####.###"; my        'MIN WINDOOW Y

FOR i = my TO mx                                 'DRAW GRID ON WINDDOW
'LINE (0, i)-(1000, i), 1
NEXT i


DO                                               'MAIN LOOP
t1 = TIMER                                       'TIMER START

'**********    GET 500 ,200 SAMPLE  ESTIMATES IE. ONE SCREEN WIDTH
FOR w% = 1 TO 500
'******** STEP 5: PERFORM N A/D CONVERSIONS AND D.M.A. ****************
' ********        TRANSFER USING FUNC 6                                  ****************
'
DAT%(0) = n%        'NUMBER OF CONVERSIONS
DAT%(1) = &H7000  'MEMORY SEGMENT TO HOLD A/D DATA
DAT%(2) = 1         'PACER TRIGGER
DAT%(3) = 0         'NON-RECYCLE SCANNING
FUN% = 6           'FUNCTION 6
CALL PCL718(FUN%, SEG DAT%(0), SEG ARY1%(0), SEG ARY2%(0), ER%)
IF ER% <> 0 THEN PRINT "PERFORM FUNCTION 6 FAILED!": STOP
n = DAT%(0)
'
'
'******** STEP 7: TRANSFER DATA TO ARRAY USING FUNC 9 ***************
'
DAT%(0) = n%        'NUMBER OF DATA TO BE MOVED
DAT%(1) = &H7000  'SOURCE MEMORY SEGMENT
```

```
DAT%(2) = 0             'STARTING DATA NUMBER
FUN% = 9                'FUNCTION 9
CALL PCL718(FUN%, SEG DAT%(0), SEG ARY1%(0), SEG ARY2%(0), ER%)
IF ER% <> 0 THEN PRINT "PERFORM FUNCTION 9 FAILED!": STOP
'

'sum samplesm& = 0FOR v% = 0 TO n%: m& = m& + ARY1%(v%): NEXT v%

'average samples
est(w%, 0) = (m& / n%)
est(w%, 2) = est(w%, 0)

GOSUB lpf     'LOW PASS FILTER SUBROUTINE

IF w% = endsampl% AND st% = 1 THEN GOSUB sampl2    'MANUAL SAMPLE  START
IF w% = endsampl% AND st% = 0 THEN GOSUB sampl1    'MANUAL SAMPLE END

iF w% > df% + 1 THEN LOCATE 2, 65: PRINT USING "####.###ohm"; (est(w% - (df% / 2), 1) / slope) + intc
IF w% > df% THEN PSET (w% - (df% / 2), est(w% - (df% / 2), 1)), 3

LOCATE 3, 65: PRINT USING "####.###S"; sbase            'SCREEN AVERAGE BASELINE
IF k$ = "s" OR k$ = "S" THEN LINE (0, sbase)-(500, sbase), 3            'ON SCREEN BASELINE
c$ = INKEY$
IF c$ = "[" AND w% < 450 THEN endsampl% = w% + 50: st% = 0 'MANUAL SAMPLE START KEY
IF c$ = "]" AND w% < 450 THEN endsampl% = w% + 50: st% = 1       'MANUAL SAMPL END KEY
IF c$ = "c" THEN k$ = c$                                'CENTRE WINDOW KEYBOARD COMMAND
IF cal < 4 THEN GOSUB calibrate                         'IF IN STARTUP THEN SELF CALIBRATE
NEXT w%                                                 'END OF SCREEN WITH OF SAMPLES LOOP

' ****** THIS CODE RUNS AFTER EACH SCREEN WIDTH OF SAMPLES
'CALCULAT E SI UNIT CONVERSION AND DISPLAY
slope = (caldat(1) - caldat(3)) / (1400 - 511.51)
LOCATE 20, 65: PRINT USING "##.##### m"; slope
intc = caldat(3) - (511.51 * slope)
LOCATE 21, 65: PRINT USING "##.##### i"; intc

df2% = df% + 50
IF k$ = "s" OR k$ = "S" THEN GOSUB setbase
IF k$ = "c" OR k$ = "C" THEN GOSUB centrewindow
IF k$ = "+" THEN r = r + 1: GOSUB centrewindow          'DECREASE SCREEN RESOLUTION
IF k$ = "-" THEN r = r - 1: GOSUB centrewindow          'INCREASE SCREEN RESOLUTION


t2 = TIMER                                              'END TIMER FOR SAMPLE RATE ESTIMATION
LOCATE 4, 65: PRINT USING "####.###Hz"; 500 / (t2 - t1)

'ESTIMATE MIN OF WINDOW ON PREVIOUS SCREEN OF DATA
l = 4096: h = 0
FOR i = 1 TO 500
IF ABS(est(i, 1) - est(i, 0)) > h THEN h = ABS(est(i, 1) - est(i, 0))
NEXT i
'LOCATE 5, 65: PRINT USING "####.####P"; h

'MOVING AVERAGE OF PREVIOUS SCREEN
mav = 0
FOR i% = 1 TO 500
mav = mav + est(i%, 0)
NEXT i%
LOCATE 6, 65: PRINT USING "####.####Av"; mav / 500
LOCATE 7, 65: PRINT USING "#########Df"; df%            'SECONDARY LOW PASS FILTER POINTS

'CHECK FOR KEYBOARD COMMANDS
LOOP WHILE k$ = "" OR k$ = "s" OR k$ = "S" OR k$ = "c" OR k$ = "C" OR k$ = "+" OR k$ = "-"


' CLEAN UP ON EXIT
'******** STEP 9: DISABLE INTERRUPT ACTIVITY USING FUNC 7 ************
'
 FUN% = 7
CALL PCL718(FUN%, SEG DAT%(0), SEG ARY1%(0), SEG ARY2%(0), ER%)
END

'******************SUBROUTINES
setbase:
tt = 0
```

```
FOR x% = 1 TO 500
tt = est(x%, 0) + tt
NEXT x%
sbase = tt / 500
RETURN

centrewindow:
my = INT(est(250, 0)) - (r * 1.5)
mx = INT(est(250, 0)) + (r * .5)
VIEW (1, 1)-(500, 348), 1, 3
WINDOW (0, my)-(500, mx)
' CLS 1
LOCATE 1, 64: PRINT USING "####.###"; mx
LOCATE 23, 64: PRINT USING "####.###"; my
FOR f = my TO mx
LINE (0, f)-(500, f), 0
NEXT f
RETURN

setad:
PORT% = &H300          'SET I/O PORT ADDRESS
DAT%(0) = PORT%        'GET I/O PORT ADDRESS
DAT%(1) = 3            'SELECT INTERRUPT LEVEL 3
DAT%(2) = 1            'SELECTE D.M.A. IRQ3
ER% = 0               'ERROR RETURN CODE
FUN% = 0              'FUNCTION 0
CALL PCL718(FUN%, SEG DAT%(0), SEG ARY1%(0), SEG ARY2%(0), ER%)
IF ER% <> 0 THEN PRINT "DRIVER INITIALIZATION FAILED!": STOP
'
'******** STEP 3: SET SCAN CHANNEL RANGE USING FUNC 1 *****************
'
DAT%(0) = ch%        'SET START CHANNEL NUMBER
DAT%(1) = ch%         'SET STOP  CHANNEL NUMBER
FUN% = 1             'FUNCTION 1
CALL PCL718(FUN%, SEG DAT%(0), SEG ARY1%(0), SEG ARY2%(0), ER%)
IF ER% <> 0 THEN PRINT "SET SCAN CHANNEL FAILED! RE-ENTER": STOP
'

'******** STEP 4: SET PACER TRIGGER USING FUNC 17 **********************
'
'SET PACER=20KHZ (2MHZ DIVIDED BY 100 <DAT%(0)*DAT%(1)>)
'
DAT%(0) = 10     'COUNTER 2 DIVISOR
DAT%(1) = 10       'COUNTER 1 DIVISOR
FUN% = 17           'FUNCTION 17
CALL PCL718(FUN%, SEG DAT%(0), SEG ARY1%(0), SEG ARY2%(0), ER%)
IF ER% <> 0 THEN PRINT "SET PACER TRIGGER FAILED!": STOP
'
RETURN

lpf:
mav = 0
IF w% > df% THEN
      FOR q% = w% TO w% - df% STEP -1
            mav = mav + est(q%, 0)
      NEXT q%
      est(w% - (df% / 2), 1) = mav / (df% + 1)
END IF
RETURN

lpf2:
      LINE (ow% - (df% / 2), est(ow% - (df% / 2), 1))-(w% - (df% / 2), est(w% - (df% / 2), 1)), 2
      ow% = w%

RETURN
FOR q% = 1 TO df2%
mav = 0
IF w% > 1 THEN mav = est(w%, 2) + est(w% - 1, 2) ELSE mav = est(w%, 2) + est(w% + 499, 2)
est(w%, 2) = mav / 2
NEXT q%
RETURN

sampl1:
'MANUAL SAMPLE  1 (REFERENCE)
d = 0
```

```
FOR i% = endsampl% - 49 TO endsampl%
d = est(i%, 0) + d
NEXT i%
LOCATE 9, 65: PRINT USING "####.####s1"; d / 50
endsampl% = 0
s1 = d / 50
RETURN

sampl2:
'MANUAL SAMPLE  2 (PEAK MEASUREMENT)
d = 0
FOR i% = endsampl% - 49 TO endsampl%
d = est(i%, 0) + d
NEXT i%
LOCATE 10, 65: PRINT USING "####.####s2"; d / 50
endsampl% = 0
s2 = d / 50
LOCATE 11, 65: PRINT USING "####.####ds"; s2 - s1
RETURN

setoutp:
'CONTROL TTL OUTPU OF INTERFACE
620 FUN% = 13
DAT%(0) = outp
CALL PCL718(FUN%, SEG DAT%(0), SEG ARY1%(0), SEG ARY2%(0), ER%)
IF ER% <> 0 THEN PRINT "WRITE DIGITAL OUTPUT FAILED": STOP
LOCATE 16, 65: PRINT USING "## Out stat"; outp
RETURN

calibrate:
'DURING THE FIRST SCREEN OF DATA CALIBRATION RESISTORS ARE SWITCHED IN TO PROVIDE
'CALIBRATION DATA FOR TRANSLATION TO SI UNITS

IF w% = 50 THEN outp = 2: GOSUB setoutp
IF w% = 149 THEN endsampl% = 149: cal = 1: GOSUB sampl
IF w% = 150 THEN outp = 1: GOSUB setoutp
IF w% = 249 THEN endsampl% = 249: cal = 2: GOSUB sampl
IF w% = 250 THEN outp = 3: GOSUB setoutp
IF w% = 349 THEN endsampl% = 349: cal = 3: GOSUB sampl
IF w% = 350 THEN outp = 4: GOSUB setoutp
IF w% = 499 THEN cal = 4
RETURN

sampl:
d = 0
FOR i% = endsampl% - 24 TO endsampl%
d = est(i%, 0) + d
NEXT i%
endsampl% = 0
caldat(cal) = d / 25
LOCATE 16 + cal, 65: PRINT USING "####.####s"; caldat(cal)
RETURN
```

10.2 B (ii) Single pulse sensor

```
"MICROSOFT QUICKBASIC 4.5"

¶SCREEN 10
DA0% = 1000
DA1% = 0
Ax = (DA0% * (5000 / 4096)) / 1000
delay = 1
N% = 20
350 DIM DAT%(4), ARY1%(N%), ARY2%(N%), est(2)

 PORT% = &H300          'SET I/O PORT ADDRESS
 DAT%(0) = PORT%        'GET I/O PORT ADDRESS
 DAT%(1) = 3            'SELECT INTERRUPT LEVEL 3
 DAT%(2) = 1            'SELECTE D.M.A. IRQ3
 ER% = 0                'ERROR RETURN CODE
 FUN% = 0               'FUNCTION 0
 CALL PCL718(FUN%, SEG DAT%(0), SEG ARY1%(0), SEG ARY2%(0), ER%)
 IF ER% <> 0 THEN PRINT "DRIVER INITIALIZATION FAILED!": STOP
 '
 '******** STEP 3: SET SCAN CHANNEL RANGE USING FUNC 1 *****************
 '
 DAT%(0) = 0       'SET START CHANNEL NUMBER
 DAT%(1) = 0        'SET STOP  CHANNEL NUMBER
 FUN% = 1           'FUNCTION 1
 CALL PCL718(FUN%, SEG DAT%(0), SEG ARY1%(0), SEG ARY2%(0), ER%)
 IF ER% <> 0 THEN PRINT "SET SCAN CHANNEL FAILED! RE-ENTER": STOP
 '
 '******** STEP 4: SET PACER TRIGGER USING FUNC 17 *********************
 '
 'SET PACER=100 HZ (2MHZ DIVIDED BY 20000 <DAT%(0)*DAT%(1)>)
 '20khz
 DAT%(0) = 200          'COUNTER 2 DIVISOR
 DAT%(1) = 10          'COUNTER 1 DIVISOR

 FUN% = 17             'FUNCTION 17
 CALL PCL718(FUN%, SEG DAT%(0), SEG ARY1%(0), SEG ARY2%(0), ER%)
 IF ER% <> 0 THEN PRINT "SET PACER TRIGGER FAILED!": STOP
 '

LOCATE 14, 63: PRINT USING "S Rate ##.##Khz"; (1000000 / (DAT%(0) * DAT%(1))) / 1000
' Set relays to both cal resistors on
DAT = (2 ^ 5) + (2 ^ 6)
GOSUB setoutp
FOR s = 1 TO delay: NEXT s

WINDOW (0, 1350)-(500, 1380)
VIEW (1, 1)-(480, 330), 0, 3

GOSUB calibrate
t1 = TIMER
WHILE INKEY$ = ""
FOR w% = 0 TO 500
   FOR drn = 0 TO 1
      DAT = (2 ^ (3 + drn)) + (2 ^ 0)'direction and electrode pair 0
      GOSUB setoutp
      GOSUB sampleInterface
      est(drn) = est
   NEXT drn
'est = (est(0) + est(1)) / 2
IF est > 4090 OR INKEY$ = " " THEN GOTO finish
'PSET (w%, est(0)), 3
PSET (w%, est(1)), 15
LOCATE 3, 63: PRINT USING "AD #####.## "; est
'LOCATE 4, 63: PRINT USING "Xn #####.## uA"; Ax * 1000
'LOCATE 5, 63: PRINT USING "R0 #####.## Ohm"; (est(0) * (2000 / 4096)) / Ax
'LOCATE 6, 63: PRINT USING "R1 #####.## Ohm"; (est(1) * (2000 / 4096)) / Ax
```

```
NEXT w%

t2 = TIMER
CLS 1
WEND
finish:
GOSUB shutdown
LOCATE 1, 64: PRINT USING ("###.##Hz ####"); 500 / (t2 - t1); N%

END

sampleinterface:
DAT%(0) = DA0% 'DA CHAN 0 0-5V
DAT%(1) = DA1%  'DA CHAN 1 0-5V
FUN% = 16
CALL PCL718(FUN%, SEG DAT%(0), SEG ARY1%(0), SEG ARY2%(0), ER%)
IF ER% <> 0 THEN PRINT "PERFORM D/A #0 AND D/A #1 FAILED!"
FOR s = 1 TO delay: NEXT s

'******* STEP 5: PERFORM n% A/D CONVERSIONS USING FUNC 4 ***********
DAT%(0) = N%
DAT%(2) = 1          'PACER TRIGGER
FUN% = 4             'FUNTION 4
CALL PCL718(FUN%, SEG DAT%(0), SEG ARY1%(0), SEG ARY2%(0), ER%)
IF ER% <> 0 THEN PRINT "PERFORM N A/D CONVERSIONS FAILED!": STOP

m& = 0

FOR v% = 0 TO N% - 1
m& = m& + ARY1%(v%)
'PSET (v%, ARY1%(v%)), 3
NEXT v%
est = m& / N%



DAT%(0) = 0 'DA CHAN 0 0-5V
DAT%(1) = 0  'DA CHAN 1 0-5V
FUN% = 16
CALL PCL718(FUN%, SEG DAT%(0), SEG ARY1%(0), SEG ARY2%(0), ER%)
IF ER% <> 0 THEN PRINT "PERFORM D/A #0 AND D/A #1 FAILED!"
RETURN



setoutp:
FUN% = 21
DAT%(1) = 0
DAT%(0) = 255 XOR DAT
CALL PCL718(FUN%, SEG DAT%(0), SEG ARY1%(0), SEG ARY2%(0), ER%)
IF ER% <> 0 THEN PRINT "PERFORM FUNC 21 FAILED!": STOP
RETURN

calibrate:
'bit 5=1400R and bit 6=806R
DAT = (2 ^ 5) + (2 ^ 6)'both cal 1400R + 806R
GOSUB setoutp
GOSUB sampleinterface
GOSUB sampleinterface
LOCATE 7, 63: PRINT USING "511.11R  = ####.##"; (est * (2000 / 4096)) / Ax

DAT = (2 ^ 6) 'cal 806R
GOSUB setoutp
GOSUB sampleinterface
GOSUB sampleinterface
LOCATE 8, 63: PRINT USING "806.00R  = ####.##"; (est * (2000 / 4096)) / Ax

DAT = (2 ^ 5) 'cal 1400R
GOSUB setoutp
GOSUB sampleinterface
GOSUB sampleinterface
LOCATE 9, 63: PRINT USING "1400.00R = ####.##"; (est * (2000 / 4096)) / Ax

DAT = (2 ^ 5) + (2 ^ 6)'cal 1400R + 806R
GOSUB setoutp
```

```
GOSUB sampleinterface
RETURN

shutdown:
DAT%(0) = 0 'DA CHAN 0 0-5V
DAT%(1) = 0  'DA CHAN 1 0-5V
FUN% = 16
CALL PCL718(FUN%, SEG DAT%(0), SEG ARY1%(0), SEG ARY2%(0), ER%)
IF ER% <> 0 THEN PRINT "PERFORM D/A #0 AND D/A #1 FAILED!"

DAT = (2 ^ 5) + (2 ^ 6)'cal 1400R + 806R
GOSUB setoutp

RETURN
```

10.3 B (iii) Multi-pulse sensor

```
'*
'*  THIS PROGRAM USES THE PCL-718 DRIVER FUNC 0, 1, 6, 7, 8,
'*  9, AND 17 TO PERFORM PACER TRIGGERED N A/D CONVERSIONS WITH
'*  D.M.A. DATA TRANSFER
'*  USES OUTPUT WAVEFORM AND INTERRUPT TIMING

'
'******** STEP 1: INITIALIZE DRIVER USING FUNC 0 **********************
'used for testing 29/12/95 in Raceway and aquarium
'used for testing multiplexer in tank 20/9/97
'modified to produce csv files 26/10/97
'fix bug which left output low at end of waveform 2/11/97
'output file contains date and time fields 2/11/97
'only pair 2 recorded 9/11/97
'all pairs recorded 13/8/98
'used for tank tests on 13/2/99
'DG7 used for real fish  JAN99


location$ = "c:\qb\tdata\"

'LINE INPUT ; "Describe experiment  "; desc$
'INPUT ; "Target length  "; tl
PRINT
INPUT ; "Water depth mm "; wdep
PRINT
INPUT ; "Water conductivity uS "; wcond
PRINT
INPUT ; "Water temp degC "; wtemp
PRINT
LINE INPUT ; "Data file name       "; fil$



SCREEN 12
drn = 0
offs = 0
fdbak = 10
DA0% = 120 'was 290 for 300us water was 580 use for setting excitation rate
DA1% = 0
v0 = 2048 'was 2048 for most ttests
Ax = (DA0% * 2 * (5000 / 4096)) / 1000 'note bipolar excitation
delay = 0
N% = 2500
DIM DAT%(4), ARY1%(N%), ARY2%(N%), est(2), dest(2), destr(2)
DIM MuxMap(0 TO 1, 1 TO 3, 0 TO 1) AS INTEGER
DIM mdat(1000)
DIM dmap(1 TO 3, 0 TO 1)
DIM bigdmap(1 TO 3, 0 TO 1, 400)
DIM timemap(400)
360 PORT% = &H300          'SET I/O PORT ADDRESS
370 DAT%(0) = PORT%        'GET I/O PORT ADDRESS
380 DAT%(1) = 3            'SELECT INTERRUPT LEVEL 3
390 DAT%(2) = 1            'SELECTE D.M.A. IRQ3
410 ER% = 0               'ERROR RETURN CODE
420 FUN% = 0               'FUNCTION 0
430 CALL PCL718(FUN%, SEG DAT%(0), SEG ARY1%(0), SEG ARY2%(0), ER%)
440 IF ER% <> 0 THEN PRINT "DRIVER INITIALIZATION FAILED!": STOP
450 '
460 '******** STEP 3: SET SCAN CHANNEL RANGE USING FUNC 1 *****************
470 '
510 DAT%(0) = 0       'SET START CHANNEL NUMBER
520 DAT%(1) = 0        'SET STOP  CHANNEL NUMBER
530 FUN% = 1           'FUNCTION 1
540 CALL PCL718(FUN%, SEG DAT%(0), SEG ARY1%(0), SEG ARY2%(0), ER%)
550 IF ER% <> 0 THEN PRINT "SET SCAN CHANNEL FAILED! RE-ENTER": STOP
560 '
spsc% = 400
'WINDOW (0, 0)-(60, 4095)
```

```
'VIEW (10, 10)-(480, 400), 0, 1

GOSUB setupwaveform
GOSUB setupmultiplexermap
SLEEP
' Set relays to both cal resistors on
REM DAT = (2 ^ 5) + (2 ^ 6)
DAT%(0) = 255
DAT%(1) = 15
GOSUB setoutp
FOR s = 1 TO delay: NEXT s


counter = 1
spsc% = 400
'WINDOW (28, 3000)-(spsc%, 4095)
VIEW (42, 20)-(480, 450), 0, 1



LOCATE 4, 63: PRINT USING "Xn #####.## uA"; Ax * 1000
GOSUB calibrate
'offs = 140
fil$ = location$ + fil$ + ".csv"
OPEN fil$ FOR APPEND AS #1

startloop:
    t1 = TIMER
    CLS
    FOR w% = 0 TO spsc% - 1' samples per screen
    'CLS
    'INPUT ; "Enter elevation cm "; elev
    'PRINT
    'IF elev = -99 THEN GOTO finish
    'INPUT ; "Enter displacement cm "; displ
    displ = 0

            FOR pair = 1 TO 3
             FOR drn = 0 TO 1

                DAT%(0) = MuxMap(drn, pair, 0)
                DAT%(1) = MuxMap(drn, pair, 1)

                GOSUB setoutp

                GOSUB sampleinterface

                destr(drn) = (dest(drn) * (2000 / 4096)) / Ax
                bigdmap(pair, drn, w%) = destr(drn)

             NEXT drn
             chk = (bigdmap(pair, 1, w%) - bigdmap(pair, 0, w%))
             ky$ = INKEY$
             IF ky$ = " " THEN GOTO finish
             IF ky$ = "S" THEN
              LOCATE 20, 65: INPUT "comment? ", COMMENT$
              saveevent = 1
              LINE (w%, -30)-(w%, 30), 1
             END IF


          NEXT pair

    timemap(w%) = TIMER
    FOR drn = 0 TO 0
        disp = 2
        IF w% > 0 THEN LINE (w% - 1, (bigdmap(disp, 1, w% - 1) - bigdmap(disp, 0, w% - 1)))-(w%, (bigdmap(disp, 1,
w%) - bigdmap(disp, 0, w%))), drn + 2
    NEXT drn
    IF delayctr < 200 AND saveevent = 1 THEN
        delayctr = delayctr + 1
        IF delayctr = 1 THEN firstsample = w%
        IF delayctr = 200 THEN
            delayctr = 0
            saveevent = 0
```

```
            'LOCATE 21, 64: PRINT "event saved"
            GOSUB recordevent
        END IF
    END IF
    mdat(w%) = est 'put average into array before recalc
    LOCATE 5, 63: PRINT USING "R0 #####.## Ohm"; (est * (2000 / 4096)) / Ax
    destr = (dest * (2000 / 4096)) / Ax          ' convert to resistance?
    span = 50

    IF w% = 0 THEN
          'CLS 0
        'WINDOW (28, INT(destr(0)) - span)-(spsc%, INT(destr(0)) + span) 'zoom in to focus
        WINDOW (0, 0 - span)-(spsc%, 0 + span) 'zoom in to focus
        LOCATE 1, 1: PRINT USING "####"; 0 + span
        LOCATE 28, 1: PRINT USING "####"; 0 - span
        FOR grid = INT(0) - span TO INT(0) + span STEP 10
            LINE (0, grid)-(spsc%, grid), 1
        NEXT grid
        LINE (0, 20)-(spsc%, 20), 1
        LINE (0, 0)-(spsc%, 0), 1

    END IF
    IF w% < 29 THEN sdestr = ((destr(0) + destr(1)) / 2) 'recursive filter seed
    sdestr = (sdestr + ((destr(0) + destr(1)) / 2)) / 2  'recursive filter

    IF est > 4090 OR ky$ = " " THEN GOTO finish


    LOCATE 3, 63: PRINT USING "AD #####.## "; est
    NEXT w%
    'CLS 1
    t2 = TIMER
    LOCATE 20, 64: PRINT USING ("###.##Hz ####"); (spsc%) / (t2 - t1); N%
GOTO startloop


finish:
CLOSE #1
GOSUB shutdown
GOSUB disableinterrupt


END

recordevent:
WRITE #1, firstsample, wdep, wcond, wtemp, COMMENT$
'NT #1, "Date,Time,TI,Dep,Temp,Cond,EI,Di,P,D,PPResist,XnuA"

'LOCATE 1, 6: PRINT "EI  Di  P  D  PPReslst  XnuA    "
FOR z = 0 TO 399
    WRITE #1, z, timemap(z), bigdmap(1, 0, z), bigdmap(1, 1, z), bigdmap(2, 0, z), bigdmap(2, 1, z), bigdmap(3, 0, z),
bigdmap(3, 1, z)

NEXT z
LOCATE 21, 65: PRINT "SAVED ", COMMENT$
RETURN



sampleinterface:

'******** STEP 6: SET D/A OPERATION ON A/D INTERRUPT USING FUNC 18 ***
'
I.MSR% = INP(&H21)
OUT &H21, (I.MSR% OR 1)
FUN% = 18
DAT%(0) = CH
DAT%(1) = LADR
DAT%(2) = N.CYC
DAT%(3) = VARPTR(ARY1%(0))
IF ADF% = 1 THEN DAT%(4) = VARPTR(ARY2%(0)) ELSE DAT%(4) = 0
CALL PCL718(FUN%, SEG DAT%(0), SEG ARY1%(0), SEG ARY2%(0), ER%)
IF ER% <> 0 THEN PRINT "FAIL!": STOP
'
'******** STEP 7: DISABLE INTERRUPT ACTIVITY USING FUNC 7 ***********
```

```
'
FUN% = 8
DO
CALL PCL718(FUN%, SEG DAT%(0), SEG ARY1%(0), SEG ARY2%(0), ER%)
LOOP UNTIL DAT%(1) = 0

FUN% = 7
CALL PCL718(FUN%, SEG DAT%(0), SEG ARY1%(0), SEG ARY2%(0), ER%)
'
OUT &H21, IMR%
'
'******** STEP 8: DISPLAY A/D DATA ***********************************
'
f% = 0
m& = 0
FOR v% = 3 TO LADR - 3 STEP 2
m& = m& + ARY2%(v%)
f% = f% + 1
NEXT v%
est(0) = m& / f%

m& = 0

FOR v% = 3 TO LADR - 3 STEP 2
m& = m& + ARY2%(v% + 1)

NEXT v%
est(1) = m& / f%


'LOCATE 14, 63: PRINT USING "AVPP ####.##"; est(0) + ABS(est(1))

'est(0) and est(1) are average +ve and negative peaks
'LOCATE 15, 63: PRINT USING "AV ####.##"; est(0) + est(1)
'so est is the average peak to peak voltage
est = ABS(est(0)) + ABS(est(1))
dest(drn) = est   'this puts the estimate in a direction variable
dest = dest(1)    'and then a general variable
imbal = (est(0) + est(1))
LOCATE 14, 63: PRINT USING "##### ##### #####"; dest(0); dest(1); dest(0) - dest(1)

' old offsetting used fixed increments of size fdbak to balance the excitation waveform
IF imbal < 0 THEN offs = offs + (imbal / 2)
'ARY1%(0) = v0 + offs ' if offsetting is required
'ARY1%(0) = v0
RETURN

disableinterrupt:
'******** STEP 9: DISABLE INTERRUPT ACTIVITY USING FUNC 7 ************

FUN% = 7
CALL PCL718(FUN%, SEG DAT%(0), SEG ARY1%(0), SEG ARY2%(0), ER%)
RETURN


setoutp:
FUN% = 21
REM DAT%(1) = 0
REM DAT%(0) = 255 XOR DAT
CALL PCL718(FUN%, SEG DAT%(0), SEG ARY1%(0), SEG ARY2%(0), ER%)
IF ER% <> 0 THEN PRINT "PERFORM FUNC 21 FAILED!": STOP
RETURN

calibrate:
'bit 5=1400R and bit 6=806R
'DAT = (2 ^ 5) + (2 ^ 6)'both cal 1400R + 806R
DAT%(0) = 255: DAT%(1) = 15
GOSUB setoutp
GOSUB sampleinterface
LOCATE 7, 63: PRINT USING "511.11R  = ####.##"; (est * (2000 / 4096)) / Ax

'DAT = (2 ^ 6) 'cal 806R
DAT%(0) = 255: DAT%(1) = 47
GOSUB setoutp
GOSUB sampleinterface
```

```
LOCATE 8, 63: PRINT USING "806.00R  = ####.##"; (est * (2000 / 4096)) / Ax

'SLEEP 2

'DAT = (2 ^ 5) 'cal 1400R
DAT%(0) = 255: DAT%(1) = 31
GOSUB setoutp
GOSUB sampleinterface
LOCATE 9, 63: PRINT USING "1400.00R = ####.##"; (est * (2000 / 4096)) / Ax

'SLEEP 2


'DAT = (2 ^ 5) + (2 ^ 6)'cal 1400R + 806R
DAT%(0) = 255: DAT%(1) = 15
GOSUB setoutp
GOSUB sampleinterface
RETURN

shutdown:
DAT%(0) = 0 'DA CHAN 0 0-5V
DAT%(1) = 0  'DA CHAN 1 0-5V
FUN% = 16
CALL PCL718(FUN%, SEG DAT%(0), SEG ARY1%(0), SEG ARY2%(0), ER%)
IF ER% <> 0 THEN PRINT "PERFORM D/A #0 AND D/A #1 FAILED!"

'DAT = (2 ^ 5) + (2 ^ 6)'cal 1400R + 806R
DAT%(0) = 255: DAT%(1) = 15
GOSUB setoutp
RETURN

setupwaveform:
'MAXIMUM RATE=4500 at PC XT(LADDER NO. *FREQ)"
LADR = 53'was 53
FREQ = 47 'was 47
T.RATE = LADR * FREQ
IF T.RATE > 4500 THEN PRINT : PRINT " OVER H/W CAN PROVIDE, RE-DO "
'NUMBER CYCLES OF OUTPUT (1-32767, 0=continuous)
N.CYC = 1
CH = 0   'da chan

ADF% = 1 'SET A/D DATA FLAG=1
CHN = 0'ad chn no
FUN% = 1
DAT%(0) = CHN: DAT%(1) = CHN
CALL PCL718(FUN%, SEG DAT%(0), SEG ARY1%(0), SEG ARY2%(0), ER%)
IF ER% <> 0 THEN PRINT "FAIL!": STOP
PRINT
'
'******** STEP 4: SET PACER TRIGGER RATE USING FUNC 17 ***************
'
DIV = 1000000! / T.RATE
IF DIV < 4 THEN PRINT " FAIL !": GOTO 470
X = 2
WHILE 1 = 1
CTR1 = X
CTR2 = INT(DIV / X)
IF CTR2 > 65535! THEN X = X + 50
IF CTR2 < 65535! GOTO nd
WEND

nd:
NDIV = CTR1 * CTR2
IF CTR1 > 32767 THEN CTR1 = CTR1 - 65536!
IF CTR2 > 32767 THEN CTR2 = CTR2 - 65536!
LOCATE 20, 62: PRINT USING "TIMER=######.###Hz"; 1000000! / NDIV
FUN% = 17
DAT%(0) = CTR1
DAT%(1) = CTR2
CALL PCL718(FUN%, SEG DAT%(0), SEG ARY1%(0), SEG ARY2%(0), ER%)
IF ER% <> 0 THEN PRINT "FAIL !": STOP
'
'DIM ARY1%(LADR - 1)
'IF ADF% = 1 THEN DIM ARY2%(LADR - 1)
'
```

```
'******** STEP 5 : CREATE BIPOLAR WAVEFORM DATA TO ARRAY ***************
'
CLS
FOR I = 1 TO LADR - 2
'ARY1%(I) = v0
'ARY1%(I) = (CINT(2048 + 2047 * SIN(3.142 * I / (LADR / 2)))) / 10
IF I MOD 2 = 1 THEN ARY1%(I) = DA0% + v0 ELSE ARY1%(I) = v0 - DA0%
'IF I = 1 THEN LINE (I, ARY1%(I))-(I + 1, ARY1%(I)), 3 ELSE LINE -(I, ARY1%(I)), 3: LINE (I, ARY1%(I))-(I + 1,
ARY1%(I)), 3
NEXT I
ARY1%(0) = v0 + offs
ARY1%(1) = v0
ARY1%(LADR - 1) = v0
ARY1%(LADR) = v0
'LINE (0, 2048)-(500, 2048), 3
'SLEEP
'ARY1%(0) = DA0%
'ARY1%(1) = 0
'PRINT : COLOR 0, 7: PRINT "  PRESS ANY KEY TO START  "; : COLOR 7, 0
'IF INKEY$ = "" GOTO 970
FOR I = 0 TO LADR
IF I = 0 THEN LINE (I, ARY1%(I))-(I + 1, ARY1%(I)), 3 ELSE LINE -(I, ARY1%(I)), 3: LINE (I, ARY1%(I))-(I + 1,
ARY1%(I)), 3
NEXT I
PRINT "waveform type"
SLEEP
CLS
RETURN

setupmultiplexermap:
MuxMap(1, 1, 0) = 149 'up,left,dat%0
MuxMap(1, 1, 1) = 63  'up,left,dat%1

MuxMap(0, 1, 0) = 106 'dn,left,dat%0
MuxMap(0, 1, 1) = 63  'dn,left,dat%1

MuxMap(1, 2, 0) = 213 'up,centr,dat%0
MuxMap(1, 2, 1) = 62  'up,centr,dat%1

MuxMap(0, 2, 0) = 234 'dn,centr,dat%0
MuxMap(0, 2, 1) = 61  'dn,centr,dat%1

MuxMap(1, 3, 0) = 213 'up,right,dat%0
MuxMap(1, 3, 1) = 59  'up,right,dat%1

MuxMap(0, 3, 0) = 234 'dn,right,dat%0
MuxMap(0, 3, 1) = 55  'dn,right,dat%1


RETURN
```

10.4 B (iv) Pattern Matching Algorithm

```
Public esdis, esel As Integer

Function CalcRange(elevation, displacement, pair)
If pair = 2 Then rng = Sqr((elevation ^ 2) + (displacement ^ 2))
If pair = 1 Then rng = Sqr((elevation ^ 2) + ((displacement + 300) ^ 2))
If pair = 3 Then rng = Sqr((elevation ^ 2) + ((displacement - 300) ^ 2))
CalcRange = Int(rng)
End Function

Static Function Log10(X)
   If X > 0 Then Log10 = Log(X) / Log(10#) Else Log10 = -3
End Function

Function CalcSignal(rng, tl)
CalcSignal = (-23.446 + (tl * 0.0288)) + (14.378 / (1 + ((rng / 477) ^ 2.36)))
End Function

Function FindTargetLength(s1, s2, s3)
mindisp = -600
maxdisp = 10
minelev = 10
maxelev = 800
absdiff = 10000
minabsdiff = 10000
mintl = 200
maxtl = 850
For elev = minelev To maxelev Step 25
   For disp = mindisp To maxdisp Step 50
      For tl = mintl To maxtl Step 20
         cs1 = (CalcSignal(CalcRange(elev, disp, 1), tl))
         cs2 = (CalcSignal(CalcRange(elev, disp, 2), tl))
         cs3 = (CalcSignal(CalcRange(elev, disp, 3), tl))
         absdiff = Abs(s1 - cs1) + Abs(s2 - cs2) + Abs(s3 - cs3)
         If absdiff < minabsdiff Then
            esttl = tl
            esel = elev
            esdis = disp
            minabsdiff = absdiff
         End If
      Next tl
   Next disp
Next elev
FindTargetLength = esttl
End Function
Sub Macro2()
''
erw = 0
For target = 300 To 700 Step 100                    ------ Calculate the number of tests required per run
   'Range("K9").Select
   'ActiveCell.FormulaR1C1 = target
   For displacement = -600 To 0 Step 50
      For elevation = 20 To 700 Step 50
         For rep = 1 To 20
            erw = erw + 1
         Next rep
      Next elevation
   Next displacement
Next target
Cells(5, 6).Value = erw
If erw > 16000 Then Exit Sub

rw = 15
For target = 300 To 700 Step 100                    --------Main program
   'Range("K9").Select
   'ActiveCell.FormulaR1C1 = target
   For displacement = -600 To 0 Step 50
```

```
        For elevation = 20 To 700 Step 50
          For rep = 1 To 20
            start = Timer
            esel = 0
            esdis = 0

            er1 = CalcRange(elevation, displacement, 1)
            er2 = CalcRange(elevation, displacement, 2)
            er3 = CalcRange(elevation, displacement, 3)
            es1 = 10 ^ (CalcSignal(er1, target) / 10) + Worksheets("noise").Cells(Int(Rnd() * 1000) + 1, 1).Value
            es1 = 10 * Log10(es1)
            es2 = 10 ^ (CalcSignal(er2, target) / 10) + Worksheets("noise").Cells(Int(Rnd() * 1000) + 1, 1).Value
            es2 = 10 * Log10(es2)
            es3 = 10 ^ (CalcSignal(er3, target) / 10) + Worksheets("noise").Cells(Int(Rnd() * 1000) + 1, 1).Value
            es3 = 10 * Log10(es3)
            Cells(rw, 2).Value = target
            Cells(rw, 3).Value = elevation
            Cells(rw, 4).Value = displacement
            Cells(14, 2).Value = target
            Cells(14, 3).Value = elevation
            Cells(14, 4).Value = displacement
            Cells(rw, 5).Value = er1
            Cells(rw, 6).Value = er2
            Cells(rw, 7).Value = er3
            Cells(rw, 8).Value = es1
            Cells(rw, 9).Value = es2
            Cells(rw, 10).Value = es3
            Cells(rw, 12).Value = FindTargetLength(es1, es2, es3)
            Cells(rw, 13).Value = esel
            Cells(rw, 14).Value = esdis
            Cells(5, 5).Value = Timer - start
            erw = erw - 1
            Cells(5, 7).Value = (erw * (Timer - start)) / 3600
            Cells(5, 8).Value = erw
            rw = rw + 1
          Next rep
        Next elevation
      Next displacement
    Next target
    End Sub

    Function FindTargetElev(s1, s2, s3, tl)
    mindisp = -600
    maxdisp = 100
    minelev = 10
    maxelev = 800
    absdiff = 10000
    minabsdiff = 10000
    mintl = 200
    maxtl = 850
    For elev = minelev To maxelev Step 25
      For disp = mindisp To maxdisp Step 50

        cs1 = (CalcSignal(CalcRange(elev, disp, 1), tl))
        cs2 = (CalcSignal(CalcRange(elev, disp, 2), tl))
        cs3 = (CalcSignal(CalcRange(elev, disp, 3), tl))
        s1 = s1
        s2 = s2
        s3 = s3
        absdiff = Abs(s1 - cs1) + Abs(s2 - cs2) + Abs(s3 - cs3)
        If absdiff < minabsdiff Then
          esttl = tl
          estel = elev
          estdisp = disp
          minabsdiff = absdiff
        End If

      Next disp
    Next elev
    FindTargetElev = estel
    End Function

    Function FindTargetDisp(s1, s2, s3, tl, elev)
    mindisp = -600
    maxdisp = 100
```

```
minelev = 10
maxelev = 800
absdiff = 10000
minabsdiff = 10000
mintl = 200
maxtl = 850
'For elev = minelev To maxelev Step 25
   For disp = mindisp To maxdisp Step 50
      'For tl = mintl To maxtl Step 25
         cs1 = (CalcSignal(CalcRange(elev, disp, 1), tl))
         cs2 = (CalcSignal(CalcRange(elev, disp, 2), tl))
         cs3 = (CalcSignal(CalcRange(elev, disp, 3), tl))
         s1 = s1
         s2 = s2
         s3 = s3
         absdiff = Abs(s1 - cs1) + Abs(s2 - cs2) + Abs(s3 - cs3)
         If absdiff < minabsdiff Then
            esttl = tl
            estel = elev
            estdisp = disp
            minabsdiff = absdiff
         End If
      'Next tl
   Next disp
'Next elev
FindTargetDisp = estdisp
End Function
```

11 APPENDIX C ADDITIONAL DATA

11.1 C (i) Water depth RCS measurements

Table 1 RCS measurements for stainless steel targets in 500 mm depth water

Resistance change signal (10 log Ω)						
Target length (mm)	306		400		700	
	Mean	Standard deviation				
Target Range (cm)	$\bar{x}$	σ	$\bar{x}$	σ	$\bar{x}$	σ
5	-1.163	0.189	2.393	0.134	8.075	0.020
10	-1.310	0.146	2.343	0.083	7.857	0.031
15	-1.675	0.241	1.948	0.060	7.277	0.018
20	-2.380	0.246	1.317	0.120	6.415	0.036
25	-3.234	0.227	0.667	0.163	5.586	0.042
30	-4.408	0.346	0.042	0.120	4.756	0.030
40	-5.637	0.454	-1.262	0.184	3.360	0.068
50	-7.685	0.933	-3.422	0.249	1.396	0.057
60						
70						
80						
85						
n=10						
Water Depth (mm)	500					
Water conductivity ($uScm^{-1}$)	470					
Water temperature (°C)	14.4					

Table 2 RCS measurements for stainless steel targets in 700 mm depth water

Resistance change signal (10 log Ω) Target length (mm)	306		400		700	
	Mean	Standard deviation				
Target Range (cm)	$\bar{x}$	σ	$\bar{x}$	σ	$\bar{x}$	σ
5	-1.758	0.253	1.590	0.117	7.422	0.018
10	-1.880	0.229	1.400	0.085	7.125	0.030
15	-2.422	0.240	0.918	0.090	6.392	0.036
20	-2.900	0.077	0.192	0.189	5.383	0.047
25	-3.907	0.366	-0.568	0.133	4.290	0.044
30	-4.797	0.257	-1.553	0.140	3.111	0.080
40	-6.873	0.548	-3.303	0.298	0.725	0.175
50	-10.701	2.048	-5.483	0.478	-1.282	0.268
60	-12.344	3.200	-6.964	0.536	-2.893	0.413
70			-9.071	1.885	-4.912	0.504
80						
85						
n=10						
Water Depth (mm)	700					
Water conductivity (uS.cm^{-1})	470					
Water temperature (°C)	14.4					

Table 3 RCS measurements for stainless steel targets in 900 mm depth water

Resistance change signal (10 log Ω) Target length (mm)	306		400		700	
	Mean	Standard deviation				
Target Range (cm)	$\bar{x}$	σ	$\bar{x}$	σ	$\bar{x}$	σ
5	-1.297	0.242	1.385	0.145	7.255	0.045
10	-1.459	0.223	1.266	0.155	7.048	0.037
15	-2.127	0.381	0.663	0.121	6.319	0.035
20	-2.553	0.384	-0.187	0.137	5.319	0.037
25	-3.571	0.395	-1.371	0.181	4.189	0.054
30	-4.643	0.428	-2.586	0.190	2.867	0.073
40	-6.234	0.584	-5.914	0.636	0.163	0.139
50	-8.802	1.239	-10.848	1.679	-2.575	0.179
60	-10.206	1.489			-5.131	0.535
70	-14.146	3.142			-7.601	0.603
80	-12.983	2.858			-8.697	1.204
85					-11.285	1.965
n=10						
Water Depth (mm)	900					
Water conductivity (uS.cm^{-1})	470					
Water temperature (°C)	14.4					

Figure 1 RCS measurements for stainless steel targets in 500 mm depth water

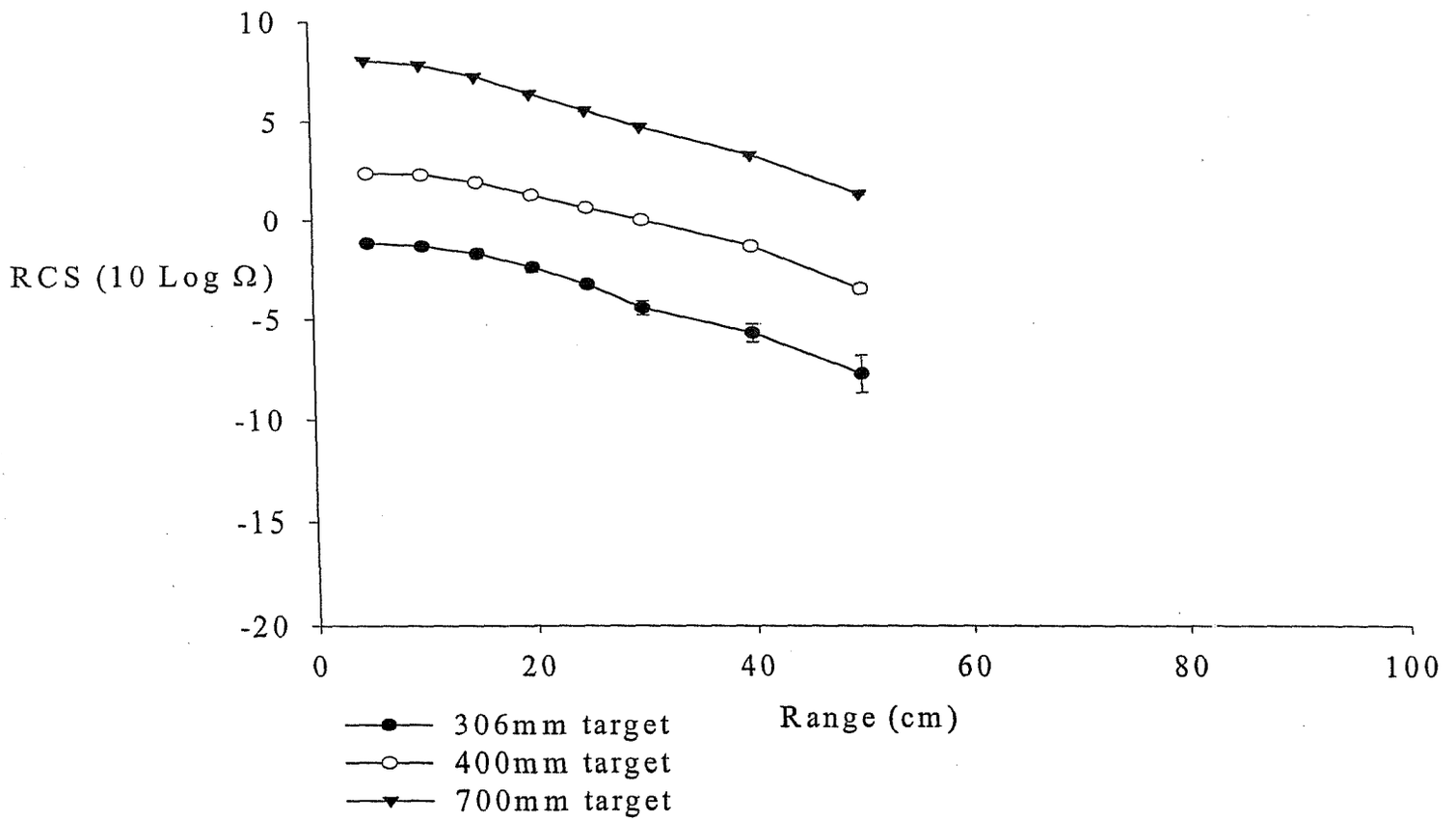

Figure 2 RCS measurements for stainless steel targets in 700 mm depth water

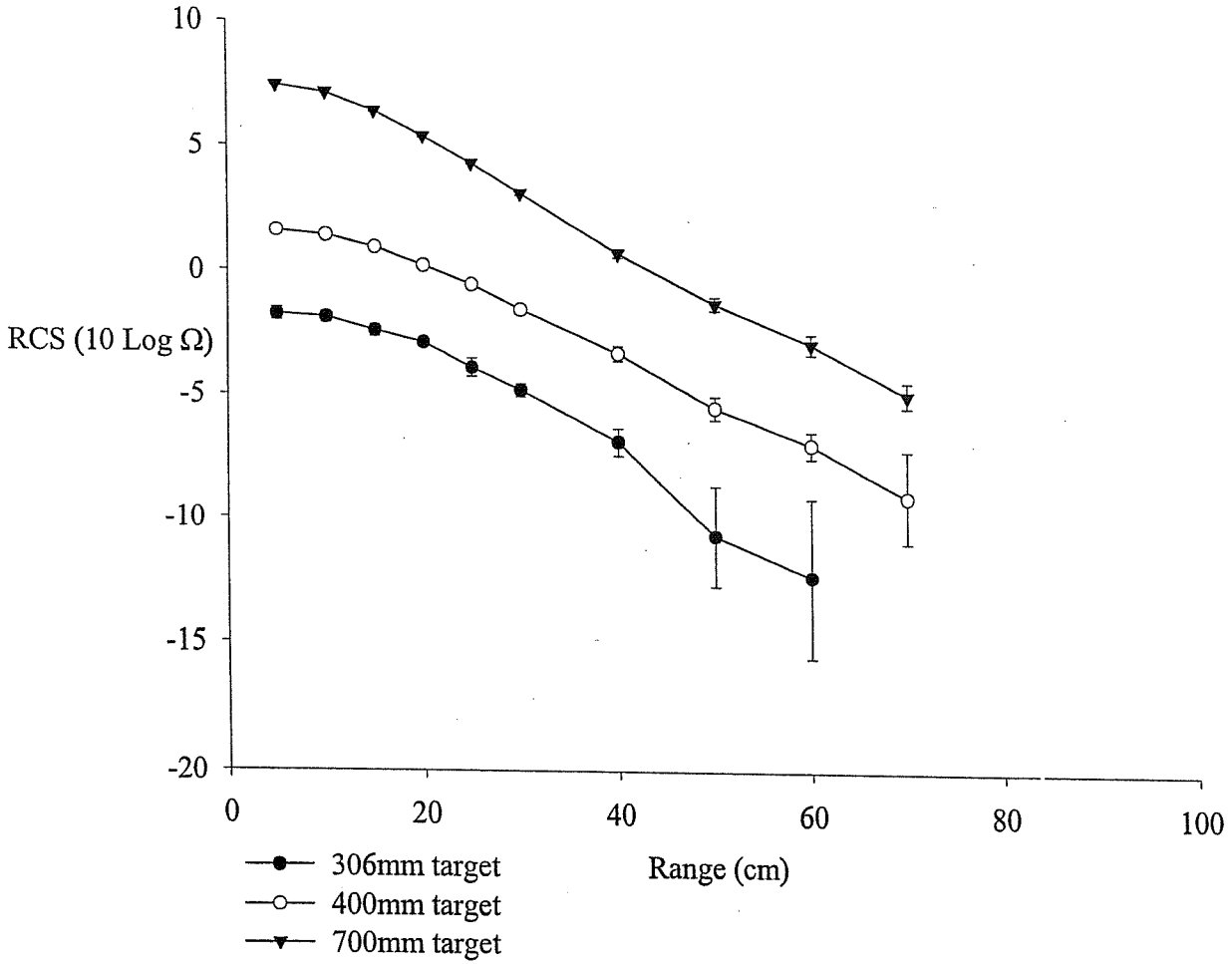

Figure 3 RCS measurements for stainless steel targets in 900 mm depth water

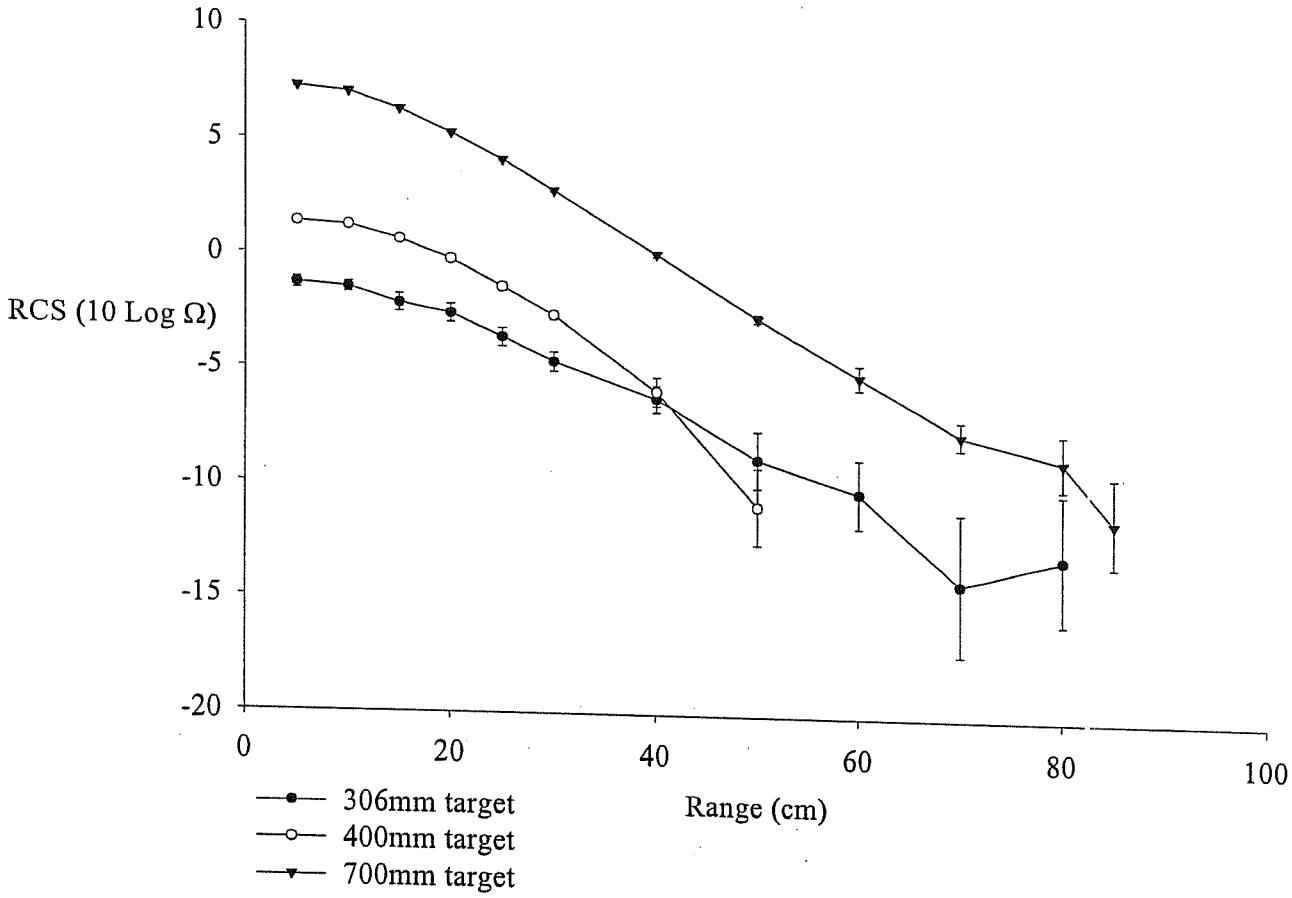

11.2 C (ii) Estimation of random lengthing errors

Table A Estimation of random lengthing error associated with resistance signal measurement with targets at 0 mm lateral displacement.

	Actual Target Length [mm] 300	300	Actual Target Length [mm] 400	400	Actual Target Length [mm] 500	500	Actual Target Length [mm] 600	600
Elevation of simulated target [mm]	Estimated mean length of target [mm]	Standard deviation of target length estimates [mm]	Estimated mean length of target [mm]	Standard deviation of target length estimates [mm]	Estimated mean length of target [mm]	Standard deviation of target length estimates [mm]	Estimated mean length of target [mm]	Standard deviation of target length estimates [mm]
20	322	27	411	19	500	0	600	0
70	309	17	410	14	502	6	600	0
120	297	25	397	22	488	10	586	9
170	288	28	398	25	499	23	597	20
220	294	43	395	17	495	16	596	19
270	324	52	410	31	496	22	608	18
320	317	50	401	28	489	20	593	18
370	313	67	403	34	504	21	606	20
420	291	59	398	35	502	19	600	19
470	312	41	414	52	496	26	600	18
520	293	76	408	49	508	37	596	17
570	295	78	388	59	509	38	602	24
620	289	60	381	50	497	33	598	26
670	269	60	401	35	492	41	595	20

Table B Estimation of random lengthing error associated with resistance signal measurement with targets at –50 mm lateral displacement.

	Actual Target Length [mm] 300	300	Actual Target Length [mm] 400	400	Actual Target Length [mm] 500	500	Actual Target Length [mm] 600	600
Elevation of simulated target [mm]	Estimated mean length of target [mm]	Standard deviation of target length estimates [mm]	Estimated mean length of target [mm]	Standard deviation of target length estimates [mm]	Estimated mean length of target [mm]	Standard deviation of target length estimates [mm]	Estimated mean length of target [mm]	Standard deviation of target length estimates [mm]
20	314	18	408	16	502	6	600	0
70	315	20	405	13	504	8	601	4
120	312	25	393	16	486	9	585	9
170	302	31	391	26	491	22	596	20
220	286	39	397	25	496	19	602	20
270	301	38	402	26	493	16	592	16
320	325	42	404	33	499	22	596	18
370	291	45	396	29	499	26	591	15
420	309	68	397	42	502	21	602	16
470	347	76	395	59	508	25	603	19
520	302	77	410	48	497	22	603	19
570	296	70	394	62	520	33	605	23
620	252	61	388	45	503	41	601	21
670	267	62	397	63	492	39	590	30

Table C Estimation of random lengthing error associated with resistance signal measurement with targets at –100 mm lateral displacement.

	Actual Target Length [mm] 300	300	Actual Target Length [mm] 400	400	Actual Target Length [mm] 500	500	Actual Target Length [mm] 600	600
Elevation of simulated target [mm]	Estimated mean length of target [mm]	Standard deviation of target length estimates [mm]	Estimated mean length of target [mm]	Standard deviation of target length estimates [mm]	Estimated mean length of target [mm]	Standard deviation of target length estimates [mm]	Estimated mean length of target [mm]	Standard deviation of target length estimates [mm]
20	308	15	409	10	502	6	600	0
70	309	21	411	17	503	7	602	6
120	299	18	400	22	497	10	591	10
170	298	40	396	28	501	18	607	16
220	310	38	402	18	501	18	593	16
270	320	38	397	30	496	17	591	15
320	287	41	401	26	502	21	592	18
370	288	44	397	32	501	25	598	20
420	286	49	401	41	500	21	595	17
470	292	77	391	24	506	21	606	20
520	308	69	406	44	508	40	601	19
570	257	64	389	62	499	38	604	24
620	268	68	397	65	507	42	605	19
670	264	65	373	65	488	36	597	28

Table D Estimation of random lengthing error associated with resistance signal measurement with targets at –150 mm lateral displacement.

	Actual Target Length [mm] 300	300	Actual Target Length [mm] 400	400	Actual Target Length [mm] 500	500	Actual Target Length [mm] 600	600
Elevation of simulated target [mm]	Estimated mean length of target [mm]	Standard deviation of target length estimates [mm]	Estimated mean length of target [mm]	Standard deviation of target length estimates [mm]	Estimated mean length of target [mm]	Standard deviation of target length estimates [mm]	Estimated mean length of target [mm]	Standard deviation of target length estimates [mm]
20	317	24	409	12	504	8	600	0
70	313	26	407	10	503	7	604	8
120	302	30	405	19	497	13	595	9
170	305	34	403	23	493	15	603	12
220	289	29	399	28	499	21	593	12
270	275	47	409	26	497	16	589	12
320	301	50	404	38	490	20	591	14
370	314	66	393	43	494	23	603	19
420	294	73	409	54	503	30	605	18
470	269	75	400	32	498	25	599	18
520	293	73	412	62	515	27	607	20
570	291	59	394	71	486	39	600	19
620	251	64	379	82	503	36	594	22
670	253	71	359	64	504	28	593	20

Table E Estimation of random lengthing error associated with resistance signal measurement with targets at –200 mm lateral displacement.

	Actual Target Length [mm] 300	300	Actual Target Length [mm] 400	400	Actual Target Length [mm] 500	500	Actual Target Length [mm] 600	600
Elevation of simulated target [mm]	Estimated mean length of target [mm]	Standard deviation of target length estimates [mm]	Estimated mean length of target [mm]	Standard deviation of target length estimates [mm]	Estimated mean length of target [mm]	Standard deviation of target length estimates [mm]	Estimated mean length of target [mm]	Standard deviation of target length estimates [mm]
20	313	21	408	12	501	4	600	0
70	309	25	405	11	501	4	602	6
120	308	38	399	19	497	10	597	7
170	302	37	400	27	496	14	601	4
220	306	54	412	23	493	13	593	12
270	312	61	401	27	499	18	593	12
320	265	61	416	48	505	23	594	16
370	263	81	398	43	505	29	604	18
420	254	57	416	58	502	29	605	20
470	275	91	429	55	498	30	599	20
520	303	72	419	69	507	28	604	22
570	270	76	397	57	493	35	612	24
620	282	63	402	60	513	43	604	24
670	279	61	374	59	503	41	597	25

Table F Estimation of random lengthing error associated with resistance signal measurement with targets at –250 mm lateral displacement.

	Actual Target Length [mm] 300	300	Actual Target Length [mm] 400	400	Actual Target Length [mm] 500	500	Actual Target Length [mm] 600	600
Elevation of simulated target [mm]	Estimated mean length of target [mm]	Standard deviation of target length estimates [mm]	Estimated mean length of target [mm]	Standard deviation of target length estimates [mm]	Estimated mean length of target [mm]	Standard deviation of target length estimates [mm]	Estimated mean length of target [mm]	Standard deviation of target length estimates [mm]
20	309	19	406	9	503	7	600	0
70	326	31	414	17	503	7	601	4
120	306	38	400	19	501	12	599	8
170	314	47	389	22	502	16	601	10
220	294	60	399	27	502	14	596	10
270	311	69	401	41	507	13	597	12
320	306	72	418	35	506	21	600	16
370	283	64	407	48	497	23	595	13
420	285	69	405	51	487	33	610	26
470	285	87	382	54	514	36	595	20
520	262	77	420	56	493	40	593	20
570	324	74	406	64	492	33	605	23
620	309	63	392	69	501	40	602	27
670	277	76	377	75	499	38	604	22

Table G Estimation of random lengthing error associated with resistance signal measurement with targets at –300 mm lateral displacement.

	Actual Target Length [mm] 300	300	Actual Target Length [mm] 400	400	Actual Target Length [mm] 500	500	Actual Target Length [mm] 600	600
Elevation of simulated target [mm]	Estimated mean length of target [mm]	Standard deviation of target length estimates [mm]	Estimated mean length of target [mm]	Standard deviation of target length estimates [mm]	Estimated mean length of target [mm]	Standard deviation of target length estimates [mm]	Estimated mean length of target [mm]	Standard deviation of target length estimates [mm]
20	311	15	408	12	506	9	602	6
70	325	35	407	10	503	7	601	4
120	314	38	416	26	498	11	598	9
170	308	53	408	35	502	17	600	6
220	292	45	411	34	504	19	599	10
270	297	42	421	43	502	19	596	18
320	320	89	393	49	497	28	599	14
370	316	81	391	50	499	19	608	21
420	289	74	399	52	506	37	600	13
470	327	67	390	71	498	45	587	23
520	294	75	389	68	503	38	604	22
570	276	70	400	63	506	32	607	23
620	292	62	379	60	486	41	608	29
670	257	58	365	50	483	52	589	27

Table H Estimation of random lengthing error associated with resistance signal measurement with targets at –350 mm lateral displacement.

	Actual Target Length [mm] 300	300	Actual Target Length [mm] 400	400	Actual Target Length [mm] 500	500	Actual Target Length [mm] 600	600
Elevation of simulated target [mm]	Estimated mean length of target [mm]	Standard deviation of target length estimates [mm]	Estimated mean length of target [mm]	Standard deviation of target length estimates [mm]	Estimated mean length of target [mm]	Standard deviation of target length estimates [mm]	Estimated mean length of target [mm]	Standard deviation of target length estimates [mm]
20	350	48	408	12	505	11	601	4
70	327	44	409	19	503	7	600	0
120	330	45	404	20	500	18	600	0
170	313	62	414	39	504	18	601	8
220	291	54	399	57	497	30	603	18
270	314	65	406	53	504	25	606	17
320	326	75	406	54	505	33	604	18
370	317	88	400	70	504	32	603	13
420	293	74	400	54	514	42	606	18
470	277	75	391	46	494	31	597	24
520	258	65	386	75	498	37	600	26
570	308	69	390	67	478	52	606	25
620	271	73	376	79	483	54	600	22
670	272	62	371	83	493	46	588	26

Table I Estimation of random lengthing error associated with resistance signal measurement with targets at –400 mm lateral displacement.

	Actual Target Length [mm] 300	300	Actual Target Length [mm] 400	400	Actual Target Length [mm] 500	500	Actual Target Length [mm] 600	600
Elevation of simulated target [mm]	Estimated mean length of target [mm]	Standard deviation of target length estimates [mm]	Estimated mean length of target [mm]	Standard deviation of target length estimates [mm]	Estimated mean length of target [mm]	Standard deviation of target length estimates [mm]	Estimated mean length of target [mm]	Standard deviation of target length estimates [mm]
20	318	35	415	28	500	0	602	9
70	316	40	416	36	509	15	602	9
120	315	53	408	33	497	18	601	4
170	310	64	395	32	499	28	599	14
220	285	62	415	47	494	27	606	17
270	317	67	396	46	502	25	595	16
320	266	75	424	52	500	28	604	19
370	315	70	408	52	505	30	604	17
420	325	67	405	53	495	41	608	21
470	284	79	399	53	511	28	601	23
520	277	69	385	65	493	37	598	18
570	280	76	401	56	487	46	602	16
620	271	60	368	83	488	41	588	26
670	247	53	392	68	497	36	602	29

Table J Estimation of random lengthing error associated with resistance signal measurement with targets at –450 mm lateral displacement.

	Actual Target Length [mm] 300	300	Actual Target Length [mm] 400	400	Actual Target Length [mm] 500	500	Actual Target Length [mm] 600	600
Elevation of simulated target [mm]	Estimated mean length of target [mm]	Standard deviation of target length estimates [mm]	Estimated mean length of target [mm]	Standard deviation of target length estimates [mm]	Estimated mean length of target [mm]	Standard deviation of target length estimates [mm]	Estimated mean length of target [mm]	Standard deviation of target length estimates [mm]
20	324	59	412	33	504	17	600	0
70	314	53	402	32	501	19	601	4
120	311	49	384	30	507	25	603	15
170	303	65	396	35	497	31	607	16
220	296	76	390	50	502	29	599	15
270	315	68	398	54	497	35	596	17
320	294	73	401	41	515	24	595	19
370	284	66	391	58	509	27	592	20
420	292	54	400	48	493	30	593	28
470	259	80	376	66	501	31	598	22
520	239	52	372	84	490	31	591	26
570	297	76	403	53	491	50	594	24
620	265	60	371	88	489	44	587	27
670	265	59	372	79	484	43	591	28

Table K Estimation of random lengthing error associated with resistance signal measurement with targets at –500 mm lateral displacement.

	Actual Target Length [mm] 300	300	Actual Target Length [mm] 400	400	Actual Target Length [mm] 500	500	Actual Target Length [mm] 600	600
Elevation of simulated target [mm]	Estimated mean length of target [mm]	Standard deviation of target length estimates [mm]	Estimated mean length of target [mm]	Standard deviation of target length estimates [mm]	Estimated mean length of target [mm]	Standard deviation of target length estimates [mm]	Estimated mean length of target [mm]	Standard deviation of target length estimates [mm]
20	285	48	411	33	500	28	601	4
70	281	51	396	35	493	22	601	10
120	293	55	409	42	497	27	602	16
170	290	72	390	51	500	24	596	19
220	294	61	403	47	507	26	608	18
270	301	63	395	50	502	25	606	13
320	284	58	394	49	496	26	599	17
370	285	74	407	44	490	38	603	18
420	272	73	381	76	491	40	606	16
470	295	59	355	58	486	41	600	19
520	262	81	372	78	503	33	595	16
570	241	48	366	73	487	34	589	26
620	274	71	392	50	491	39	595	24
670	243	57	358	86	490	38	592	23